Impacts of Cascadia Subduction Zone M9 Earthquakes on Bridges in Washington State: Three-Dimenstional Bridge Models

WA-RD 908.2

Kan-Jen Liu
Zachary Kortum
Jeffrey W. Berman
Brett Maurer
Addie Lederman
Marc O. Eberhard
Nasser A. Marafi

November 2022

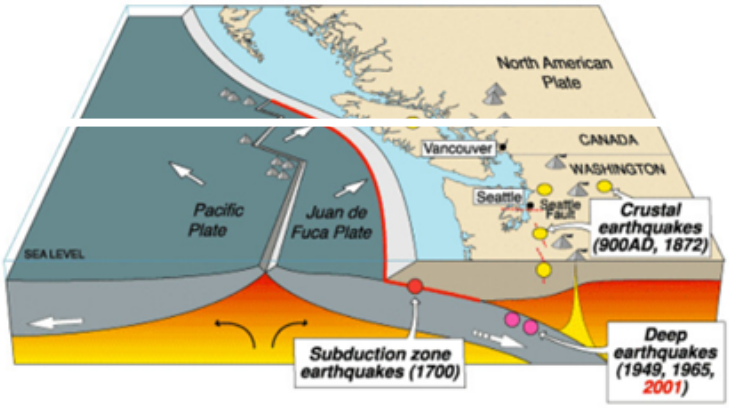

Source	Affected area	Max. Size	Recurrence
Subduction Zone	W.WA, OR, CA	M 9	500-600 yr
Deep Juan de Fuca plate	W.WA, OR,	M 7+	30-50 yr
Crustal faults	WA, OR, CA	M 7+	Hundreds of yr?

Cascadia Subduction Zone
USGS, 2017

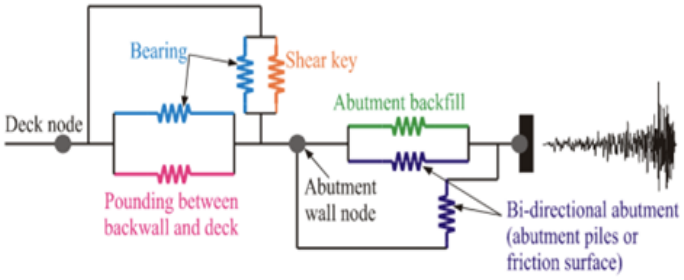

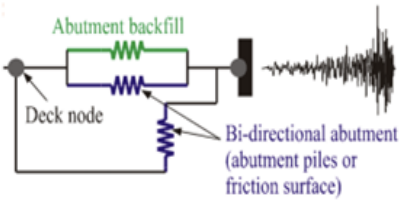

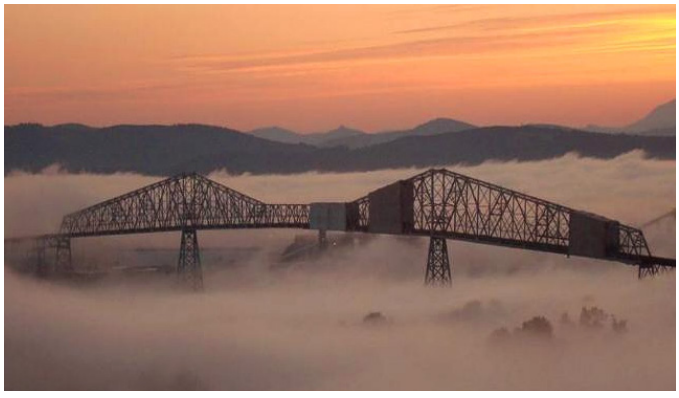

Washington State Department of Transportation
Office of Research & Library Services

WSDOT Research Report

Research Report
Agreement T1461, Task 74
M9 WSDOT Bridges
WA-RD 908.2

IMPACTS OF CASCADIA SUBDUCTION ZONE M9 EARTHQUAKES ON BRIDGES IN WASHINGTON STATE: THREE-DMENSIONAL BRIDGE MODELS

by

Kan-Jen Liu, Research Assistant
Civil and Env. Engineering

Addie Lederman
Civil and Env. Engineering

Zachary Kortum, Research Assistant
Civil and Env. Engineering

Marc O. Eberhard, Professor
Civil and Env. Engineering

Jeffrey W. Berman, Professor
Civil and Env. Engineering.

Nasser A. Marafi, Senior Modeler
Risk Management Solutions, Inc

Brett Maurer, Assistant Professor
Civil and Env. Engineering

University of Washington
Seattle, Washington 98195

Washington State Transportation Center (TRAC)
University of Washington, Box 359446
University Tower, 4333 Brooklyn Ave NE
Seattle, Washington 98195-9446

Washington State Department of Transportation Technical Monitor
Bijan Khaleghi
State Bridge Design Engineer
Bridge and Structures Office

Prepared for
The State of Washington
Department of Transportation
Roger Millar, Secretary

November 2022

TECHNICAL REPORT STANDARD TITLE PAGE

1. REPORT NO.	2. GOVERNMENT ACCESSION NO.	3. RECIPIENT'S CATALOG NO.
WA-RD 908.2		

4. TITLE AND SUBTITLE	5. REPORT DATE
Impacts of Cascadia Subduction Zone M9 Earthquakes on Bridges in Washington State: Three-Dimensional Bridge Models	November 2022
	6. PERFORMING ORGANIZATION CODE
7. AUTHOR(S)	8. PERFORMING ORGANIZATION REPORT NO.
Liu, Kan-Jen, Lederman, Addie, Kortum, Zachary, Eberhard, Marc O., Berman, Jeffrey W., Marafi, N., Maurer, Brett	
9. PERFORMING ORGANIZATION NAME AND ADDRESS	10. WORK UNIT NO.
Washington State Transportation Center University of Washington, Box 359446 University Tower, 4333 Brooklyn Ave NE Seattle, Washington 98195-9446	11. CONTRACT OR GRANT NO. Agreement T1461, Task 74
12. SPONSORING AGENCY NAME AND ADDRESS	13. TYPE OF REPORT AND PERIOD COVERED
Washington State Department of Transportation Transportation Building, MS 47372 Olympia, Washington 98504-7372 14 Mustafa Mohamedali, Project Manager, 360-704-6307	Research Report
	14. SPONSORING AGENCY CODE

15. SUPPLEMENTARY NOTES

This study was conducted in cooperation with the U.S. Department of Transportation, Federal Highway Administration and the University of Washington.

16. ABSTRACT

Large-magnitude earthquakes generated by the Cascadia Subduction Zone (CSZ) pose major risks to the western portions of Washington state, Oregon, and Northern California. The performance of bridges during such events is an essential feature of the resilience of these regions because bridges will be needed for pre-tsunami evacuation, emergency response, and economic recovery.

Washington State Department of Transportation (WSDOT) and University of Washington engineers identified typical properties of bridges along some of the major highways in the Puget Sound region. These properties guided the development of a three-dimensional, nonlinear model of a typical bridge, which was subjected to sets of simulated M9 earthquake ground motions for six locations, four site classes, and a variety of abutment characteristics and column properties.

The calculated displacements of the bridges were consistently smaller in the longitudinal direction than in the transverse direction because of the high resistance provided by the backwall, abutment, and backfill soil. In the transverse direction, the likelihoods of flexural damage for the reference bridge were largest for locations on the Olympic Peninsula, reaching maximum values of 31% for concrete column spalling (Forks, Wash., Site Class D1) and 6.1% for longitudinal bar buckling (Port Angeles, Wash., Site Class D3). Neglecting the abutment resistance greatly increased the transverse displacements for all locations and site classes, with the largest increases occurring for long-period bridges in sedimentary basins. When the shear key resistance was neglected, and the column height was doubled for a bridge in Seattle, the maximum likelihoods of spalling and bar buckling increased from 1.53% to 32% and from 0.3% to 5.6%, respectively. These analyses suggest that, for typical bridges, WSDOT should prioritize retrofit efforts on bridges without shear keys or those in which a curved or discontinuous superstructure makes the shear key less effective.

17. KEY WORDS	18. DISTRIBUTION STATEMENT
Bridges, Earthquakes, Abutments, Cascadia, Damage	No restrictions. This document is available to the public through the National Technical Information Service, Springfield, VA 22616

19. SECURITY CLASSIF. (of this report)	20. SECURITY CLASSIF. (of this page)	21. NO. OF PAGES	22. PRICE
None	None	230	

DISCLAIMER

The contents of this report reflect the views of the authors, who are responsible for the facts and the accuracy of the data presented herein. The contents do not necessarily reflect the official views or policies of the Washington State Department of Transportation, Federal Highway Administration, or United States Department of Transportation. This report does not constitute a standard, specification, or regulation.

CONTENTS

FIGURES

Figure *Page*

TABLES

Table *Page*

ACKNOWLEDGMENTS

The research presented here builds on analyses performed as part of the MSCE thesis research by Gloria De Zamacona Cervantes (2019) and Zach Kortum et al. (2022).

The authors are greatly indebted to their colleagues from the United States Geological Survey, Arthur Frankel and Erin Wirth. They worked with Nasser Marafi (RMS Associates) to generate the baseline simulated motions that underlie the research results presented in this report (Frankel et al. 2018, Wirth et al. 2018). USGS researcher alex grant performed the analyses to account for the effects of local site conditions (Marafi et al. 2017).

The research described in this report was funded jointly by the Washington State Department of Transportation (WSDOT) and the United States Department of Transportation Pacific Northwest Transportation Consortium (Pactrans) University Transportation Center. WSDOT engineers Chase Weeks, Amy Leland, Geoff Swett, and Bijan Khaleghi provided valuable assistance in assembling the database and helping researchers understand current and past WSDOT practices. Additional analyses were supported by the Pacific Earthquake Engineering Research center.

EXECUTIVE SUMMARY

Large-magnitude earthquakes generated by the Cascadia Subduction Zone (CSZ) pose a major hazard to the western portions of Washington state, Oregon, and Northern California. It is important to understand the impacts of such earthquakes on typical highway bridges because these bridges will be critical to the post-event emergency response and to the longer-term economic recovery of many communities. Coastal communities will also need these bridges to evacuate rapidly in the time interval between the end of earthquake shaking and possible subsequent tsunami inundation.

Previous researchers developed 30 sets of ground motions, corresponding to a variety of M9 rupture scenarios, at numerous locations throughout Washington state (Frankel et. al 2018). De Zamacona Cervantes (2019) and Kortum et al. (2022) combined these motions with single-degree-of-freedom (SDOF) models to investigate bridge performance for several site classes. SDOF models are computationally efficient, but they have limitations in predicting bridge seismic response. In particular, such models neglect the lateral-force resistance provided by the bridge abutments.

As part of this study, typical characteristics of bridges along major highways in the Puget Sound region were identified from a database compiled by the Washington State Department of Transportation (WSDOT) and University of Washington engineers. The presence of shear keys and of a continuous superstructure are important features of a bridge because both features are needed to engage the abutment resistance in the transverse direction. Of the 505 multi-span bridges for which span continuity was documented, 76 percent (302/399) of the bridges built before 1976 and 97 percent (103/106) of the newer bridges had continuous superstructures (Figure 3.5). Of the 94 bridges in which the shear-key configuration was surveyed, 90 percent (65/72) of the bridges built before 1976 and 100 percent (19/19) of the newer bridges had internal or external shear keys (Figure 3.20).

On the basis of the properties that were common in the database, a three-dimensional, multi-degree-of-freedom model was developed to represent typical highway bridges in Washington state (tables 3.2 and 3.3). The reference bridge model had three spans, a continuous superstructure, and an L-type (Seat) abutment with bearing pads and internal transverse shear keys (Figure 4.2). Using that model, a series of parametric studies was conducted to evaluate the effects of bridge location (6), site class (4), abutment

characteristics, and the properties of the columns at the intermediate supports. For each of the combinations of bridge abutment characteristics, column properties, location, site class, and ground motion realization, there were 300 analyses, of which at least 296 were completed.

The simulated deformation responses of the bridges in the longitudinal direction were consistently smaller than those in the transverse direction because of the high resistance provided by the backwall, abutments, and backfill soil (Figure 6.1). In the longitudinal direction, the worst combination of location and site class (Forks, Site Class D1) for the reference bridge resulted in median and 85th percentile column drift ratios of only 0.67 percent and 0.83 percent, respectively (Figure 6.2). These values were far below the median drift ratio for spalling of the column concrete cover (2.1 percent).

In the transverse direction, the largest median displacement responses for the reference bridge were calculated for the coastal cities and for site class D1, resulting in median bent drift ratios of 1.64 percent and 85th percentile values of 2.3 percent (Figure 6.3, Forks, Site Class D1). The corresponding likelihood of spalling for these conditions was 31 percent (Figure 6.4). Depending on the location and site class, the likelihood of bar buckling for the three cities nearest the coast ranged from 0.25 percent (Figure 6.6, Forks, Site Class D1) to 6.0 percent (Figure 6.6, Port Angeles, Site Class D3). The deformations responses and likelihoods of damage of the reference bridge tended to decrease as the distance from the CSZ increased. For example, the likelihood of cover spalling and bar buckling for the three cities farthest from the coast (Olympia, Seattle, and Everett) reached maxima of only 4.5 percent and 0.32 percent, respectively.

The calculated maximum transverse displacements (Figure 7.8) and likelihood of column damage increased significantly when the shear keys were removed for all locations and site classes (figures 7.9 and 7.10). These increases were particularly large for bridges with tall columns located on sedimentary basins. For example, for the reference bridge located in the city of Seattle on Site Class D3, the likelihoods of concrete spalling and bar buckling were small (1.25 percent and 0.16 percent). For the same bridge without a shear key (but with bearing resistance), the corresponding likelihoods increased to 8.4 percent (Figure 7.9) and 1.3 percent (Figure 7.10). For the same bridge with a column height equal to double the reference height, the likelihoods increased further to 32 percent and 5.6

percent (figures 8.3 and 8.4). The likelihood of damage increased even further when both the shear key and bearing resistances were neglected (figures 7.9 and 7.10).

These findings provide WSDOT an opportunity to develop cost- and time-efficient prioritization bridge retrofit plans. Many factors affect the decision to retrofit a bridge, including the importance of the bridge to the community and highway system, the bridge's possible functional obsolescence, and the cost of retrofitting the bridge. The results of this study suggest that, for typical bridges, WSDOT should consider prioritizing retrofit efforts on bridges in which the abutments do not effectively constrain the column displacements of the bridges, either because the bridge has no shear key or because the superstructure is curved or discontinuous. These results can also use the developed damage fragility curves to make regional estimates of bridge damage for large numbers of bridges. Such regional estimates could serve as the basis for future emergency management planning.

It is important to note that this research did not address some critical aspects of bridge vulnerability. In particular, the research did not consider "atypical" bridges, including major bridges or bridges with high skew or curved alignment. Most importantly, the effects of liquefaction and the possibility of shear failure were not considered. Column shear failure is one of the most common causes of bridge collapse (Moehle and Eberhard 2000).

CHAPTER 1 INTRODUCTION

1.1 BACKGROUND

The Cascadia Subduction Zone (CSZ) runs over 1,000 kilometers from Northern Vancouver Island to Cape Mendocino, California (Figure 1.1). It is the boundary between the Juan de Fuca and the North American tectonic plates. The subduction zone has the potential of generating large "megathrust" earthquakes with magnitudes over 9.0. Geological evidence indicates that at least seven such events occurred in the last 3,500 years, and the last event happened in 1700. Such events have the potential to cause tremendous damage to the western portions of Washington state, Oregon, and Northern California. (PNSN 2021).

The post-earthquake functionality of the transportation system for communities in these regions is critical because the highway transportation system will be needed to recover from the effects of an earthquake, and possibly, an ensuing tsunami. Coastal communities in Washington state are close to the CSZ source, so it is expected that these locations will experience intense ground motions with large spectral accelerations. It is also expected that the motions will have long durations. The major cities in the Puget Sound region, including Seattle, are farther from the sources of M9 earthquakes, but these cities lie on top of deep sedimentary basins. The presence of such basins is a concern because deep basins are known to affect ground motions as a result of impedance contrast at the boundary of the basin, focusing (and de-focusing) because of the irregular geometry of the basin and surface-wave conversion at the edge of basins (Figure 1.2).

Basins tend to amplify the longer period content of the motion (above 1 sec) and can have damaging spectral shapes (Marafi et al. 2017). The resulting, basin-modified CSZ ground motions pose a considerable risk to these highly populated areas, particularly to structures with periods of 1 second and above (Marafi et al. 2017, 2020). Nevertheless, the current United States seismic hazard design maps for bridges do not consider the effect of basin amplification.

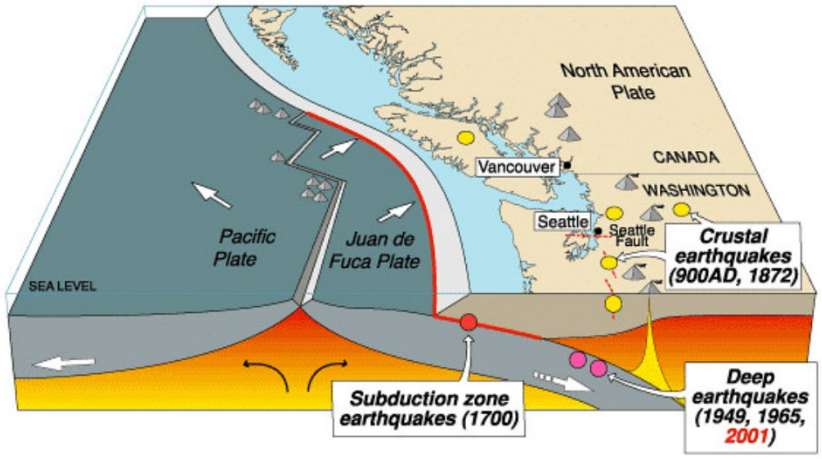

Source	Affected area	Max. Size	Recurrence
Subduction Zone	W.WA, OR, CA	M 9	500-600 yr
Deep Juan de Fuca plate	W.WA, OR,	M 7+	30-50 yr
Crustal faults	WA, OR, CA	M 7+	Hundreds of yr?

Figure 1.1: Cascadia Subduction Zone (USGS 2017)

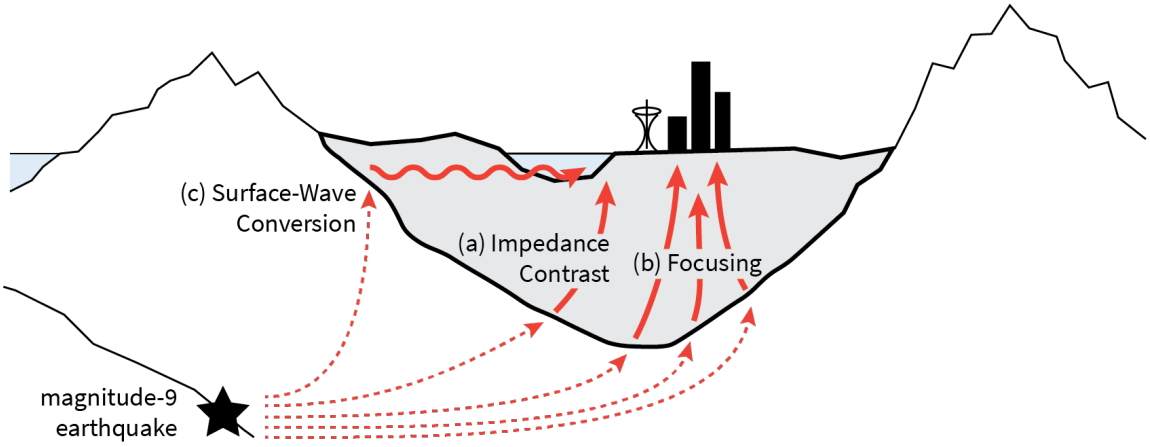

Figure 1.2: Cities located above a sedimentary basin (Marafi 2018)

1.2 RESEARCH OBJECTIVES

Communities rely on their transportation infrastructure after an earthquake for the delivery of relief supplies, for evacuation following an earthquake and tsunami (along the coasts), and for longer-term economic recovery. Consequently, the performance of bridges in a CSZ event is an essential feature of the resilience of these communities. Considering six representative cities in Western Washington, this study aimed to investigate the impacts of these earthquakes on typical bridges for a variety of site classes, source distances, presence of basin, and key features of the abutments and the columns at intermediate supports.

Previous researchers developed suites of ground motions resulting from an M9 CSZ earthquake for the western portions of Washington and Oregon (Frankel et al. 2018, Wirth et al. 2018). De Zamacona (2019) evaluated the effects of these motions for ten cities in Washington state by using single-degree-of-freedom (SDOF) models of bridges, assuming that the lateral strength of the system was 50 percent above the minimum strength required by the AASHTO bridge design provisions (AASHTO, 2017). Kortum et al. (2022) also modeled bridges as nonlinear, SDOF oscillators, but they also considered how various site classes might affect motions, and they estimated the strength of the oscillators on the basis of the actual properties of bridges on major highways within the Puget Sound region.

The previous research, which is summarized in Chapter 2, had some limitations.

- The SDOF oscillators neglected the resistance provided by the end abutments, including the effects of the bearings, end walls, and shear keys.
- The SDOF oscillators used simple relationships to represent the cyclic deterioration of the reinforced concrete columns.
- The SDOF models did not consider the 3D behavior of the bridges (e.g., skew, curve) and effects of simultaneous application of both horizontal components of ground motion.
- Shear failure of columns was not considered.
- Foundation failure, including the possibility of liquefaction, was not considered.

This study aimed to resolve some of these limitations by using a three-dimensional, nonlinear, multi-degree-of-freedom (MDOF) finite-element bridge model that captures more detailed behaviors of critical bridge components. This model can better characterize

the risk to Washington state bridges in the event of an M9 earthquake. The characteristics modeled for the various bridge components were developed through the study of a bridge database compiled by the Washington Statement Department of Transportation (WSDOT) and university researchers. Furthermore, the researchers reviewed 94 bridge plans to extract data for modeling the abutments, which had not been previously available from the WSDOT database.

The main research goals of this study were as follows:

- Identify key characteristics of bridges that are typical in Washington state.
- Evaluate the effects of geographic location and soil class on the expected performance of a bridge with typical characteristics.
- Investigate the effects of variations in the key characteristics of the abutments and columns on the expected performance of typical bridges.
- Develop damage fragility curves for typical bridges.

1.3 RESEARCH APPROACH

The research described in this report built directly on the results of recent research. Chapter 2 summarizes the development of the M9 baseline motions (Frankel et al. 2018), the effects of sedimentary basins (Marafi et al. 2019), and the effects of local site conditions on ground motions (de Zamacona 2019). This chapter also reviews previous investigations of the effects of such ground motions on SDOF bridge structures (de Zamacona 2019, Kortum et al. 2022).

With data from a newly assembled database, the distribution of key properties was established for bridges along major highways in the Puget Sound region (Chapter 3). These properties were used to define a typical reference bridge. The bridges were modeled with OpenSeesPy (Zhu et al. 2018) by combining finite-element methodologies used in previous research (Ranf 2007, Ramanathan et al. 2012, and Mangalathu et al. 2017). Chapter 4 reviews these methodologies and illustrates the development of the reference bridge model in OpenSeesPy. This model was used as a baseline for the parametric study described in later chapters.

The performance of the reference bridge model was interrogated in detail to confirm that it performed as expected. Chapter 5 presents the results of a series of analyses

of the bridge model, including pushover analyses, cyclic analyses, and bi-directional, dynamic analyses. This chapter also compares the dynamic response of the managed three-dimensional, MDOF model and the SDOF model from previous research (Kortum et al. 2022).

The reference bridge model was used to perform a comprehensive parametric study to evaluate the impacts on bridge performance of bridge location, site class, abutment properties, and column properties. Chapter 6 describes the effects of geographic location and site class on bridge response, and chapters 7 and 8 discuss the effects of variation of abutment and column properties on bridge performance, respectively. Bridge performance was quantified in terms of the following:

- displacements of the superstructure at the end of the bridge,
- drift ratio of the columns at intermediate supports,
- maximum force in the shear key, normalized by the weight of the bridge,
- maximum force in the columns, normalized by the weight of the bridge,
- likelihood of column spalling, and
- likelihood of buckling of the column longitudinal bars.

Chapter 9 summarizes the results of this research, and Chapter 10 provides recommendations for WSDOT retrofit prioritization, identifies the limitations of the research, and proposes new directions for future research.

CHAPTER 2 PREVIOUS RESEARCH ON BRIDGE PERFORMANCE DURING CSZ M9 EARTHQUAKES

This chapter provides an overview of the development of M9 ground motions, as well as of previous studies that investigated the impacts of these simulated ground motions on bridges in Washington state. The previous work included the following:

- The development of a methodology to simulate ground motions for a set of 30 M9 earthquake scenarios for the Cascadia Subduction Zone (Section 2.1)
- The selection of ten cities to represent a variety of distance-to-source and basin combinations (Section 2.2)
- The evaluation of the effects of site-source distance and basins on the resulting ground motions (Section 2.3)
- The generation of soil-adjusted ground motions that take into account the effects of local site conditions. (Section 2.4)
- Simulation of bridges with single-degree-of-freedom (SDOF) models (de Zamacona 2019, Kortum et al. 2022) to simulate impacts on bridges in Washington state under M9 ground motions (Section 2.5).

2.1 MODELING OF CASCADIA SUBDUCTION ZONE M9 EARTHQUAKES

Synthetic seismograms for magnitude 9 earthquakes for the Cascadia Subduction Zone were generated by researchers from the United States Geological Survey (USGS) and the University of Washington (UW) (Frankel et. Al. 2018, Wirth et. Al. 2018). To develop these simulated ground-motions, synthetic seismograms derived from 3D finite difference simulations were combined with finite-source, stochastic synthetics (Frankel et al. 2018). The synthetic seismograms were designed to capture a wide range of possible M9 events by including a variety of rupture features (Frankel et al. 2018). The motion's hypocenter, rupture velocity, and the number and location of subevents were all factors in the rupture simulation (Wirth et al. 2018). The ground motions were generated by using a two-component model: first, massive slip motions with long durations and second, large stress-drop magnitude 8 subevents (Frankel et al. 2018). The final simulated M9 motions were created by superimposing these two components on top of each other.

The baseline ground-motion pairs were computed for 30 rupture scenarios (30 realizations) for 169 locations within the Cascadia Subduction Zone model, corresponding to a soil profile with a V_{s30} of 1968 ft./s (600 m/s). These ground motions can be accessed through the online data repository DesignSafe (https://www.designsafe-ci.org/), supported by the National Science Foundation, under the citation Frankel et al. (2018).

2.2 SELECTION OF REPRESENTATIVE LOCATIONS

To understand the impacts of M9 ground motions over a wide range of conditions in Washington state, de Zamacona (2019) selected ten cities that had a variety of site-to-source distances and sedimentary basin conditions. The locations of these cities are shown in Figure 2.1, and their coordinates are listed in Table 2.1. For each of the 10 cities, Table 2.1 also provides the corresponding location and station ID of the nearest locations where ground motions were computed with the seismic model (Section 2.1).

The depth from the surface to a soil layer with shear-wave velocity of 2,500 m/s (8,200 ft/s), $Z_{2.5}$, had been used as a measure of the depth of sedimentary basins (Marafi et al. 2021). Locations with thick sedimentary deposits within the basin tended to have lower shear wave velocities, so these locations tended to have higher values of $Z_{2.5}$ (Marafi et al. 2019). The cities were categorized into four groups based on distance to the faults and the values of $Z_{2.5}$. Cities with a $Z_{2.5}$ lower than 2.0 km were categorized as having no basin. Cities with a $Z_{2.5}$ of between 2.0 and 3.0 km were classified as having a shallow basin, and cities with a $Z_{2.5}$ greater than 3.0 km were classified as having a deep basin. The ten cities were grouped as follows:

- Coastal cities (closer to the fault) outside of the basin (Forks and Ocean Shores),
- Inland cities (farther from the fault) outside of the basin (Olympia, Vancouver, and Graham),
- Inland cities on a shallow/medium-depth basin (Port Townsend, Port Angeles, and Tacoma), and
- Inland cities on a deep basin (Seattle and Everett).

Note that Port Angeles was classified as "inland" because it is located much farther from the Pacific Coast than are Ocean Shores and Forks. However, Port Angeles is located closer to the rupture zone than the other inland cities, such as Seattle, Tacoma, and Everett.

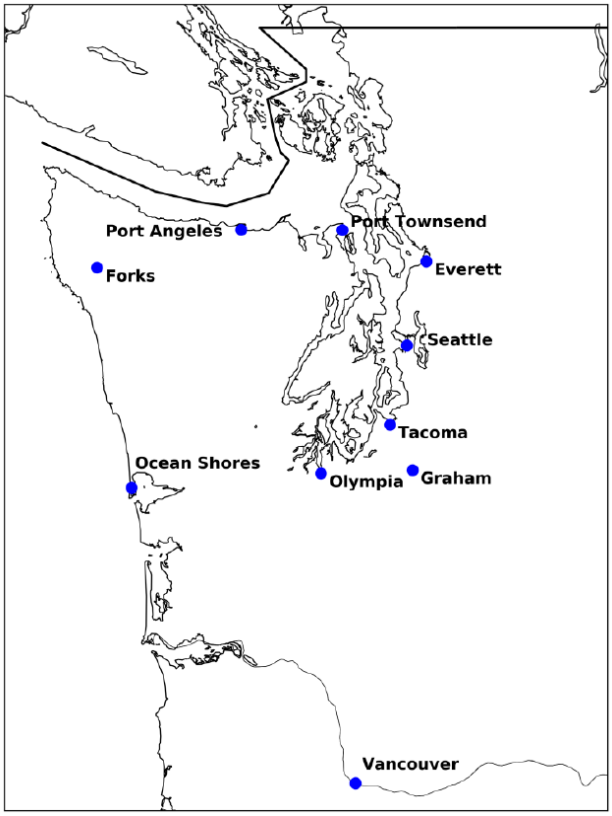

Figure 2.1: Locations of ten representative cities (de Zamacona 2019)

The coastal locations had large spectral accelerations for low periods, with a maximum value above 1.5 g occurring in Forks, Wash. The spectral accelerations rapidly decreased with increasing periods for periods above 0.3 to 0.5 s. None of the coastal locations are located on sedimentary basins. The inland locations that are outside of basins had similar spectral shapes, but the spectral accelerations were much lower. For example, the largest spectral acceleration for an inland location without a basin was approximately 0.6 g (Olympia, Wash.), which was less than half the maximum value for Forks, Wash.

Table 2.1: Ten representative cities in Western Washington state (de Zamacona 2019)

City Locations			Closest Station Locations			Basin Depth (km)	Classification
City Name	Latitude	Longitude	Station ID	Latitude	Longitude		
Forks	47.9504	-124.386	Z0FORK	47.9456	-124.566	0.76	Coastal Outside of Basin
Ocean Shores	46.9737	-124.156	Z0XOCS	46.9778	-124.154	0.98	Coastal Outside of Basin
Port Angeles	48.1181	-123.431	Z0XANG	48.1191	-123.431	2.29	Inland Shallow Basin
Olympia	47.0379	-122.901	Z00CPW	46.9717	-123.138	1.96	Inland Outside of Basin
Port Townsend	48.117	-122.76	Z0XTWN	48.1146	-122.756	2.84	Inland Shallow Basin
Vancouver	45.6272	-122.673	Z0HUBA	45.6287	-122.653	1.76	Inland Outside of Basin
Tacoma	47.2529	-122.444	Z0TBPA	47.2559	-122.368	2.86	Inland Shallow Basin
Seattle	47.6062	-122.332	Z0XWLK	47.612	-122.338	6.70	Inland Deep Basin
Graham	47.0529	-122.294	Z00GHW	47.0395	-122.274	0.20	Inland Outside of Basin
Everett	47.979	-122.202	Z0EVCC	48.0056	-122.204	3.42	Inland Deep Basin

2.3 BASELINE GROUND MOTIONS

Figure 2.2 shows the response spectra of the baseline M9 ground motions for the ten cities listed in Table 2.1. The spectral accelerations shown in each figure correspond to the geometric mean (of the 30 realizations) of both the North-South and East-West components at a given period.

The spectral accelerations for inland sites with shallow or deep basins were similar to those of the inland sites without basins for periods below 0.5 s. The amplification of the ground motion by the sedimentary basins at longer periods (>1.0 sec) can be seen in Figure 2.2. In these locations, the spectral acceleration increased once the period reached 1.0 sec, a result of basin amplification at the longer periods

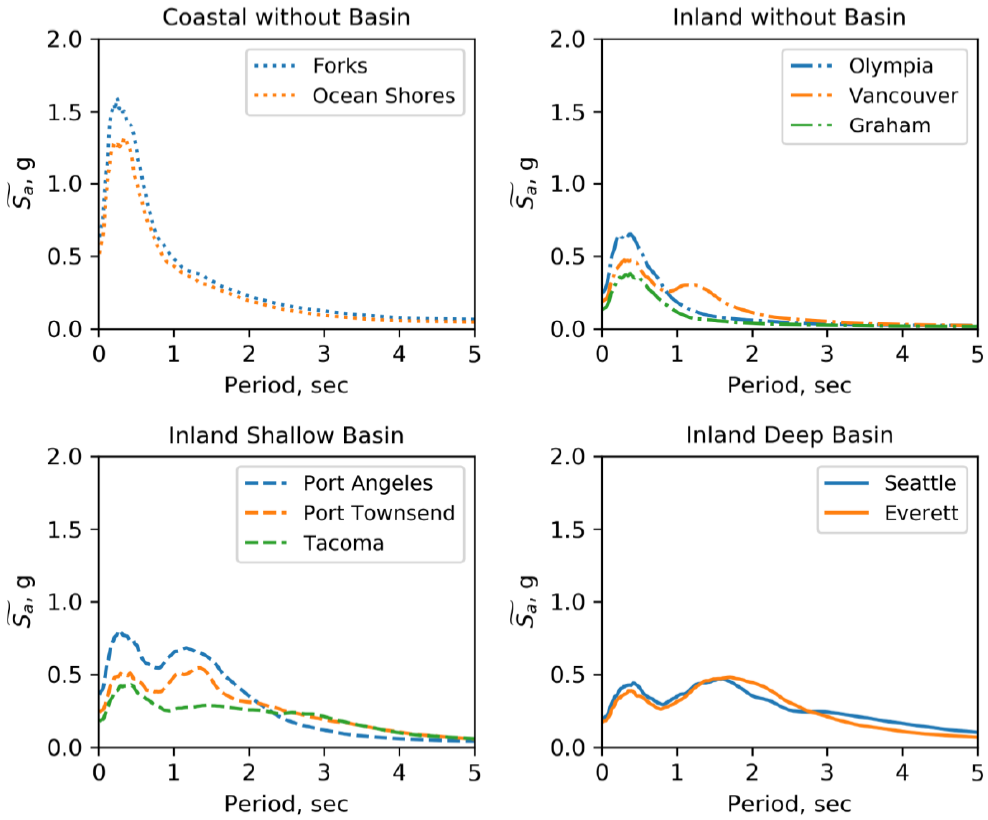

Figure 2.2: Response spectra from baseline simulated M9 ground motions, categorized by location category (de Zamacona 2019)

2.4 SOIL-ADJUSTED GROUND MOTIONS

The M9 baseline ground motions described above were developed for a site with a soil profile with a V_{s30} value of 1,968 ft/s (= 600 m/s, corresponding to NEHRP site class C). This section describes the modifications made to the baseline ground motions to account for the effects of various soil types.

Figure 2.3 shows the geographic distribution of site classes in King County, Wash. Large portions of major highways are located in areas that are categorized as site class C,

D, E, and F. To account for effects of local site conditions, alex grant from the United States Geological Survey (USGS) generated soil-adjusted M9 ground motions (de Zamacona 2019, Marafi et al. 2021).

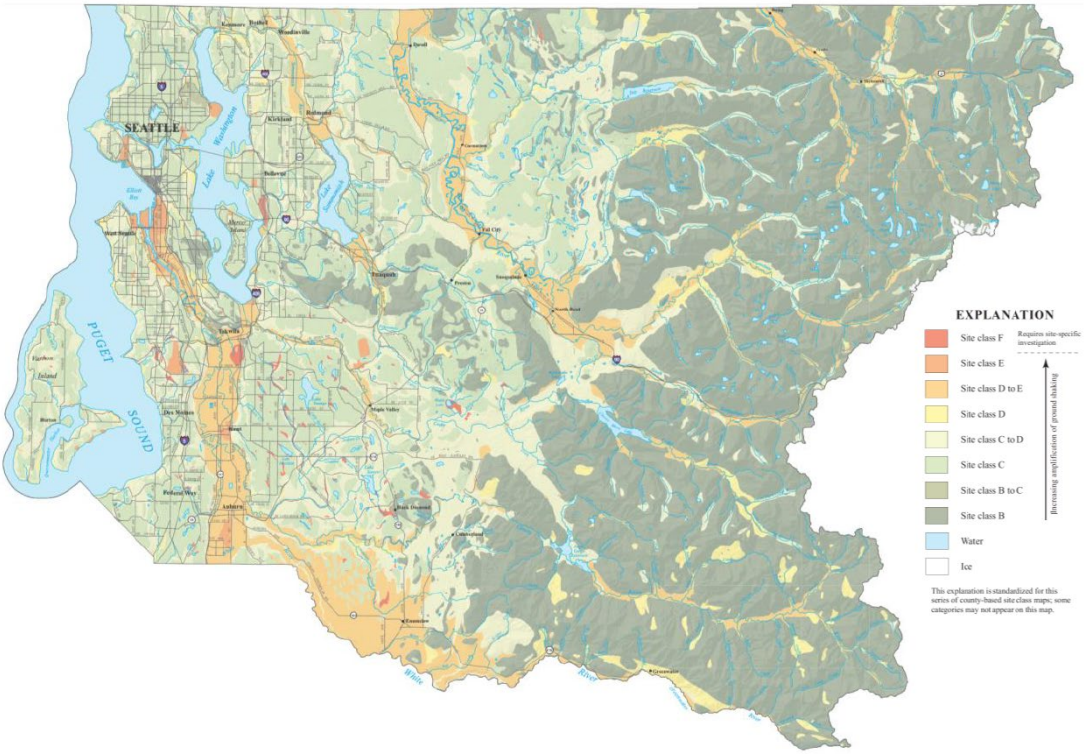

Figure 2.3: Site class map of King County, Washington (Palmer et al. 2007)

The solid-adjusted M9 ground motions were generated by using equivalent site response analysis and the soil profiles provided by Pacific Northwest shear-wave velocity profiles by Adhi et al. (2017). The soil profiles shallower than 32.8 feet and deeper than 3,281 feet were removed because of insufficient data. Figure 2.4 shows the number of soil profiles within each site class before and after the reduction.

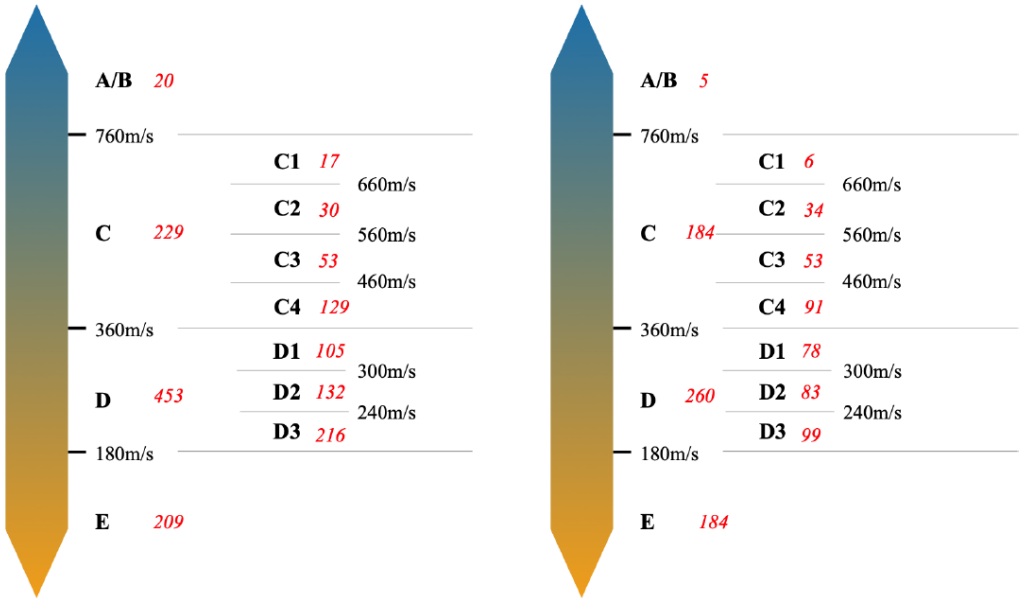

a) Full Set of Profiles b) Reduced Set of Profiles

Figure 2.4: Data available from Ahdi et al. for PNW velocity profiles (de Zamacona 2019)

Figure 2.5 illustrates the median spectral accelerations of the geometric mean of the two horizontal components for the 30 baseline and soil-adjusted M9 grounds for site subclasses C2, C4, D1 and D3. These site classes were chosen because their V_{s30} ranges are commonly found within Washington state. For each soil subclass, 30 soil profiles were randomly selected from the reduced set. Site class C2 had the closest value to the baseline spectral accelerations, which was expected, as site class C2 had values of V_{s30} that were closer to that used to develop baseline M9 ground motions. At longer periods, the effect of soil site class on site amplification was most apparent. The softest site class that was considered, D3, had the highest spectral acceleration at periods greater than 1.0 sec, followed by site class D1, C4, and C2. This phenomenon was due to the amplification of softer soils at longer periods. Notably, the site class D3 profiles deamplified the strong short period content of the ground motions for the coastal locations.

Motions for site classes C2, C4, D1, and D3 were selected for the parametric studies in Chapter 6 to investigate the effects of various site conditions on M9 ground motions. For computational expediency, ten soil profiles were randomly selected from the reduced set in Figure 2.4 for each site class to use in the analyses. As discussed later (Section 6.2),

each of the ten soil profiles in each of the four site classes were used with the 30 M9 earthquake realizations to create the ground motion sets used for analysis here.

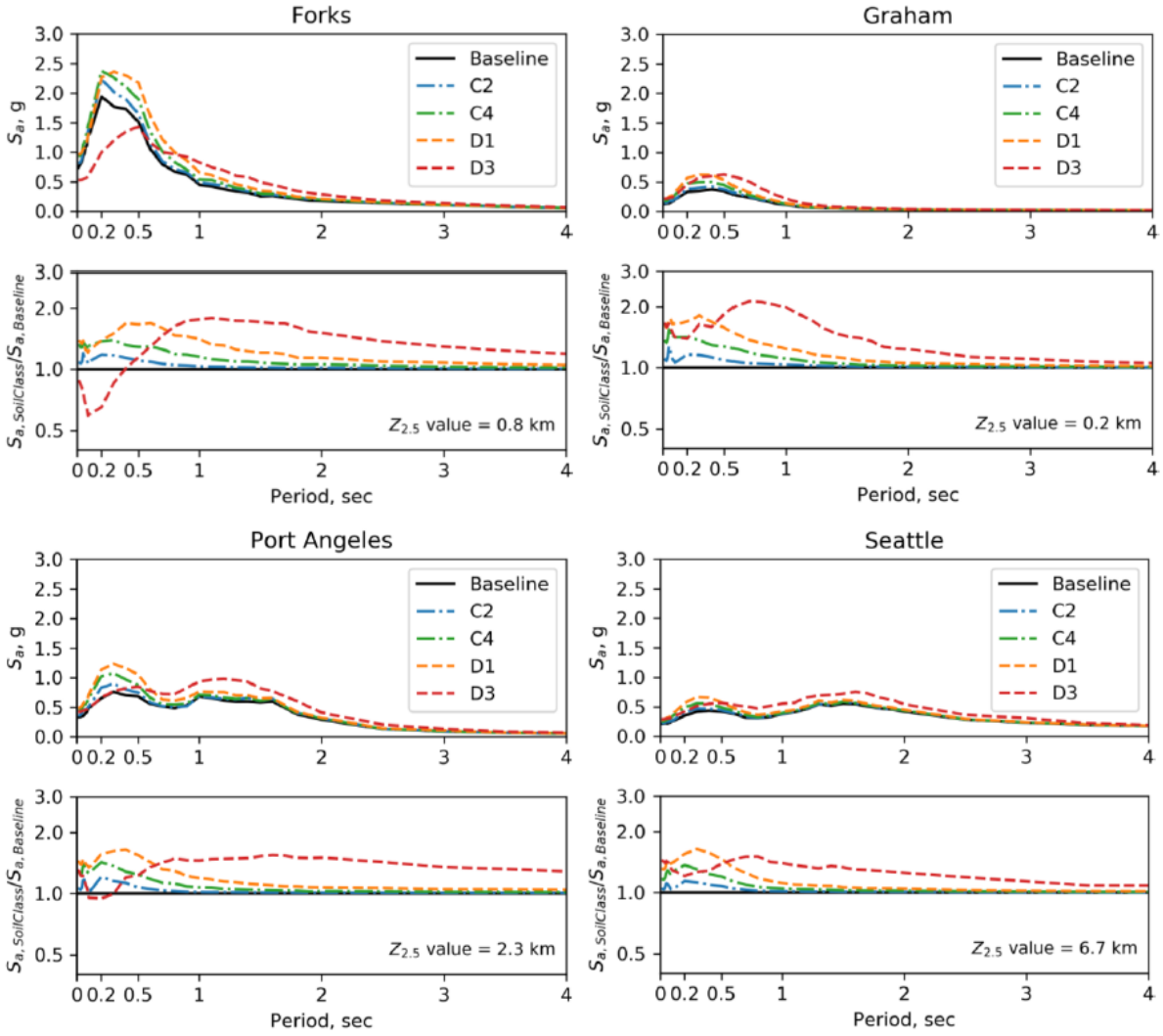

Figure 2.5: Median spectral accelerations for site-adjusted M9 ground motions and median spectral acceleration normalized by the baseline ground motion spectra (de Zamacona 2019)

2.5 EFFECTS OF M9 GROUND MOTIONS ON SDOF MODELS OF BRIDGES

To understand the impacts ofM9 earthquakes on bridges in Western Washington state, de Zamacona (2019) and Kortum et al. (2022) developed single-degree-of-freedom models in OpenSees. The strengths of de Zamacona's (2019) oscillators were set to be 50 percent higher than the 2019 WSDOT code-minimum values for bridges at each of the ten locations. Her results showed that structures with a short period were severely damaged in

cities along the fault, whereas those with a longer period were severely damaged in cities located on sedimentary basins.

Kortum et al. (2022) further improved the single-degree-of-freedom oscillator by considering the actual properties of the bridges (based on bridge plans), rather than based on past or current design specifications. Kortum et al. also included more detailed model parameters and covered a wider range of oscillator periods, locations, and soil types to better understand the impact of M9 earthquakes on bridges. Each bridge was simplified to a single-degree-of-freedom with a mass and nonlinear spring. The effect of cycling was considered with the Modified Ibarra-Medina Krawinkler (IMK) Deterioration Model with Peak-Oriented Hysteretic Response material in OpenSees.

The Kortum et al. study showed that spectral acceleration amplification effects were observed in cities that lie on top of sedimentary basins at higher periods (> 1 sec) and that strong shaking along the coast could be potentially damaging to bridges. They also found that the strength of most bridges in the database greatly exceeded the strength required by the design code, and as a result, they performed better than predicted by de Zamacona.

The following sections describe in detail the modeling methodologies of the SDOF model from Kortum et al. (2022).

2.5.1 Development of SDOF Bridge Models

The identification of key properties of the SDOF model was based on the bridge database compiled by WSDOT and University of Washington engineers. Kortum et al. (2022) utilized the compiled database and conducted regression analyses to approximate the relationship between bridge strength and bridge period for the lifeline bridges. The stiffnesses were calculated on the basis of the recommendations of Elwood and Eberhard (2009); the masses were estimated by extrapolating from detailed calculations for typical bridges; and the strengths were estimated by moment-curvature analysis with the column properties provided by the database. Figure 2.6 shows the relationship between normalized lateral strengths (with respect to bridge weight) and periods of the old (pre-1976) and new (1976-2018) bridges.

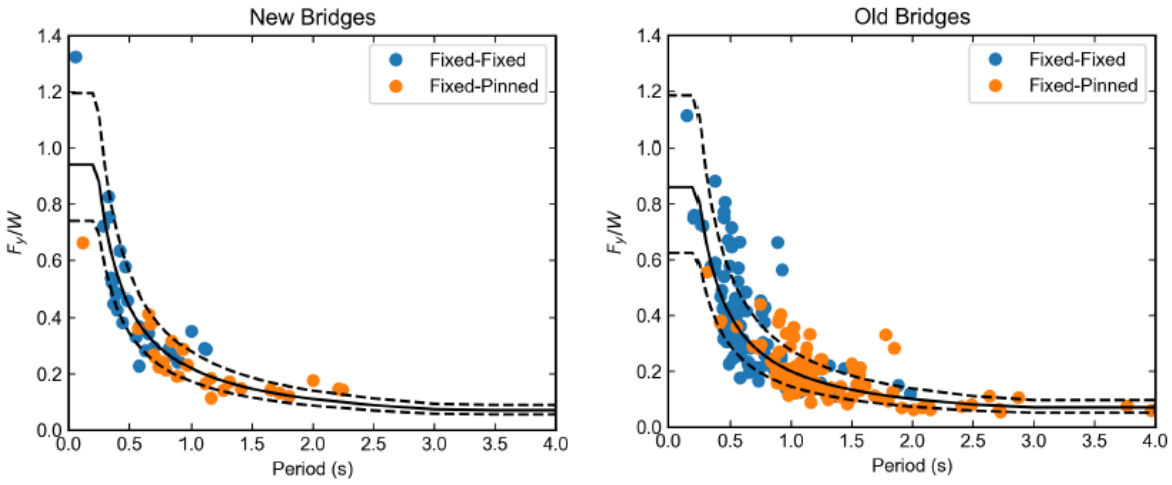

Figure 2.6: Normalized base shear strength for new and old bridges (Kortum et al. 2022)

The SDOF model used the Modified Ibarra-Medina-Krawinkler (IMK) Deterioration Model with Peak-Oriented Hysteretic Response material in OpenSees to consider the deterioration of bridge columns. The IMK model required several input parameters to define the backbone curve (Figure 2.7).

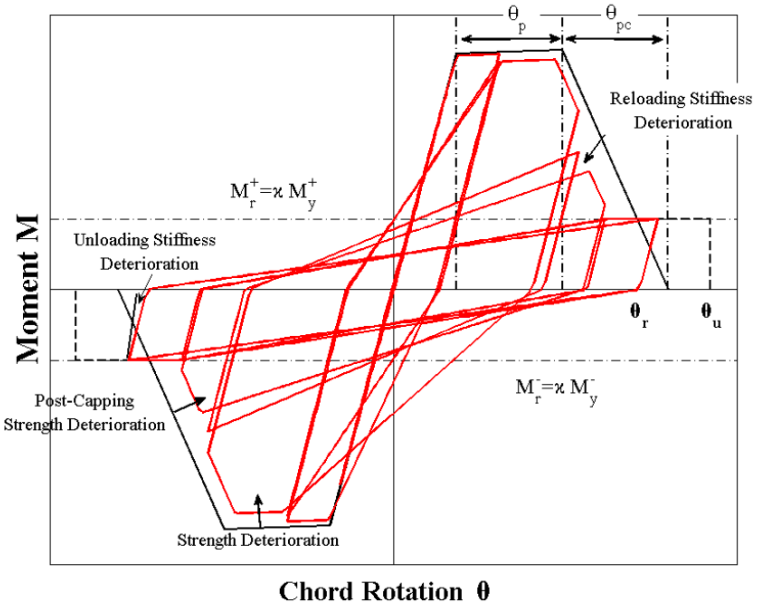

Figure 2.7: IMK model behavior (Lignos and Krawinkler 2012)

To model the behavior of the bridge columns, the response of the IMK model was calibrated to match the cyclic force-displacement response of selected reinforced concrete circular columns from the UW-PEER Structural Performance Database (UW-PEER 2020). In particular, two of the input parameters, λ and θ_p, of the IMK model were used for the calibration against the transverse reinforcement ratio. A series of calibration results for the cyclic loading tests are shown in Figure 2.8.

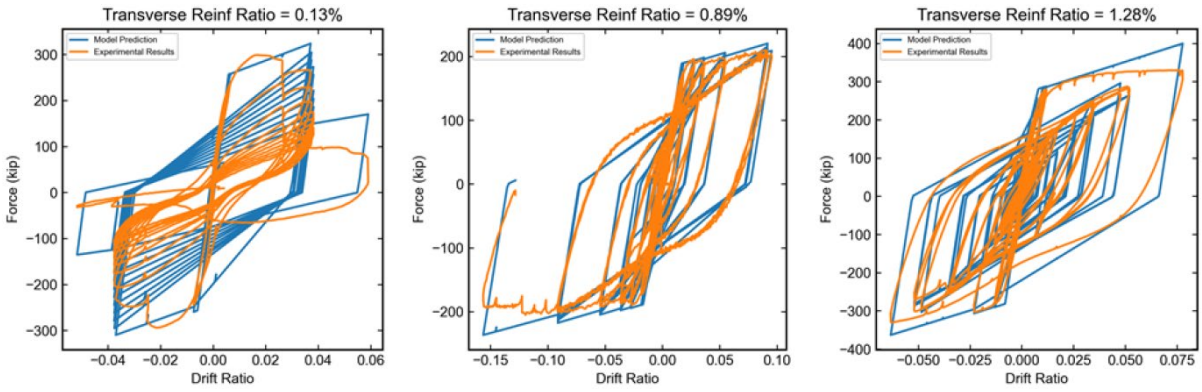

Figure 2.8: Fully calibrated IMK results for a lightly reinforced column (left), moderately reinforced column (center), and heavily reinforced column (right) (Kortum et al. 2022)

2.5.2 Effects of M9 Ground Motions on SDOF Bridge Model

Ground motions for ten cities (Table 2.1), 30 scenarios, four site classes, and 30 soil profiles for each site class were considered to study the effects of M9 earthquakes on highway bridges in Washington. The Kortum et al. (2022) study found that the response of the model varied among the different cities and site classes.

Figure 2.9 shows the median ductility demands of older bridges for different site classes in various cities. The bridges tended to have a higher response in coastal cities that were closer to the fault line at lower periods (< 0.5 sec). For various site classes, the response of the model had greater ductility demands at sites that had softer soil (site class D3) at higher periods (around or greater than 1.0 sec).

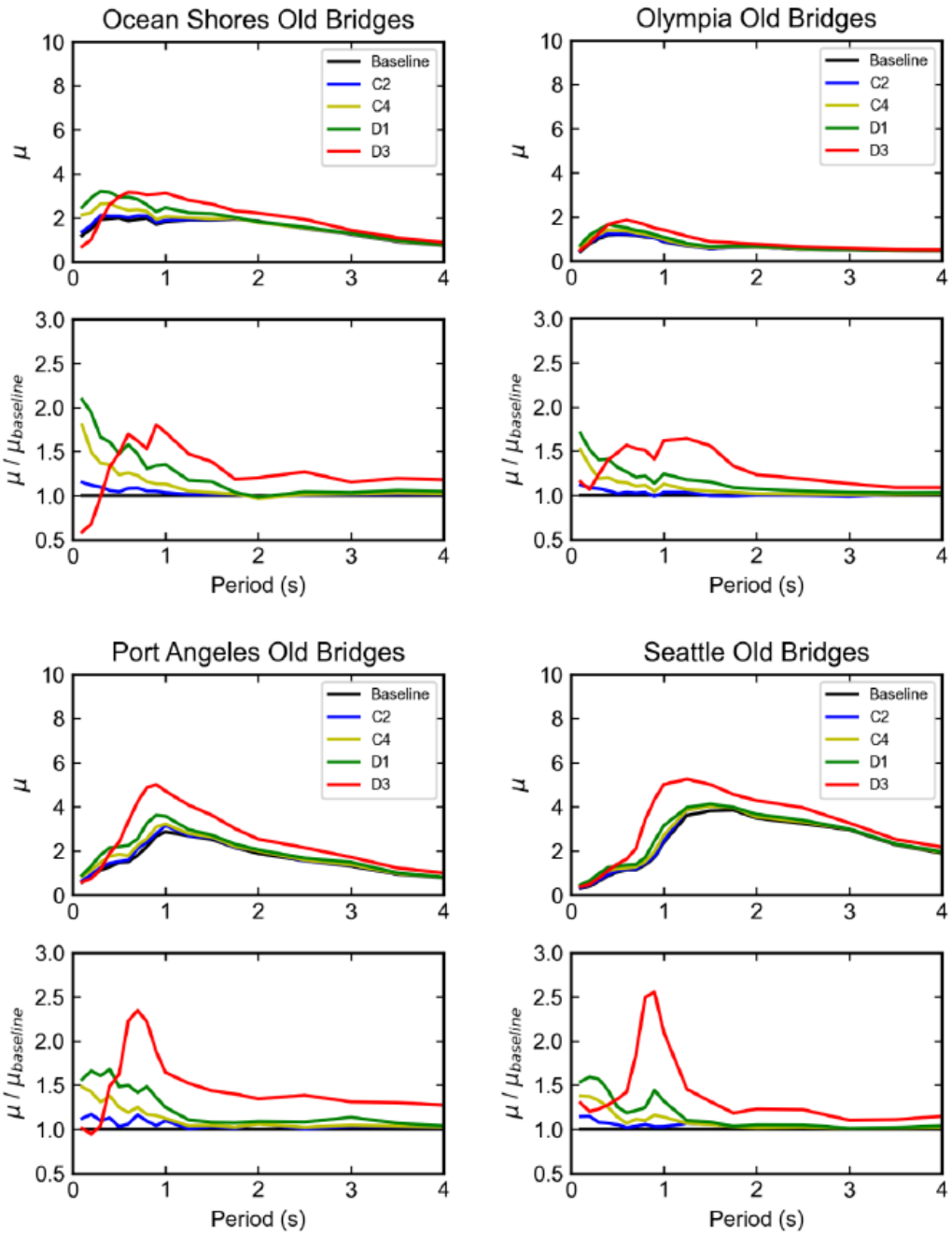

Figure 2.9: Median displacement ductility demands and median displacement ductility demands normalized by baseline values for various soil types (Kortum et al. 2022)

CHAPTER 3 PROPERTIES OF TYPICAL WSDOT BRIDGES

This chapter provides statistics of key properties of bridges that are documented within a database compiled by Washington State Department of Transportation (WSDOT) and University of Washington engineers. The structural properties for these bridges were extracted from the bridge plans.

The database provides properties of 609 structures along major highways in the Puget Sound region (Figure 3.1, Table 3.1), including 582 highway bridges. The database documents key properties of bridges along the following routes:

- I-5 from Fort Lewis to Arlington
- I-405 from Tukwila to Lynnwood
- I-90 from Bellevue to the Snoqualmie Summit, and
- SR 512 and SR 167 from Lakewood to Tukwila.

The database does not include some major highways in the Puget Sound region, including state routes 2, 99, and 526. Some of the properties of bridges along other highways will likely vary from those documented in this database because bridge properties tend to vary according to the era of construction, width of highway (e.g., two lanes versus six lanes), and the obstacle the bridge spans (e.g., overpass versus river crossing).

- Section 3.1 provides properties of the highway bridges within the bridge database.
- Section 3.2 discusses the properties of the 416 multi-span bridges with columns.
- The original WSDOT database did not include information about the bridge abutments, so the research team identified the abutment properties for 94 bridges with multiple spans by reviewing bridge plans that WSDOT made available. These abutment properties are discussed in Section 3.3.
- The properties of these bridges were used to identify typical characteristics of bridges within the database. A set of typical bridge properties (Section 3.4) was then selected on the basis of these data and used to develop a reference model for a typical bridge (Chapter 4).

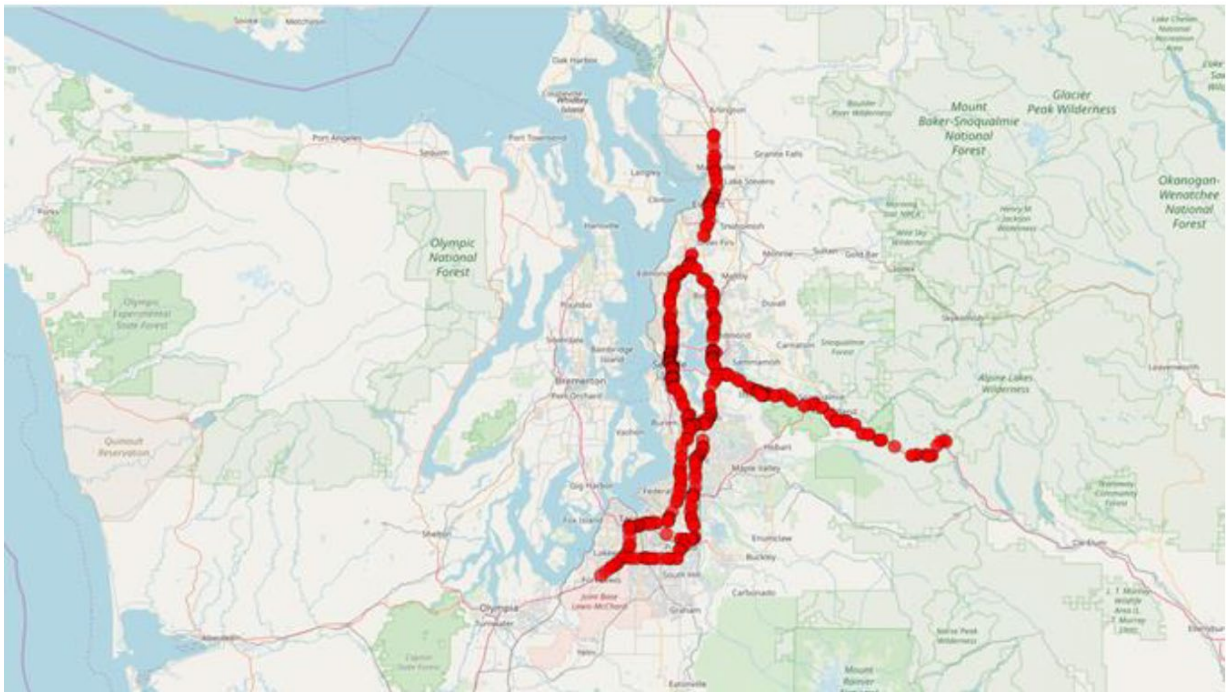

Figure 3.1: Locations of bridges documented in the bridge database (Kortum et al. 2022)

Table 3.1: Key characteristics of bridge populations in the database

Characteristic	Total	pre-1976	1976-2018
Number of Structures	609	448	156
Number of Highway Bridges	582	435	147
Number of Single-Span Bridges	74	34	40
Number of Bridges with Multiple Spans	508	401	107
Number of Bridges Supported by Columns	416	318	98
Number of Bridges Supported by Circular Columns	318	274	44

3.1 PROPERTIES OF BRIDGES WITHIN BRIDGE DATABASE

The bridge database documents key properties for 609 structures, including 582 highway bridges, four culverts, ten tunnels, two detention vaults, and one pedestrian bridge. This report discusses only the properties of the highway bridges. Among other properties, the database documents the year of construction, superstructure type, column dimensions, column transverse and longitudinal reinforcement, and number of spans of each bridge.

The year of construction of the highway bridges in the database ranges from 1930 to 2018. Earthquake design practice in Washington state changed significantly near 1976 following the 1971 San Fernando earthquake, so the statistics presented in this chapter are usually provided for two categories: pre-1976 (435 bridges, 74.7 percent) and 1976-2018 (147 bridges, 25.2 percent). Table 3.1 provides statistics for the bridge inventory for these two year-of-construction categories.

3.1.1 Year of Construction

As shown in Figure 3.2, nearly 70 percent of the bridges (398, 68.4 percent) were built between 1960 and 1975. Only 37 (6.4 percent) of these bridges were built before 1960, 83 (14.3 percent) were built between 1976 and 2000, and 64 (11 percent) bridges were built after 2000.

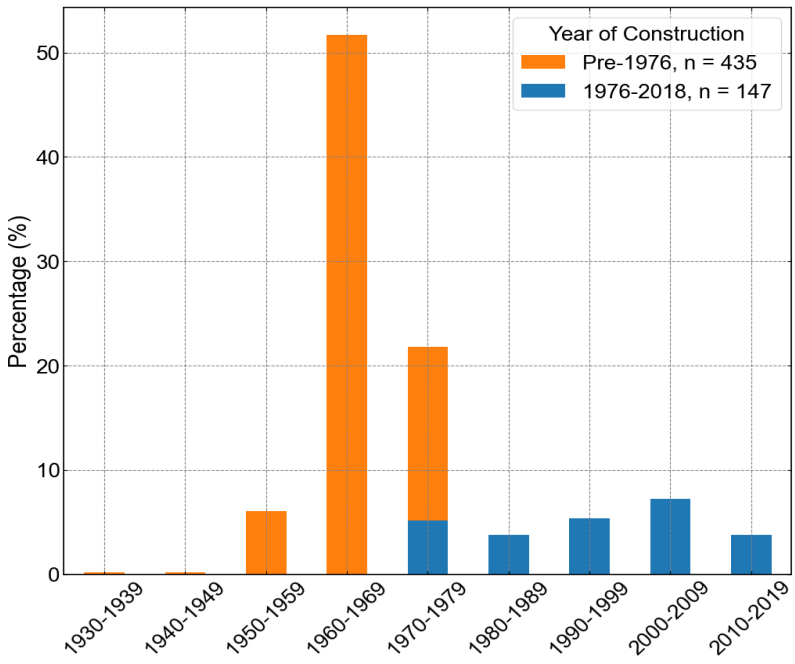

Figure 3.2: Year of construction

3.1.2 Superstructure Type

The database provided information for 582 bridges, but 18 of those had two superstructure types, so for the purpose of compiling superstructure statistics, each superstructure was counted independently, resulting in 600 (582+18) incidences of superstructure type.

As shown in Figure 3.3, nearly 90 percent (538, 89.7 percent) of the superstructures were constructed of concrete, with the most common types being prestressed concrete girders (294, 49.0 percent), concrete boxes (154, 25.7 percent), concrete slabs (86, 14.3 percent), and concrete tee beams (21, 3.5 percent). An additional 39 (6.5 percent) bridges had steel superstructures, most of which were steel girders (35). The percentage of prestressed concrete girder bridges, concrete slab bridges, and concrete tee-beam bridges did not differ greatly between the pre-1976 and 1976-2018 age ranges. However, in comparison with superstructures in the older age range, bridges built more recently had approximately half the percentage of concrete box superstructures and approximately three times the percentage of steel superstructures.

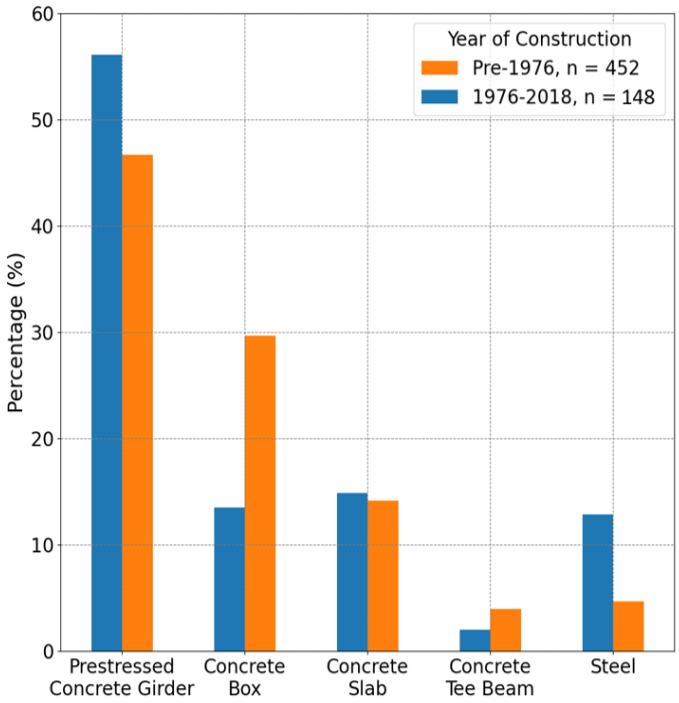

Figure 3.3: Superstructure types

3.1.3 Substructure Type at Intermediate Supports

The substructure at the intermediate supports was not documented clearly for one of the 582 bridges, so the substructure statistics are reported for 581 bridges. A total of 74 bridges had a single span and therefore did not have any intermediate supports. Out of 508 bridges with multiple spans, 416 (71.6 percent) of the intermediate supports contained at least one column, with 102 (17.6 percent) bridges supported by single-column bents and 314 (54.0 percent) supported by multiple-column bents (Figure 3.4). A smaller number of other bridges were supported by pier walls (44, 7.6 percent) or piles (42, 7.2 percent), or had unknown support types (6, 1.0 percent). The statistics did not vary greatly between the two age ranges.

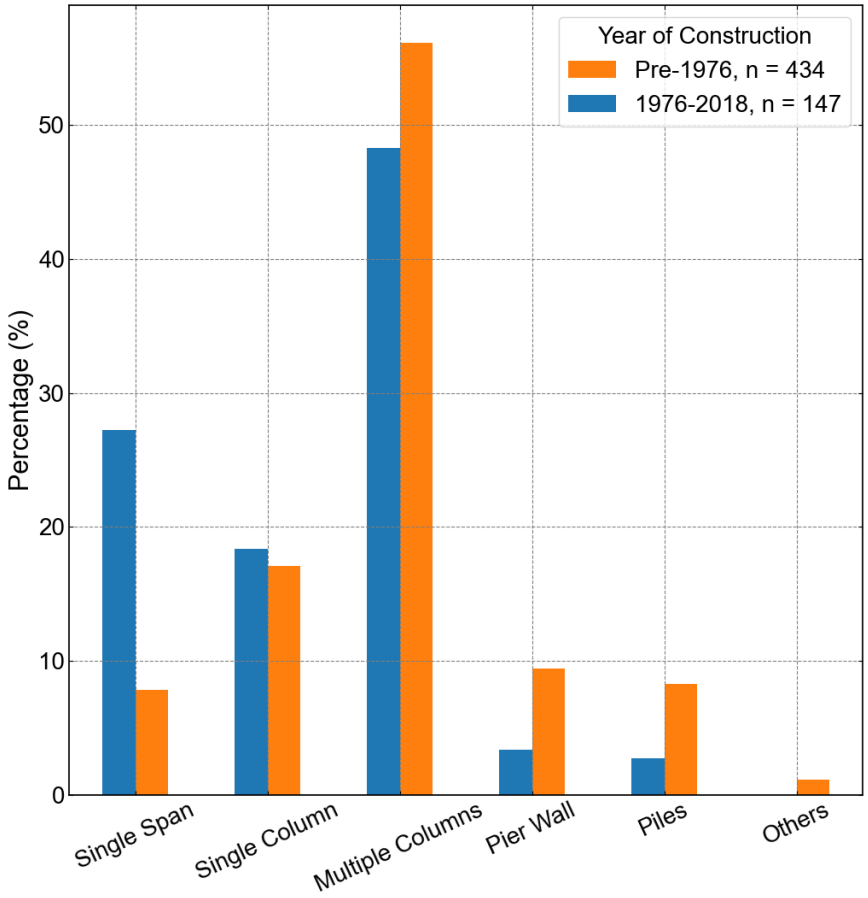

Figure 3.4: Substructure types

3.1.4 Span Continuity

Span continuity refers to the end conditions of the spans within the superstructure. A continuous superstructure can resist negative moments at the end of each span, whereas in simply supported structures, the end moment is equal to zero and there is usually a joint at each intermediate support. The presence of a joint limits the forces that are transmitted along the length of the superstructure to the abutments. The span continuity was documented for 504 of the 508 multi-span bridges, and one bridge had a portion that was continuous and a portion that was simply supported, so statistics were computed for 505 incidences of span continuity.

Most multi-span bridges (80.2 percent, 405 out of 505) had continuous spans. As can be seen in Figure 3.5, the percentage of multi-span bridges with continuous spans was

higher for newer bridges (97.2 percent, 103 bridges) than for older bridges (75 percent, 302 bridges).

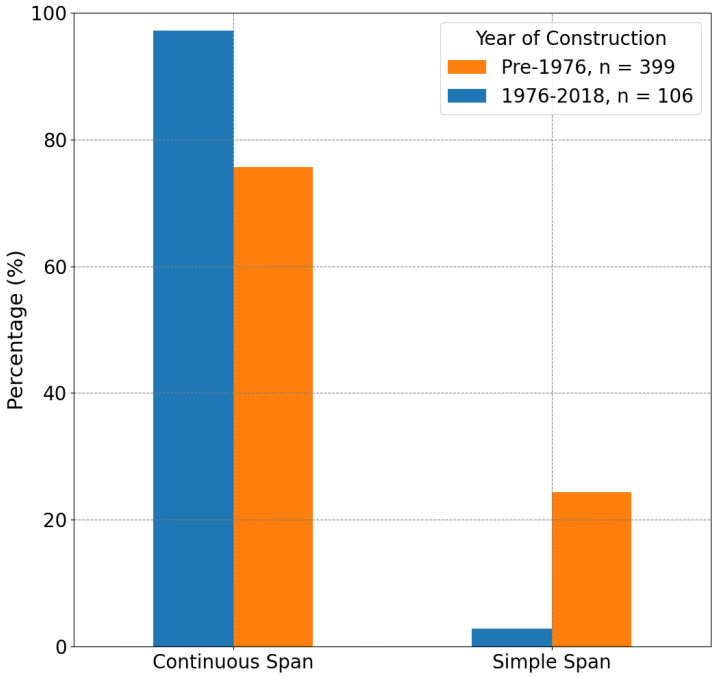

Figure 3.5: Span continuity for multiple-span bridges

3.2 PROPERTIES OF BRIDGES WITH COLUMNS

Early WSDOT retrofit efforts focused on preventing unseating of bridges at abutments and intermediate hinges. In bridges that did not unseat, most earthquake damage has been observed in the columns. Of the 582 highway bridges, 74 (12.7 percent) had only one span, and 508 (87.3 percent) had multiple spans. The vast majority (416 bridges, 81.9 percent) of these multiple-span bridges were supported by columns. The 416 bridges with columns are discussed in this section. Of the 416 bridges with columns, 318 (76.4 percent) of them were built before 1976, whereas 98 (23.6 percent) were built from 1976-2018 (Figure 3.6).

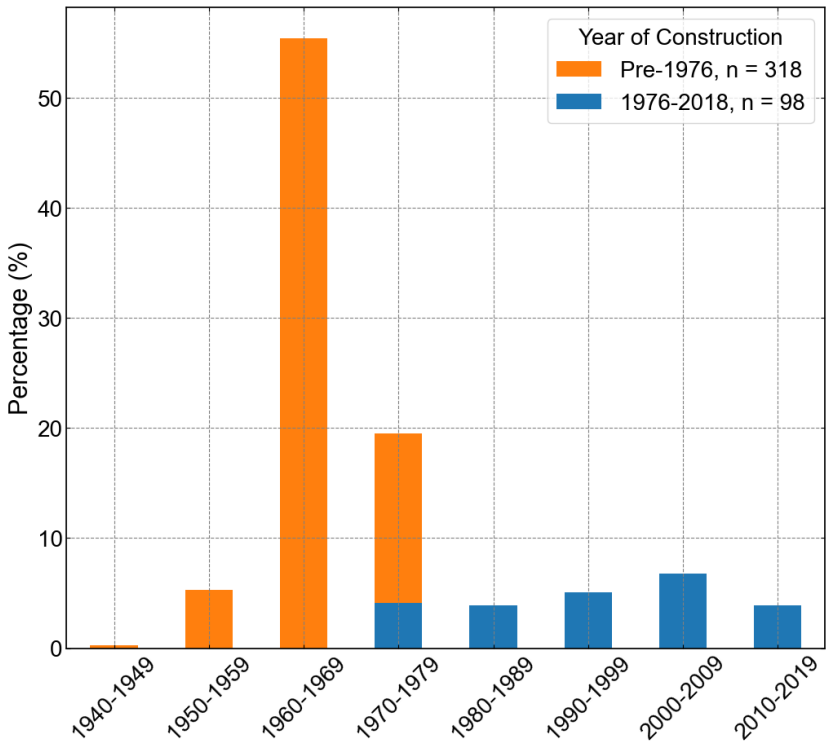

Figure 3.6: Years of construction (bridges with columns)

3.2.1 Number of Spans

The numbers of spans for bridges with columns at intermediate supports are shown in Figure 3.7. Although the bridges had a wide variety of span numbers, ranging from two to 48, most of them fell between two and four for bridges in both eras. Of these 416 bridges, 316 (76 percent) had span numbers within this range. The main difference between the age categories was that the percentage of bridges built with two spans was larger for the 1976-2018 age range than for the earlier age range. This difference might be attributable to the increased number of spans that is possible for newer bridges built of stronger materials.

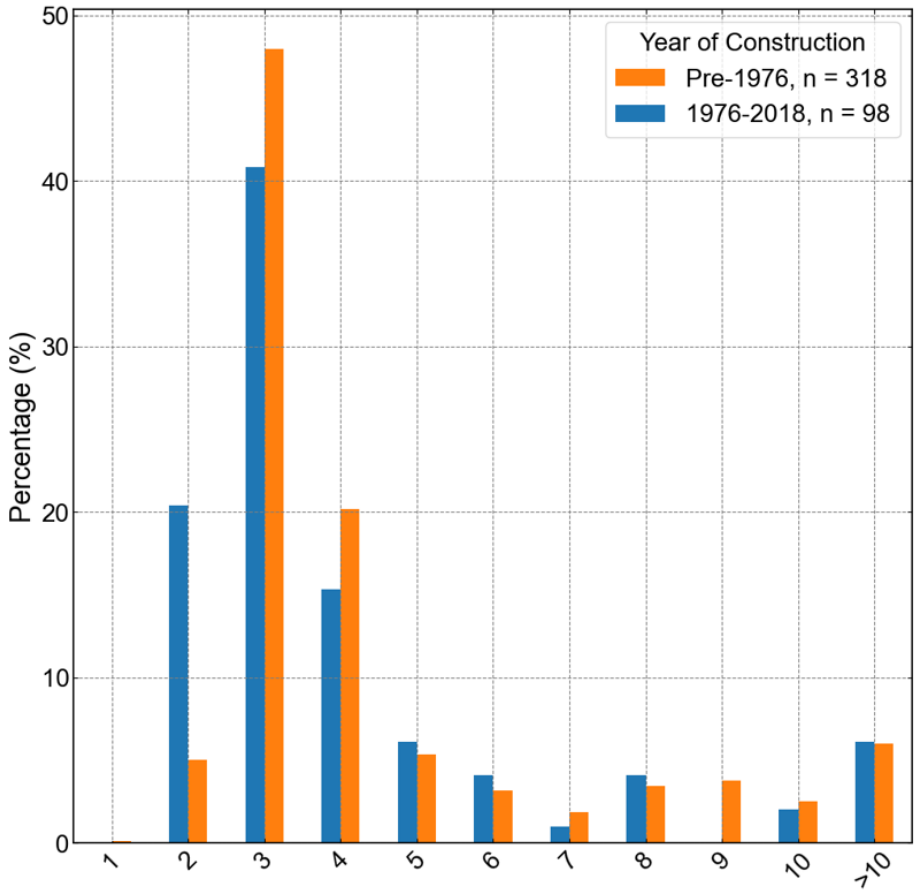

Figure 3.7: Number of spans

3.2.2 Foundation Type at Intermediate Piers

Foundation types are usually related to the bearing capacity of the soils and to the space available to construct the foundations. In most cases, spread footings are used at sites with stronger/stiffer soils, whereas shafts and piles tend to be used in structures located on softer soils. Additionally, some bridges have a combination of foundation types, which is commonly found in bridges whose decks were expanded later than the rest of the bridge.

As shown in Figure 3.8, for both newer and older bridges, spread footings were the most common foundation types (43 percent for older and 37 percent for newer bridges). Drilled shafts were more common in newer bridges than older ones. The larger percentage of "combination" foundations in older bridges is likely attributable to the fact the older bridges were more likely to have been widened.

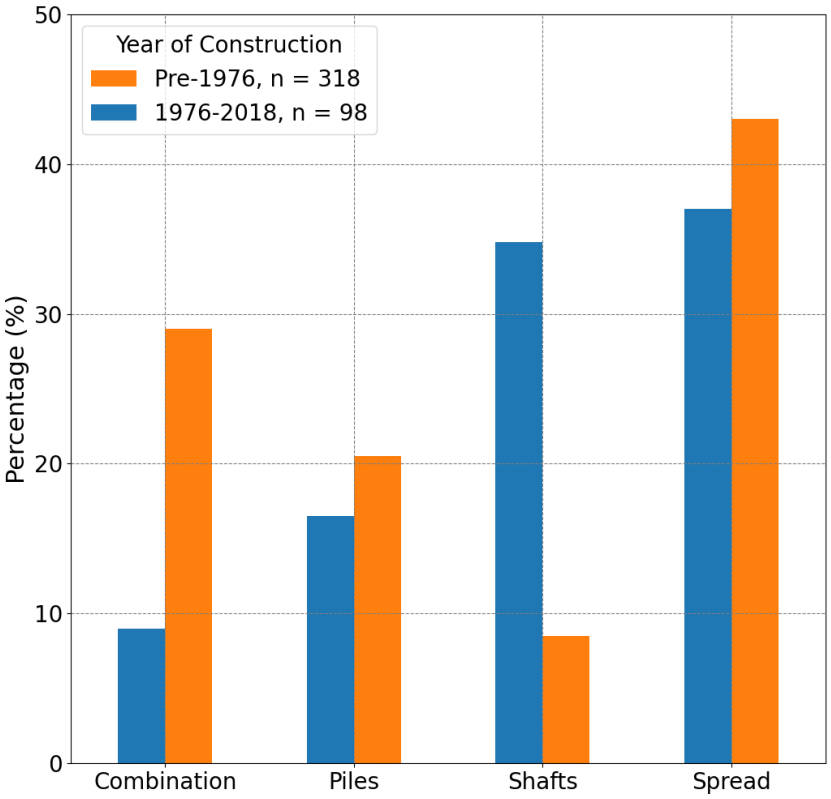

Figure 3.8: Intermediate bent foundation types

3.2.3 Column Shape

The cross-section shapes of the columns were divided into three groups: circular, rectangular, and others (e.g., octagonal or oval) (Figure 3.9). Circular column cross-sections were most common (348, 76 percent), particularly for bridges built before 1976 (274 bridges, 86.2 percent). The percentage of circular columns was lower for more recently constructed bridges (44 bridges, 44.9 percent). For newer bridges, circular and rectangular columns had about the same percentage (~40 percent).

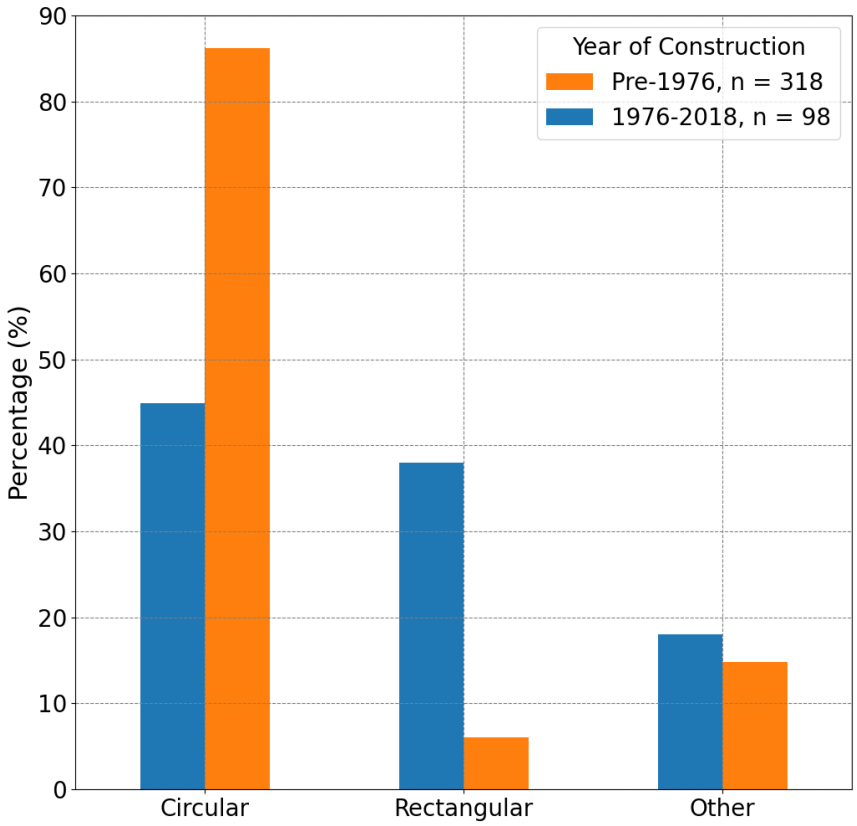

Figure 3.9: Column cross-section shapes

3.2.4 Diameters of Circular Columns

For bridges that had intermediate supports consisting of circular columns and with available diameter data (n=318), almost all of them had cross-section diameters ranging from 30 to 60 inches for older columns (306, 93 percent) and newer columns (77, 88 percent). Approximately half of the columns had a diameter of between 31 (space) and 40 inches (Figure 3.10).

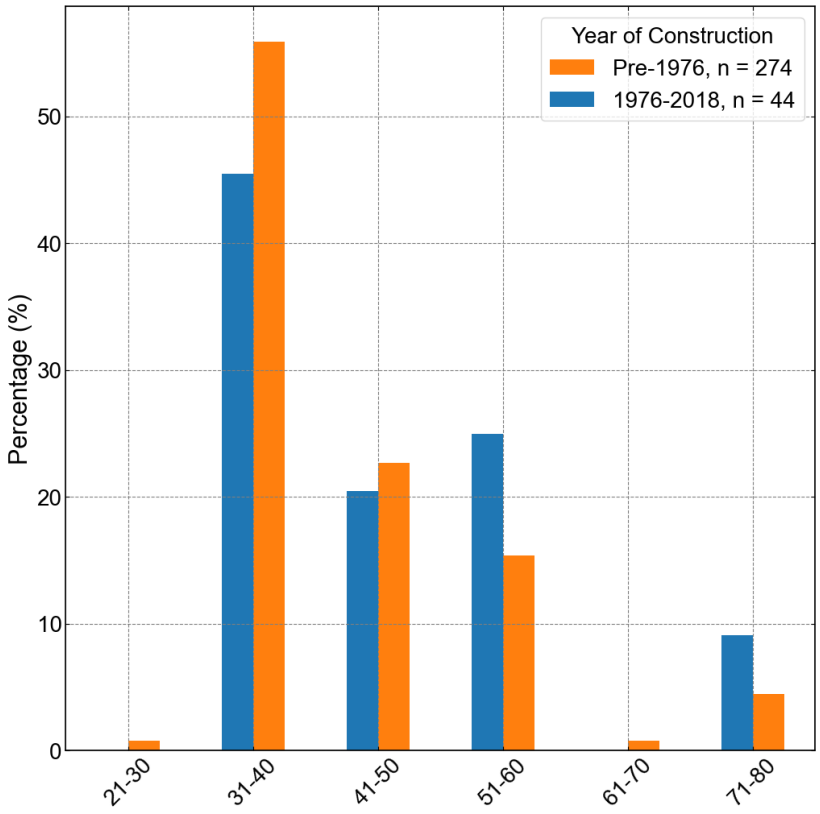

Figure 3.10: Distribution of diameters for bridges with circular columns

3.2.5 Number of Columns at Intermediate Piers

The distribution of the number of columns at each pier is shown in Figure 3.11. If this number was equal to 1, then the bridge was categorized as a single-column bridge, and it was categorized as a multiple-column bridge when this number was greater than or equal to 2. As shown in Figure 3.11, regardless of the age of the bridge, the number of columns supporting the intermediate bent was mostly within one to five, with nearly 83.2 percent (254) of the older bridges in this range and almost all (85) of the newer bridges.

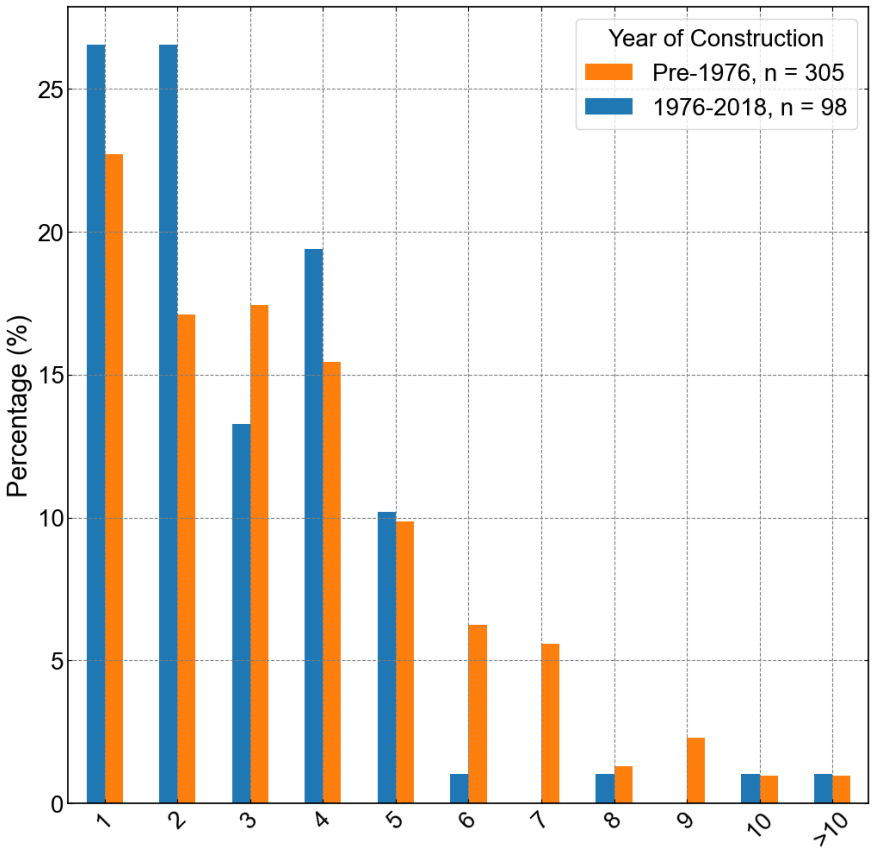

Figure 3.11: Number of columns at each pier

3.2.6 Effective Column Height

The bridge database provided column heights for the shortest and tallest columns on each bridge. Column heights vary within each bridge, so to capture the overall column behavior with an idealized bridge that has columns of the same length, Kortum et al. (2022) proposed the calculation of an effective column height. A bridge with all columns of the effective column height provides approximately the same stiffness as a bridge with its original varying heights.

Effective column height information is summarized in Figure 3.12, with most of them ranging between 11 and 30 feet for bridges in both eras. Furthermore, effective column heights between 21 and 25 feet were particularly common (89 (27.9 percent) for older bridges and 29 (30.5 percent) for newer bridges).

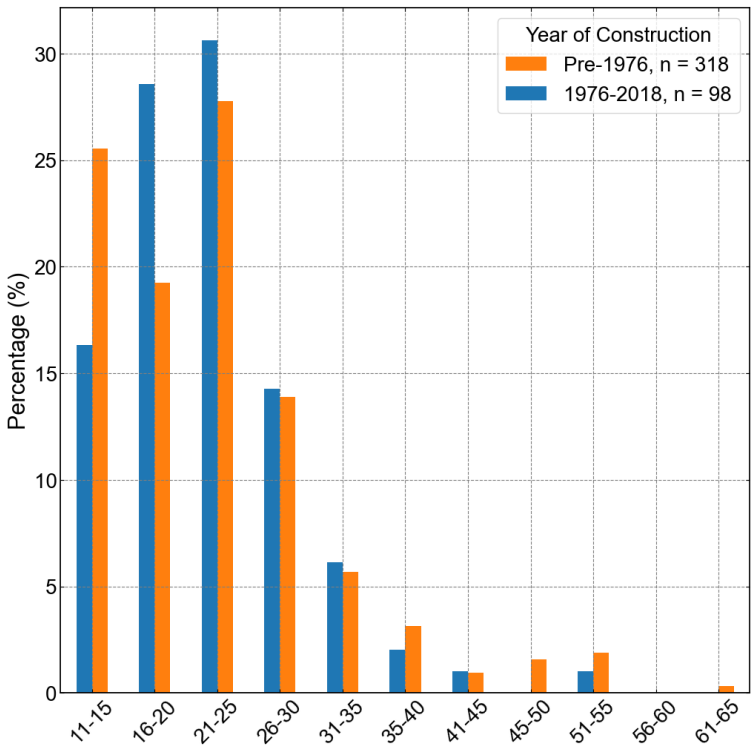

Figure 3.12: Effective column heights

3.2.7 Longitudinal Reinforcement Ratio

The longitudinal reinforcement ratio strongly affects the flexural strength of bridge columns. The longitudinal reinforcement ratio is calculated as the total area of longitudinal reinforcement, normalized by the gross-section area of the column. Although the reinforcement ratio varied greatly, the majority (70 percent) of bridge column reinforcement ratios for both new and old bridges fell between 1 percent and 2.5 percent. Furthermore, the longitudinal reinforcement ratio did not appear to differ considerably between old and new bridge columns (Figure 3.13).

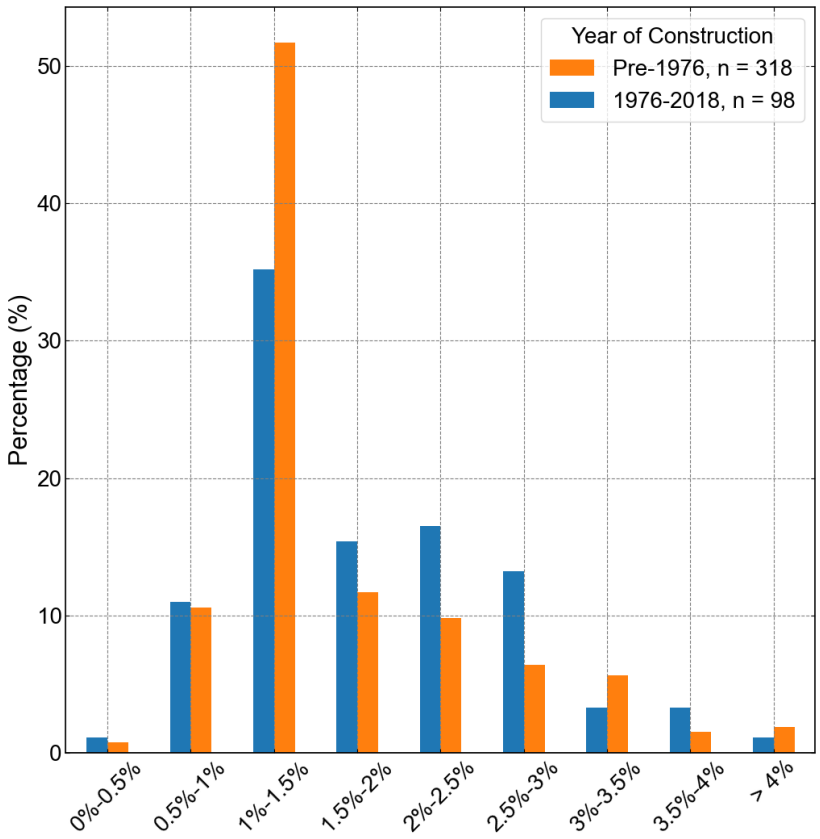

Figure 3.13: Longitudinal reinforcement ratio of the shortest columns

3.2.8 Transverse Reinforcement Ratio

Transverse reinforcement enhances the ductility of reinforced concrete columns by providing confinement to the concrete within the spiral and by providing lateral support to the longitudinal reinforcement. WSDOT provided reinforcement ratios for the shortest and tallest columns of bridges.

The transverse reinforcement ratio is computed as the ratio of the volume of transverse bars to the volume of the confined concrete core, with the confined core extending to the centerline of the transverse reinforcement. In comparison to the longitudinal reinforcement ratio, the difference of transverse reinforcement ratio between older and newer bridges was far more significant (Figure 3.14). Most older bridge columns (~85 percent) had a reinforcement ratio of between 0 and 0.5 percent, while for newer bridge columns, nearly 50 percent of them had a ratio of greater than 1.0 percent. This phenomenon reflects the change in design code that happened in the mid-1970s.

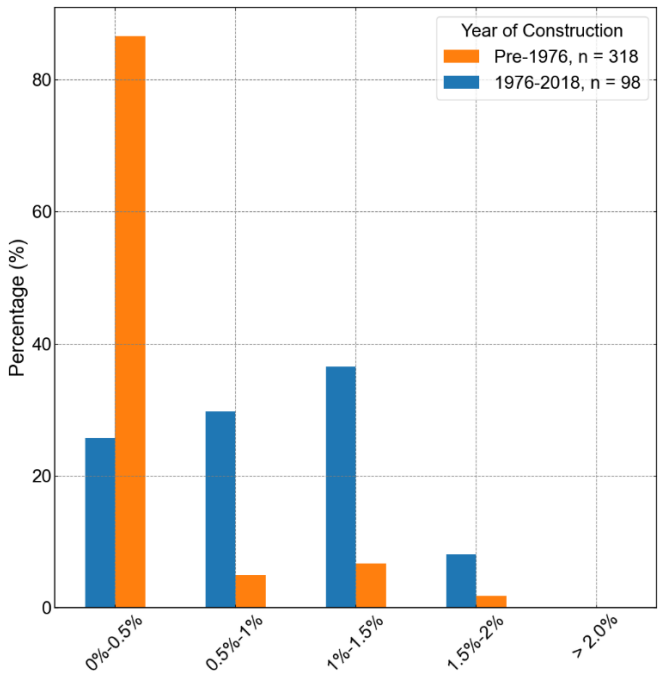

Figure 3.14: Transverse reinforcement ratio of the tallest columns

3.2.9 Column Retrofit

The determination of whether a bridge had experienced a column retrofit (Figure 3.15) was based on the information about column jacket existence provided by WSDOT. Bridges with column jackets were classified as retrofitted, whereas those without were classified as non-retrofitted. The reported data showed that more than half of the bridges (~64 percent) built before 1976 were non-retrofitted, and as expected, almost none of the newer bridges (1 percent) had been retrofitted.

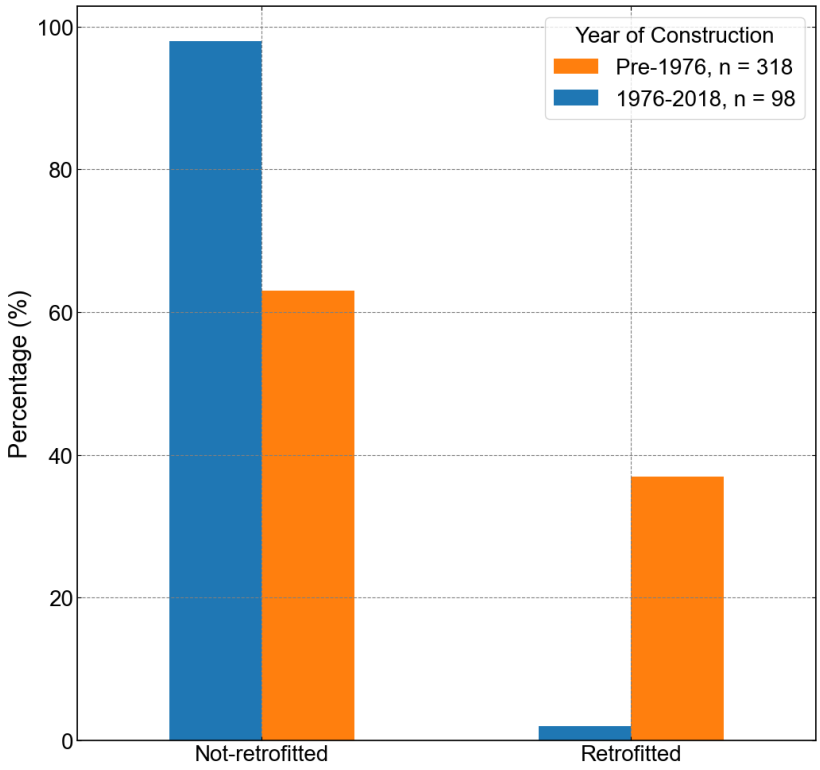

Figure 3.15: Percentage of retrofitted column-supported bridges

3.3 ABUTMENT PROPERTIES

Key features of the abutments were identified from the construction documents for 94 of the 416 bridges with columns in the bridge inventory. The list of selected bridges is provided in Appendix A. For these bridges, the researchers compiled information about the abutment type, abutment foundation type, and shear key existence.

Of these 94 bridges, 75 (79.8 percent) had been built before 1976 and 19 (20.2 percent) had been built between 1976 and 2018. In this report, this subset of 94 bridges is referred to as the "Abutment Database." The bridges were selected such that the distribution of year-of-construction and intermediate pier type would be similar for the 94 selected bridges and the bridges supported on columns. Figure 3.16 and Figure 3.17 show that these two bridge populations had roughly similar years of construction and intermediate support foundation type distribution.

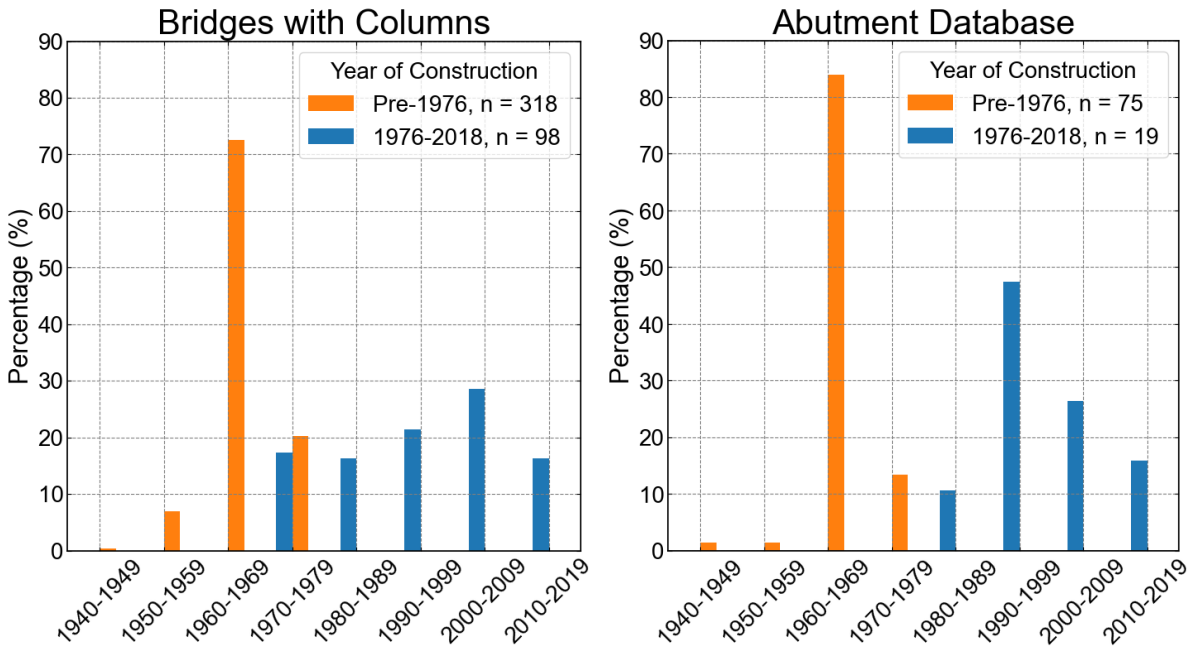

Figure 3.16: Years of construction for Bridges with Columns (left) and Abutment Database (right)

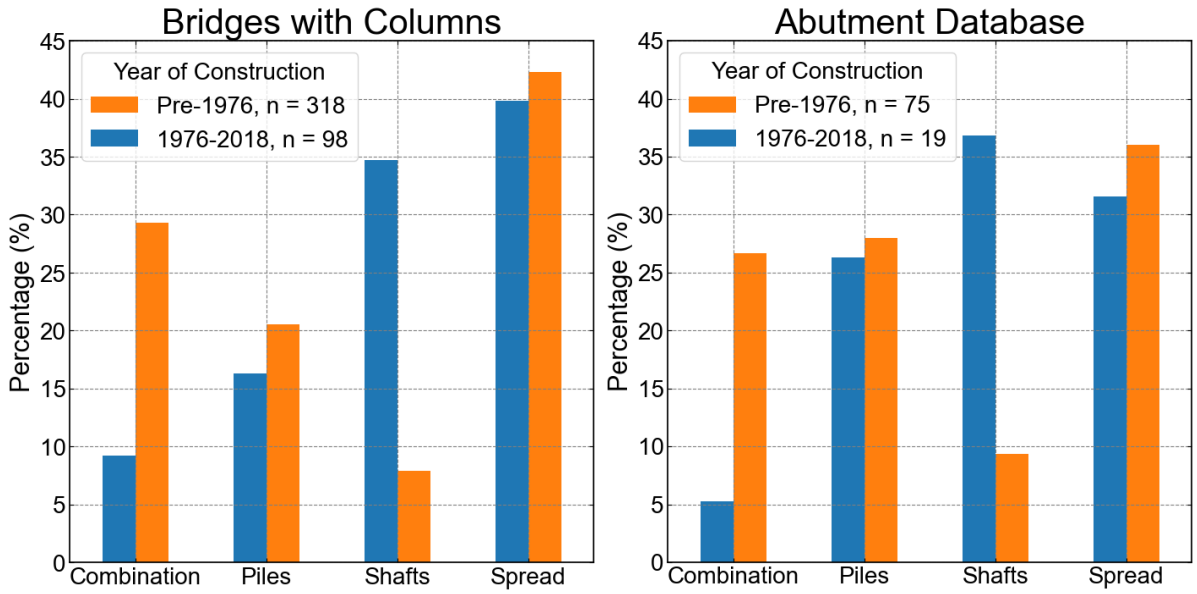

Figure 3.17: Intermediate foundation types for Bridges with Columns (left) and Abutment Database (right)

3.3.1 Abutment Type

Abutment type is one of the most important features that determines the resistance provided by the abutment. Detailed information about the various abutment types can be found in the bridge modeling chapter (Section 4.4). L-type abutments were the most common type of abutment in general, and their percentages were similar for both the older (41/75 bridges, 54.6 percent) and newer bridges (9/19 bridges, 47.3 percent) (Figure 3.18). Semi-integral abutments were the second most commonly used, but they were more frequent in newer bridges. Semi-integral abutments were used in 16 percent (12) of the older bridges and 47.3 percent (nine) of newer bridges (same percentage as for L-type abutments).

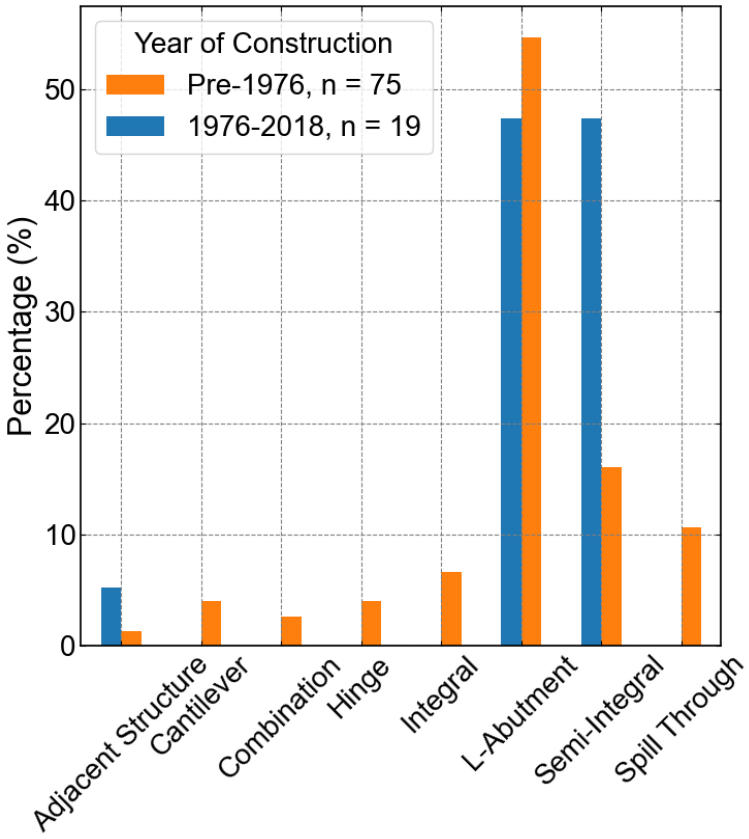

Figure 3.18: Abutment types

3.3.2 Abutment Foundation Type

The abutment foundation plays an important role in providing lateral-load resistance for an abutment. Figure 3.19 shows that, for both older and newer bridges, spread

footings and piles were the most common abutment foundation types, followed by shafts and combinations of spread and piles. The main difference between the two populations was that new bridges tended to have piles less frequently and shafts more frequently than older bridges.

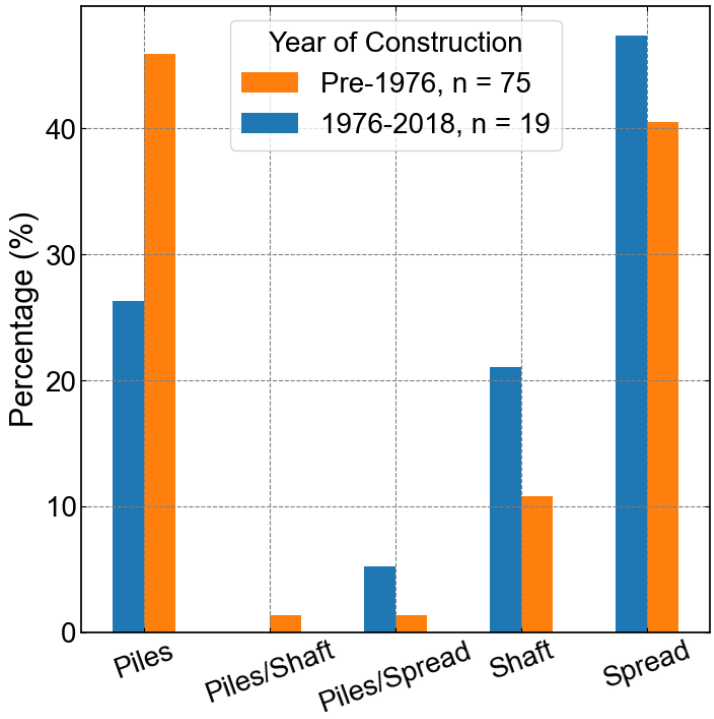

Figure 3.19: Foundation types

3.3.3 Presence of Shear Key

Shear keys provide a significant amount of resistance in the transverse direction, preventing restraint to relative displacement between the superstructure deck and the abutments. As a result, the existence of shear keys is expected to strongly affect the performance of bridges during earthquakes.

The shear-key configurations for three bridges constructed before 1976 were unclear in the drawings, so these bridges were excluded from the statistical calculations. Almost all the bridges had shear keys, including 90.3 percent (65/72 bridges) of the older bridges and 100 percent (19 bridges) of newer bridges. As shown in Figure 3.20, the bridges with box girders tended to have external shear keys, whereas the bridges with prestressed girders or beams tended to have internal shear keys.

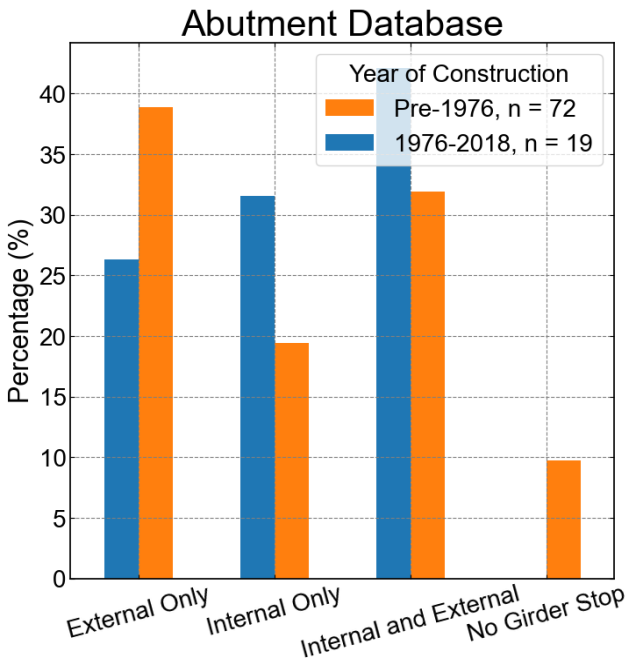

(a) Abutment Database bridges

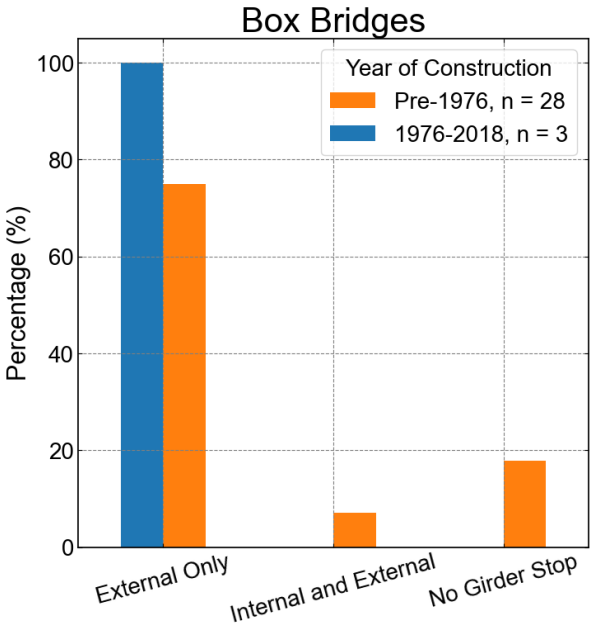

(b) Abutment Database bridges with box girders

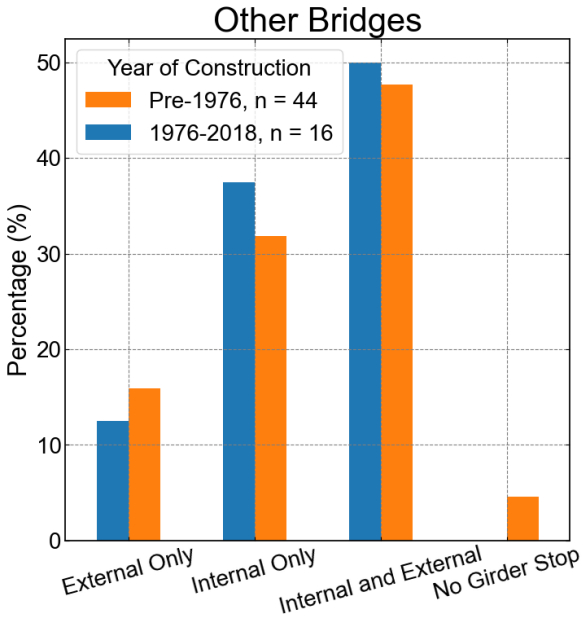

(c) Abutment Database bridges with other types of girders

Figure 3.20: Presence of shear key for (a) all Abutment Database bridges, (b) Abutment Database bridges with box girders, and (c) Abutment Database bridges with other girder types for which that property was characterized.

3.4 REPRESENTATIVE BRIDGE

Based on the statistics of the bridge properties presented in previous sections, Table 3.2 provides a summary of the desired characteristics to represent bridges constructed before 1976 and from 1976 to 2018. The table also provides references to the relevant report section.

One bridge (405/23E-N) built in 1997 approximately matched the identified features and was selected as a reference bridge. This selected bridge was built upon for the reference bridge that was used for the model development and the parametric study discussed in subsequent chapters. The key features of the reference bridge features are also listed in Table 3.2. Additionally, as mentioned in section 3.2.8, because transverse reinforcement ratio reflects the code change that occurred around 1976, it is not surprising that the transverse reinforcement ratio appears to be the only major parameter listed in Table 3.2 that is different between older and newer bridges. As a result, the transverse reinforcement ratio sufficiently reflects the age of the bridges.

Table 3.2: Properties of target and selected bridges

	Pre-1976 (target)	**1976-2018 (target)**	**Report Section**	**Identified Bridge 405/23E-N**	**Reference Bridge**
Column cross-section	Circular	Circular, Rectangular	3.2.3	Circular	Circular
Column diameter (in.)	30~40	30~60	3.2.4	36	36
Effective column height (ft)	10~25	10~25	3.2.6	21.3	21.3
Tallest column long reinf. ratio (%)	1.0~1.5	1.0~1.5	3.2.8	1.3	1.3
Shortest column long reinf. ratio (%)	1.0~1.5	1.0~1.5	3.2.7	1.3	1.3

	Pre-1976 (target)	1976-2018 (target)	Report Section	Identified Bridge 405/23E-N	Reference Bridge
Tallest column trans reinf. ratio (%)	0.0~0.5	1.0~1.5	3.2.8	0.7	0.5
Shortest column trans reinf. ratio (%)	0.0~0.5	1.0~1.5	3.2.7	0.7	0.5
Span numbers	3, 4	2, 3	3.2.1	3	3
Span continuity	Continuous	Continuous	3.1.4	Continuous	Continuous
Superstructure type	Prestressed -girder	Prestressed -girder	3.1.2	Prestressed -girder	Prestressed -girder
Intermediate pier type	Multiple columns	Multiple columns	3.1.3	Multiple columns	Multiple columns
Intermediate pier column numbers	1~5	1~5	3.2.5	3	3
Retrofit	Not-retrofitted	Not-retrofitted	3.2.9	Not-retrofitted	Not-retrofitted
Intermediate foundation type	Spread	Spread	3.2.2	Spread	Spread
Abutment type	L, semi-integral	L, semi-integral	3.3.1	Semi-integral	L
Abutment foundation type	Spread, Piles	Spread, Piles	3.3.2	Spread	Piles
Shear key existence	Yes	Yes	3.3.3	Yes	Yes

The geometry of the reference bridge is consistent with the bridge plans for the identified bridge 405/23E-N. The original bridge plans of bridge 405/23E-N can be found in Appendix B. Table 3.3 lists the important dimensions for the bridge superstructure, substructure, and abutment of the reference bridge.

Table 3.3: Dimensions of the reference bridge

Bridge Element	Expression	Value	Measurement
Superstructure Dimensions			
Span 1 length	L_{span1}	61	ft
Span 2 length	L_{span2}	110	ft
Span 3 length	L_{span3}	61	ft
Deck width	W_{deck}	37.4	ft
Deck depth	D_{deck}	5.75	ft
Deck length	L_{deck}	232	ft
Substructure Dimensions			
Cross-beam width	W_{beam}	5.33	ft
Cross-beam depth	D_{beam}	4	ft
Cross-beam length	L_{beam}	39.3	ft
Column spacing	S_{col}	16.2	ft
Column height	H_{col}	21.3	ft
Column diameter	d_{col}	36	in.
Column clear cover	d_{cover}	2	in.
Concrete core diameter	d_{core}	31.5	in.
Number of rebars	$\#_{rebar}$	13	
Column rebar diameter	d_{rebar}	1.128	in.
Column rebar area	A_{rebar}	1	in^2
Spiral confined reinforcement diameter	d_{spiral}	0.5	in.
Spiral confined	A_{spiral}	0.196	in2

Bridge Element	Expression	Value	Measurement
reinforcement diameter rebar area			
Spiral confined reinforcement spacing	$D_{spacing}$	3.5	in.
Abutment Dimensions			
Abutment width	W_{abut}	37.4	ft
Abutment back wall height	H_{abut}	7.5	ft

CHAPTER 4 MODEL DEVELOPMENT

This chapter documents the strategies that were implemented to model the reference reinforced concrete highway bridge. The model was used in a parametric study to evaluate the effects of geographic location and site class (Chapter 6) on bridge performance. Variations of this model were used to evaluate the effects of variations in abutment properties (Chapter 7) and properties of the columns at the intermediate bents (Chapter 8).

4.1 OVERVIEW OF BRIDGE MODEL

The properties of the reference bridge (Section 3.4) were the result of the identification of typical properties of bridges in the database. The modeling strategies were extended from, and built upon, the work of Ranf (2007), Ramanathan et al. (2012) and Mangalathu et al. (2017). The three-dimensional numerical model of the reference bridge was developed in OpenSeesPy (Zhu et al. 2018), a Python-compiled version of the finite element modeling package OpenSees, to simulate the dynamic response of the three-span, two-bent structure.

As shown in Figure 4.1, a typical highway reinforced concrete bridge has two primary components: the superstructure and substructure. The superstructure of a typical reinforced concrete bridge consists of traffic barriers/parapet, deck slab, and girders, and the substructure includes intermediate bent supports (cross-beams, columns, and foundation) and abutments (shear keys, bearings, backwalls, and foundations).

Figure 4.2 shows a schematic of the overall bridge model. The bridge deck was expected to remain elastic during earthquakes, so the bridge superstructure was modeled as a spine of multiple elastic beam-column elements in OpenSeesPy. Where the deck was connected to substructures (intermediate bents and abutments) a series of stiff elastic beam-column elements were used to extend from the centerline spine of the deck out to the full deck width (Section 4.2).

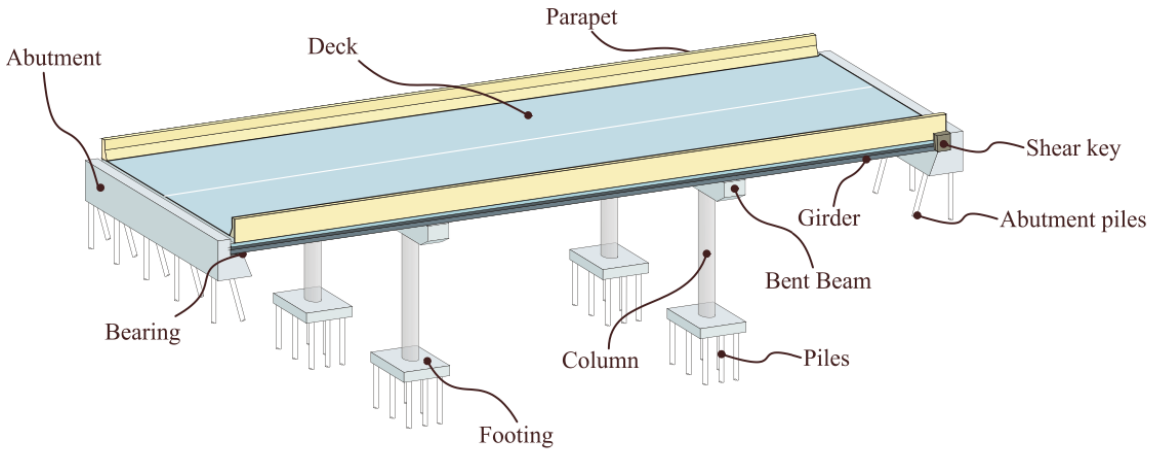

Figure 4.1: Typical highway concrete bridge components (Mangalathu 2017)

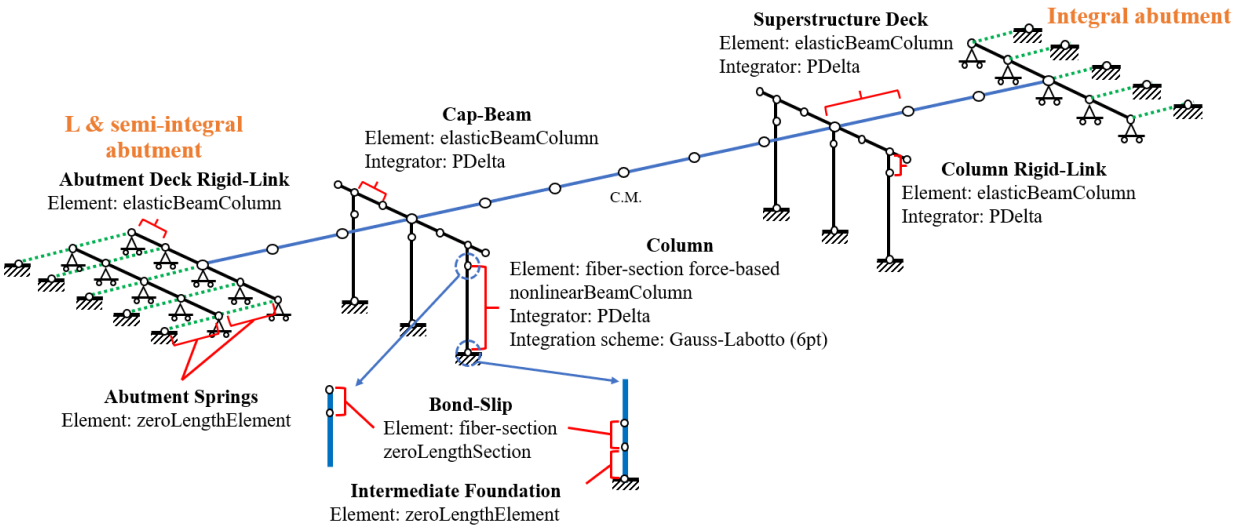

Figure 4.2: Overview of the bridge model

At the bents, rigid links were used to connect the extension of the deck to the top of columns. The column flexural deformation was modeled with nonlinear beam-column elements. Zero-length fiber sections were assigned to both ends of the columns to simulate the anchorage flexibility due to bond slip. Rotational and translational springs were attached to the base of columns to capture the behavior of the intermediate bent foundations (Section 4.3).

Three types of abutments—integral, semi-integral, and L (seat) abutments—were considered in this study. Zero-length elements capturing backfill soil and bi-directional forces (abutment piles/spread footings and friction surface) were connected in parallel and linked to the ends of deck elements for the integral abutment case. For semi-integral and L (seat) abutments, a zero-length element was connected in series with the backfill element to reflect pounding between the backfill soil and deck. Additionally, zero-length elements for the shear keys and bearing pads were also placed in parallel with the pounding elements (Section 4.4).

4.2 SUPERSTRUCTURE

The superstructure was modeled with elastic beam-column elements that remained elastic during earthquake shaking. The mass of the superstructure was uniformly assigned to the longitudinal deck nodes according to the tributary area of the deck and the length of the traffic barrier. Rigid and massless elastic beam-column elements were used for the transverse deck elements. The elastic modulus, E_c, and shear modulus, G_c, for the deck elements were computed with equations. 4-1 and 4-2, a concrete strength, f_c, equal to 6 ksi, and the concrete material Poisson's ratio, ν_c, equal to 0.2. The resulting E_c and G_c were 4,415.2 psi and 1,839.7 ksi, respectively.

$$E_c = 57000\sqrt{f_c}\ (psi) \qquad \textit{(Equation. 4-1)}$$

$$G_c = \frac{E_c}{2*(1+\nu_c)}\ (ksi) \qquad \textit{(Equation. 4-2)}$$

4.3 INTERMEDIATE BENTS

As illustrated in Figure 4.3, the intermediate bents included cross-beams, columns, and foundations. The intermediate bents were modeled with a combination of nonlinear beam-column elements and rigid links that captured the transfer of moments and forces among the bent members. The rotational and translational springs were placed at the base of the columns for foundations. Detailed properties for each component are described in the following sections.

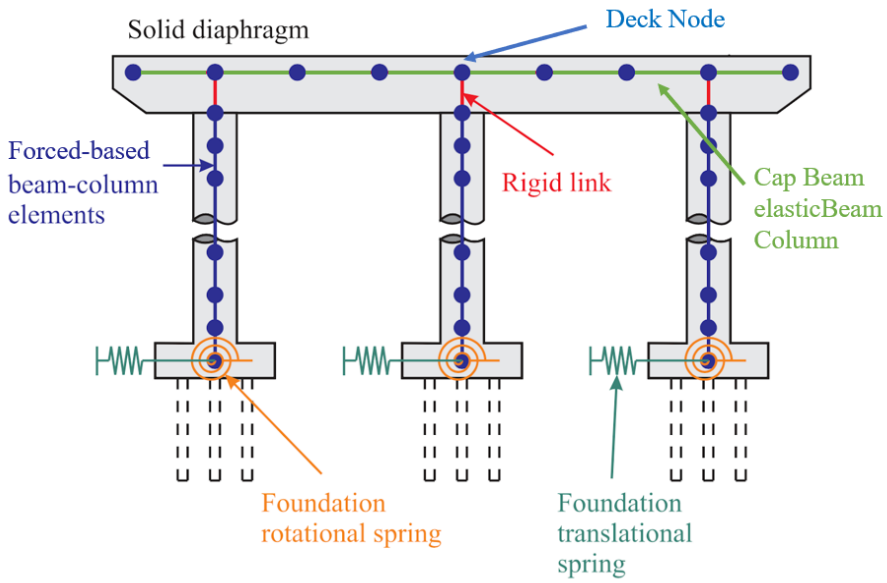

Figure 4.3: Finite element discretization of bents (Ramanathan et al. 2012)

4.3.1 Cross-Beams

Elastic beam-column elements with large elastic modulus and shear modulus (E_c and G_c in Section 4.2 times a factor of 100) were used to model cross-beams and were connected to the top of columns with rigid links. The resulting elastic modulus, E_{c-beam}, and shear modulus, G_{c-beam}, for cross-beams were 4,415,200 ksi and 1,839,700 ksi, making these elements essentially rigid.

4.3.2 Columns

As shown in Figure 4.4, the model for the circular columns was composed of four parts. The inelastic flexural response was modeled using distributed plasticity forced-based beam column elements (nonlinearBeamColumn), which captured the local strain response at the column-anchorage interfaces and required cross-sections to be defined at each of the integration points. The elastic shear and torsional behaviors were aggregated to the cross-sections using the Section Aggregator command in OpenSeesPy. Furthermore, the anchorage rotation was simulated with a zero-length element at both ends of the column. Each column component is discussed in the following sections.

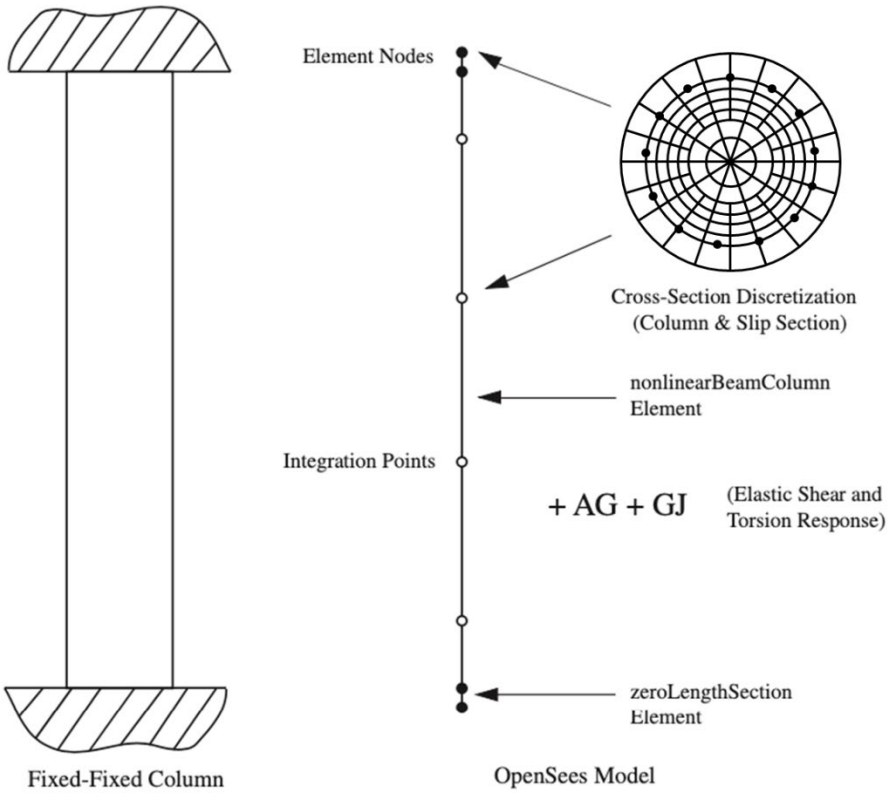

Figure 4.4: Components of the numerical column model (Ranf 2007)

4.3.2.1 Column Nonlinear Material Models

One of the advantages of the fiber-section defined nonlinear beam-column element is its ability to assign unique material properties over the cross-section. The Mander and Priestley (1988) model was used to define the monolithic stress-strain curve of the confined and unconfined concrete. The unconfined maximum concrete stress, f_c, was assumed to be 1.5 times the specified concrete strength, f'_c, and the corresponding unconfined strain was given as ϵ_c. For the reference bridge, f_c was assumed to be 6 ksi and ϵ_c was 0.002. Based on these values of f_c and ϵ_c, the confined concrete strength, f_{cc}, and its corresponding strain, ϵ_{cc}, were calculated with the following equations:

$$f_{cc} = f_c * [-1.254 + (2.254\sqrt{1 + \frac{7.94 f_{lp}}{f_c}}) - 2\frac{f_{lp}}{f_c}] \qquad \textit{(Equation. 4-3)}$$

$$\epsilon_{cc} = \epsilon_c \left(5\frac{f_{cc}}{f_c} - 4\right) \qquad \textit{(Equation. 4-4)}$$

The resulting values for f_{cc} and ϵ_{cc} were 7.11 ksi and 0.00385, where f_{lp} is the effective lateral confining pressure and can be given as:

$$f_{lp} = k_e * \frac{\rho_{hoop} * f_y}{2} \quad \text{(Equation. 4-5)}$$

where ρ_{hoop} is the transverse reinforcement ratio, f_y is the yield strength of the transverse reinforcement, and k_e is the effective confinement coefficient. The effective confinement coefficient, k_e, is given as the ratio of effective confined concrete area and the area of concrete core. The transverse reinforcement ratio, ρ_{hoop}, is provided as a user input for the bridge model to reflect columns designed pre- and post-1976 (0.5 percent for old columns and 1.5 percent for new columns).

The ultimate confined concrete stress and strain was calculated as:

$$\epsilon_{cu} = \epsilon_u + \frac{1.4\rho_{hoop} * f_y * \epsilon_{su}}{f_{cc}} \quad \textit{(Equation. 4-6)}$$

$$f_{cu} = \frac{f_{cc} * x_{conf} * r_{conf}}{r_{conf} - 1 + x_{conf}^{\ r_{conf}}} \quad \textit{(Equation. 4-7)}$$

where ϵ_{su} is the ultimate strain of reinforcement equal to 0.12, and ϵ_u is the unconfined concrete ultimate strain equal to 0.004. In addition, r_{conf} and x_{conf} can be given as:

$$r_{conf} = \frac{E_c}{E_c - E_{secant}} \quad \textit{(Equation. 4-8)}$$

$$E_{secant} = \frac{f_{cc}}{\epsilon_{cc}} \quad \textit{(Equation. 4-9)}$$

$$x_{conf} = \frac{\epsilon_{cu}}{\epsilon_{cc}} \quad \textit{(Equation. 4-10)}$$

where E_{secant} denotes the concrete secant elastic modulus. The resulting values for f_{cu} and ϵ_{cu} are 4,855.6 psi and 0.0122, respectively.

Additionally, a linear model up to an assumed strength was used to model the tensile behavior of both the confined and unconfined concrete. The maximum tension stress and strain, f_t and ϵ_t, were the same for both the confined and unconfined concrete models and were calculated as:

$$f_t = 0.1 f_{cc} \quad \textit{(Equation. 4-11)}$$

$$\epsilon_t = \frac{f_t}{E_c} \qquad \textit{(Equation. 4-12)}$$

The resulting values for f_t and ϵ_t were 0.711 ksi and 0.000136, respectively. The residual stresses (at large deformations) were assumed to be 0.2 and 0.01 of f_t for confined and unconfined concrete, resulting in values of 0.142 ksi (f_{r-c}) and 0.00711 ksi (f_{r-uc}), respectively.

For both longitudinal and transverse reinforcement, the ultimate tensile strength, f_y (equal to 69.6 ksi), was assumed to be 1.16 of the specified steel strength to capture overstrength (Bournonville et al. 2004). The steel elastic modulus, E_s, was assumed to be 29,000 ksi, and the strain hardening ratio, b_{col}, of the reinforcement was assumed to be 1.5 percent.

Concrete04 and Steel02 material models in OpenSeesPy were used to represent the behavior of concrete and reinforcement over the column fiber-sections; the stress-strain curves for these materials are given in Figure 4.5 and Figure 4.6.

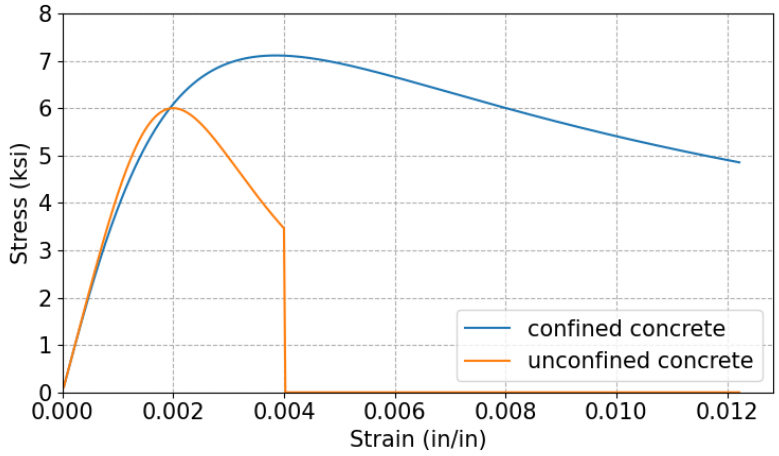

Figure 4.5: Concrete04 material model for the column fiber section

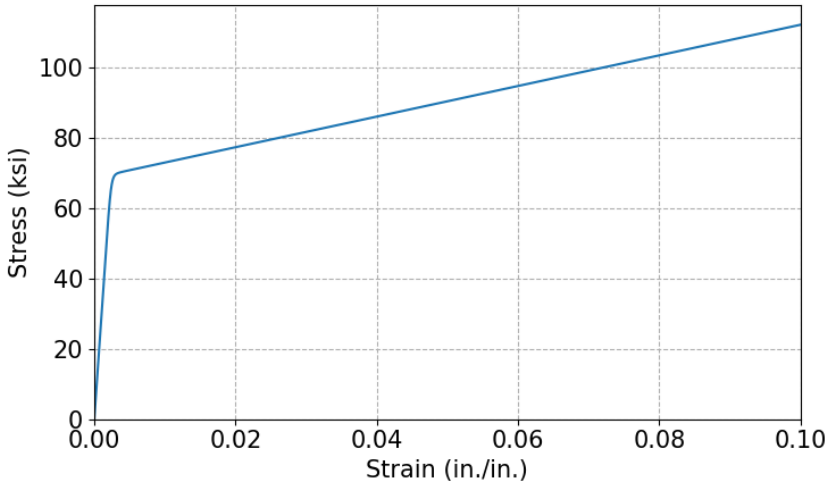

Figure 4.6: Steel02 material model for the column fiber section

4.3.2.2 Column Elastic Shear and Torsional Response

The elastic shear and torsional properties were calculated on the basis of the shear modulus of concrete and the gross area of the column, assuming the Poisson's ratio, ν_c, of the cross-section to be 0.2. The shear modulus, G_c, was 1,839.7 and the torsional constant J was 164,896 in^4. The elastic properties were then aggregated to the inelastic flexural response to capture the overall behavior of the column elements. The "Aggregator" command was used to integrate the elastic and inelastic properties in OpenSeesPy.

4.3.2.3 Cross-Section Discretization

The number of fibers defined for the cross-section of the columns was a balance between the efficiency and accuracy of the analysis. Berry (2006) conducted a convergence study with a variety of discretization schemes and compared analysis results to column test results from the UW-PEER column database (Berry et al. 2004). The study found that the discretization scheme shown in Figure 4.7 adequately captured the moment-curvature relationship while maintaining computational efficiency. This modeling strategy was adopted for the fiber-sections of the column and the anchorage slip in this study.

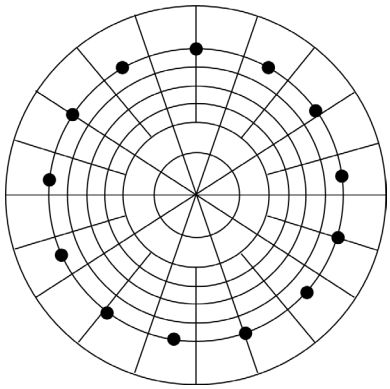

Section	Disc. Dir.	Disc. #
cover	tangential	20
	radial	1
inner core	tangential	10
	radial	2
outer core	tangential	20
	radial	5

Figure 4.7: Bond-slip and column fiber-section discretization (Berry et al. 2004)

4.3.2.4 Anchorage Slip

The anchorage slip models were included to capture slip of the longitudinal reinforcing steel at both ends of columns. The zeroLength section was used in OpenSeesPy with the cross-section discretization scheme as described in Section 4.3.2.3.

The steel stress-displacement relationship for a bar was based on a bond slip model (Lehman and Moehle 2000) and later modified by Ranf (2006). As shown in Figure 4.8, the shear-stress relationship with bar anchorage can be ideally described in three segments as follows:

$$\tau(\sigma)\{\tau_e \frac{\sigma}{\sigma_d} = a\frac{\sigma}{\sigma_d}\sqrt{f_c'} \qquad \sigma < \sigma_d \; \tau_e = \lambda_e\sqrt{f_c'} \qquad \sigma_d \le \sigma \le \sigma_y \; \tau_i = \lambda_i\sqrt{f_c'} \qquad \sigma_y \le \sigma \qquad \textit{(Equation. 4-13)}$$

where τ is the bar shear, σ is the bar stress, and λ_e and λ_i are the elastic and inelastic bond-stress coefficients, respectively.

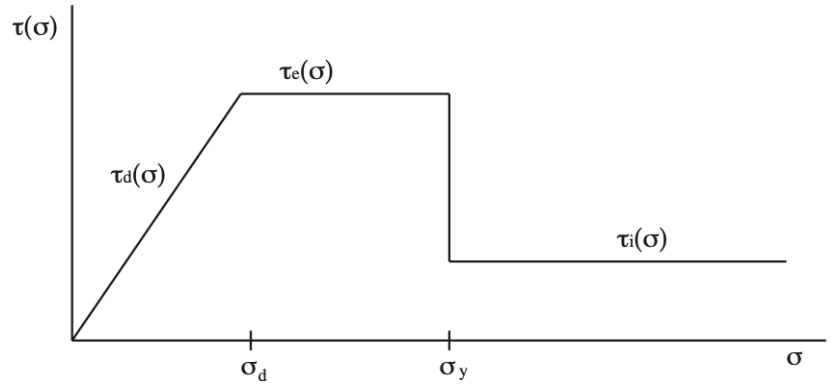

Figure 4.8: Bond slip shear-stress relationship (Berry and Eberhard, 2007)

The change in strain (change in stress) along the reinforcement can then be calculated as:

$$\frac{dF}{dx} = \frac{\pi d_b^2 d\sigma}{4}\frac{d\sigma}{dx} = \tau(\sigma)\pi d_b \qquad \textit{(Equation. 4-14)}$$

$$\frac{d\sigma}{dx} = \frac{4\tau(\sigma)}{d_b} \qquad \textit{(Equation. 4-15)}$$

By integrating the strain along the anchorage zone, the stress-displacement envelope of the rebar can be calculated. The final relationship along with a simplified bi-linear model, which was used in the bridge model here and implemented with the Steel02 material model in OpenSeesPy, is illustrated in Figure 4.9. The resulting reinforcement elastic modulus, E_{s-slip}, and the yield strength, f_{y-slip}, were calculated as 2,085.12 ksi/in and 60 ksi. The bond slip rebar strain hardening ratio, b_{slip}, was 1.08 percent.

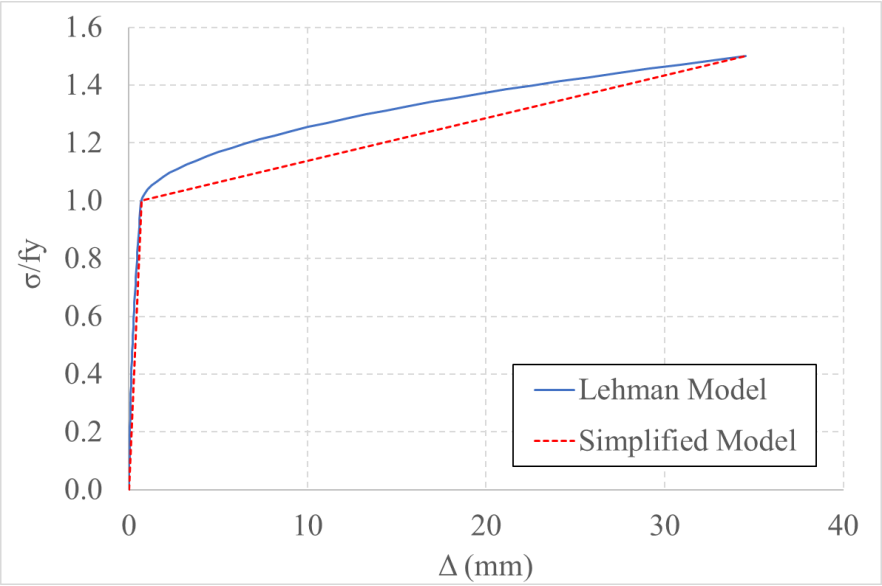

Figure 4.9: Comparison of the stress-displacement curve for modeling bond slip as proposed by Lehman and Moehle (2000) and the simplified bi-linear response

For the concrete material model used at the bond slip section, because of the sufficient confinement provided by the steel and the surrounding concrete around the anchorage zone, the concrete was assumed to not degrade after the maximum stress. This behavior can be accomplished by multiplying the ultimate concrete strain by an effective concrete depth. Berry (2006) used eight test columns from the UW-PEER column database (Berry et al. 2004) and calibrated the effective concrete depth, e_{depth}. The result suggested e_{depth} to have a value of approximately 29 percent of the column diameter, which was adopted in the concrete model of this study. The concrete strain at peak strength, ϵ_{c-slip} , and the ultimate concrete strain, ϵ_{u-slip}, were 0.04 and 127, respectively.

The Concrete01 model was used in OpenSeesPy for this study to model the concrete at bond slip sections. The stress-displacement relationship is illustrated in Figure 4.10.

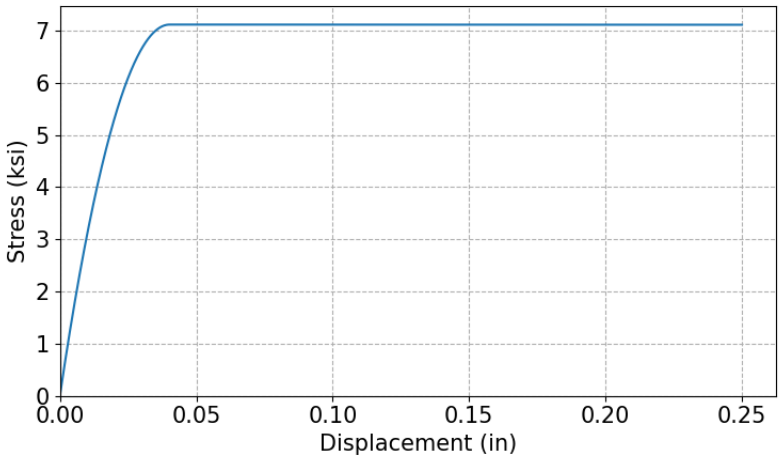

Figure 4.10: Concrete01 stress-displacement relationship for the bond-slip section

4.3.3 Intermediate Foundations

As presented in Figure 4.11, the intermediate foundations were modeled as elastic rotational and translational springs modeled as zero-length elements at the base of columns. Ramanathan (2012) studied the numerical values of the spring stiffnesses according to the configurations of various bridge structures. In this study, the numbers for multiple-span continuous concrete I-girder (MSCC-IG) bridges from that previous work were used for the reference bridge model, and they can be found in Section 4.4. The rotational spring stiffness, K_r, and translational spring stiffness, K_t, were taken to be 7*1e06 (kip-in/rad) and 1,300 (kip/in), respectively (Ramanathan 2012).

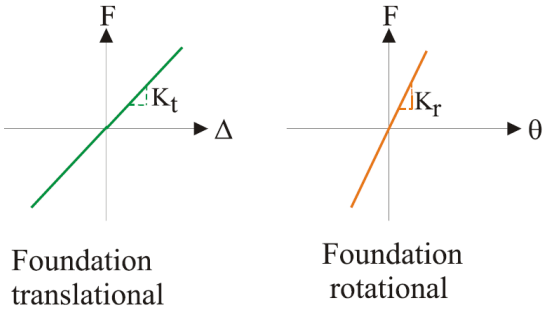

Figure 4.11: Rotational and translational spring for foundations (Mangalathu 2017)

4.4 ABUTMENTS

The abutments that were most commonly observed in the bridge inventory can be classified into three categories: integral, semi-integral, and L abutments. Integral abutments are cast monolithically with the superstructure and provide restriction for the movement of the deck in both the transverse and longitudinal directions. The stiffness and resistance of integral abutments are high and are limited only by the backfill soil and the abutment foundations.

Whereas semi-integral abutments are not cast together with the superstructure, they have the same behavior in the longitudinal direction as integral abutments, as the deck goes beyond the abutment backwall and engages directly with the backfill soil. In the transverse direction, semi-integral and L abutments provide bearing supports to the superstructure whose motion is restrained by shear keys (internal or external) at both ends of the bridge. Both semi-integral and L abutments are typically supported on piles, but they may also be found on spread footings. The longitudinal motion of the superstructures in the case of L abutments is restrained by bearing pads, the abutment backwall, and the backfill soil. To capture the abutment behaviors described above, two different spring systems consisting of various types of zero-length elements were used as shown in Figure 4.12. Although semi-integral and L abutments use the same type of spring systems, the stiffness of the bearing springs differs in the longitudinal direction, with semi-integral abutments modeled as rigid and L abutments as flexible.

The following sections introduce the numerical models used for the spring elements that appear in Figure 4.12 and were used to simulate various bearing, abutment, and soil behaviors.

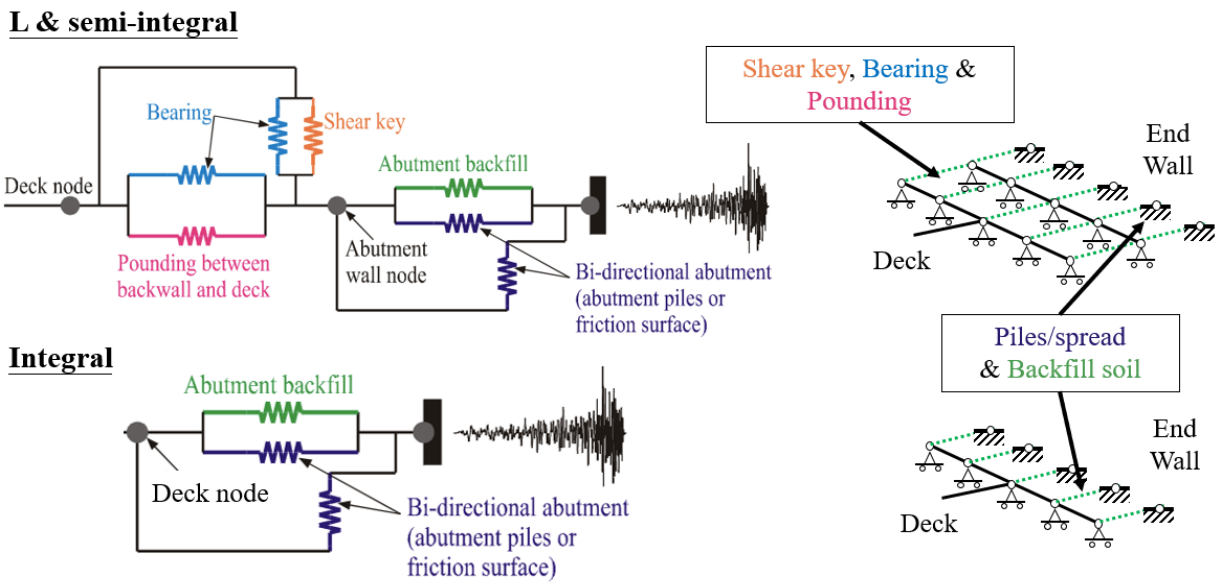

Figure 4.12: Zero-length spring system for L and semi-integral abutment (upper) types, and for integral abutments (lower)

4.4.1 Backfill Soil

The passive response of the abutment backwall was captured by a hyperbolic soil model established by Shamsabadi and Yan (2008). The model was based on experiments conducted at the University of California Los Angeles using a test specimen with a 4.5-ft high abutment backwall. The closed form force-displacement response can be described as:

$$F(\Delta) = \frac{8\Delta}{1+3\Delta} H^{1.5} \qquad Granular\ backfills \qquad (Equation.\ 4\text{-}16a)$$

$$= \frac{8\Delta}{1+1.3\Delta} H \qquad Cohesive\ backfills \qquad (Equation.\ 4\text{-}16b)$$

where F is the interaction force (kip/in) per width of backwall, Δ is the displacement given in inches, and H is the back wall height in feet. Note that the equation for cohesive soil was used for this study, as it is conservative in terms of calculated strength and stiffness.

The maximum displacements for granular and cohesive soils are $0.05H$ and $0.1H$, respectively (Shamsabadi and Yan 2008). Using these maximum displacements and the 7.5-ft backwall height for the reference bridge in Equation 4.16, the ultimate force, F_{ult}, was calculated to be equal to 2,735 kip for cohesive soils. Furthermore, the stiffness at

specific displacements could be calculated by differentiating Equation 4.16 with respect to delta, with Equation 4.17 for the case of cohesive soil.

$$K(\Delta) = F'(\Delta) = \frac{8H^{1.5}(1+6\Delta)}{(1+3\Delta)^2} \qquad \textit{(Equation. 4-17)}$$

The HyperbolicGapMaterial in OpenSeesPy, shown in Figure 4.13, was adopted for modeling the backfill soil, and its behavior is given as:

$$F(\Delta) = \frac{\Delta}{\frac{1}{K_{max}} + R_f \frac{\Delta}{F_{ult}}} \qquad \textit{(Equation. 4-18)}$$

where R_f is failure ratio given as 0.7 (Mangalathu, 2017), and K_{max} , the initial stiffness, was calculated to be 15,503 kip/in from Equation 4.17 by substituting Δ equal to 0. The gap distance in the HyberbolicGapMaterial is assumed to be a small value, as the backfill soil is likely to be compacted against the back wall and is neglected. However, once the material has compressed, a gap is created and increases with repeated cycling.

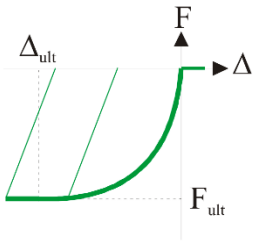

Figure 4.13: HyperbolicGapMaterial model for abutment backfill (Mangalathu 2017)

4.4.2 Abutment Foundations

Two types of abutment foundations were considered in this study. The modeling for abutment foundations included six soil types: soft clay, medium clay, stiff clay, soft sand, medium sand, and stiff sand. (The reference bridge was set to sit on medium sand, and medium clay soil was considered for the parametric study in Chapter 6). The soil types influenced the input parameters for the abutment foundation material models and reflected the effects of different soil types.

4.4.2.1 Abutment Spread Footing

The abutment spread footings were assumed to have elastic-plastic behavior, and the yield force was obtained by multiplying the normal force and the friction coefficient,

μ_{spread}. The friction coefficients were assumed to have different values for different types of soils, and they are listed in Table 4.1, where the bold value is that used for the reference bridge.

Table 4.1: μ_{spread} for different soil types (with bold value used for the reference bridge)

	Soft clay	**Medium clay**	**Stiff clay**	**Soft sand**	**Medium sand**	**Stiff sand**
μ_{spread}	0.3	0.4	0.5	0.31	**0.47**	0.79

The normal force was assumed to be half of the self-weight of the span that sits on the bearing pads, and the yield displacement, $\Delta_{y-spread}$, was set to be 0.75 in. (Mangalathu, 2017). The stiffness, E_{spread}, was then calculated to be 37.1 kip/in. The ElasticPP model shown in Figure 4.14 was used to simulate spread footings.

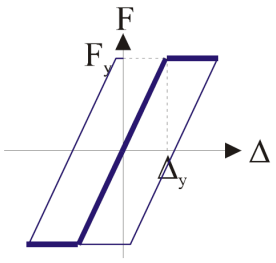

Figure 4.14: Piles spread footing material model (Mangalathu 2017)

4.4.2.2 Abutment Piles

Modeling of the abutment piles followed the lateral pile force-deflection curves developed by Evans and Duncan (1982). Evans and Duncan proposed charts describing the relationship between pile lateral load and lateral deflection for different soil types. The soil types were described in terms of the axial strain at which 50 percent of the soil strength is mobilized, denoted as ϵ_{50}.

The characteristic shear load of a pile, V_c, is defined as:

$$V_c = \lambda B^2 E R_I \left(\frac{\sigma_p}{E R_I}\right)^m {\epsilon_{50}}^n \qquad \textit{(Equation. 4-19)}$$

where $R_I = 1.0$ for circular cross-sections (considered in this study).

For plastic clay and sand:

$$\lambda = 1.00 \qquad \textit{(Equation. 4-20)}$$

For brittle clay:

$$\lambda = (0.14)^n \qquad \textit{(Equation. 4-21)}$$

For clay:

$$\sigma_p = 4.2S_u \qquad \text{(Equation. 4-22)}$$

For sand:

$$\sigma_p = 2C_{p\phi}\gamma B tan^2(45 + \phi'/2) \qquad \textit{(Equation. 4-23)}$$

where:

λ = A dimensionless parameter dependent on the soil's stress-strain behavior

B = Diameter of the foundation pile

E = Modulus of elasticity of the foundation piles (assumed equal to Ec for this study)

I = Moment of inertia of the foundation piles ($= \pi B^4/64$ for circular piles)

R_I = Moment of inertia ratio ($= \frac{I}{\pi B^4/64}$, 1.0 for circular piles)

σ_p = Representative passive pressure of the soil

ϵ_{50} = Axial strain at which 50 percent of the soil strength is mobilized (Table 4.2)

m, n = Exponents terms (Table 4.2)

S_u = Undrained shear strength of the soil (Table 4.2)

ϕ' = Effective friction angle of the soil (deg) (Table 4.2)

$C_{p\phi}$ = Passive pressure factor = $\phi'/10$

γ = Unit weight of the soil (assumed to be 110 (lb/ft^3) in this study)

Table 4.2: Soil parameters for clay and sand soil types (with bold values indicating those used for the reference bridge) (Evan and Duncan 1982)

Soil type	ϵ_{50}	**m**	**n**	ϕ' **(deg)**	S_u **(kPa)**
Soft clay	0.02	0.683	-0.22	-	25
Medium clay	0.01	0.683	-0.22	-	50
Stiff clay	0.005	0.683	-0.22	-	75
Soft sand	0.002	0.57	-0.22	25	-
Medium sand	0.002	0.57	-0.22	50	-
Stiff sand	0.002	0.57	-0.22	75	-

Figures 4.15 and 4.16 show the lateral force versus deflection curves for soil types from Evans and Duncan (1982) for clay and sand, respectively.

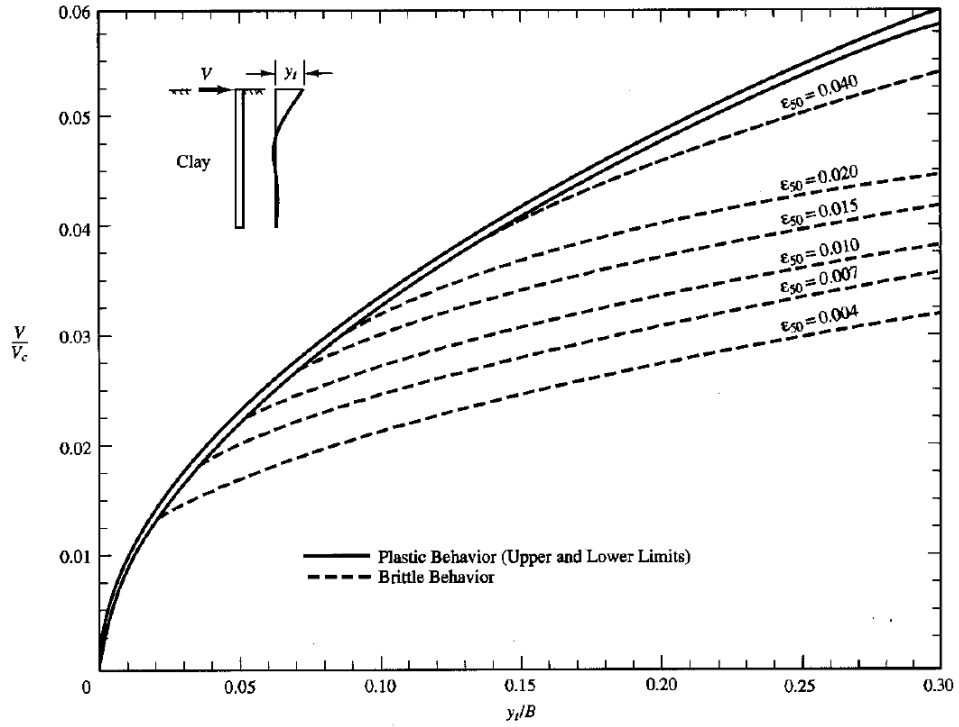

Figure 4.15: Piles lateral load and deflection relationship for clay (Evan and Duncan 1982)

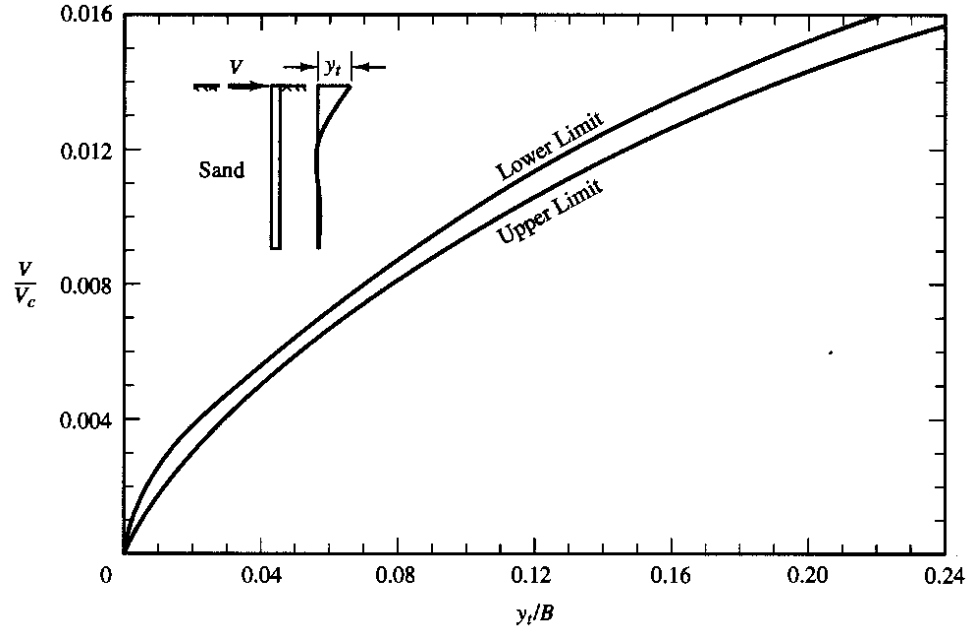

Figure 4.16: Piles lateral load and deflection relationship for sand (Evan and Duncan 1982)

The total lateral load of abutment piles, $V_{c_{total}}$, was calculated by:

$$V_{c_{total}} = V_c * (\#piles) \qquad \textit{(Equation. 4-24)}$$

where $\#piles$ is the equivalent number of 13-inch diameter piles at the abutments and was derived from the deck width. The 13-inch pile diameter is often the standard among bridges.

The equivalent number of 13-inch piles at the abutments, $\#piles$, was calculated as:

$$\#piles = \#piles_{actual} * d_{actual} \,/\, 13 \qquad \textit{(Equation. 4-25)}$$

where $\#piles_{actual}$ is the actual number of piles and d_{actual} is the actual pile diameter.

For the selected bridges from the Abutment Database (Chapter 3) that had sufficient information for abutment piles, Figure 4.17 shows the relationship between $\#piles$ and bridge deck width.

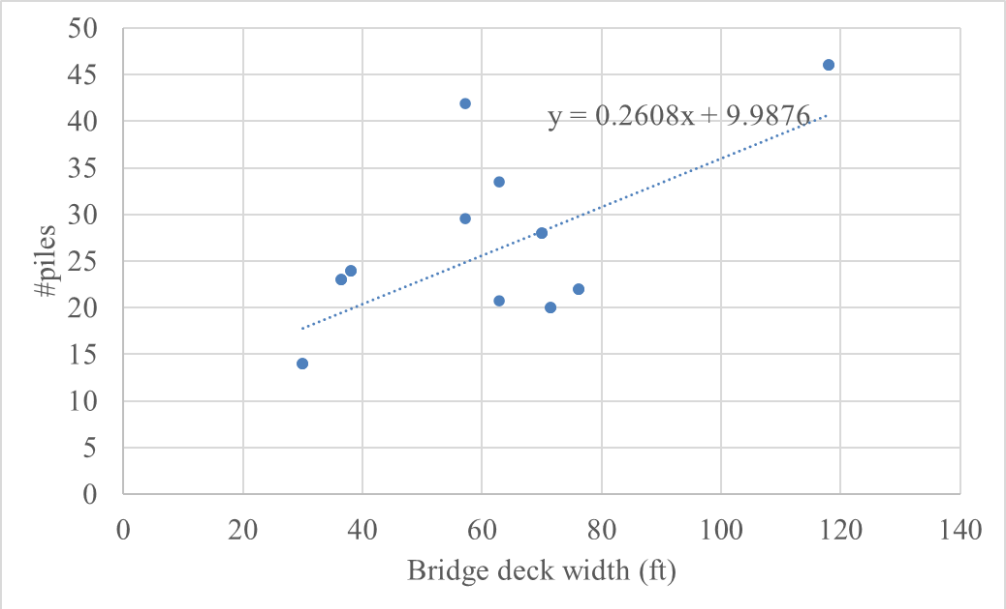

Figure 4.17: Equivalent 13-inch-diameter pile numbers versus bridge deck width

In this study, the curves in figures 4.15 and 4.16 were modeled as bi-linear curves followed by a constant relationship between pile lateral load and the deflection, and they were modeled with the Hysteretic material model in OpenSeesPy. Figure 4.18 illustrates the hysteretic model for the abutment piles and the first and second yield points, (Δ_{1-pile},

F_{1-pile}) and (Δ_{2-pile}, F_{2-pile}), for the different soil types listed in Table 4.3. The pinching parameters in the hysteretic material model, $pinchX_{pile}$ and $pinchY_{pile}$, were set to be 0.75 and 0.5, respectively (Mangalathu 2017).

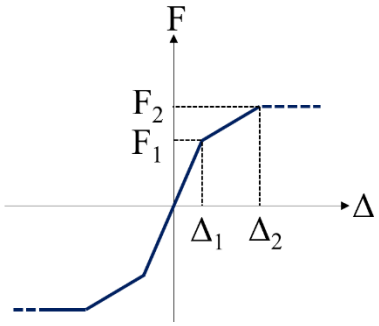

Figure 4.18: Abutment pile hysteretic model (Mangalathu 2017)

Table 4.3: Abutment pile hysteretic model force and displacement input values (with the bold values indicating the reference bridge)

Soil types	**Δ_1 (in)**	**Δ_2 (in)**	**F_1 (kip)**	**F_2 (kip)**
Soft clay	1.13	3.9	30	45
Medium clay	0.65	3.9	42	71
Stiff clay	0.34	3.9	42	97
Soft sand	1.17	2.99	31	56
Medium sand	**1.17**	**2.99**	**88**	**157**
Stiff sand	1.17	2.99	356	633

4.4.3 Shear Keys

Shear keys provide important constraints for the superstructure in the transverse direction at semi-integral and L abutments during earthquakes.

Megally (2002) studied the capacity of a series of interior and exterior shear keys at the University of California San Diego. An example of the experimental results is shown in Figure 4.19 in terms of shear force versus displacement. As seen in Figure 4.19, the

shear key reached its capacity at a displacement that was equal to the gap between the deck and the shear key and then started deteriorating until a maximum displacement of 4.0 inches was reached, when it lost all resistance.

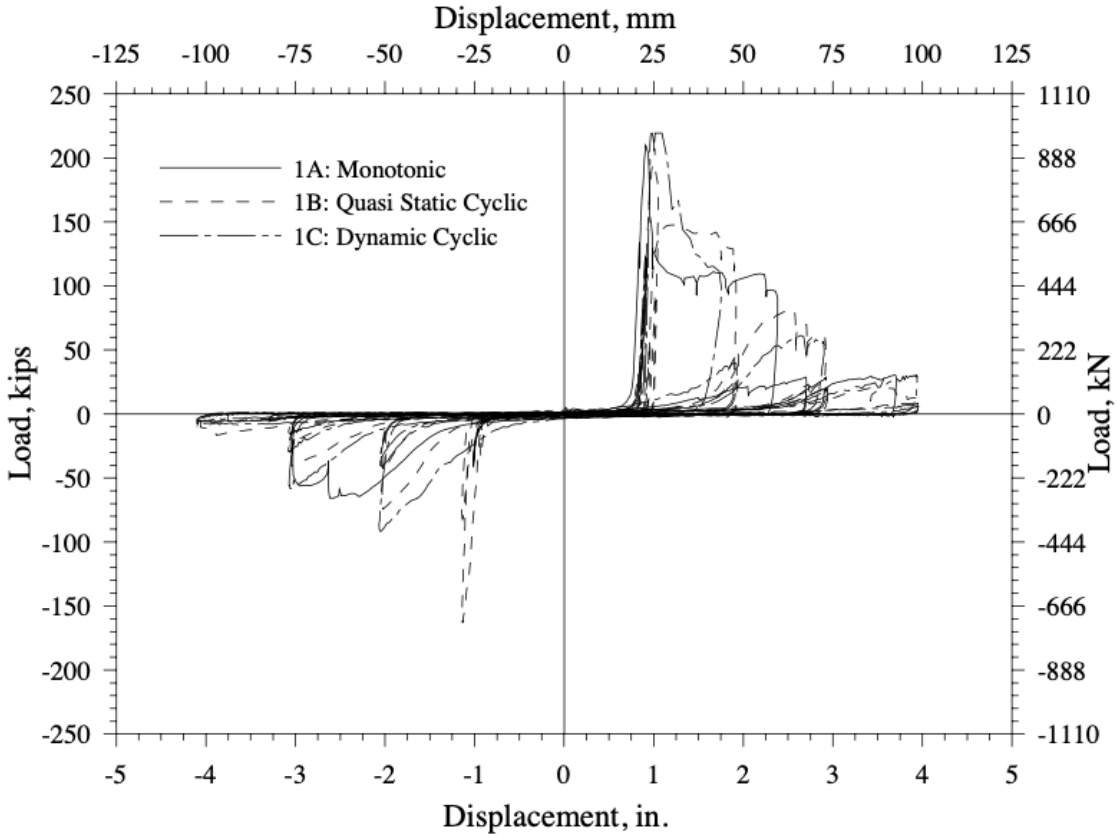

Figure 4.19: Shear key experimental results from Megally (2002)

Figure 4.20 shows an example schematic of a typical interior shear key, where b is width, d is depth, and h is height. The interior shear key capacity can be calculated for different failure mechanisms based on its aspect ratio, α (which is equal to h/d).

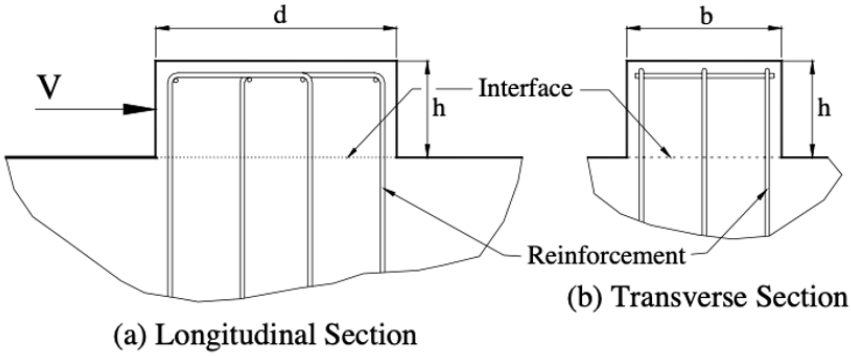

Figure 4.20: Shear key material model (Megally 2002)

Table 4.4 lists three capacity calculations with their corresponding failure modes, where $f'c$ is the concrete strength in psi.

Table 4.4: Shear key capacities according to failure mechanism

Aspect Ratio (α)	**Failure Mechanism**	**Shear Stress (V_N) (psi)**
$\alpha < 0.5$	Shear Friction	$11.3\sqrt{f'c}$
$0.5 < \alpha < 1.0$	Bracket and corbel	$800\ f'c$
$1.0 < \alpha$	Flexural (cantilever beam)	$0.2\ f'c$

In this study, only interior shear keys at the abutments were considered, with their capacities integrated and assigned to two shear key models at opposite ends of the abutments. Interior shear keys were found in the survey of WSDOT bridges to be most common. With this simplification, four shear key spring elements were included for the entire bridge model. The derived shear key capacity, F_{shear}, was 2,240.25 (kip) for a shear key model in the reference bridge.

The Hysteretic material model in OpenSeesPy was used to simulate the force-displacement curve and deterioration after maximum strength of the shear keys. The initial gap, Δ_{init}, was assumed to be 0.5 inches and the maximum displacement, Δ_{max}, was assumed to be Δ_{init} + 3.5 inches (Megally et. al 2002). The pinching parameters in the hysteretic material model, $pinchX_{shear}$ and $pinchY_{shear}$, were set to be 1.0 and 0.0,

respectively, to produce the pinched behavior observed in Figure 4.19. Figure 4.21 shows the material model of the shear key.

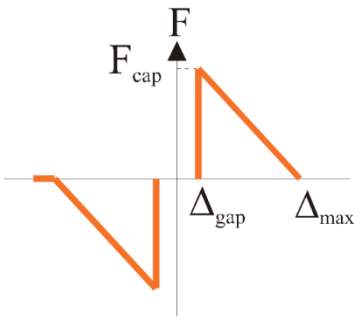

Figure 4.21: Shear key material model (Mangalathu 2017)

4.4.4 Bearings

Since the reference bridge contains elastomeric bearings, elastomeric bearing pads were considered for the study. The bearing pads were assumed to have elastic-plastic behavior (Mangalathu 2017), where the elastic portion represented the deformation of the bearing pads, and the portion after yielding represented the slip between the girder and the end plate of the bearings. The yield force, $F_{y-bearing}$, was obtained by the multiplication of normal force, N_b, subjected to bearing pads and the friction coefficient, μ_b. N_b was equal to 59.6 (kip), and μ_b was set to be 0.3 (Mangalathu 2017). The stiffness for the bearing pad, K_{pad}, following the suggestion by Mangalathu (2017), was set to be 14.51 (kip/in). The Steel02 material model in OpenSeesPy was used to simulate the bearing pads and is shown in Figure 4.22 with a hardening ratio, $b_{bearing}$, assumed to be 1 percent.

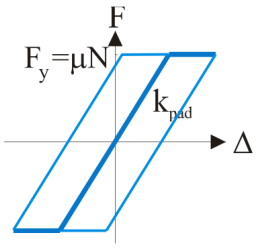

Figure 4.22: Elasto-plastic bearing model (Mangalathu 2017)

4.4.5 Pounding

Pounding elements are used to reflect the impact between the bridge decks and the abutments during seismic events. The ImpactMaterial model is used to model pounding at these locations in OpenSeesPy. The material model was based on work proposed by Muthukumar and DesRoches (2006) that accounts for hysteretic energy loss caused by the impact (Figure 4.23). Following the assumptions from Mangalathu (2017), the maximum displacement, Δ_m, was 1.0 inches, and the yield deformation, $\Delta_{y-pounding}$, was $0.10\Delta_m$. The stiffnesses, $k_1$and k_2, were assumed to be 1,022.3 (kip/in) and 351.755 (kip/in) per ft width of backwall, respectively (Mangalathu 2017).

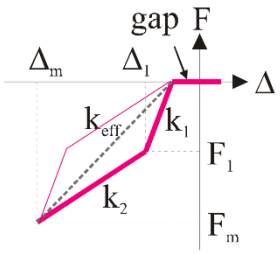

Figure 4.23: ImpactMaterial for pounding elements (Mangalathu 2017)

4.5 SUMMARY OF PARAMETERS USED TO MODEL REFERENCE BRIDGE

This section summarizes the important input parameters for the material models described in the earlier sections of this chapter. Tables 4.5 through 4.7 provide the parameters for bridge deck, column, cross-beam, and bond-slip, and tables 4.8 through 4.13 provide the parameters for the various components of the bridge abutments.

Table 4.5: Parameters for bridge deck, column, and cross-beam

Parameter	Expression	Value	Measurement
concrete elastic modulus	E_c	4415.2	ksi
concrete shear modulus	G_c	1839.7	ksi
concrete poisson's ratio	ν_c	0.2	
concrete strength	f_c	6	ksi
cross-beam concrete elastic modulus	E_{c-beam} $(=E_c * 1000)$	441520	ksi

Parameter	Expression	Value	Measurement
cross-beam concrete shear modulus	G_{c-beam} $(=G_c * 1000)$	183970	ksi
specified concrete strength	f'_c	4	ksi
unconfined concrete strain at peak strength	ϵ_c	0.002	
unconfined concrete ultimate strain	ϵ_u	0.004	
confined concrete strength	f_{cc}	7.11	ksi
confined concrete strain at peak strength	ϵ_{cc}	0.00385	
confined concrete ultimate stress	ϵ_{cu}	0.0122	
confined concrete ultimate strain	f_{cu}	4855.6	ksi
concrete maximum tension stress	f_t	0.711	ksi
concrete maximum tension strain	ϵ_t	0.000136	
confined concrete residual stress	f_{r-c}	0.142	ksi
unconfined concrete residual stress	f_{r-uc}	0.00711	ksi
transverse reinforcement ratio	ρ_{hoop}	0.5	%
reinforcement ultimate strain	ϵ_{su}	0.12	
column reinforcement yield strength	f_y	69.6	ksi
reinforcement elastic modulus	E_s	29000	ksi
column reinforcement strain hardening ratio	b_{col}	1.5	%
column torsional constant	J	164896	in4

Table 4.6: Parameters for bond-slip

Parameter	Expression	Value	Measurement
bond-slip reinforcement strain hardening ratio	b_{slip}	1.08	%
bond-slip reinforcement yield strength	f_{y-slip}	60	ksi

Parameter	Expression	Value	Measurement
bond slip reinforcement elastic modulus	E_{s-slip}	2085.12	kip/in
effective concrete depth	e_{depth}	10.44	in
bond slip concrete ultimate strain	ϵ_{u-slip} $(= \epsilon_{u-slip} * e_{depth})$	12.7	
bond slip concrete strain at peak strength	ϵ_{c-slip}	0.04	

Table 4.7: Parameters for intermediate foundation springs

Parameter	Expression	Value	Measurement
Intermediate foundation rotational spring stiffness	K_r	7000000	kip-in/rad
Intermediate foundation translational spring stiffness	K_t	1300	kip/in

Table 4.8: Parameters for backfill soil

Parameter	Expression	Value	Measurement
backfill soil initial stiffness	K_{max}	15503	kip/in
backfill soil ultimate force	F_{ult}	-2375	kips
backfill soil failure ratio	R_f	0.7	
backfill gap distance	Δ_{abut}	1.00E-05	in

Table 4.9: Parameters for the abutment spread footing

Parameter	Expression	Value	Measurement
spread footing yield displacement	$\Delta_{y-spread}$	0.75	in
spread footing initial stiffness	E_{spread}	37.1	kip/in

Table 4.10: Parameters for the abutment pile

Parameter	Expression	Value	Measurement
abutment piles first yield displacement	Δ_{1-pile}	1.17	in
abutment piles first yield force	F_{1-pile}	88	kip
abutment piles second yield displacement	Δ_{2-pile}	2.99	in
abutment piles second yield force	F_{2-pile}	157	kip
pinchX	$pinchX_{pile}$	0.75	
pinchY	$pinchY_{pile}$	0.5	

Table 4.11: Parameters for the shear key

Parameter	Expression	Value	Measurement
shear key capacity	F_{shear}	2240.25	kips
shear key initial gap	Δ_{init}	0.5	in
shear key maximum displacement	Δ_{max}	4	in
pinchX	$pinchX_{shear}$	1	
pinchY	$pinchY_{shear}$	0	

Table 4.12: Parameters for the bearing pad

Parameter	Expression	Value	Measurement
bearing yield force	$F_{y-bearing}$	17.88	kips
bearing friction coefficient	μ_b	0.3	
bearing initial stiffness	K_{pad}	14.51	kip/in
Bearing strain hardening ratio	$b_{bearing}$	1	%

Table 4.13: Parameters for pounding

Parameter	**Expression**	**Value**	**Measurement**
pounding yield deformation	$\Delta_{y-pounding}$	0.1	in
pounding maximum displacement	Δ_m	1	in
pounding initial stiffness	k_1	1022.3	kip/in/ft
pounding secondary stiffness	k_2	351.755	kip/in/ft

CHAPTER 5 RESPONSE OF THE REFERENCE BRIDGE MODEL

The three-dimensional, multiple-degree-of-freedom model of the reference bridge described in Chapter 4 was developed using detailed numerical modeling strategies for the columns and abutments. To understand the static and dynamic behaviors of the reference bridge model (before variations in key parameters are described in later chapters), this chapter presents a set of simple analyses. The analyses were used to verify the behaviors of various components of the reference MDOF bridge model and to compare them with those of the SDOF bridge model (Kortum et al. 2022) from an earlier study (Section 2.4).

Section 5.1 presents the pushover analyses that were used to ensure the model components behaved as expected. Section 5.2 reports the response of the bridge columns to quasi-static cyclic loading. Section 5.3 discusses the responses of the bridge as well as various detailed bent and abutment components under bi-directional earthquake excitation. Finally, in Section 5.4, a comparison of the dynamic analysis response of the MDOF reference model and the SDOF model for selected ground motions is described.

5.1 PUSHOVER ANALYSES

The purpose of this section is to show that under static pushover loading, the key components of the model developed in Chapter 4 behaved as expected. As shown in Figure 5.1, the abutment model developed in Chapter 4 consisted of a set of spring elements acting in parallel or in series. The semi-integral and L abutments included detailed models of the shear keys, bearing pads, pounding elements, spread footings/piles, and backfill soil. For integral abutments, only the spread footings/piles and backfill soil were included.

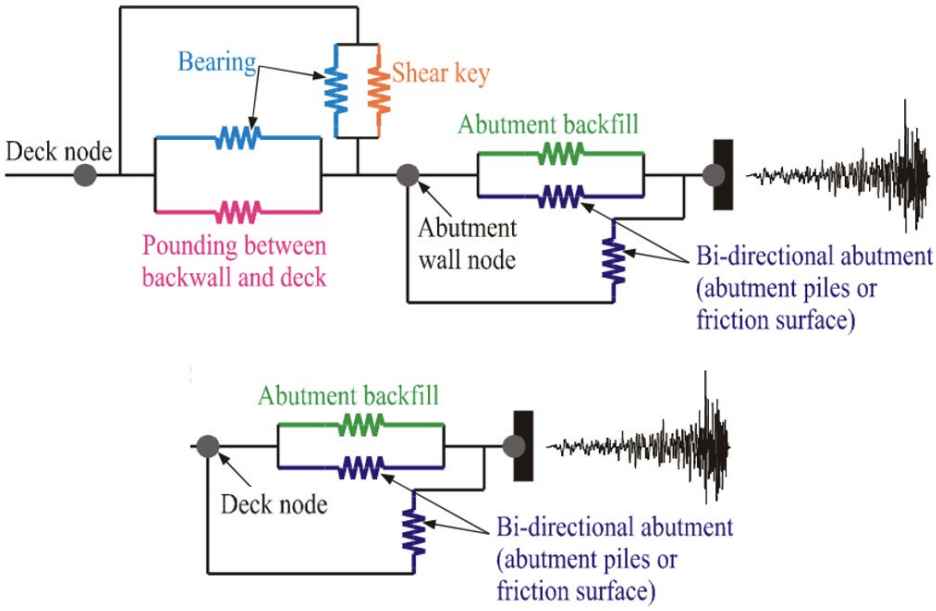

Figure 5.1: Zero-length spring system for semi-integral and L abutment types (upper) and for integral abutments (lower)

Pushover analyses were performed with a variety of stiffness assumptions for each spring element. Only the L abutment model was included for the pushover analyses since it included all the spring elements shown in the figure. Table 5.1 lists four cases of the abutment model for the reference bridge that were used for the pushover analysis in both horizontal directions (transverse and longitudinal) to validate the modeling approach. The pushover analyses assumed that each spring in the abutment model had one of three possible stiffness conditions in the horizontal directions, namely:

- soft: the element was assumed to have negligible stiffness
- stiff: the element was assumed to have large stiffness and to behave like a rigid element
- actual: the element had the actual material model properties for the reference bridge (Chapter 4).

Table 5.1: L-type abutment model cases for modeling approach validation

Case number	Shear keys stiffness	Bearing stiffness	Pounding stiffness	Piles/Spread footings stiffness	Backfill Soil stiffness
1	Soft	Soft	Soft	Stiff	Stiff
2	Soft	Actual	Soft	Stiff	Stiff
3	Actual	Actual	Actual	Stiff	Stiff
4	Actual	Actual	Actual	Actual	Actual

The results for Case 1 are shown in Figure 5.2, which compares the calculated forces in each abutment element with the sum of the shear forces in the columns, as well as the total base shear for the bridge. In Case 1, the forces for all the abutment springs were zero, since the bearings, shear keys, and pounding elements had no significant resistance because of their negligible stiffnesses. The piles or spread footing springs and backfill springs also had no force because they were connected in series to the bearing, shear keys, and pounding elements. As a result, the lateral load for the bridge was resisted only by the columns, causing the force-displacement relationship for the entire bridge (black curve) to be the same as the force-displacement relationship of the columns (red curve). Furthermore, the pushover curves were almost identical in the transverse and longitudinal directions. The slight difference between the pushover response in the longitudinal and transverse directions resulted from the overturning resistance provided by the bent in the transverse direction that came from the column axial-force couple.

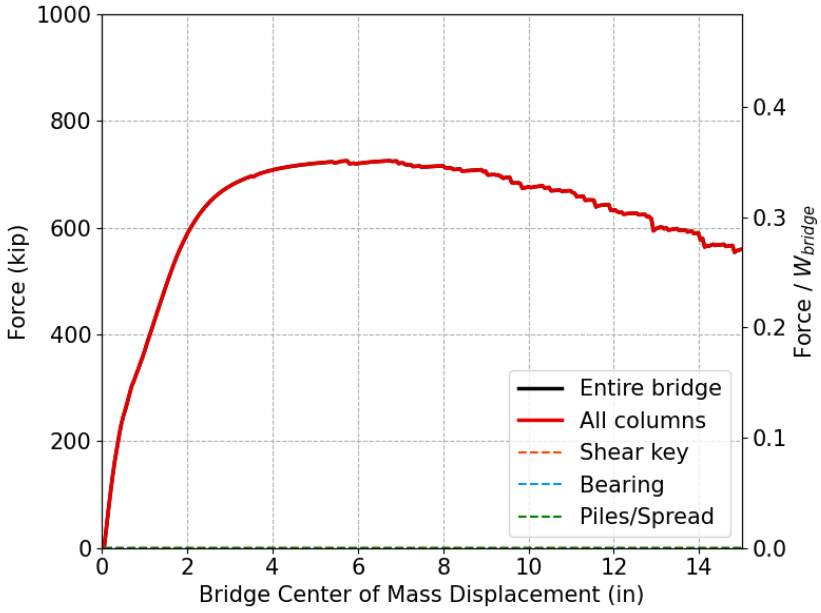

(a) Transverse direction

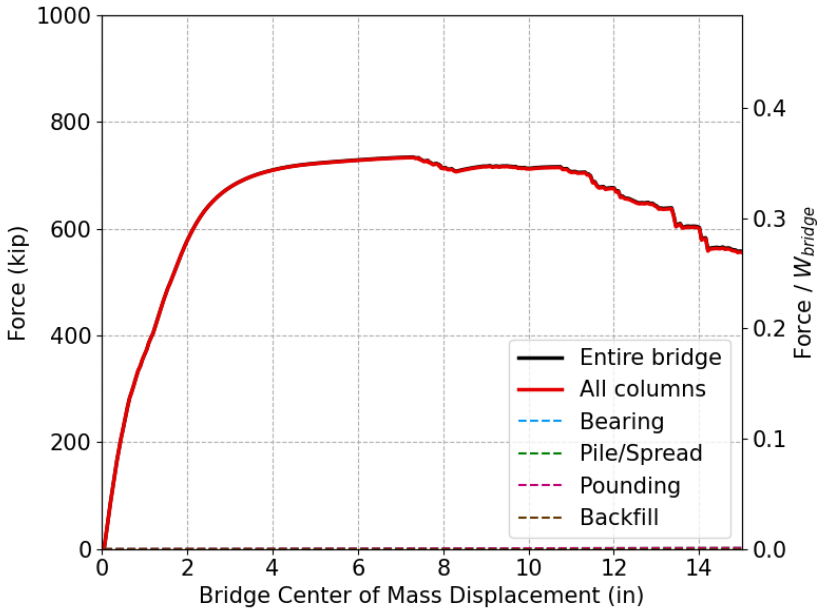

(b) Longitudinal direction

Figure 5.2: Case 1 pushover curves in the (a) transverse and (b) longitudinal directions

Case 2 was the same as Case 1, except that the actual stiffness of the bearings in Case 2 were computed as in Chapter 4. The pushover results for Case 2 are shown in Figure 5.3, and again, the responses are shown for the transverse and longitudinal directions. In

the transverse direction, the bearing pads resisted their maximum force, and that force was transmitted to the transverse piles/spread springs, resulting in the overlapping bearing (light blue) and piles/spread (green) lines. The difference between total pushover force and the sum of the load in the columns was the force resisted by the bearings. In the longitudinal direction, the bearing pads also resisted loads that were then transmitted to the piles/spread springs. Although both the piles/spread springs and backfill elements were set to "stiff," the stiffness for the piles/spread springs was considerably larger, resulting in the bearing force being largely transferred to the piles/spread elements. Pounding and shear key elements resisted no force because their resistance was negligible.

Figure 5.4 shows the pushover response for Case 3, in which the shear key, bearing, and pounding elements had their actual stiffnesses, whereas the piles/spread springs and backfill stiffnesses were set to be stiff. In the transverse direction, when displacement was less than the shear key gap (around 0.5 inches), the bearings and piles/spread springs had the same forces because of their series connection. The forces in the shear key elements started increasing when the shear key gap was closed and eventually peaked at around 5,500 kips, followed by its failure, consistent with the prescribed behavior discussed in Chapter 4. The remaining resistance was then only from the bearing, piles/spread elements, and the columns. In the longitudinal direction, when displacement was less than the pounding gap (approximately 0.95 inches), the bearings and piles/spread elements had the same forces because of their series connection. The forces in the pounding elements started increasing after the pounding gap was closed. Furthermore, the sum of the force in the bearing and pounding elements was equal to the sum of forces in the piles/spread elements and the backfill elements.

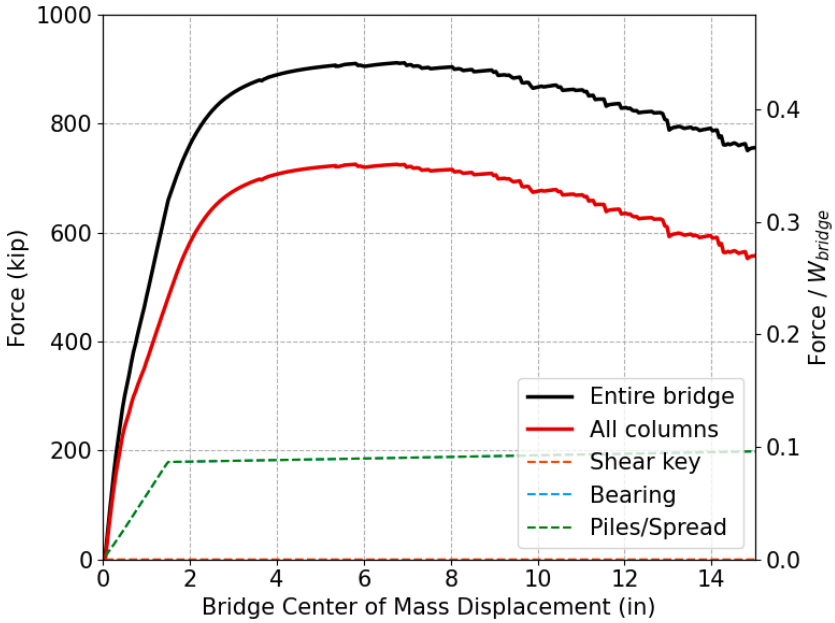

(a) Transverse direction

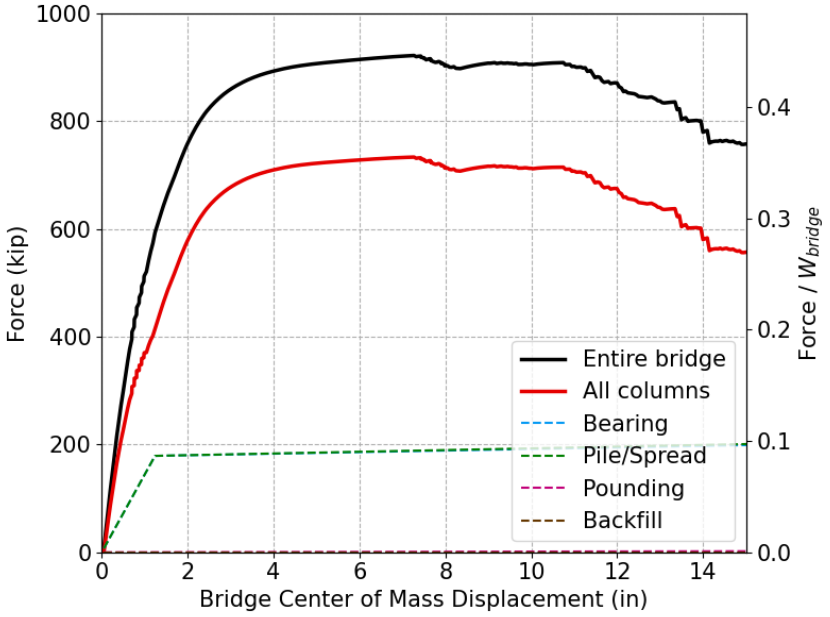

(b) Longitudinal direction

Figure 5.3: Case 2 pushover curves in the (a) transverse and (b) longitudinal directions

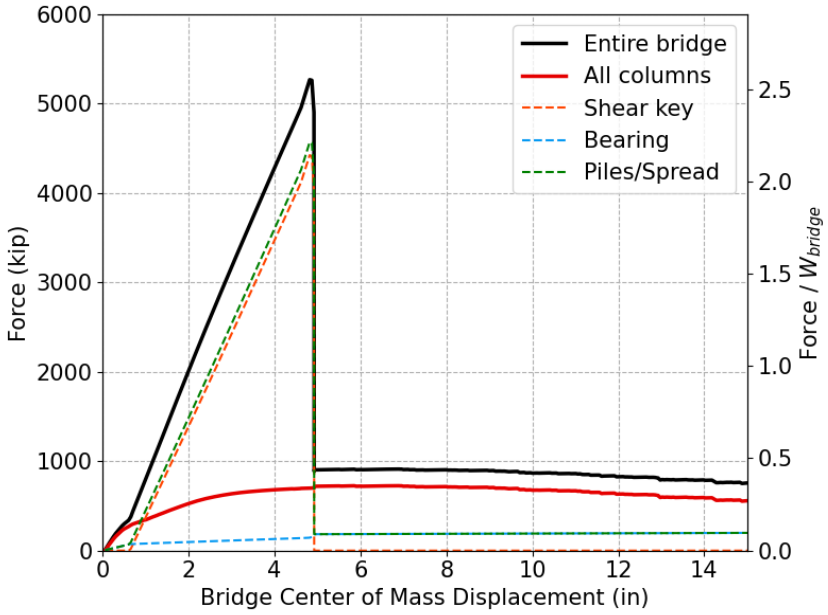

(a) Transverse direction

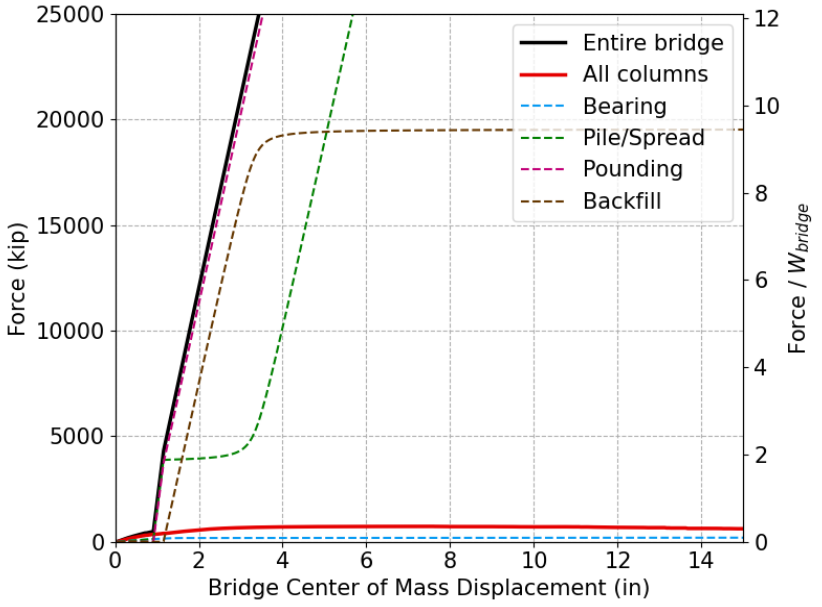

(b) Longitudinal direction

Figure 5.4: Case 3 pushover curves in the (a) transverse and (b) longitudinal directions

Figure 5.5 presents the pushover results for the bridge model with all of the abutment elements having the actual stiffnesses discussed in Chapter 4. In the transverse

direction, the lateral force began to increase rapidly after the shear key gap was closed. Then, the lateral force was limited by the piles/spread elements until the maximum capacity of the piles/spread elements (approximately around 2,300 kips) was reached. In the longitudinal direction, the lateral force began increasing after the pounding gap was closed. Then the lateral force was capped at the maximum capacity of the backfill elements (around 20,000 kips), and the pushover curve matched the hyperbolic curve prescribed for the backfill elements.

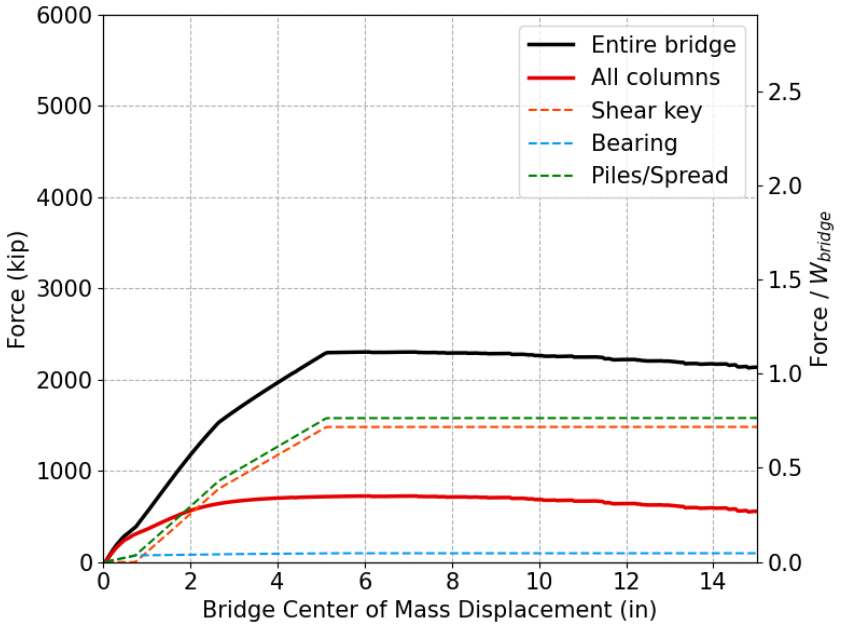

(a) Transverse direction

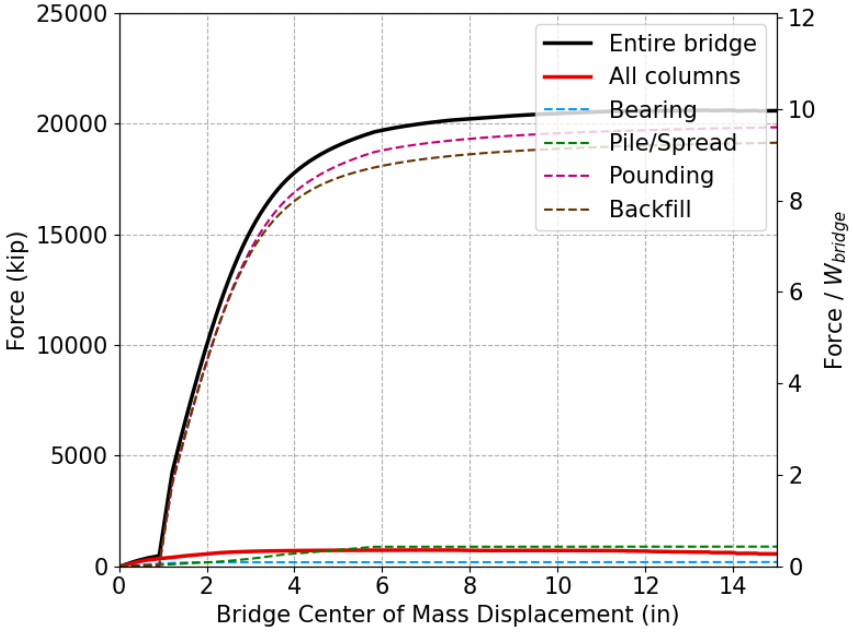

(b) Longitudinal direction

Figure 5.5: Case 4 pushover curves in the (a) transverse and (b) longitudinal directions

5.2 QUASI-STATIC CYCLIC ANALYSIS OF BRIDGE COLUMNS

To show the deterioration behavior of the columns in the reference bridge model, quasi-static cyclic loading was applied in the transverse direction to the bridge model, corresponding to Case 1 in Table 5.1. Cycles were applied at increasing amplitude drift ratios that ranged from 0.2 percent (0.5 inches) to approximately 5.0 percent (13.0 inches).

As shown in Figure 5.6, the columns yielded at a bridge lateral force of about 625 kips and a center of mass displacement of 2.5 inches. Yielding was followed by a secondary slope resulting from strain-hardening in the reinforcing steel. Stiffness deterioration and pinching were evident in the cyclic response, and the overall response was consistent with the expectations for the column models discussed in Chapter 4.

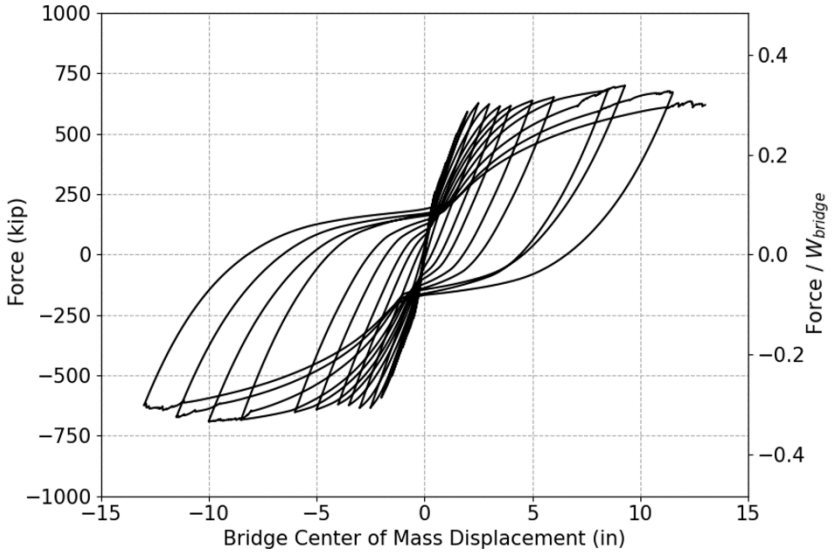

Figure 5.6: Cyclic lateral force versus center of mass displacement for Case 1

5.3 BI-DIRECTIONAL DYNAMIC ANALYSES

This section presents detailed results for a bi-directional dynamic analysis for the reference bridge (corresponding to Case 4 in Table 5.1). The baseline M9 ground motion selected for this analysis was realization csz002 for the Ocean Shores site. Figure 5.7 shows the original ground motion time history in units of the gravitational constant, g. Both horizontal components of the ground motions were applied, with the x-direction component applied in the transverse direction and the y-direction component applied in the longitudinal direction.

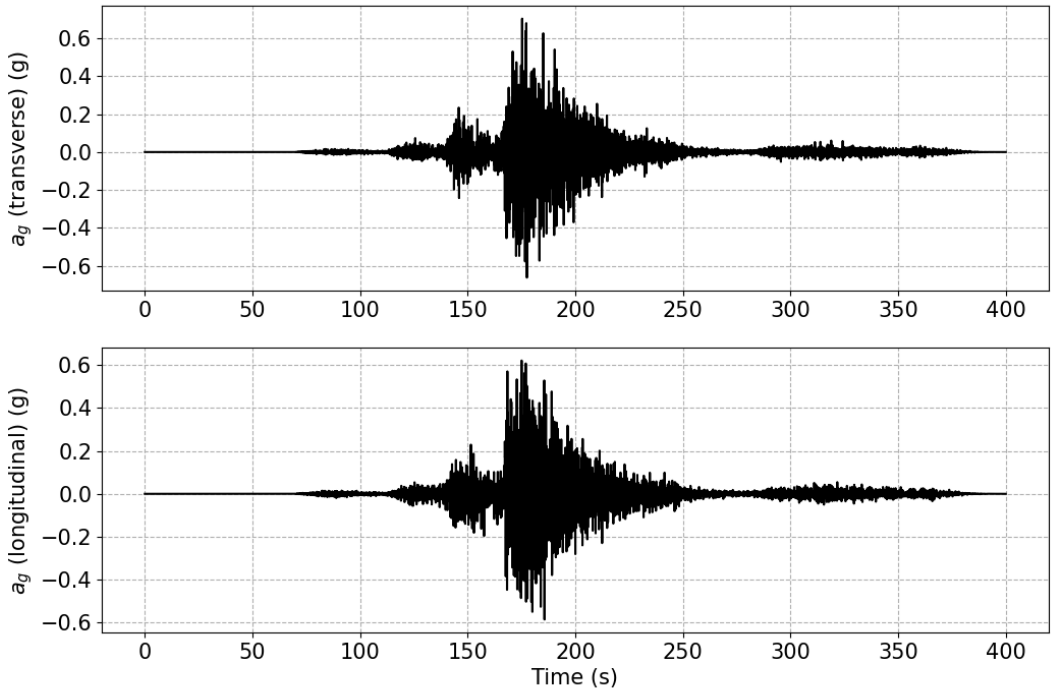

Figure 5.7: Baseline ground motion time history for realization csz002 for Ocean Shores

Figure 5.8 presents the dynamic force-displacement response of the bridge columns under the sample M9 ground motions. Although the ground motion time history in the x- and y-directions were similar (with peak ground acceleration values close to 0.6 g), the maximum displacement in the transverse direction (3.18 inches) was almost two times that in the longitudinal direction (1.65 inches). This difference resulted from the presence of the pounding elements in the longitudinal direction, whose stiffness was large in comparison to that provided in the transverse direction (Figure 5.5). Furthermore, from the almost identical displacements at Bent 1, at the center of mass of the bridge, and at Bent 2, the bridge deck behaved like a rigid body during the earthquake excitation.

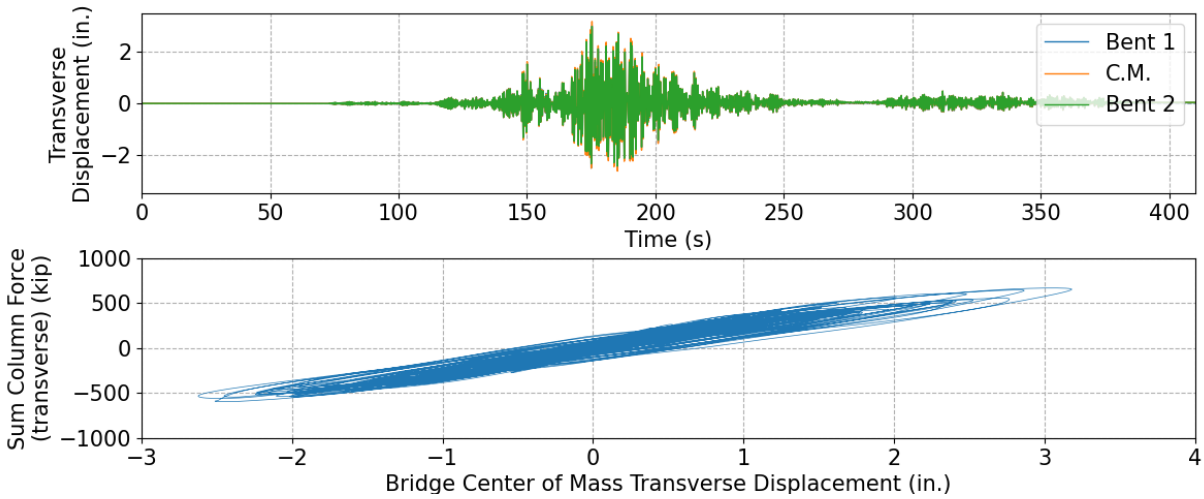

(a) Transverse direction

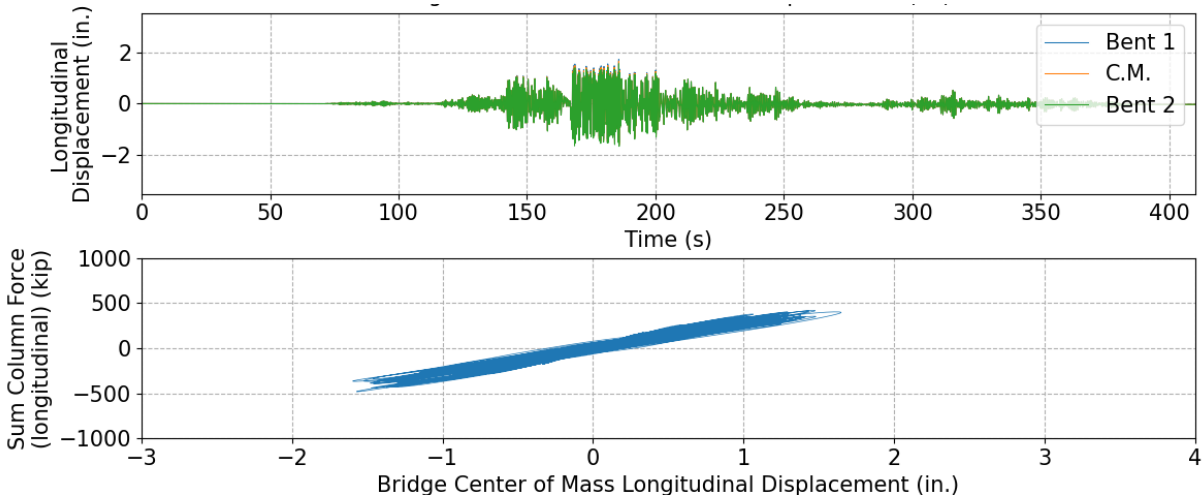

(b) Longitudinal direction

Figure 5.8: Dynamic response of bridge columns in the transverse and longitudinal directions

The responses of the abutment springs to the same ground motions are shown in figures 5.9 and 5.10 for the left and right abutments, respectively. The bearing springs had elastic plastic material models and reached a maximum capacity of 17.79 kips. Shear key springs began to resist seismic forces when the shear key gap was closed at 0.5-inch deck displacement in the transverse direction. The piles/spread springs had a hysteretic bi-linear material model and had larger responses in the transverse direction. The pounding and backfill springs had large forces because of their high stiffness values, which resulted in

smaller displacement response for the bridge in the longitudinal direction than in the transverse direction. Furthermore, the displacement responses were symmetric in the longitudinal direction, which was expected for the left and right abutments.

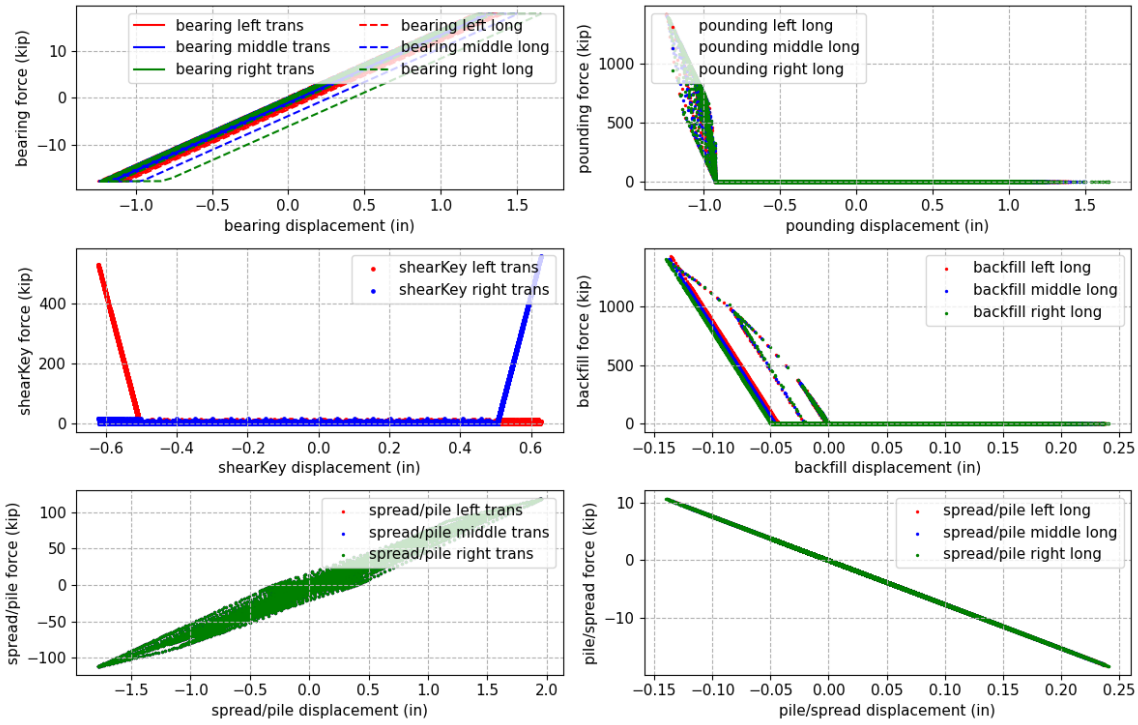

Figure 5.9: Dynamic response of springs at the left abutment

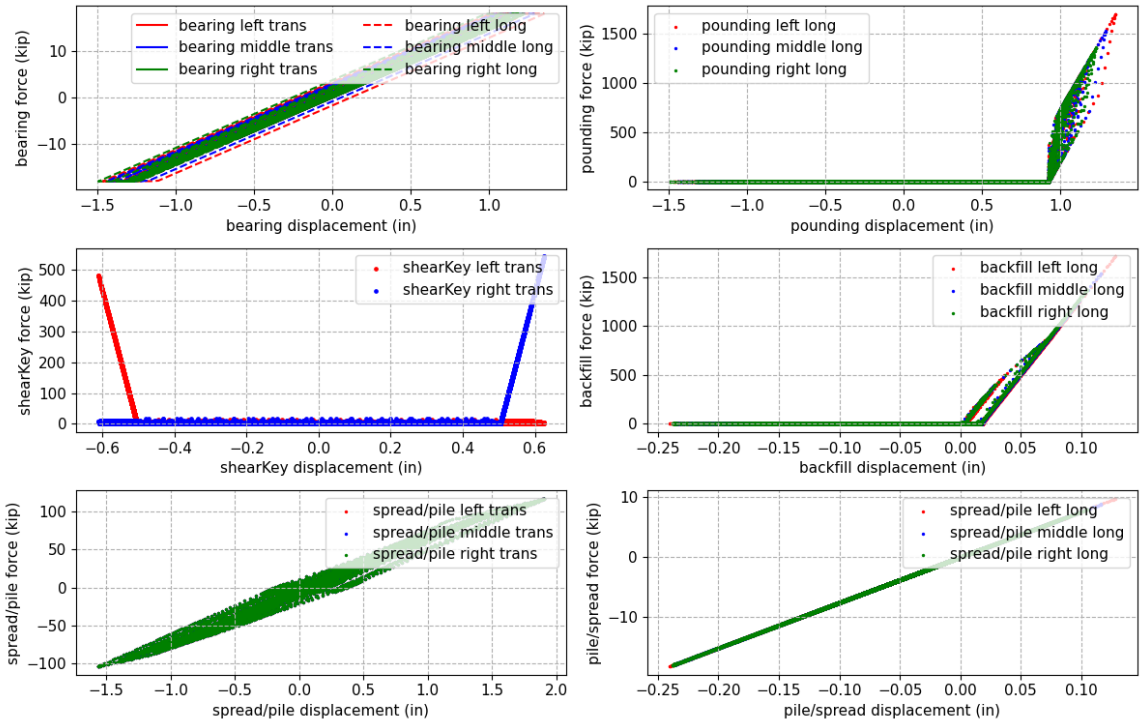

Figure 5.10: Dynamic response of springs at the right abutment

5.4 COMPARISON WITH SDOF BRIDGE MODELS

Kortum et al. (2022) developed an SDOF model methodology to study the impacts of M9 ground motions on highway bridges, without considering the existence of abutments (Section 2.4). The SDOF model used the stiffness and the lateral capacity of the columns along with other input parameters (i.e., the total bridge mass) to approximate the force-displacement response of the entire bridge. This section describes comparisons of dynamic response made between the SDOF model (Kortum et al. 2022) and the MDOF model described in Chapter 4 before the parametric study described in chapters 6, 7, and 8. Furthermore, the MDOF model for the analysis described in this section corresponded to Case 1 shown in Table 5.1, as that was comparable to the SDOF model that neglected the abutment response.

Section 5.4.1 describes the methodology of the comparison, and Section 5.4.2 presents the results of the dynamic analyses for the SDOF and MDOF models.

5.4.1 Pushover Curves

The input effective stiffness and lateral capacity for the SDOF model were derived from the pushover curve of the MDOF model following the recommendations of Elwood-Eberhard (2009). The resulting bi-linear force-displacement relationship was then used for the SDOF model. Figure 5.11 shows the definition of the measured yield displacement and the effective stiffness that were used to construct the bi-linear force-displacement relationship for the SDOF.

The effective stiffness of the bridge was calculated by connecting the origin with the point of first yield of steel (most outer steel strain equal to 0.002). The lateral capacity of the bridge was the force where the extension of this curve intersected with the point where the concrete strain equaled 0.004. The line was then continued with a slope of 1.5 percent. Figure 5.12 shows the MDOF pushover curve along with the bi-linear force-displacement relationship following the recommendations of Elwood-Eberhard (2009). The resulting curve had an effective stiffness of 377.66 kip/in and a lateral capacity of 710 kips.

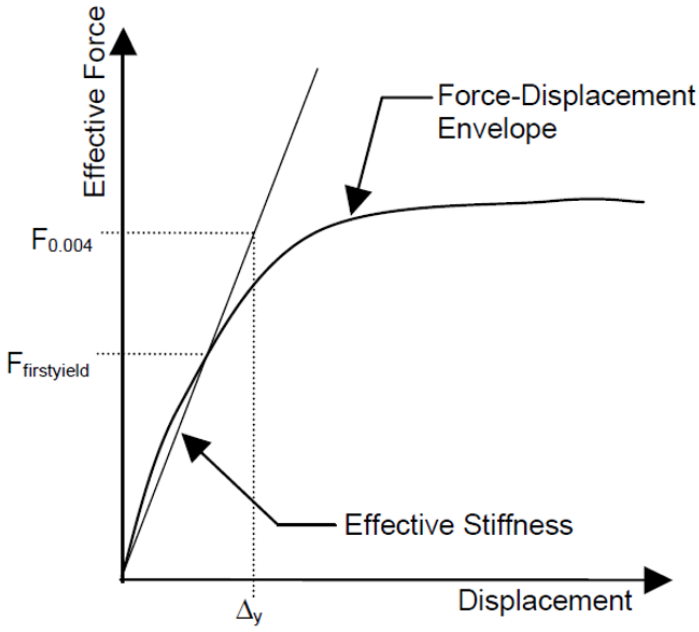

Figure 5.11: Definition of measured yield displacement and effective stiffness

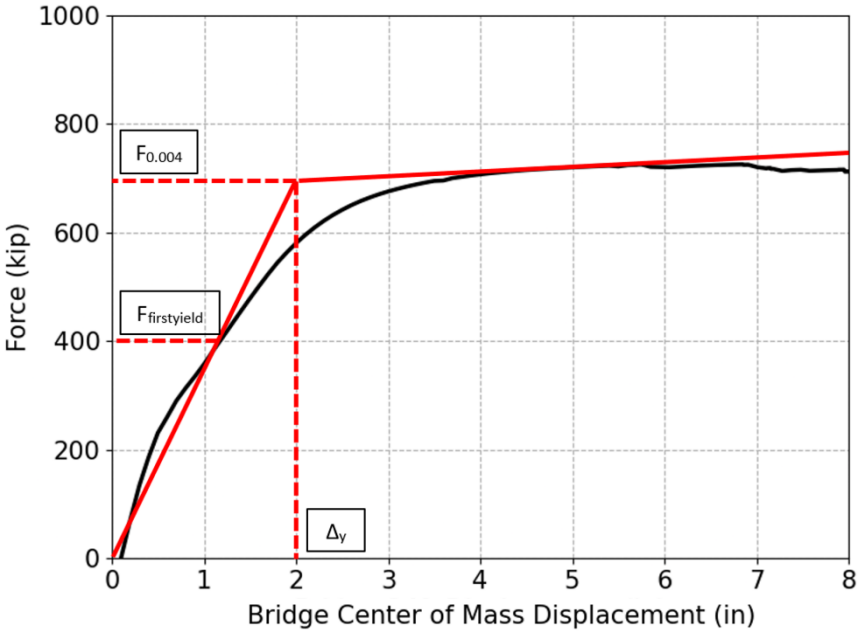

Figure 5.12: Pushover curve for the Case 1 MDOF model (black) and the bi-linear (red) curves

5.4.2 Comparison of MDOF and SDOF Dynamic Responses

The M9 ground motions used for comparing the dynamic response of the SDOF model and the MDOF model are listed in Table 5.2. Ground motions from two cities (Ocean Shores and Seattle) were chosen. For each location the x-component of all 30 realizations were run, each using ten randomly chosen soil profiles for site class C2. This resulted in a total of 600 analyses (300 for each city). The ground motions were applied in the transverse directions of both the MDOF and SDOF model.

Table 5.2: Selected ground motions for comparison of the dynamic response of the SDOF and MDOF bridge models

Cities	Number of Realizations	Site Class	Soil profile category	Direction	Number of ground motions
Ocean Shores	30	C2	Random 10	X	300
Seattle	30	C2	Random 10	X	300

Figures 5.13 and 5.14 compare the maximum displacement dynamic response for the SDOF and MDOF models for Ocean Shores and Seattle. The displacement responses

for Ocean Shores were larger than those for Seattle. For both cities, the responses of the SDOF and the MDOF models were close to each other, as illustrated by how close they track to the 1-to-1 line in the figures. These results provided confidence in the dynamic results of the more complicated MDOF mode.

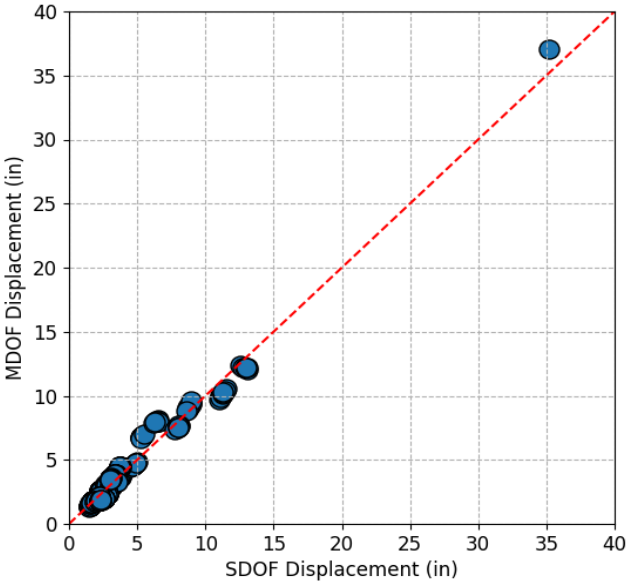

(a)

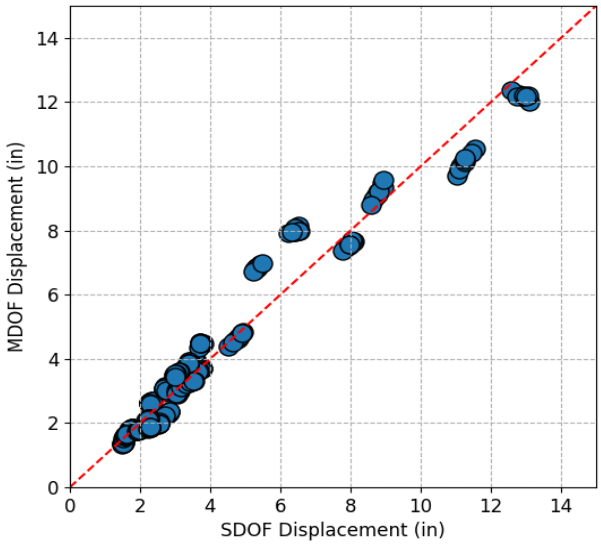

(b)

Figure 5.13: Comparison of dynamic responses of the SDOF and MDOF models for Ocean Shores for (a) all data, (b) data between 0 and 15 inches of bridge displacement

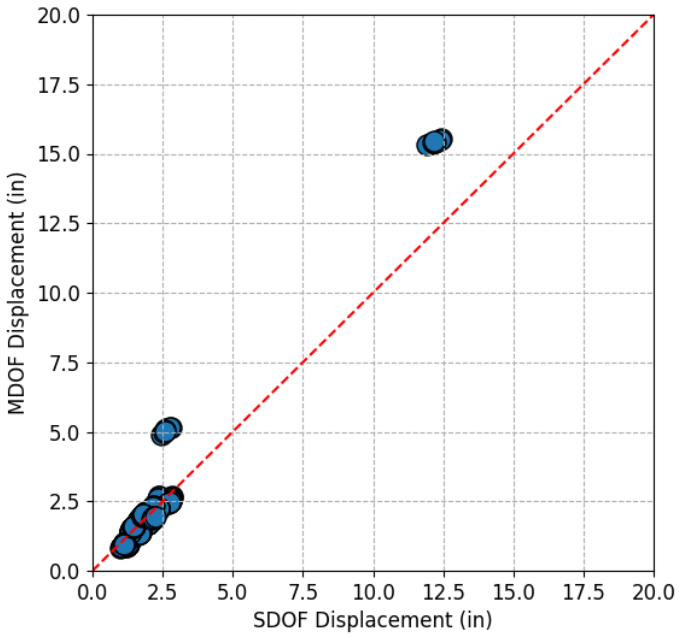

(a)

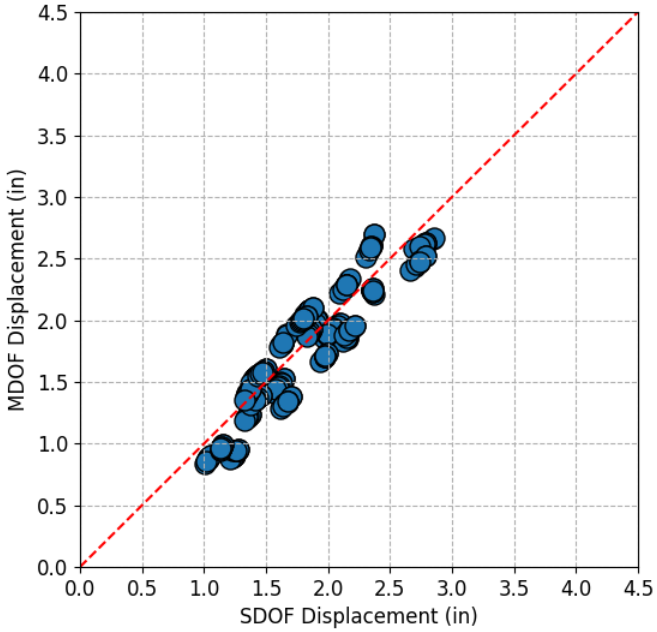

(b)

Figure 5.14: Comparison of dynamic responses of the SDOF and MDOF models for Seattle. (a) Figure shows all data, (b) Figure shows the data between 0 and 4.5 inches of bridge displacement

CHAPTER 6 EFFECTS OF GEOGRAPHIC LOCATION AND SITE CLASS

This chapter describes a parametric study of the effects of geographic location, site class, and baseline ground motions (Section 2.3) on the simulated performance of the reference bridge during an M9 CSZ earthquake. The development of the ground motions is described in Chapter 2, the OpenSeesPy model of the reference bridge is discussed in Chapter 4, and the behavior of that model is examined in Chapter 5.

The ground motions used for the parametric study included all 30 realizations (Section 2.3) of the M9 ground motions (Frankel et al. 2018). For each simulation, the orientation of the horizontal components (North-South or East-West) were randomly assigned to the transverse and longitudinal directions of the bridge model. The parametric study was conducted using the Stampede2 supercomputer at the Texas Advanced Computing Center (TACC) at the University of Texas at Austin.

Sections 6.1 and 6.2 discuss the selection of geographic locations and site classes, respectively, for the parametric study. Section 6.3 discusses the effects of geographic location and site class on the deformation demands for the reference bridge. Sections 6.4 and 6.5 provide estimates of the likelihood of column spalling and bar buckling, and Section 6.6 discusses the force demands. Lastly, in Section 6.7, the effects of individual earthquake scenarios (30 realizations) on the reference bridge are presented.

6.1 SELECTION OF REPRESENTATIVE LOCATIONS

In their SDOF studies, de Zamacona (2019) and Kortum et al. (2022) selected ten locations (Section 2.2) to represent a variety of source-to-site distances and basin depths. The three-dimensional MDOF model developed for this parametric study required considerably more computational effort per simulation than the SDOF models, so to reduce the computational demands, this study considered only six of these ten locations while maintaining a variety of geographic locations and basin depths. Table 6.1 lists some of the key characteristics of these cities. All six selected cities were included in the analyses of the reference bridge, but only three of them were selected for the abutment (Chapter 7) and column (Chapter 8) parametric studies.

Table 6.1: Selected representative locations

City Name	Latitude	Longitude	Basin Depth $Z_{2.5}$ (km)	Site Classification	Analyses Performed
Forks	47.9504	-124.386	0.76	Coastal, Outside of Basin	Reference Bridge Only (Ch. 6)
Ocean Shores	46.9737	-124.156	0.98	Coastal, Outside of Basin	All Bridge Cases (Ch. 6, 7 and 8)
Port Angeles	48.1181	-123.431	2.29	Inland, Shallow Basin	All Bridge Cases (Ch. 6, 7 and 8)
Olympia	47.0379	-122.901	1.96	Inland, Outside of Basin	Reference Bridge Only (Ch. 6)
Seattle	47.6062	-122.332	6.70	Inland, Deep Basin	All Bridge Cases (Ch. 6, 7 and 8)
Everett	47.979	-122.202	3.42	Inland, Deep Basin	Reference Bridge Only (Ch. 6)

6.2 SELECTION OF REPRESENTATIVE SOIL PROFILES

De Zamacona (2019) and Kortum et al. (2022) used 30 soil profiles (Section 2.4) to represent the variation in soil profiles within each of four site classes (C2, C4, D1 and D3). These profiles are listed in Table 6.2. To reduce computational demands, ten of the 30 soil profiles were randomly selected (for each combination of city, site class, and realization) for this study. The selection procedure resulted in 300 analyses (30 realizations times ten randomly selected soil profiles) for each combination of location and site class (Section 2.4). To evaluate the impacts of selecting the profiles, the results for Ocean Shores were compared for analyses, including all 30 soil profiles, with the results using ten randomly selected soil profiles. The differences were negligible. This suggests that the downsizing of the 30-soil profile set (300 combinations, rather than 900 combinations) did not significantly affect the results of the analyses. This downsizing was used in the parametric study discussed in this chapter, as well as in the studies discussed in chapters 7 and 8.

Table 6.2: Soil profile identifiers used for random selection (Adhi et al. 2017)

Site Class C2	Site Class C4	Site Class D1	Site Class D3
WA-DNR-08_87	7026	WA-DNR-08_210	DOGAMI-13_196
WA-DNR-08_90	WA-DNR-08_69	WA-DNR-08_24	WA-DNR-08_196
WA-DNR-08_41	KIMB-1	WA-DNR-08_68	DOGAMI-13_179
SFER	WA-DNR-08_91	DOGAMI-13_255	SCPT94-1
WA-DNR-08_57	WA-DNR-08_14	DOGAMI-13_74	DOGAMI-13_233
WA-DNR-08_164	PCFR	WA-DNR-08_39	FD86-4
WA-DNR-08_161	DOGAMI-13_132	WA-DNR-08_171	DOGAMI-13_131
ALKI	WA-DNR-08_20	7041	DOGAMI-13_223
GL2	WISH	DOGAMI-13_89	SCP95-24
WA-DNR-08_85	WA-DNR-08_73	LAWT	DOGAMI-13_123
BUCK	DOGAMI-13_79	WA-DNR-08_97	WA-DNR-08_225
HAO	DOGAMI-13_146	7043	DOGAMI-13_180
LTY	WA-DNR-08_12	WA-DNR-08_172	DOGAMI-13_141
DOGAMI-13_102	WA-DNR-08_45	WA-DNR-08_165	WA-DNR-08_190
WA-DNR-08_21	WA-DNR-08_217	ROSS	FD97-5
WA-DNR-08_77	LANE	DOGAMI-13_187	WA-DNR-08_143
WA-DNR-08_231	WA-DNR-08_28	WA-DNR-08_123	WA-DNR-08_5
WA-DNR-08_3	WA-DNR-08_75	DOGAMI-13_106	DOGAMI-13_20
WA-DNR-08_26	WA-DNR-08_187	DOGAMI-13_78	DOGAMI-13_38
BEVT	MRIN	WA-DNR-08_121	WA-DNR-08_232
WA-DNR-08_62	DOGAMI-13_76	WA-DNR-08_65	DOGAMI-13_181
WA-DNR-08_128	WA-DNR-08_175	WA-DNR-08_129	DOGAMI-13_98

Site Class C2	Site Class C4	Site Class D1	Site Class D3
WA-DNR-08_176	WA-DNR-08_219	WA-DNR-08_33	DOGAMI-13_31
WA-DNR-08_44	WA-DNR-08_81	WA-DNR-08_208	DOGAMI-13_28
WA-DNR-08_36	DOGAMI-13_114	7027-A	WA-DNR-08_46
WA-DNR-08_6	WA-DNR-08_83	DOGAMI-13_164	WA-DNR-08_199
LYNC	7034	DOGAMI-13_150	WA-DNR-08_115
WA-DNR-08_18	QKTN	2172	WA-DNR-08_234
ERW	WA-DNR-08_151	WA-DNR-08_169	DOGAMI-13_64
BH_DEEPBH	SEW	WA-DNR-08_48	KNEL

6.3 EFFECTS ON DEFORMATION DEMANDS

This section presents the results of the parametric study on the effects of geographic location (Section 6.1) and site class (Sections 6.2) on the computed deformation demands induced by the M9 earthquake motions on the reference bridge.

The computed maximum displacements at the ends of the bridge in the transverse and longitudinal directions are summarized in Figure 6.1. Specifically, the figure shows the 15th, 50th (median), and 85th percentiles of displacement at the end of the superstructure as a function of location (six cities) and site class (baseline, C2, C4, D1, and D3). These displacements were slightly higher than the displacements of the foundations because the reference bridge model included a 0.5-in. gap between the end of the superstructure and shear key (transverse direction) and backwall (longitudinal direction). The cities were arranged in the same order that they are listed in Table 6.1 and were characterized as follows: coastal outside of basin (Forks, Ocean Shores), inland shallow basin (Port Angeles), inland outside of basin (Olympia), and inland deep basin (Seattle, Everett). Note that Port Angeles is closer to the Cascadia Rupture Zone than are the other inland cities.

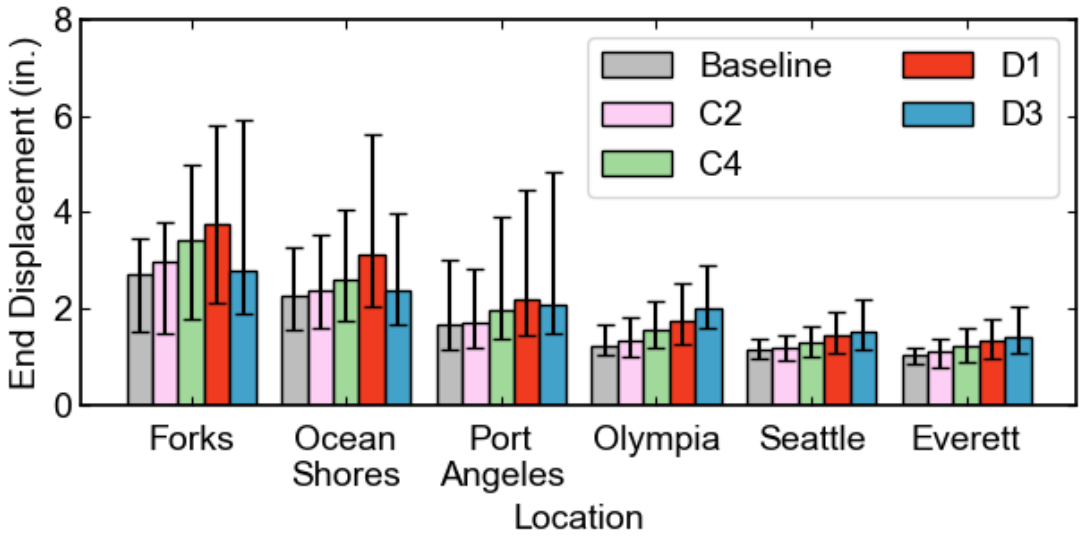

(a) Transverse direction

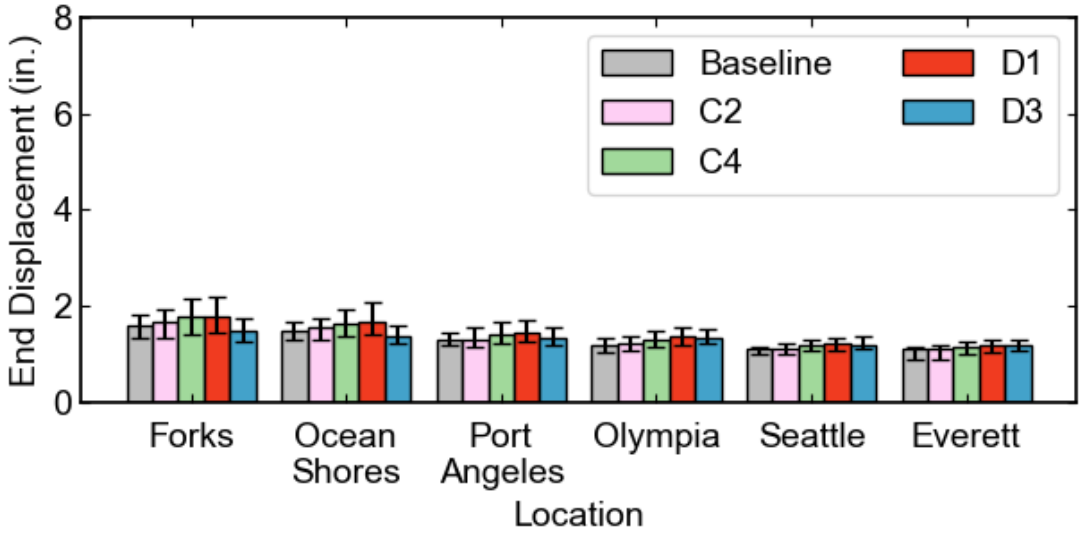

(b) Longitudinal direction

Figure 6.1: Effects of location and site class on maximum displacements at the end of the deck

Following a similar format, Figure 6.2 summarizes the maximum drift ratios for the bents in the transverse and longitudinal directions. The drift ratios were calculated as the maximum displacement (of either bent) divided by the clear column height, which was equal to 21.3 ft (256 inches) for the reference bridges. Correspondingly, a bent drift ratio

of 1.0 percent corresponded to a bent displacement of 2.6 inches. By comparison, the calculated effective bent yield displacement (Section 5.4.1) was 1.88 inches for the reference bridge, which corresponded to a drift ratio of 0.73 percent. Note that the relative magnitudes of the values in figures 6.1 and 6.2 are similar because the superstructure was stiff in comparison to the columns.

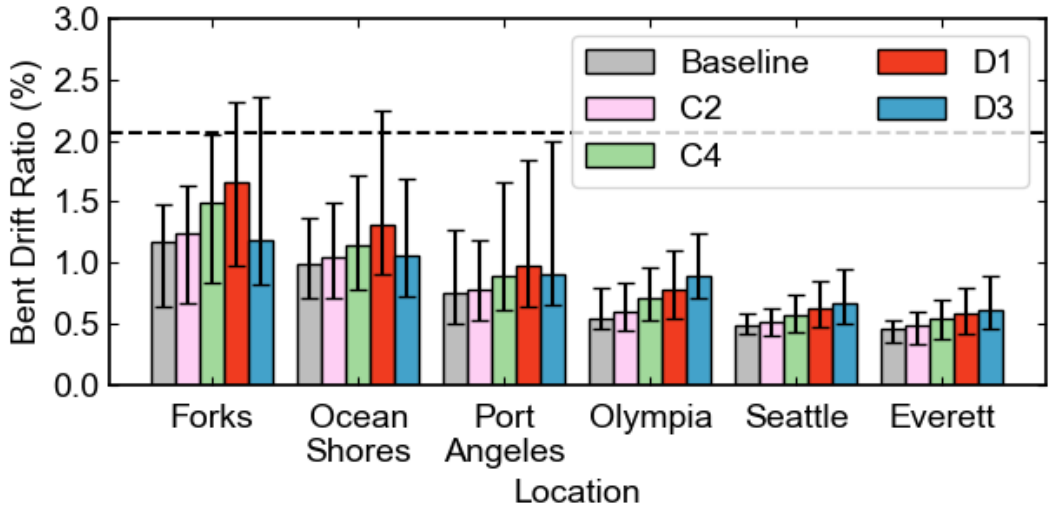

(a) Transverse direction

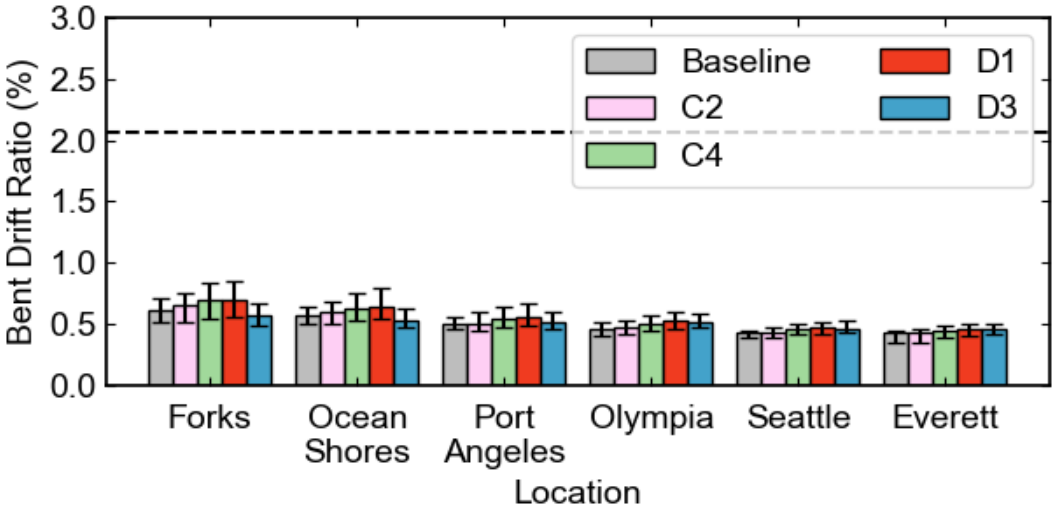

(b) Longitudinal direction

Figure 6.2: Effects of location and site class on maximum bent drift ratio (Dashed line corresponds to spalling of column concrete cover)

Some key observations from figures 6.1 and 6.2 are as follows:

- In the longitudinal direction, the computed end displacements and bent drift ratios varied little among the various locations and site classes. The longitudinal displacements were consistently small, reflecting the displacement constraint provided by the foundation backwall, backfill soil, and pounding element. Across all six cities, the largest median longitudinal end displacement was equal to 1.79 inches, and the largest median longitudinal bent drift ratio was equal to 0.69 percent, which was below the drift ratio at the effective yield (0.74 percent). Even the 85th percentile values were small, reaching maximum values of 2.19 inches at the ends and 0.85 percent for the bent columns (Forks, Site Class D1).
- In the transverse direction, the median displacement responses tended to increase as the site classes became softer, but the site class that resulted in the maximum response at each location varied among the locations. The largest responses for the three cities closest to the coast (Forks, Ocean Shores, and Port Angeles) occurred for Site Class D1. The largest responses for the cities located farther inland occurred for Site Class D3.
- In the transverse direction, the coastal locations (Forks and Ocean Shores) had the largest displacement responses. The largest median end displacements (Figure 6.2) and bent drift ratios (Figure 6.3) were 3.7 in. and 1.65 percent (Site Class D1, Forks). The corresponding 85th percentile values were 5.9 in. and 2.35 percent.
- The magnitudes of the transverse displacements tended to decrease as the distance from the coast increased. The median transverse displacements were 2 inches or less at the bridge ends, and the median bent drifts were less than 0.8 percent for the two cities located farthest from the coast and on deep basins (Seattle and Everett). The largest median end displacement and bent drift ratio for Seattle were 1.52 in. and 0.66 percent (Site Class D3). The corresponding 85th percentile values were 2.16 in. and 0.94 percent.

6.4 EFFECTS ON THE LIKELIHOOD OF COLUMN CONCRETE SPALLING

The bent drift ratios reported in Figure 6.2 were compared with the estimates of the drift ratios at the onset of column spalling. This damage state is important because spalling

generally represents the first level of column damage that may require significant repairs. The median drift ratio at onset of spalling of the column concrete was computed following the recommendations of Berry and Eberhard (2003, 2007):

$$\frac{\Delta_{sp,calc}}{H_{col}}(\%) = 1.6\left(1 - \frac{P}{A_g f_c'}\right)\left(1 + \frac{L}{10D}\right) \qquad \textit{(Equation. 6-1)}$$

where the axial-load ratio, $\frac{P}{A_g f_c'}$, was taken as 0.05, and the ratio of the distance to the inflection point, normalized by the column depth, was taken as $\frac{21.3/2\ (ft)}{3\ (ft)} = 3.55$. The resulting calculated median drift ratio at spalling was 2.1 percent, which is shown as a horizontal, dashed line in Figure 6.2. In the longitudinal direction, the 85th percentile bent drift ratios were far below the median spalling values for all cities and soil classes. In the transverse direction, the median values never exceed 2.1 percent, but the 85th percentile values did exceed this value for the two coastal cities (Forks, Ocean Shores).

The accuracy of Equation 6-1 is shown evaluated in Figure 6.3 (Berry and Eberhard 2003) for a set of experimental observations of concrete spalling for spiral-reinforced concrete columns. The maximum observed drift ratio at concrete spalling was 195 percent of the calculated value, and the minimum observed drift ratio was 45 percent of the calculated value. The uncertainty in the drift ratio at spalling can be represented with a lognormal distribution with a coefficient of variation of 35 percent.

For each combination of location and site class, the ratio of the demand to capacity was calculated for each of the 300 combinations (30 realizations times ten soil profiles) by dividing the column deformation demand for each combination by the value calculated with Equation 6-1. The likelihood of concrete spalling for each combination was then calculated as the value of the lognormal distribution (median = 1.0, COV = 35 percent) for that ratio. Assuming that each simulation and soil profile was equally probable, the overall likelihood of spalling was calculated as the average of the 300 estimates of likelihood of concrete spalling.

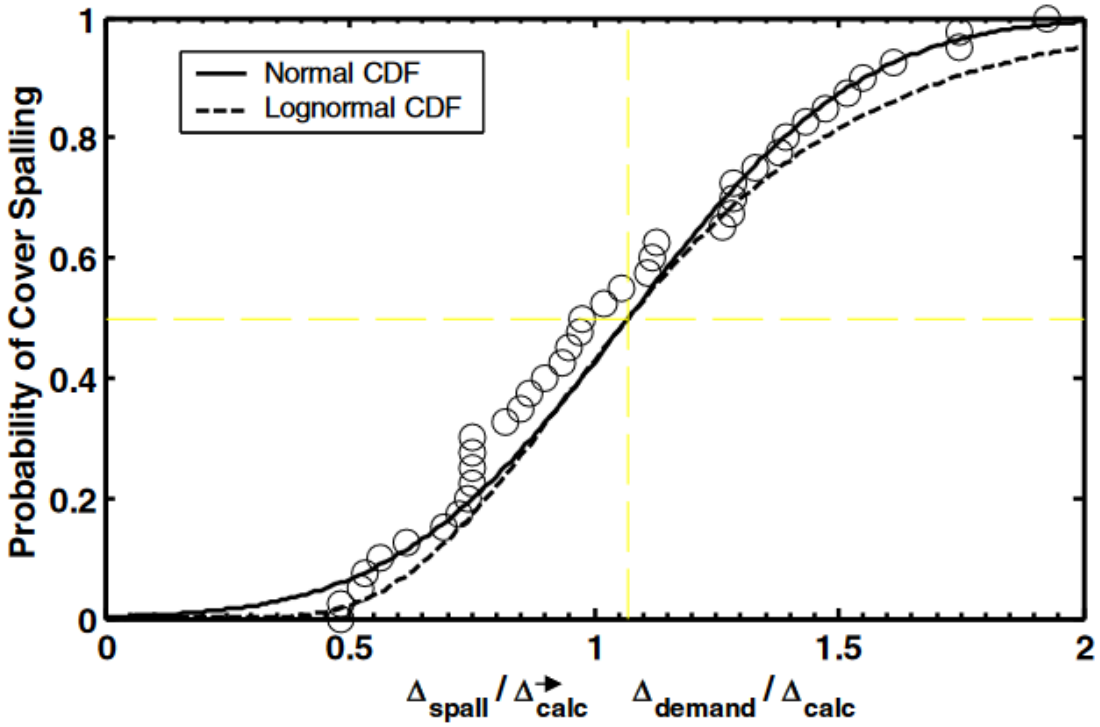

Figure 6.3: Likelihood of column concrete spalling as a function of normalized deformation demand (Berry and Eberhard 2007)

Figure 6.4 shows the calculated likelihood of concrete cover spalling for each combination of location and site class. In comparison with the other cities, the likelihoods of concrete spalling were much higher for the two coastal cities (Forks and Ocean Shores). For Forks, the likelihood of spalling ranged from 12.6 percent (Site Class C2) to 31.3 percent (Site Class D1), with the site classes C4 and D3 falling in between. The likelihood of concrete spalling for Ocean Shores followed the same pattern, but the maximum value (Site Class D1, 23.2 percent) was smaller. In contrast, the likelihoods of spalling for the inland cities (Olympia, Seattle, and Everett) reached a maximum of 4.6 percent for Site Class D3 in Olympia. The spalling probabilities for Port Angeles fell between the values for the coastal cities and cities that were located farther inland.

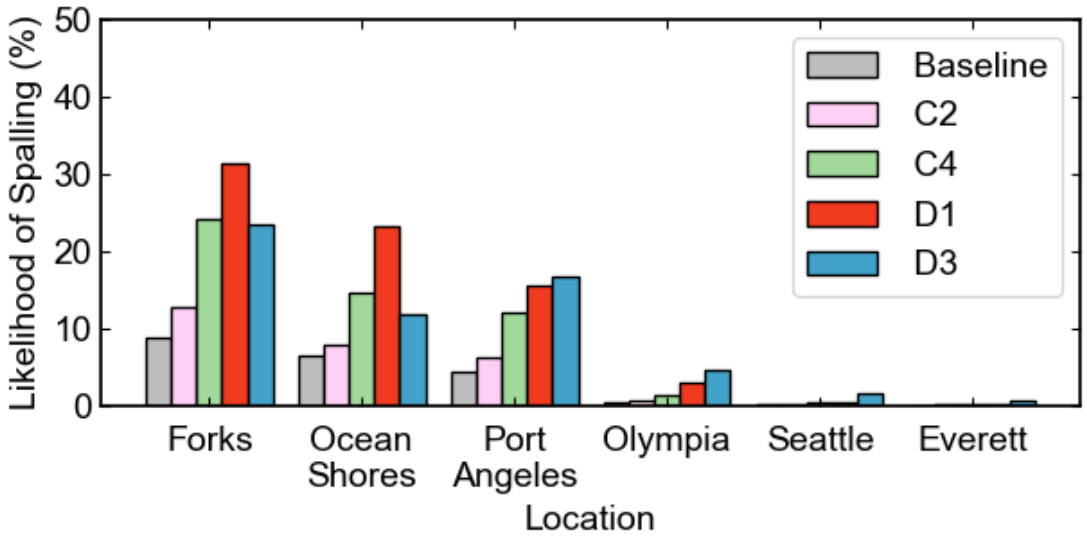

Figure 6.4: Effects of location and site class on the likelihood of column concrete cover spalling

6.5 EFFECTS ON THE LIKELIHOOD OF COLUMN BAR BUCKLING

The drift ratios in Figure 6.2 can also be compared with estimates of the drift ratios at the onset of buckling of the column longitudinal bars. This damage state is important because bar buckling represents a severe form of damage that may require expensive repairs, long-term bridge closure, and possibly column replacement.

The mean drift ratio at the onset of buckling of the column longitudinal bars was calculated following the recommendations of Berry and Eberhard (2005, 2007), where the median drift ratio causing bar buckling was given by:

$$\frac{\Delta_{bb,calc}}{H_{col}}(\%) = 3.25(1 + k_{e,bb}\rho_{eff}\frac{d_b}{D})(1 - \frac{P}{A_g f_c'})(1 + \frac{L}{10D}) \qquad \textit{(Equation. 6-2)}$$

where $k_{e,bb}$ was taken as 150, and the ratio of the longitudinal bar diameter to the column depth, $\frac{d_b}{D}$, was taken as 0.0313. The quantity $\rho_{eff} = \rho_s \frac{f_{ys}}{f'_c}$, where ρ_s is the volumetric transverse reinforcement ratio, f_{ys} is the yield stress of the transverse reinforcement, and f'_c is the concrete compressive strength, was taken as 0.058 for the reference bridge. Based on Equation 6.2, the mean drift ratio at the onset of bar buckling was 5.3 percent. For the reference bridge, this drift ratio at bar buckling greatly exceeded the 85th percentile values

of bent deformation demands for all combinations of location and site class. Therefore, bar buckling was expected to occur seldomly for all locations.

For a set of spiral-reinforced concrete columns, Figure 6.5 shows an evaluation of the likelihood of bar buckling as a function of the ratio of the column deformation demand to the drift ratio calculated with Equation 6-2. All the observed demand/capacity ratios fall between ratios of 0.65 and 1.45. The uncertainty in the drift ratio at spalling can be represented with lognormal distribution with a coefficient of variation of 25 percent.

For each combination of location and site class, the ratio of the deformation demand to capacity was calculated for each of the 300 combinations (30 realizations and ten soil profiles) by dividing the column deformation demand for each combination by the value calculated with Equation 6-2. The likelihood of bar buckling for each combination was calculated as the value of the lognormal distribution (median = 1.0, COV = 25 percent) for that ratio. Assuming that each simulation and soil profile was equally probable, the overall likelihood of buckling was calculated as the average of the 300 estimates of likelihood of bar buckling.

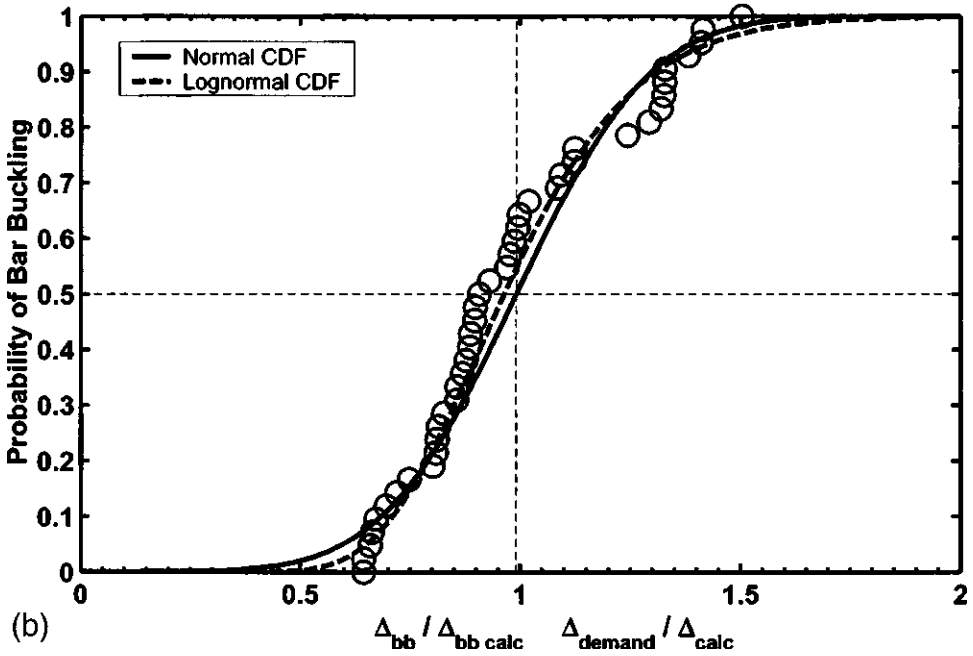

Figure 6.5. Likelihood of bar buckling as a function of normalized deformation demand (Berry and Eberhard 2005)

Figure 6.6 shows the calculated likelihood of the onset of buckling of the longitudinal bars. As expected from the deformation demands (Figure 6.2), the likelihoods of bar buckling were far below the likelihoods of column concrete spalling. Depending on the particular city and soil class, the likelihood of bar buckling for the three cities nearest the coast ranged from 0.01 percent to 7.9 percent. The likelihoods of bar buckling were even smaller for the three most inland cities, reaching a maximum of only 0.31 percent.

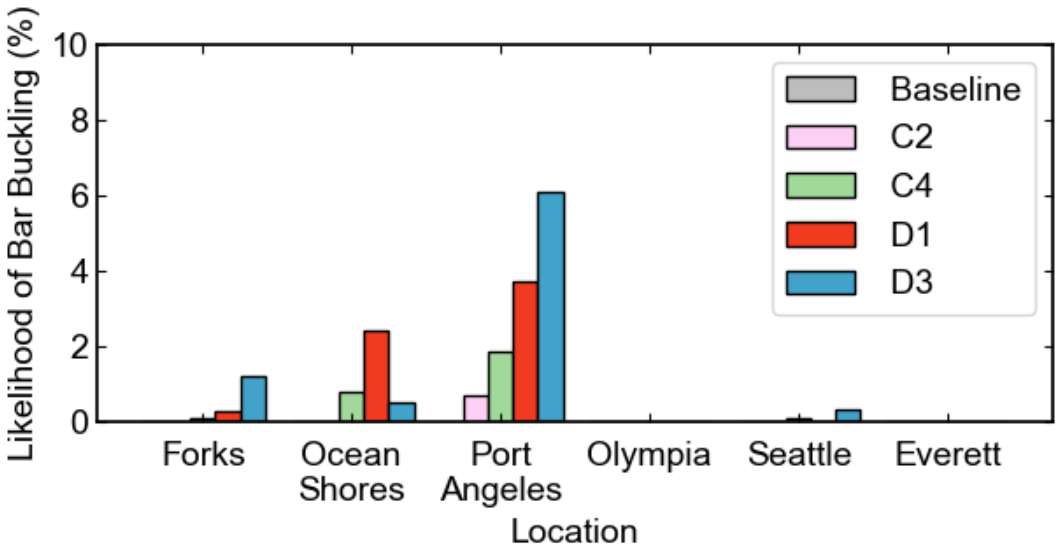

Figure 6.6: Effects of location and site class on the likelihood of onset of buckling of column longitudinal bars

6.6 EFFECTS ON MAXIMUM FORCES

This section presents the results of the parametric study of the effects of geographic location (Section 6.1) and site class (Section 6.2) on the computed column and shear-key force demands induced by the earthquake motions for the reference bridge.

Figure 6.7 shows the maximum sum of column lateral forces normalized by the bridge weight (2,066 kips). The lateral load at effective yield was 118 kips for each column, so the sum of the column resistances at effective yield of the six columns was approximately equal to 710 kips (Section 5.4.1), which corresponded to a base-shear strength ratio of 0.32. This value is shown as a horizontal dashed line in Figure 6.7.

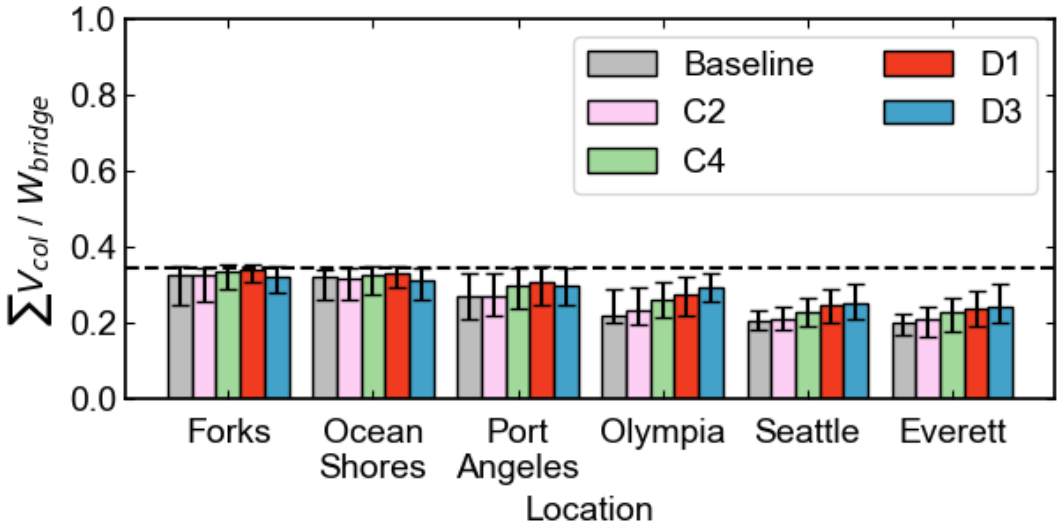

(a) Transverse direction

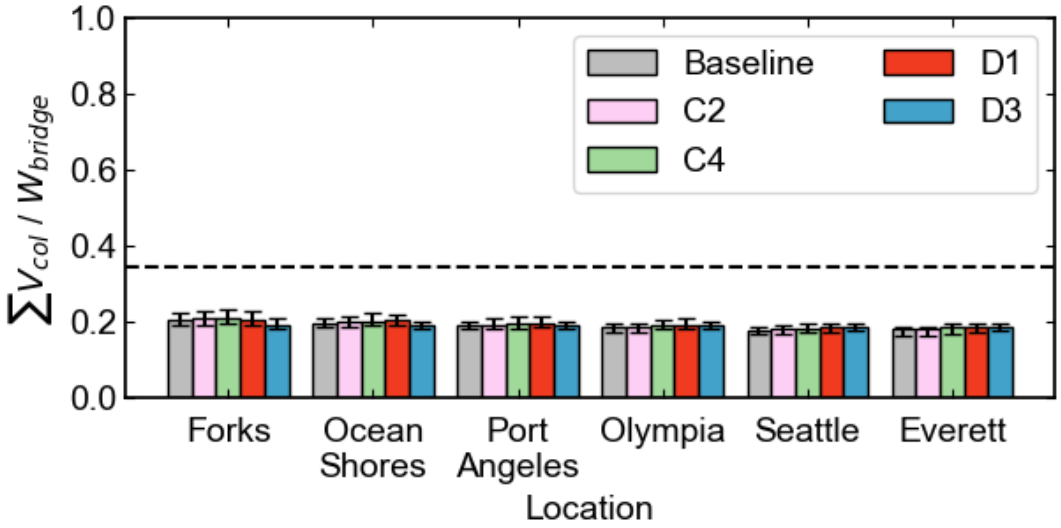

(b) Longitudinal direction

Figure 6.7: Sum of column maximum lateral forces normalized by bridge weight for median, 15th, and 85th percentiles. (Dashed line represents the effective yield of the bridge columns)

In the longitudinal direction, the computed column horizontal forces varied little among the various locations and site classes. Because of the constraint provided by the foundation backwall and backfill soil in the longitudinal direction, the column forces were consistently small. Across all six cities, the median longitudinal sum of column forces

never exceeded 20 percent of the bridge weight, which corresponded to 58 percent of the effective yield force. The 85th percentile values never reached 23 percent of the bridge weight, which corresponded to 67 percent of the effective yield force.

In the transverse direction, the sums of the column horizontal forces were considerably larger than those in the longitudinal direction. For the two coastal cities, both the median and 85th percentile values of column resistance were near the yield values for all site classes. The forces were largest in the coastal cities for site class D1, but the effect of site class was small.

The maximum column forces tended to decrease with increasing distance from coast. As the location moved inland, the responses of the softest soil site class (D3) in the transverse direction increased in comparison to the responses for other soil site classes at the same location.

Figure 6.8 shows the maximum sum of the shear key transverse lateral forces normalized by bridge weight. The shear capacity of each modeled shear-key element was calculated as 2,240 (kips) (Section 4.4.3), which corresponded to the resistance provided by the five internal shear keys of the reference bridge. So each shear-key element had a total capacity of 4,481 (kips), which corresponded to a lateral strength ratio of 2.17 (with respect to bridge weight), which is shown as a horizontal, dashed in Figure 6.8.

The trends in shear-key forces were similar to the trends in maximum column forces. The shear-key forces were highest in coastal cities (for Site Class D1) and tended to decrease with increasing distance from the coast. As the location moved inland, the forces at each location tended to increase as the soil site class became softer. Most importantly, regardless of the location and site class, the force demands on the shear keys were far below their calculated capacity. The maximum 85th percentile value for the shear-key force (Forks, site class D1) was only 34 percent of the nominal capacity of the shear key.

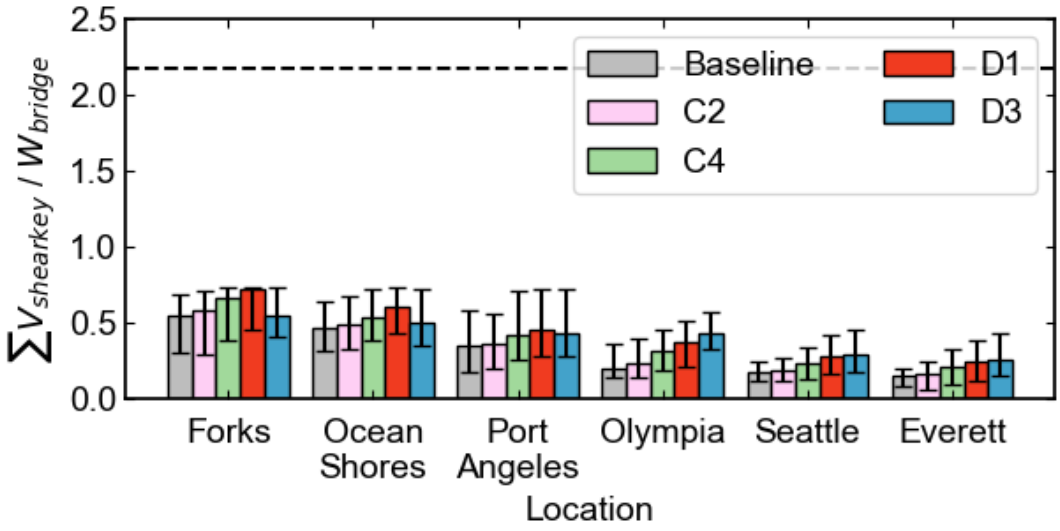

Figure 6.8: Effects of location and site class on sum of shear key maximum transverse force normalized by bridge weight. (Black dashed line represents the capacity of shear keys)

6.7 VARIATIONS OF BENT DRIFT RATIOS AMONG EARTHQUAKE SCENARIOS

In the previous sections, the reported 15th percentile, median, and 85th percentile values were computed by combining the results of all 30 possible earthquake rupture scenarios and ten soil profiles, resulting in 300 realization-profile combinations for each city and site class. This section investigates the variability of the individual earthquake scenarios in relation to the performance of the reference bridge. This information is reported for three cities: Ocean Shores, Port Angeles, and Seattle.

Figure 6.9 and Table 6.3 show the 15th percentile, median, and 85th percentile of the maximum bent transverse drift ratio for Ocean Shores, for the baseline motions, as well as soil site classes C2 and D1. Unlike previous plots, each bar in Figure 6.9 represents the results of analyses of a particular realization (one out of 30) for ten randomly selected soil profiles.

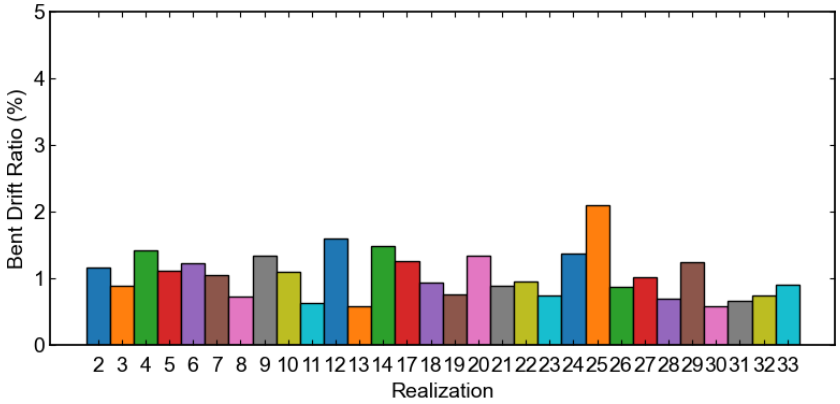

(a) Baseline

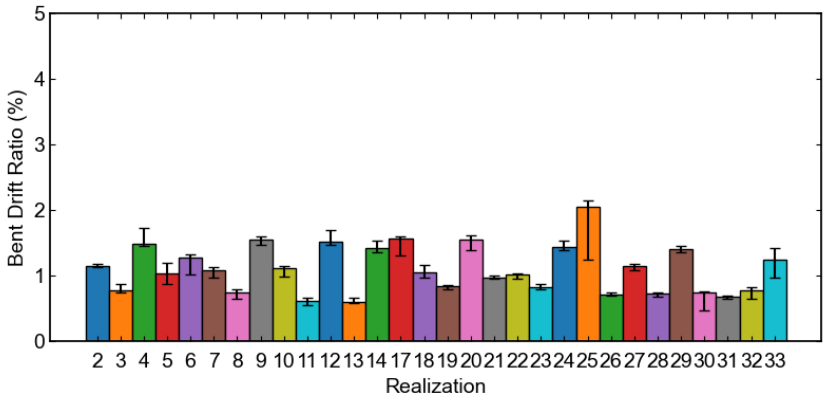

(b) Site class C2

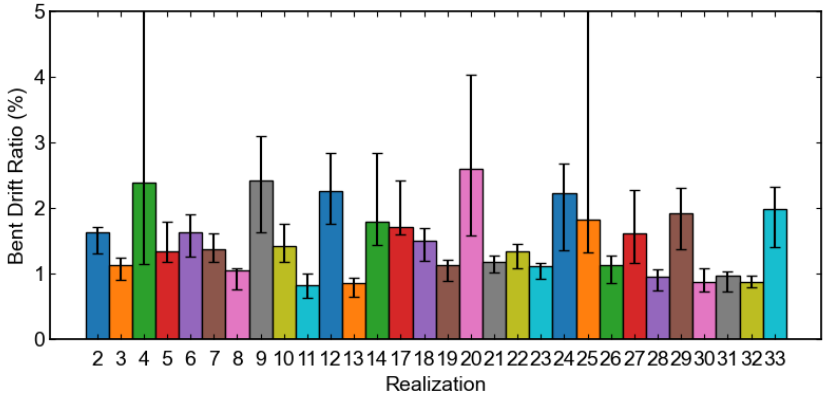

(c) Site class D1

Figure 6.9: Median, 15th, and 85th percentiles of maximum bent drift ratios in the transverse direction for Ocean Shores

Table 6.3: Bent transverse drift ratios for Ocean Shores (%)

Realization	Baseline	C2			D1		
		15th Percentile	Median	85th Percentile	15th Percentile	Median	85th Percentile
csz002	1.163	1.127	1.155	1.181	1.311	1.629	1.712
csz003	0.894	0.750	0.772	0.883	0.901	1.140	1.251
csz004	1.423	1.461	1.481	1.722	1.152	2.391	5.042
csz005	1.123	0.872	1.044	1.194	1.175	1.336	1.797
csz006	1.234	1.026	1.274	1.332	1.261	1.637	1.906
csz007	1.049	0.969	1.083	1.135	1.180	1.371	1.610
csz008	0.737	0.650	0.753	0.794	0.765	1.060	1.083
csz009	1.343	1.474	1.545	1.605	1.633	2.415	3.094
csz010	1.106	0.988	1.117	1.154	1.174	1.417	1.754
csz011	0.634	0.555	0.623	0.659	0.638	0.820	1.000
csz012	1.608	1.476	1.523	1.699	1.760	2.260	2.834
csz013	0.583	0.582	0.595	0.669	0.654	0.859	0.945
csz014	1.492	1.362	1.427	1.531	1.433	1.787	2.837
csz017	1.263	1.317	1.569	1.593	1.598	1.711	2.418
csz018	0.944	0.977	1.046	1.163	1.202	1.497	1.698
csz019	0.770	0.799	0.841	0.867	0.892	1.131	1.217
csz020	1.344	1.386	1.546	1.609	1.581	2.601	4.037
csz021	0.899	0.958	0.973	1.011	1.016	1.186	1.272
csz022	0.951	0.958	1.019	1.036	1.079	1.340	1.450
csz023	0.754	0.794	0.822	0.879	0.918	1.121	1.158
csz024	1.380	1.391	1.443	1.529	1.365	2.224	2.678
csz025	2.098	1.246	2.055	2.150	1.332	1.827	11.030
csz026	0.876	0.703	0.710	0.745	0.861	1.139	1.270
csz027	1.028	1.077	1.143	1.182	1.170	1.620	2.274
csz028	0.698	0.675	0.726	0.741	0.745	0.957	1.064
csz029	1.244	1.361	1.408	1.463	1.379	1.925	2.308
csz030	0.588	0.470	0.741	0.765	0.725	0.876	1.085
csz031	0.667	0.648	0.684	0.700	0.730	0.968	1.031
csz032	0.749	0.655	0.777	0.835	0.790	0.868	0.966
csz033	0.910	0.965	1.247	1.419	1.414	1.993	2.320
Median	0.989	0.967	1.065	1.158	1.172	1.394	1.705
15% Value	0.687	0.649	0.721	0.744	0.740	0.929	1.053
85% Value	1.395	1.388	1.531	1.606	1.485	2.237	2.927

For Ocean Shores, seven rupture scenarios generated the highest drift ratios: csz004, csz009, csz012, csz14, csz17, csz020, and csz025. Among these scenarios, the order of the maximum drift ratios depended on the site conditions. For example, the calculated drift ratios for the baseline motion and Site C2 (the stiffer of the two site classes) motions were significantly larger for the csz25 realization than for the other realizations. In contrast, the largest drift ratios for Site Class D1 were calculated for realizations csz004, csz009, csz012, and csz020. The softer site condition produced larger drift ratios with a large increase in variability due to varying the site profiles. The highest median bent drift ratio was around 2.6 percent (csz020, Site Class D1) with 85th percentile values that exceeded 4 percent. Note that the median drift ratio for that scenario exceeded the median drift ratio at concrete spalling.

Figure 6.10 and Table 6.4 show the maximum bent drift ratios for Port Angeles for all 30 realizations. For most scenarios, the responses for Port Angeles were smaller than those calculated for Ocean Shores. As was the case for Ocean Shores, the drift ratios were larger for the softer soil site class. Three rupture scenarios induced significantly higher responses: csz003, csz019, and csz030. Note that for csz019, the median response exceeded the largest value from Ocean Shores for the same site class, and the highest 85th percentile value exceeded 13 percent. The largest recorded median value was close to 5.6 percent, which was much larger than the highest median response from Ocean Shores.

Figure 6.11 and Table 6.5 show the maximum bent drift ratios for Seattle due to the 30 realizations. The drift ratios were significantly smaller than those calculated for Ocean Shores and Port Angeles. The responses from two rupture scenarios were the largest: csz010 and csz029. The highest median response was close to 1 percent while the highest 85th percentile value was around 1.1 percent. The softer site class was observed to magnify the overall responses across different rupture scenarios.

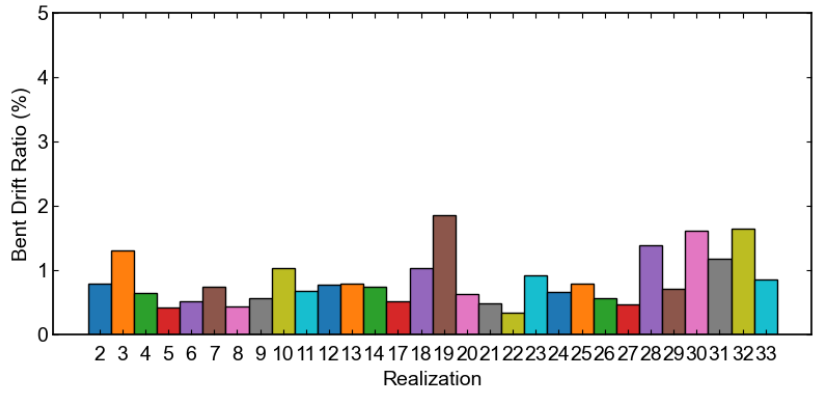

(a) Baseline

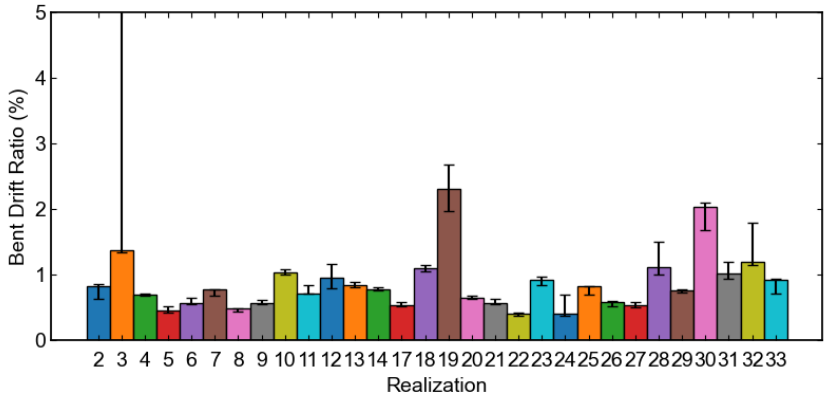

(b) Site class C2

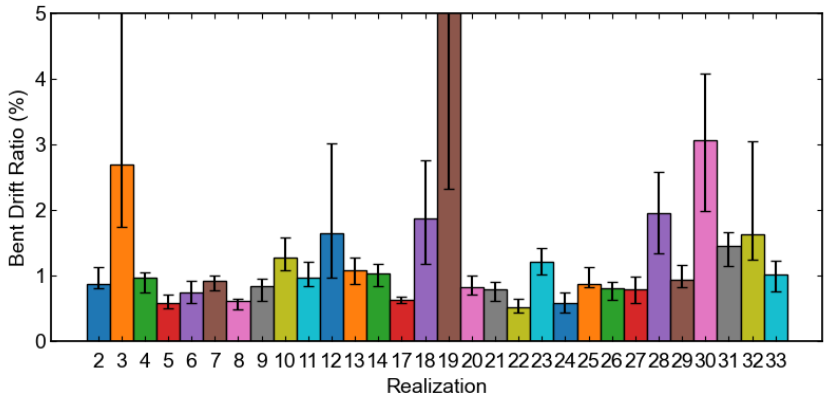

(c) Site class D1

Figure 6.10: Median, 15th, and 85th percentiles of maximum bent drift ratios in the transverse direction for Port Angeles

Table 6.4: Bent transverse drift ratios for Port Angeles, according to realization (%)

Realization	Baseline	C2			D1		
		15th Percentile	Median	85th Percentile	15th Percentile	Median	85th Percentile
csz002	0.795	0.642	0.824	0.855	0.809	0.868	1.139
csz003	1.305	1.346	1.370	7.049	1.752	2.691	10.055
csz004	0.644	0.684	0.703	0.708	0.750	0.967	1.051
csz005	0.421	0.432	0.453	0.517	0.504	0.583	0.720
csz006	0.525	0.552	0.567	0.653	0.588	0.744	0.923
csz007	0.749	0.687	0.778	0.785	0.774	0.923	1.002
csz008	0.440	0.443	0.484	0.494	0.488	0.625	0.656
csz009	0.565	0.552	0.570	0.613	0.617	0.851	0.949
csz010	1.036	1.011	1.037	1.078	1.090	1.286	1.589
csz011	0.687	0.709	0.715	0.844	0.837	0.971	1.208
csz012	0.775	0.790	0.953	1.160	0.976	1.641	3.020
csz013	0.793	0.817	0.846	0.893	0.877	1.083	1.286
csz014	0.752	0.762	0.780	0.816	0.840	1.036	1.174
csz017	0.515	0.526	0.532	0.583	0.587	0.640	0.687
csz018	1.034	1.047	1.100	1.149	1.188	1.877	2.764
csz019	1.858	1.978	2.309	2.685	2.323	5.610	13.865
csz020	0.638	0.639	0.656	0.674	0.707	0.827	1.001
csz021	0.495	0.547	0.573	0.630	0.610	0.795	0.901
csz022	0.350	0.369	0.401	0.421	0.436	0.528	0.649
csz023	0.920	0.841	0.931	0.966	1.015	1.206	1.431
csz024	0.672	0.381	0.411	0.696	0.444	0.581	0.744
csz025	0.802	0.693	0.824	0.834	0.830	0.883	1.129
csz026	0.568	0.515	0.582	0.595	0.629	0.809	0.913
csz027	0.478	0.502	0.535	0.579	0.593	0.790	0.981
csz028	1.394	1.008	1.112	1.497	1.345	1.958	2.583
csz029	0.721	0.736	0.768	0.779	0.821	0.946	1.161
csz030	1.613	1.688	2.034	2.106	1.982	3.064	4.085
csz031	1.177	0.940	1.017	1.202	1.144	1.455	1.659
csz032	1.650	1.155	1.201	1.797	1.249	1.641	3.052
csz033	0.861	0.707	0.916	0.943	0.761	1.017	1.233
Median	0.750	0.700	0.779	0.825	0.815	0.957	1.150
15% Value	0.489	0.482	0.515	0.581	0.558	0.635	0.735
85% Value	1.336	1.085	1.143	1.602	1.283	1.905	3.031

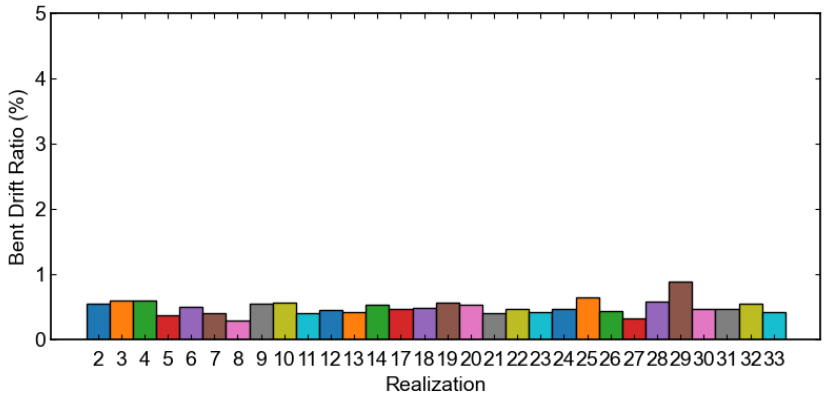

(a) Baseline

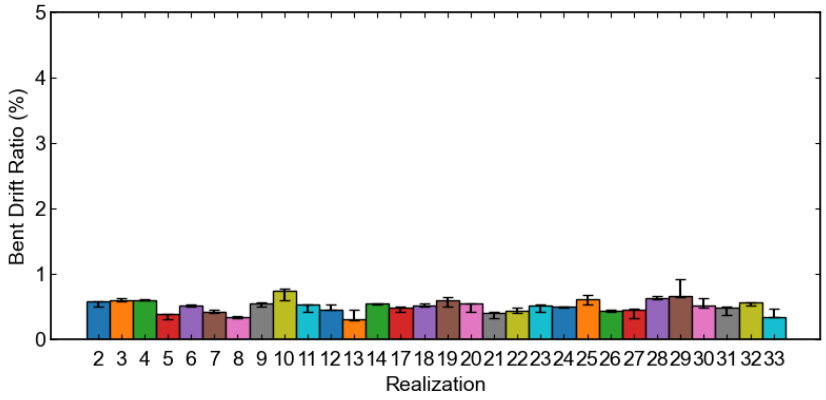

(b) Site class C2

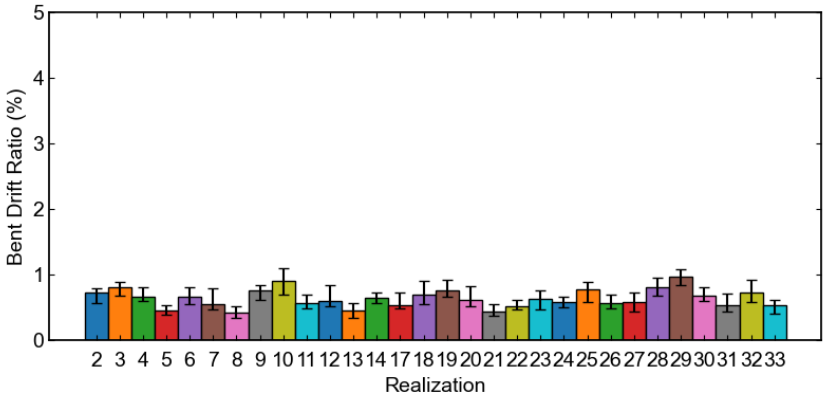

(c) Site class D1

Figure 6.11: Median, 15th, and 85th percentiles of maximum bent drift ratios in the transverse direction for Seattle

Table 6.5: Bent transverse drift ratios for Seattle (%)

Realization	Baseline	C2			D1		
		15th Percentile	Median	85th Percentile	15th Percentile	Median	85th Percentile
csz002	0.560	0.509	0.580	0.588	0.571	0.724	0.797
csz003	0.609	0.589	0.609	0.638	0.685	0.810	0.896
csz004	0.600	0.595	0.603	0.614	0.606	0.673	0.806
csz005	0.380	0.313	0.385	0.399	0.399	0.449	0.533
csz006	0.500	0.506	0.524	0.536	0.561	0.668	0.814
csz007	0.403	0.409	0.421	0.462	0.470	0.559	0.800
csz008	0.301	0.320	0.345	0.352	0.347	0.419	0.524
csz009	0.552	0.500	0.557	0.575	0.611	0.756	0.837
csz010	0.571	0.597	0.747	0.779	0.697	0.900	1.105
csz011	0.406	0.432	0.531	0.539	0.488	0.561	0.700
csz012	0.457	0.460	0.465	0.538	0.521	0.596	0.851
csz013	0.427	0.302	0.308	0.461	0.341	0.462	0.565
csz014	0.544	0.543	0.548	0.561	0.571	0.643	0.732
csz017	0.479	0.432	0.487	0.499	0.490	0.536	0.734
csz018	0.493	0.511	0.518	0.555	0.547	0.703	0.905
csz019	0.570	0.501	0.605	0.650	0.663	0.770	0.928
csz020	0.532	0.419	0.553	0.560	0.517	0.617	0.827
csz021	0.412	0.329	0.414	0.417	0.369	0.436	0.557
csz022	0.479	0.412	0.437	0.489	0.473	0.519	0.616
csz023	0.420	0.428	0.521	0.531	0.467	0.633	0.763
csz024	0.473	0.490	0.497	0.506	0.513	0.592	0.671
csz025	0.657	0.544	0.617	0.679	0.586	0.772	0.892
csz026	0.440	0.426	0.441	0.462	0.483	0.564	0.704
csz027	0.330	0.332	0.457	0.478	0.443	0.589	0.734
csz028	0.582	0.621	0.638	0.660	0.683	0.814	0.951
csz029	0.889	0.650	0.662	0.921	0.836	0.968	1.091
csz030	0.470	0.489	0.529	0.641	0.603	0.676	0.812
csz031	0.473	0.382	0.484	0.501	0.448	0.529	0.715
csz032	0.552	0.513	0.561	0.571	0.579	0.733	0.920
csz033	0.417	0.340	0.347	0.465	0.402	0.545	0.622
Median	0.479	0.474	0.523	0.538	0.519	0.625	0.799
15% Value	0.405	0.331	0.404	0.462	0.401	0.499	0.598
85% Value	0.588	0.591	0.612	0.654	0.670	0.785	0.923

CHAPTER 7 EFFECTS OF ABUTMENT PROPERTIES

This chapter describes a parametric study of the effects of variations in abutment properties on the performance of the reference bridge during an M9 earthquake. In this study, the performance of the bridges was investigated for three cities: Ocean Shores, Port Angeles, and Seattle. Ocean Shores is near the Pacific Coast (and earthquake source), Seattle is located inland on a deep sedimentary basin, and Port Angeles combines an intermediate source-to-site distance and a moderate basin depth. Because of the constraint provided by the abutment resistance in the longitudinal direction (Section 6.3), this chapter discusses only the results in the transverse direction. In the abutment parametric study, the column height remained constant at 21.3 ft, and the transverse reinforcement ratio remained constant at 0.5 percent, which was representative of older bridges.

Section 7.1 discusses how the properties of the abutments were varied in the parametric study. Section 7.2 discusses the effects of abutment configuration, foundation type, and soil type (sand versus clay). Section 7.3 discusses the effects of the contributions of the shear keys and bearing pads.

7.1. VARIATION OF ABUTMENT PROPERTIES

The abutment parametric study considered the following abutment characteristics, which were selected on the basis of the variations of abutment characteristics in the abutment database (Section 3.4):

- Abutment configuration: L, semi-integral, and integral abutment (Section 4.4.1).
- Abutment foundation type: spread footings, piles (Section 4.4.2)
- Soil type: medium sand and medium clay (Section 4.4.2)
- Shear key: present or absent (Section 4.4.3)
- Bearings: present or absent (Section 4.4.4).

Table 7.1 shows the cases considered in the abutment parametric study, which included the reference bridge (Section 3.4, Chapter 6) and six cases that were variations of the reference bridge. Cases 1 and 2 considered the effects of changes in abutment configuration, Case 3 changed the abutment foundation type from piles to spread footings, and Case 4 assumed that the soil at the abutment was medium clay instead of medium sand.

Cases 5 and 6 varied the contributions of the shear keys and bearing pads. Case 5 represented a bridge that does not have shear keys, whereas Case 6 represented a bridge with no transverse resistance at the abutments. This case indirectly represented the response of a bridge with a discontinuous superstructure that cannot transmit lateral forces to the abutments.

Table 7.1: Cases for abutment parametric study

Parameter	**Reference Bridge**	**Case 1**	**Case 2**	**Case 3**	**Case 4**	**Case 5**	**Case 6**
Shear Key Stiffness/Strength	Present	Present	N/A-	Present	Present	**Absent**	**Absent**
Bearing Stiffness/ Strength	Present	Present	N/A-	Present	Present	Present	**Absent**
Abutment Type	L	**Semi-integral**	**Integral**	L	L	L	L
Abutment Foundation Type	Piles	Piles	Piles	**Spread**	Piles	Piles	Piles
Soil Type	Medium sand	Medium sand	Medium sand	Medium sand	**Medium clay**	Medium sand	Medium sand

For each of the 15 combinations of location (three) and site class (four), 300 analyses were performed, corresponding to 30 earthquake rupture scenarios and ten site profiles.

7.2 EFFECTS OF VARIATION IN ABUTMENT AND SOIL TYPES

The reference bridge had an L-type abutment, supported on piles with a medium-sand soil type. In this section, four other configurations at the abutment were considered: semi-integral abutment (Case 1 in Table 7.1), integral abutment (Case 2), abutment foundation of spread footing (Case 3), and abutments supported on medium clay (Case 4).

This section discusses the effects of the abutment configurations and soil types on the deformation demands, likelihood of damage, and force demands.

7.2.1 Effects on Deformation Demands

Figure 7.1 shows the median as well as the 15th and 85th percentiles of the maximum displacement at the end of the bridge deck. Figure 7.2 presents the same sets of plots for maximum bent drift ratio. Because the superstructure behaved nearly rigidly during the earthquake, the trends in both figures are similar.

Some of the trends observed were similar for all of the abutment configurations, including the reference bridge (Chapter 6):

- The median end displacements and bent drift ratios tended to be largest for Ocean Shores, somewhat smaller for Port Angeles, and significantly smaller for Seattle.
- For Ocean Shores, the largest displacements tended to occur for Site Class D1, whereas the largest deformation for Seattle tended to occur for D3. For Port Angeles, the median displacements tended to be the same for the D1 and D3 site classes.
- The deformations calculated for the softer site classes tended to have more variability, as measured from the ratio of the 85^{th} percentile displacement divided by the median displacement.

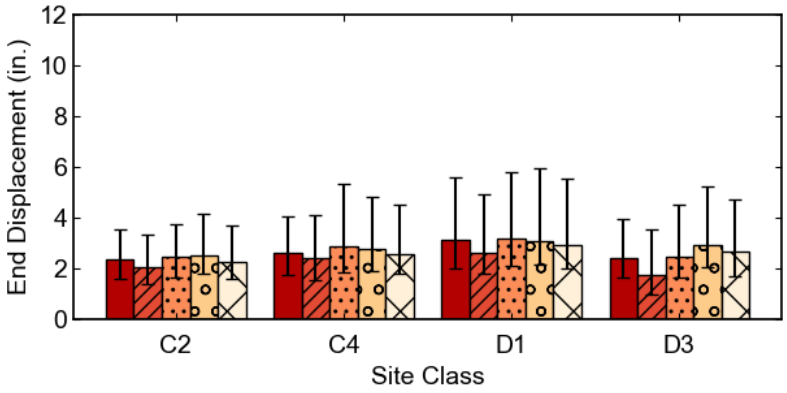

(a) Ocean Shores

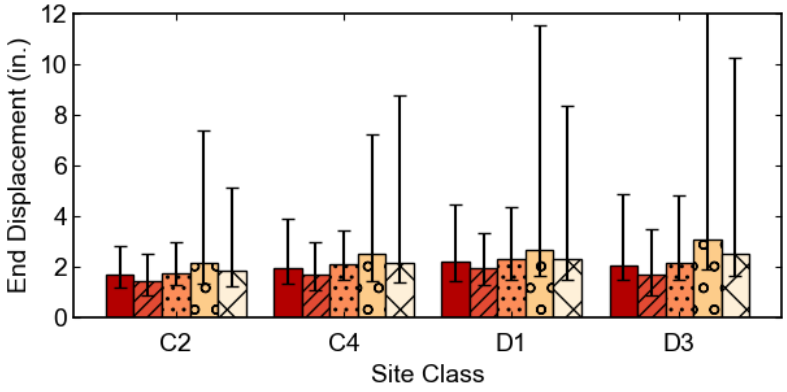

(b) Port Angeles

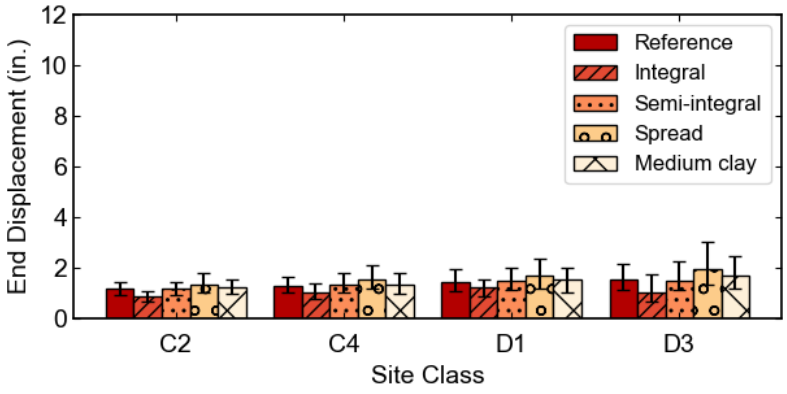

(c) Seattle

Figure 7.1: Effects of abutment and soil types on maximum end displacements for (a) Ocean Shores, (b) Port Angeles, and (c) Seattle

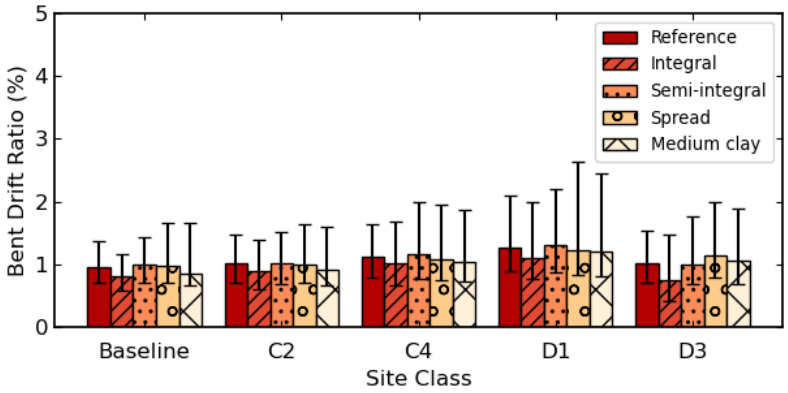

(a) Ocean Shores

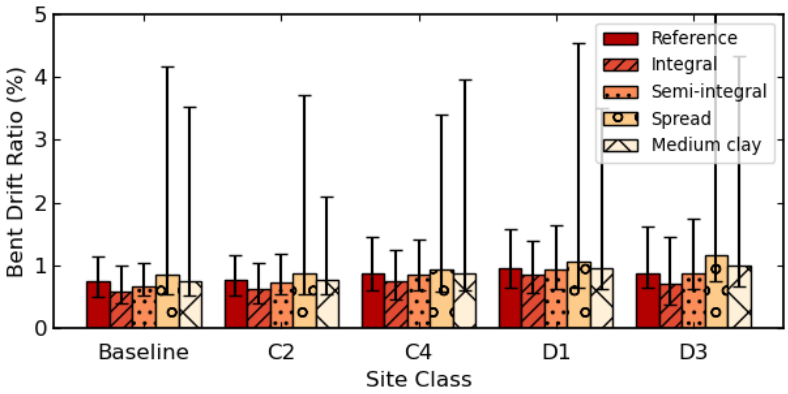

(b) Port Angeles

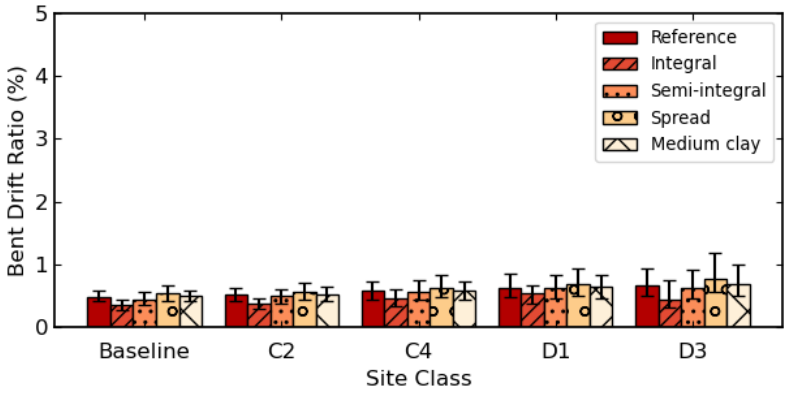

(c) Seattle

Figure 7.2: Effects of abutment and soil types on maximum bent drift ratio for (a) Ocean Shores, (b) Port Angeles, and (c) Seattle

There were also some differences among the responses for the five cases:

- For all 15 combinations of cities and site classes, the bridge with the integral abutment had the smallest median displacement responses, and for nearly all cases (13 of 15), it had the smallest 85th percentile displacement response. This trend was expected because the displacement in the transverse direction was restrained by the integral abutments without there being a gap between the bridge deck and the shear keys.
- The median transverse displacements for the bridges with L-abutment (reference bridge) and semi-integral abutment were nearly identical. This trend was also expected because the two abutment types had the same constraint in the transverse direction. The difference between the two abutment types was the presence/absence of a gap in the longitudinal direction.
- The largest end displacements and bent drift ratios tended to occur for the spread footings. For almost all (13 of 15) combinations of cities and site classes, bridges with spread footings had the largest median response. This result was attributed to the slightly lower lateral resistance of the spread footing (140 kips per footing, 7 percent of bridge weight) than that of the piles (157 kips per abutment, 8 percent of bridge weight).
- The change from medium sand to medium clay increased the median end displacements and bent drift ratios, but this difference was smaller than that of the change in foundation from piles to spread footings. The softer soil type (medium clay) had a lower first yield force (88 kips versus 42 kips per pile), which resulted in a lower transverse strength for the abutment foundation piles.

For the spread foundations and medium-clay-supported foundations located in Port Angeles, the calculated end displacements and drift ratios varied much more than for other abutment configurations and locations. For these two abutment conditions, the 85th percentile drift ratios were often near 4 percent.

7.2.2 Effects on the Likelihood of Column Flexural Damage

Figure 7.3 shows the effects of changes in abutment properties on the likelihood of spalling of the column concrete cover. The likelihood of spalling was calculated following the procedure described in Section 6.4.

For Ocean Shores and Port Angeles, the likelihood of spalling of the reference, integral, and semi-integral bridges ranged from 1.01 percent to 23.2 percent, with the larger values corresponding to Site Class D. For these two cities, the likelihood of spalling was significantly larger for the spread footings and piles found in medium clay. For these two conditions, the likelihood of spalling ranged from 8.6 percent to 33.3 percent. The likelihood of spalling was small for the Seattle locations. The maximum likelihood of spalling was 5.5 percent for the spread footing located on Site Class D3. These trends were observed not only in the median values of column deformation demand but they were also observed in the 85the percentile values.

Figure 7.4 shows the effects of changes in abutment properties on the likelihood of buckling of the column longitudinal bars. The likelihood of the onset of buckling of the longitudinal bars was calculated following the procedure described in Section 6.5. The maximum likelihood of bar buckling in the bridges with L-abutment (reference), integral abutment, and semi-integral abutment was 6.1 percent for the cities on the Olympic Peninsula and negligible for Seattle. For the spread and medium-clay bridges, the likelihood of buckling ranged from 0.0 percent in Seattle to 18.5 percent in Port Angeles.

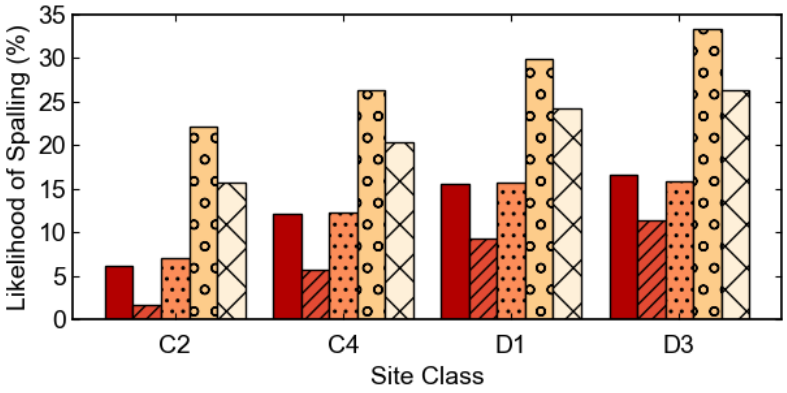

(a) Ocean Shores

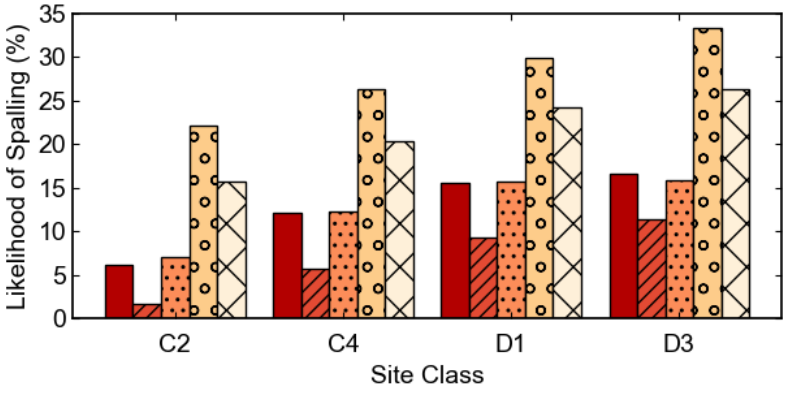

(b) Port Angeles

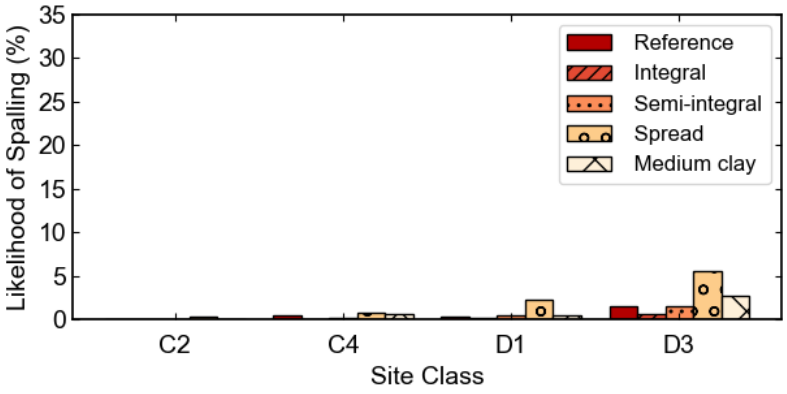

(c) Seattle

Figure 7.3: Effects of abutment and soil types on the likelihood of spalling of column cover concrete for (a) Ocean Shores, (b) Port Angeles, and (c) Seattle

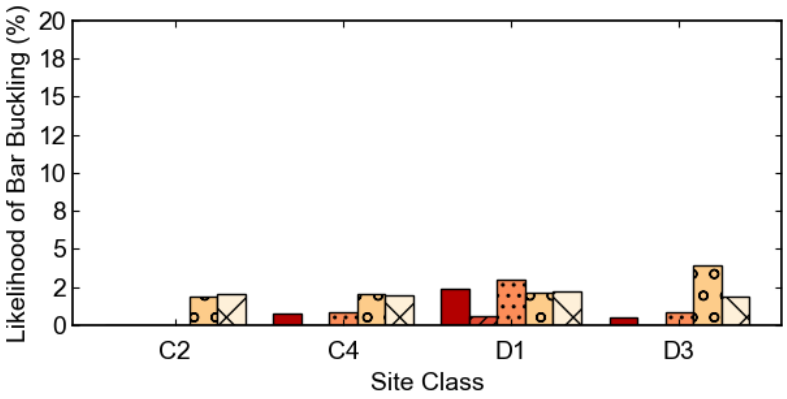

(a) Ocean Shores

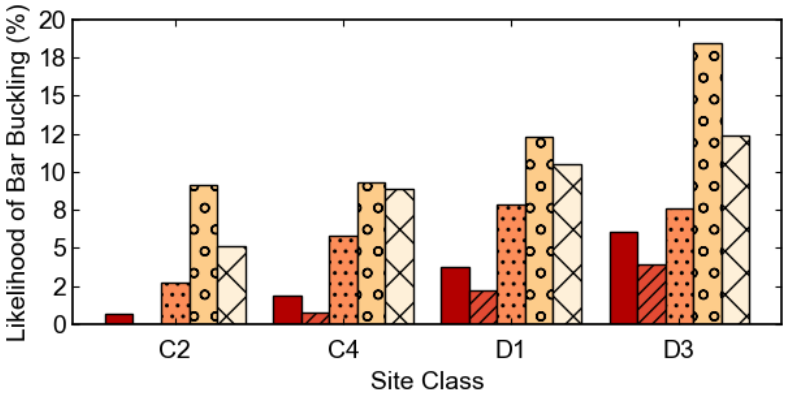

(b) Port Angeles

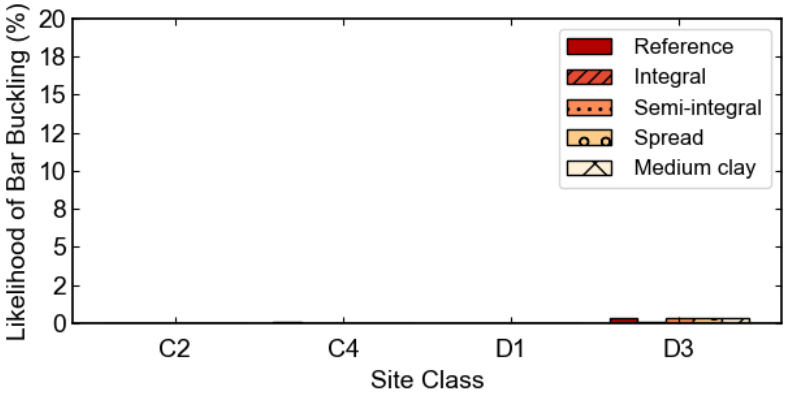

(c) Seattle

Figure 7.4: Effects of abutment and soil types on likelihood of onset of buckling of column longitudinal bars for (a) Ocean Shores, (b) Port Angeles, and (c) Seattle

7.2.3 Effects on Force Demands

Figure 7.5 shows the median, 15th, and 85th percentile values of the maximum sum of column transverse forces normalized by bridge weight. As was the case for the deformation responses (Section 7.2.1), the maximum column forces were higher in cities closer to the coast and tended to decrease as the location moved inland. For all three cities, the column forces did not change significantly among the soil site classes. Additionally, although the differences were small, the bridges with the integral abutment tended to have the lowest median sum of column forces except for some site classes in Ocean Shores. This could be explained by the high restraint that the integral abutments provided for the deck, which resulted in smaller column deformations and thus lower forces.

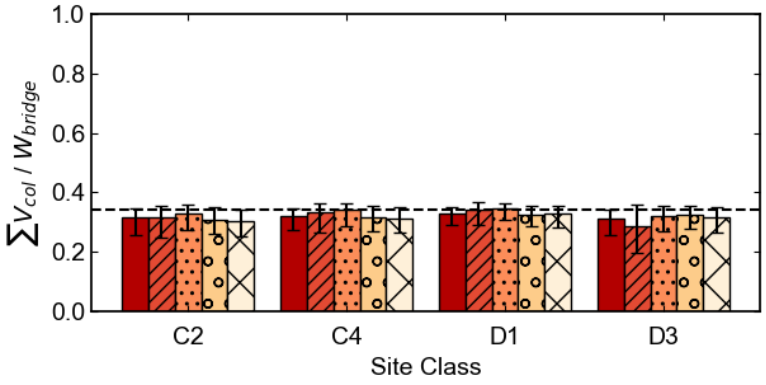

(a) Ocean Shores

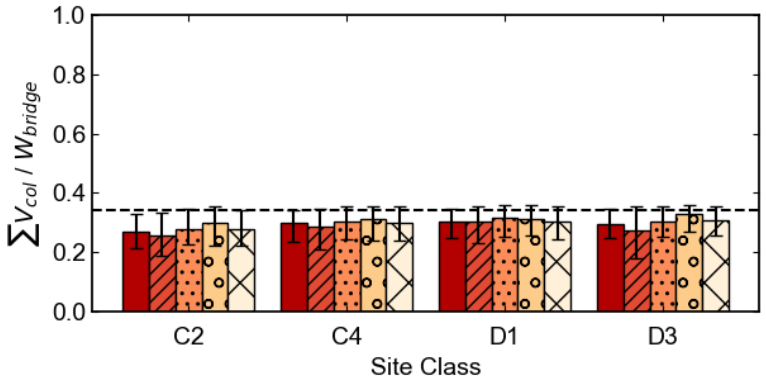

(b) Port Angeles

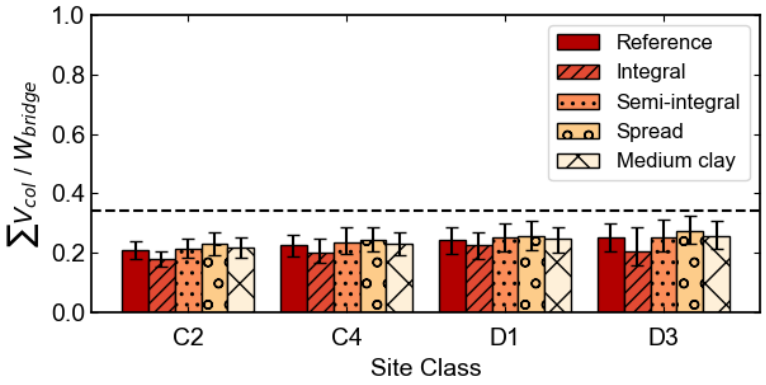

(c) Seattle

Figure 7.5: Effects of abutment and soil types on sum of column maximum lateral forces normalized by bridge weight for (a) Ocean Shores, (b) Port Angeles, and (c) Seattle (Black dashed line represents the effective yield of the bridge columns)

Figure 7.6 shows the maximum sum of the shear key forces normalized by bridge weight. Note that the integral abutment did not have a shear key, so no bar is shown for that configuration. As was observed for the deformation responses, the maximum shear key forces tended to decrease as the location moved away from the coast.

The highest median value was around 0.7 for site class D1 in Ocean Shores, and it also had the highest 85th percentile, with a value close to 1.3. Even for this location, the shear keys still did not reach their capacity (2.17 when normalized by the bridge weight). For the inland cities, the shear key forces tended to increase as the soil site class became softer, but again, the force demands were far below the capacities.

The responses of the reference bridge (L-abutment) and the case with a semi-integral abutment were very similar for all locations and site classes, as they had the same force-resisting elements in the transverse direction. The change of abutment foundation type to spread footing significantly decreased the forces of shear keys. This was because of the lower lateral capacity (140 kips, 7 percent of the bridge weight) of the spread footing, which directly limited the maximum lateral force that could be applied to the shear keys. Lastly, the variation of soil type also decreased the shear key force for similar reasons, as the softer soil type (medium clay) had a lower first yield force (88 kips versus 42 kips per pile), which resulted in lower transverse strength at the abutment foundation piles.

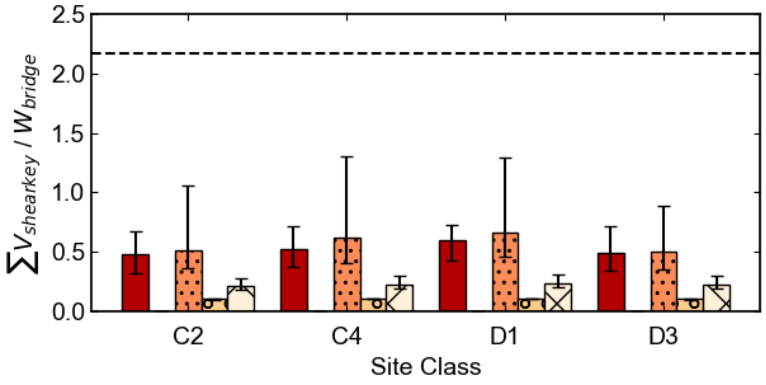

(a) Ocean Shores

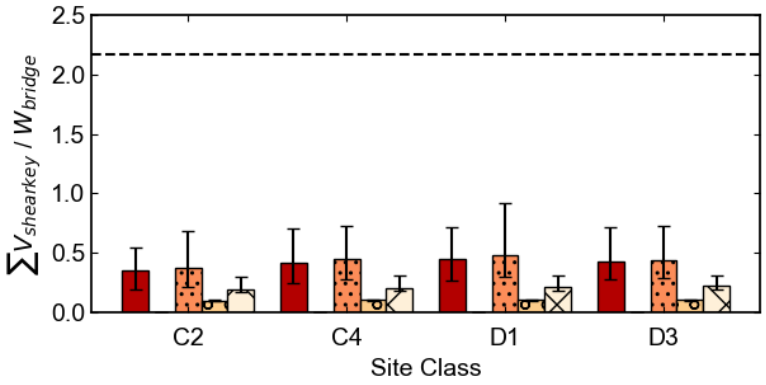

(b) Port Angeles

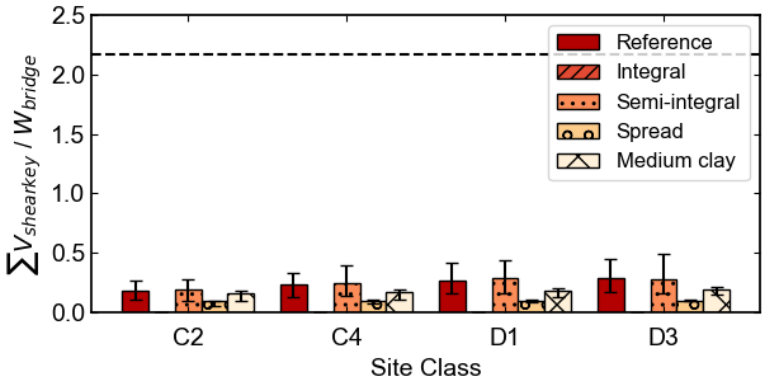

(c) Seattle

Figure 7.6: Effects of abutment and soil types on the sum of shear key maximum transverse force normalized by bridge weight for (a) Ocean Shores, (b) Port Angeles, and (c) Seattle (Black dashed line represents the capacity of the shear keys)

7.3 EFFECTS OF SHEAR KEYS AND BEARINGS

This section discusses the effects of various stiffnesses of shear key and bearing pads on deformation, column damage, and force demands. The reference bridge had shear keys and bearing pads. Two other situations were considered to represent circumstances in which there is no shear key (Case 5 in Table 7.1), or the bridge has neither a shear key nor bearing pads (Case 6 in Table 7.1). This last case was intended to conservatively represent the conditions in which a superstructure is not continuous, so it cannot transmit transverse forces to the abutment

7.3.1 Effects on Deformation Demands

For all the cities and site classes (15 combinations), the displacements at the end of the deck (Figure 7.7) and bent drift ratio (Figure 7.8) increased significantly when the resistance provided by the shear key was removed (Case 5). The displacements further increased when the resistance of the bearing pads was removed (Case 6). For both cases, the median displacement responses tended to increase as the site class became softer. For both cases, the largest displacements were computed for Port Angeles, which is on the Olympic Peninsula (but not on the Pacific Coast, so it has an "intermediate" source-to-site distance) and located on a medium-depth sedimentary basin. The effect of basin amplification would likely be larger for the bridges without shear keys, whose period would be longer than that of bridges with shear keys.

For the no-shear key situation (Case 5), the maximum median end displacement was around 4 inches, and the highest 85th percentile was over 15 inches for the Port Angeles of site class D3. The corresponding median and 85th percentile drift ratio values were about 1.5 percent and above 6 percent, respectively.

For the no-shear key and no-bearing simulations (Case 6), the displacements had a median value of over 7 inches, and the 85th percentile value was over 20 inches for Site Class D3. For Port Angeles, the maximum median bent drift ratio was 2.8 percent, and the 85th percentile value was 8.2 percent.

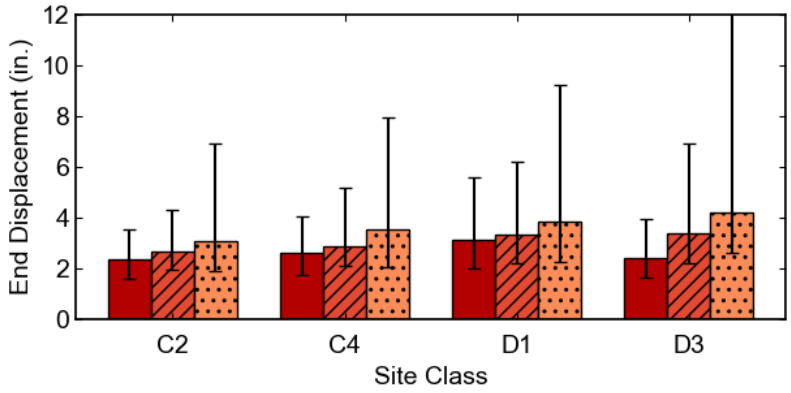

(a) Ocean Shores

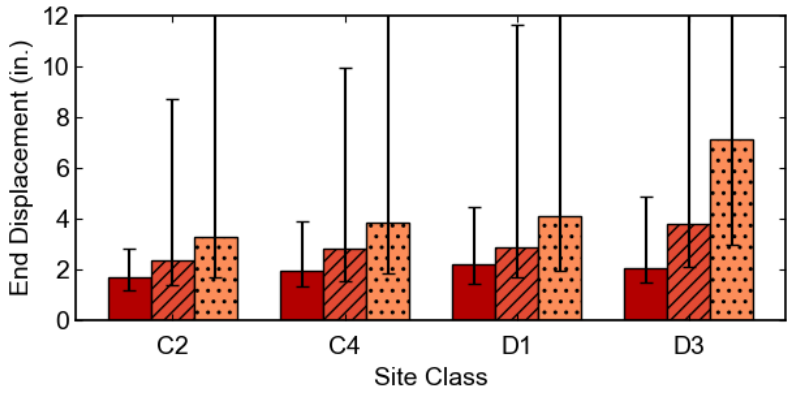

(b) Port Angeles

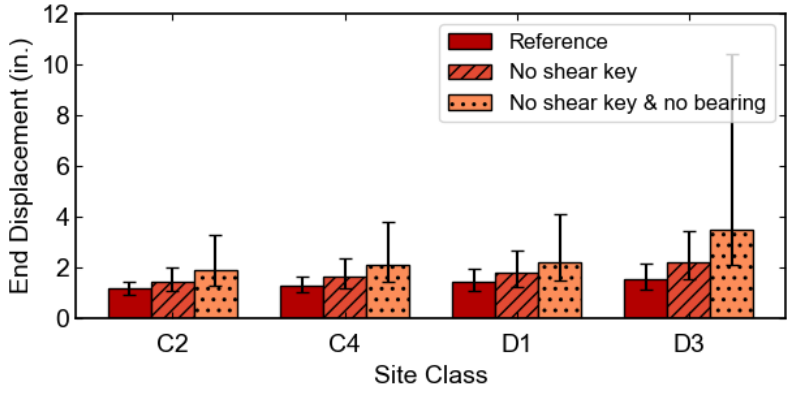

(c) Seattle

Figure 7.7: Effects of shear keys and bearings on maximum displacements at the end of the deck for (a) Ocean Shores, (b) Port Angeles, and (c) Seattle

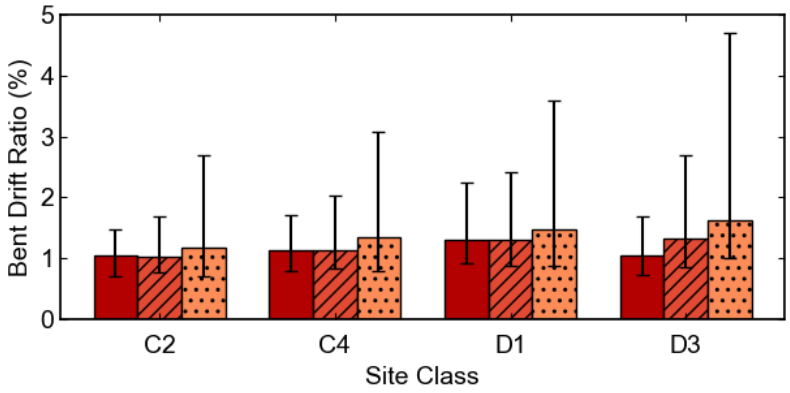

(a) Ocean Shores

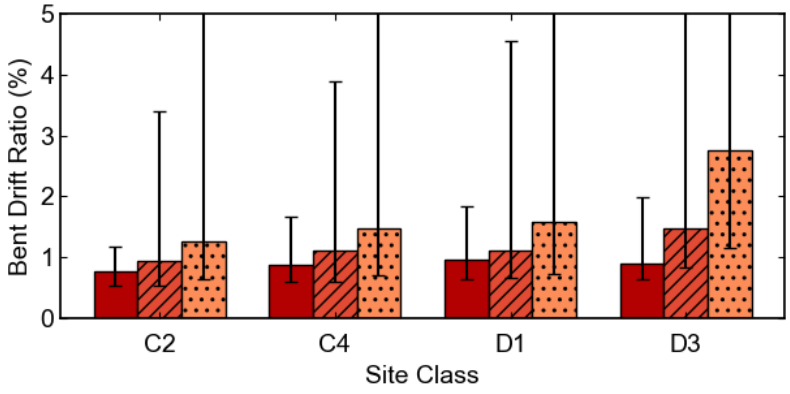

(b) Port Angeles

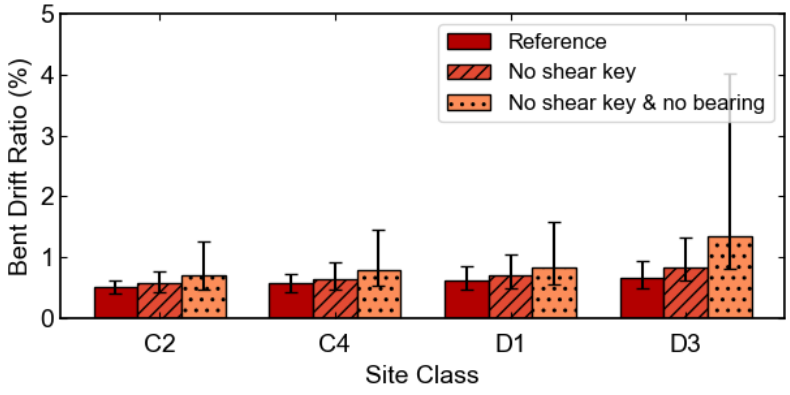

(c) Seattle

Figure 7.8: Effects of shear keys and bearings on maximum bent drift ratios for (a) Ocean Shores, (b) Port Angeles, and (c) Seattle

7.3.2 Effects on the Likelihood of Column Damage

Figure 7.9 shows the effects of shear keys and bearings on the likelihood of spalling of the column concrete cover. The likelihood of spalling was calculated following the procedure described in Section 6.4. For all 15 combinations of three cities and five site classes, the removal of the shear key greatly increased the likelihood of spalling, and the likelihood of spalling increased further when the bearing resistance was also removed.

For the bridge without a shear key (but with a bearing), the likelihood of spalling for Ocean Shores and Port Angeles ranged from 12.5 percent to 41 percent, with the larger values corresponding to Site Class D. For the bridge without a shear key nor a bearing, the likelihood of spalling ranged from 21.5 percent to 60.7 percent. For the Seattle location, the likelihood of spalling ranged from 10 percent to a maximum of 35 percent for Site Class D3.

Figure 7.10 shows effects of shear keys and bearing on the likelihood of buckling of the column longitudinal bars. The likelihood of the onset of buckling of the longitudinal bars was calculated following the procedure described in Section 6.5. As was observed for spalling, the likelihood of bar buckling increased greatly when the shear-key resistance was removed, and it increased even more when the bearing resistance was neglected. The values were largest for Port Angeles, where the likelihood of bar buckling ranged from 10.6 percent to 17.1 percent for the no-shear key analyses, and it ranged from 14 percent to 28.9 percent for the simulations without shear keys and without bearings.

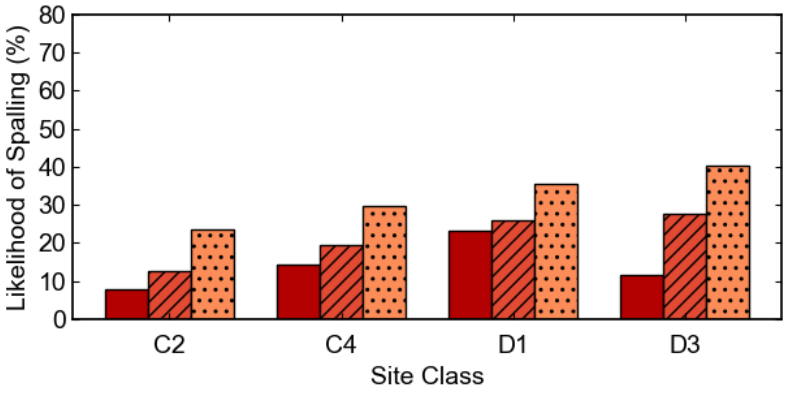

(a) Ocean Shores

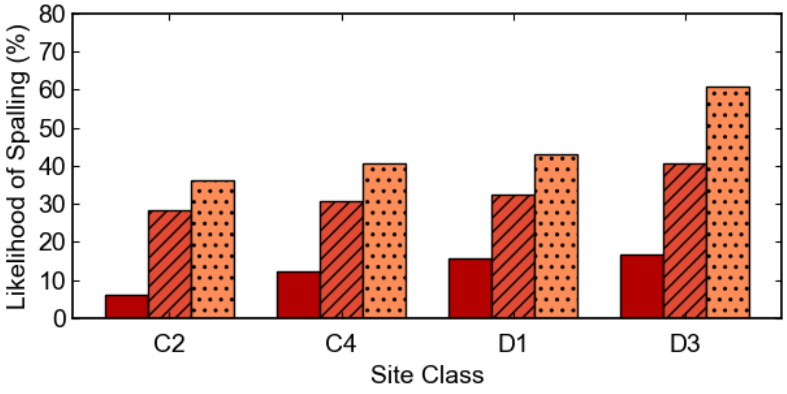

(b) Port Angeles

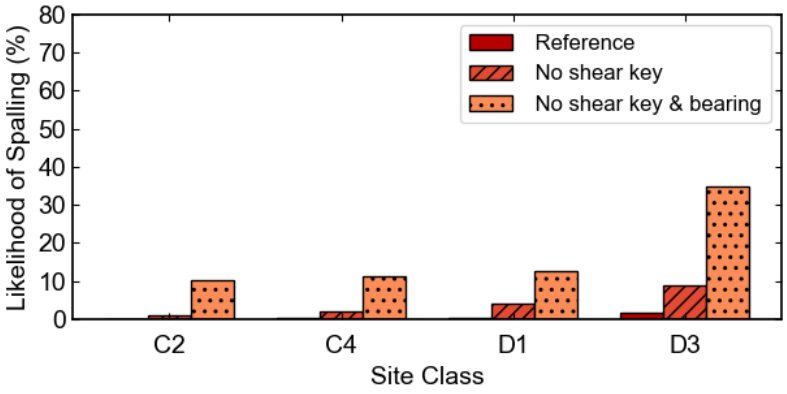

(c) Seattle

Figure 7.9: Effects of shear keys and bearings on the likelihood of spalling of the column concrete cover for (a) Ocean Shores, (b) Port Angeles, and (c) Seattle

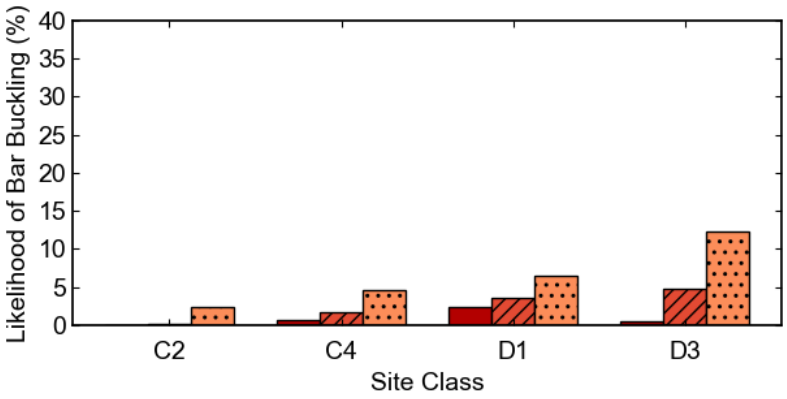

(a) Ocean Shores

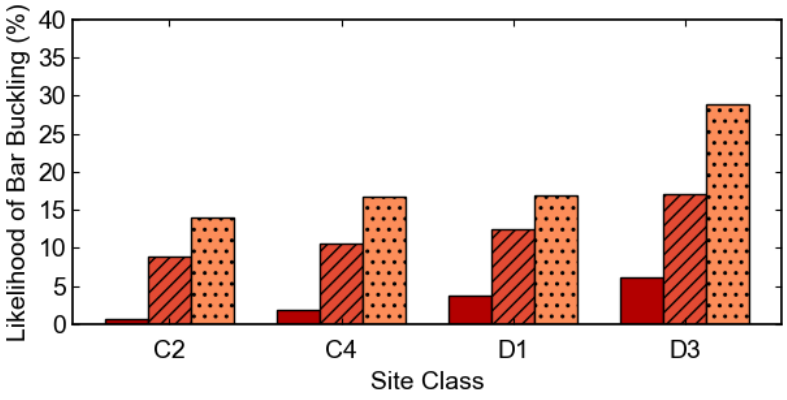

(b) Port Angeles

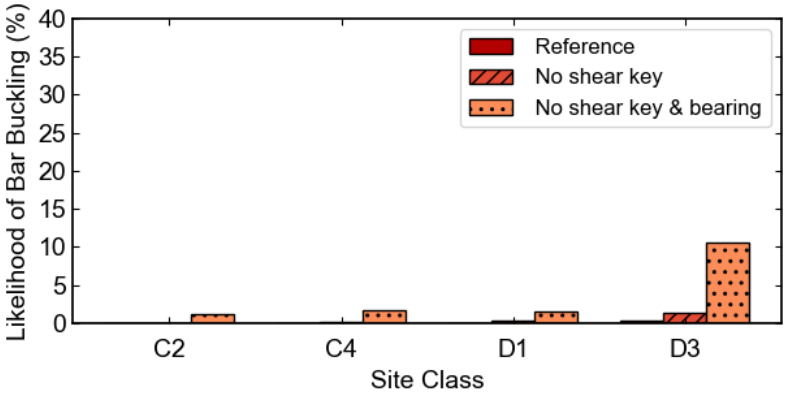

(c) Seattle

Figure 7.10: Effects of shear keys and bearings on the likelihood of the onset of buckling of the column longitudinal bars for (a) Ocean Shores, (b) Port Angeles, and (c) Seattle

7.3.3 Effects on Force Demands

Figure 7.11 shows the effects of shear keys and bearings on the maximum sum of column forces. For the two cases (cases 5 and 6), the forces tended to be higher in cities closer to the coast and also as the soil site classes became softer. The removal of shear keys caused an overall increase in the forces in the columns, and the removal of the bearing pads had a similar influence on the column forces.

The maximum sum of shear key forces is not discussed in this section because these cases did not include shear keys in the analyses

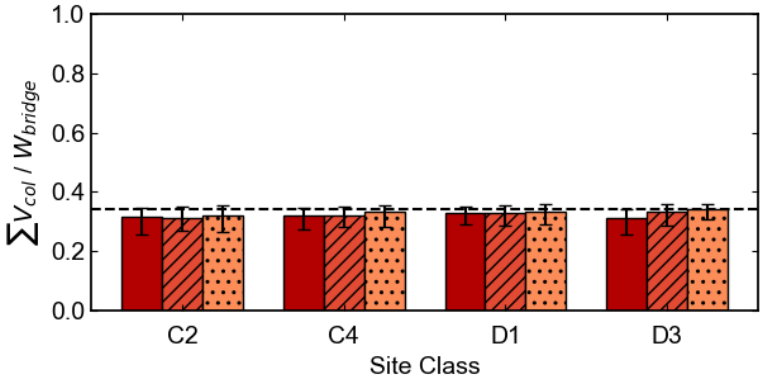

(a) Ocean Shores

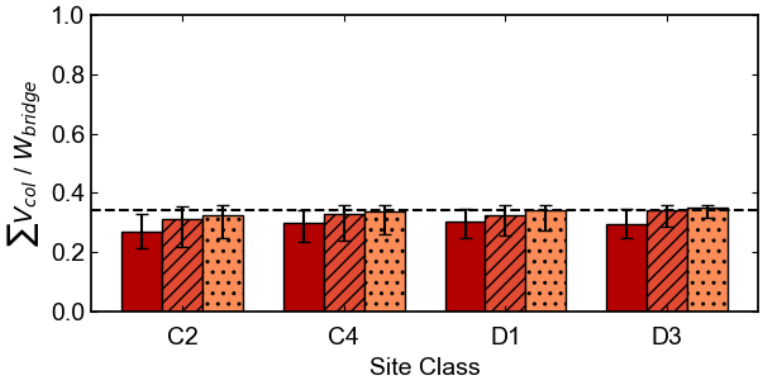

(b) Port Angeles

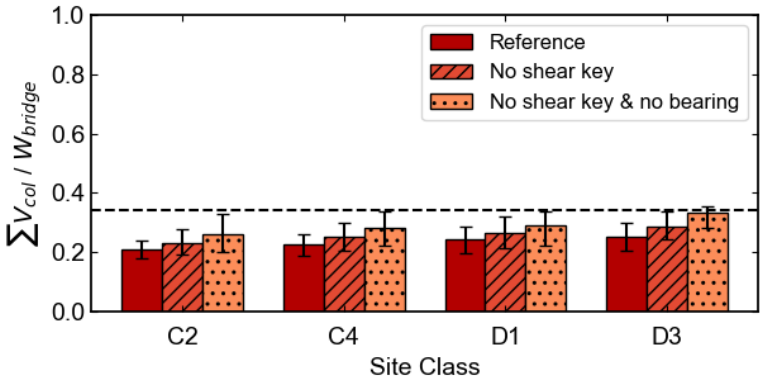

(c) Seattle

Figure 7.11: Effects of shear keys and bearings on the sum of column maximum lateral forces normalized by bridge weight for (a) Ocean Shores, (b) Port Angeles, and (c) Seattle (Black dashed line represents the effective yield of bridge columns)

CHAPTER 8 EFFECTS OF COLUMN PROPERTIES

This chapter discusses a parametric study of the effects of column properties on the performance of the reference bridge. Similar to the abutment parametric study (Chapter 7), the results are shown only for the transverse direction and for three cities: Ocean Shores, Port Angeles, and Seattle. In the column parametric study, the bridges all had an L-abutment type with pile abutment foundations founded on medium sand. The abutment parametric study (Chapter 7) considered a case in which both the resistance of the shear key and bearing pads were neglected (Case 6, Table 7.1), but in this parametric study, the resistance of the bearing pads was included in all of the analyses.

Section 8.1 introduces the analysis cases considered to evaluate the effects of variations in the column properties. Section 8.2 discusses the effects of column height, and Section 8.3 discusses the effects of column transverse reinforcement ratio.

8.1. VARIATION OF COLUMN PROPERTIES

Table 8.1 documents key analysis parameters for all the cases considered to evaluate the effects of the column characteristics. The effects of column height, both with and without shear keys, were investigated for older bridges in which the transverse reinforcement was assumed to be 0.5 percent. These analyses considered the following conditions.

- Reference bridge with reference column height (21.3 ft) (reference bridge)
- Reference bridge with double column height (42.6 ft) (Case 7)
- Reference bridge with double column height and no shear key (10.65 ft) (Case 8)
- Reference bridge with half column height (42.6 ft) (Case 9)
- Reference bridge with half column height (10.65 ft) (Case 10).

In addition, the effects of the transverse steel ratio in columns was investigated by comparing the response of a bridge with column transverse reinforcement ratios of 1.5 percent (Case 11) and 0.2 percent (Case 12) with that of a bridge with a transverse reinforcement ratio of 0.5 percent (reference bridge).

Table 8.1: Column parametric study cases

Parameter	Reference Bridge	Case 7	Case 8	Case 9	Case 10	Case 11	Case 12
Effective Height of Column (ft)	21.3	**21.3 x 2**	**21.3 x 2**	**21.3 x 1/2**	**21.3 x 1/2**	21.3	21.3
Transverse Reinforcement Ratio (%)	0.5 (old bridge)	0.5 (old bridge)	0.5 (old bridge)	0.5 (old bridge)	0.5 (old bridge)	**1.5 (new bridge)**	**0.25 (low transverse reinf.)**
Shear Key Stiffness/ Strength	Present	Present	**Absent**	Present	**Absent**	Present	Present

8.2 EFFECTS OF COLUMN HEIGHT

The reference bridge had a column height of 21.3 ft, a transverse reinforcement ratio of 0.5 percent, and shear keys. This section describes and investigation of the effects of doubling or halving the column heights with four analysis cases: double the column height of the reference bridge (42.6 ft) with shear keys (Case 7 in Table 8.1), double the column height of the reference bridge without shear keys (Case 8), half of the column height of the reference bridge (10.65 ft) with shear keys (Case 9), and half of the column height of the reference bridge without shear keys (Case 10). Sections 8.2.1, 8.2.2, and 8.2.3 discuss the effects of column height on the deformation demands, likelihood of flexural damage in the column, and force demands, respectively.

8.2.1 Effects on Deformation Demands

Figure 8.1 shows the effects of varying the column height on the displacement at the end of the bridge for the cities of Ocean Shores, Port Angeles, and Seattle. For the reference bridge, the displacements at the end of the bridge were largest for Ocean Shores and smallest for Seattle for all site classes. The largest median end displacements for the two locations closest to the coast occurred for Site Class D1 (3.12 in., Ocean Shores). The largest median end displacement for Seattle (1.52 in.), which is located farther inland, occurred for Site Class D3.

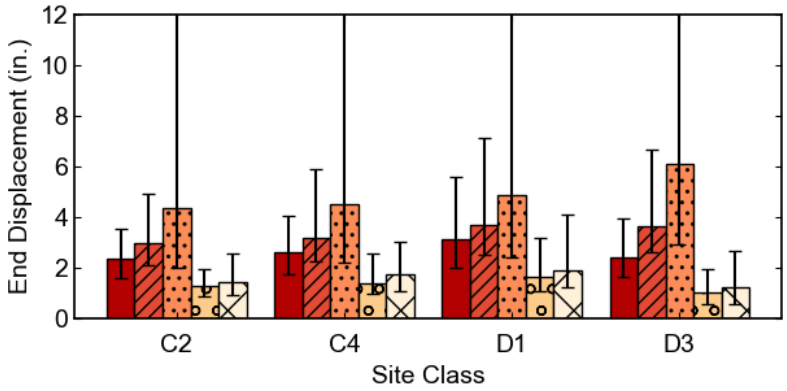

(a) Ocean Shores

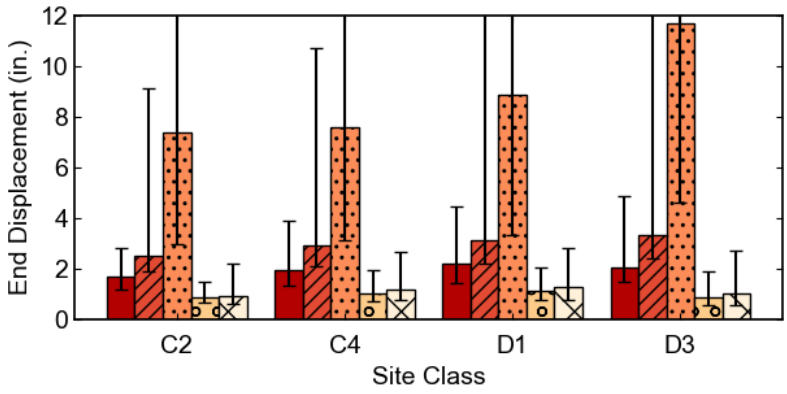

(b) Port Angeles

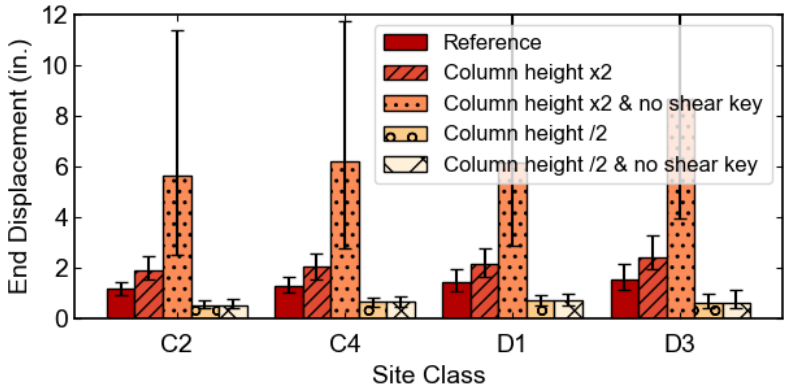

(c) Seattle

Figure 8.1: Effects of column height on maximum displacements at the end of the deck for (a) Ocean Shores, (b) Port Angeles, and (c) Seattle

When the column height was doubled (with shear key, Case 7), the end displacements increased for all locations and all site classes. For this case, the maximum displacements for site classes D1 and D3 were similar. The maximum median displacement among all three cities and all four soil types was 3.7 inches (Ocean Shores, same values for site classes D1 and D3).

When the column height was doubled and the shear key was removed (Case 8), the median displacements increased greatly for all locations and site classes. The increase was particularly large for the two locations on a basin (Port Angeles, Seattle), where the median displacement increased by a factor of approximately five. Site Class D3 always had the largest median end displacement. The highest median value was 11.7 in. (Port Angeles, Site Class D3). This large increase could be explained by the longer period of this bridge and the ground motion amplification of higher periods by the sedimentary basin.

When the column height was reduced by half of the reference value, the end displacement significantly decreased, either with or without the existence of shear keys (cases 9 and 10). These decreases were attributable to the increased stiffness of the short columns. Theoretically, the elastic flexural displacement (neglecting the effects of bond slip and shear deformations) would be inversely proportional to the cube of the column height (Elwood and Eberhard, 2009). The highest median end displacement of the half column height cases reached a maximum of only 1.9 inches (Ocean Shores, Site Class D1), even in the absence of a shear key.

Figure 8.2 shows the maximum bent drift ratios for the same three cities. The effects of model changes on drift ratios were not the same as the effects on abutment displacement because the drift ratio was computed as the maximum bent displacement divided by the column height, which varied among the cases. Specifically, the column height for the reference bridge and the other cases varied by factors of 2.0 (double column height) or 0.5 (half column height); therefore the denominators for the calculations of the drift ratio varied, too.

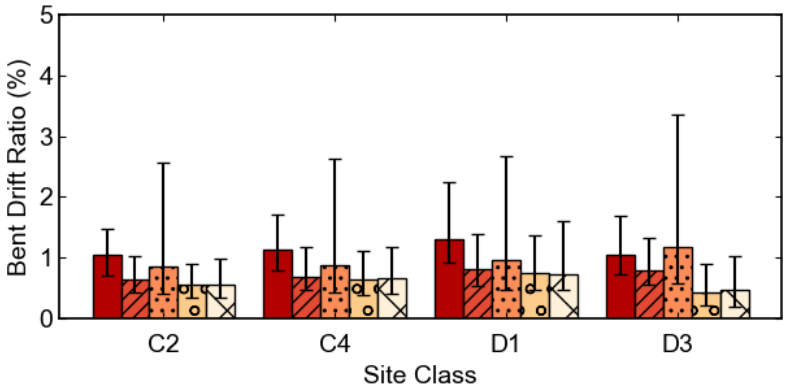

(a) Ocean Shores

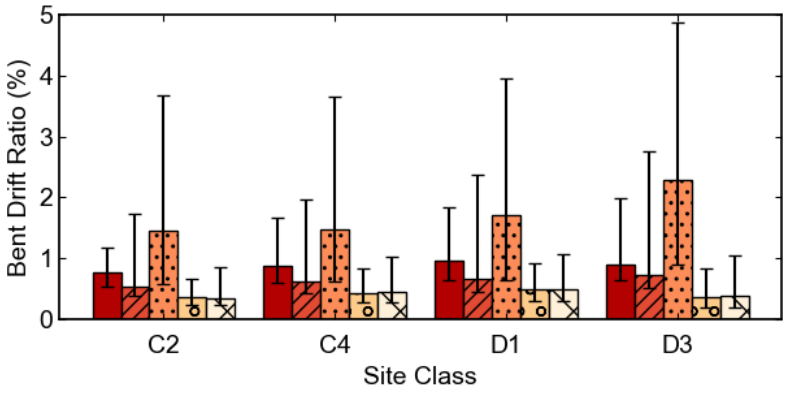

(b) Port Angeles

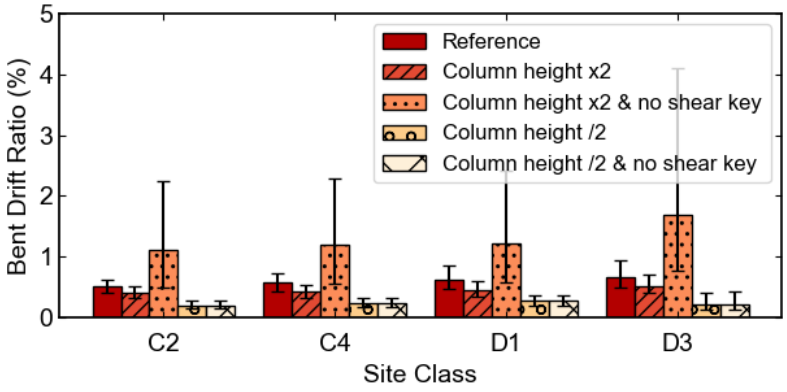

(c) Seattle

Figure 8.2: Effects of column height on maximum bent drift ratio for (a) Ocean Shores, (b) Port Angeles, and (c) Seattle

In comparison to the reference bridge, the bridge with double the column height (with shear key) had lower drift ratios for all locations and site classes because the increased column length (factor of 2.0 in denominator) more than compensated for the increased displacement demands (Figure 8.1). The effects of removing the shear key and doubling the column varied with location. For Ocean Shores, the increased displacement demands were approximately compensated for by doubling the column height in the denominator of the drift calculation. In contrast, the increased displacement demands (Figure 8.1) greatly overwhelmed the effect of the increased column length on the drift calculation for the cities of Port Angeles and Seattle, both of which are located on sedimentary basins. The highest median drift ratio was 2.3 percent and the 85th percentile value was 4.9 percent for the worst case, Port Angeles, Site Class D3.

For bridges with half the column height, the computed bent drift ratios were similar to those of the reference bridge. For these bridges, the drift ratios were below 1 percent for all locations and site classes. The drift ratios for the bridges without shear keys were only slightly larger than those for bridges with shear keys.

8.2.2 Effects on Likelihood of Column Flexural Damage

Figures 8.3 and 8.4 show the effects of varying the column height on the likelihood of spalling of the column concrete cover and onset of buckling of the longitudinal bars. The likelihoods of spalling and bar buckling were calculated following the procedures described in sections 6.4 and 6.5. Table 8.2 summarizes some of the analysis results for Port Angeles, Site Class D1. Note that the median drift ratios at spalling and bar buckling varied with the shear-span-to-depth ratio, L/D, so the longer columns had a median drift ratio for each damage level that was larger than that of the shorter columns.

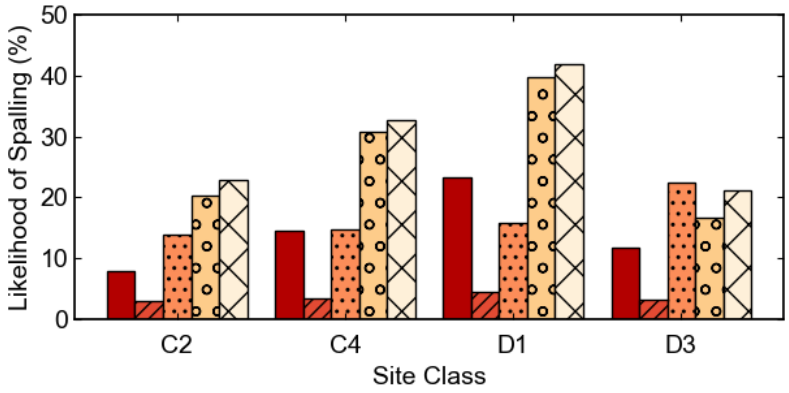

(a) Ocean Shores

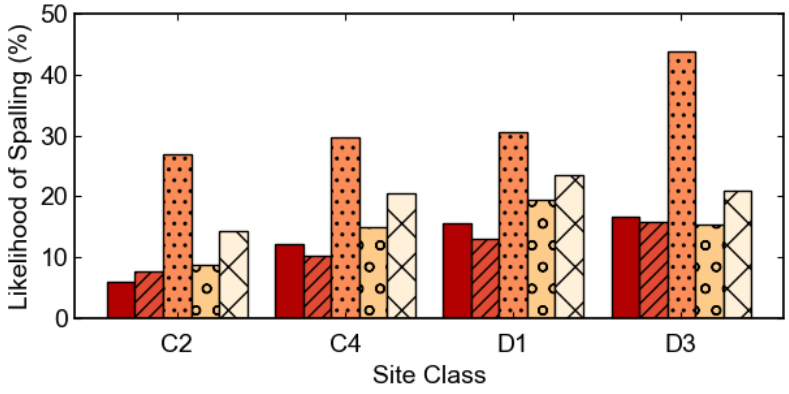

(b) Port Angeles

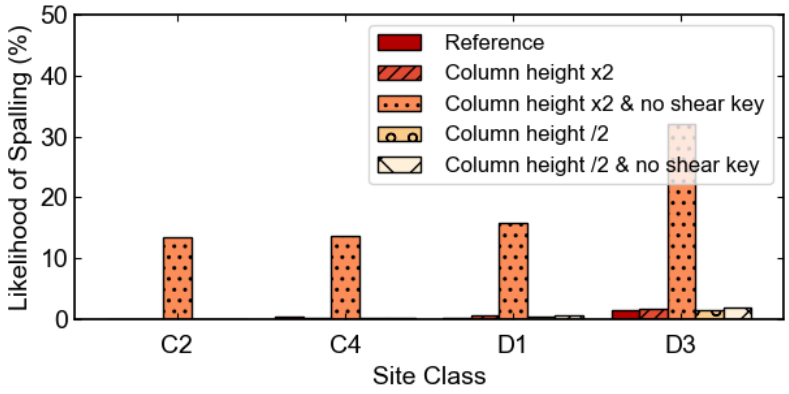

(c) Seattle

Figure 8.3: Effects of column height on the likelihood of spalling of the column cover concrete for (a) Ocean Shores, (b) Port Angeles, and (c) Seattle

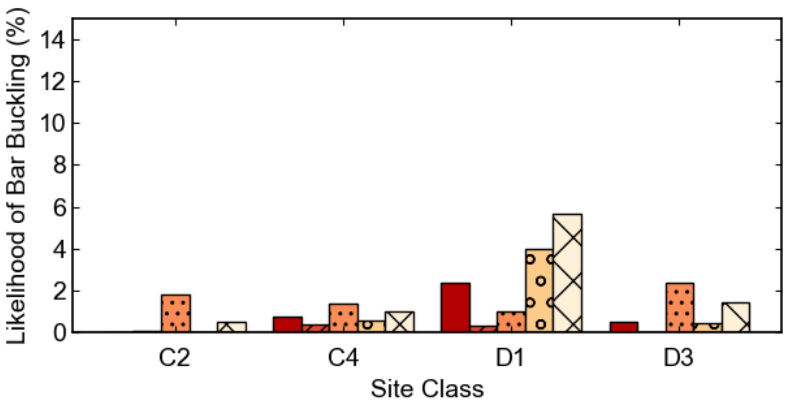

(a) Ocean Shores

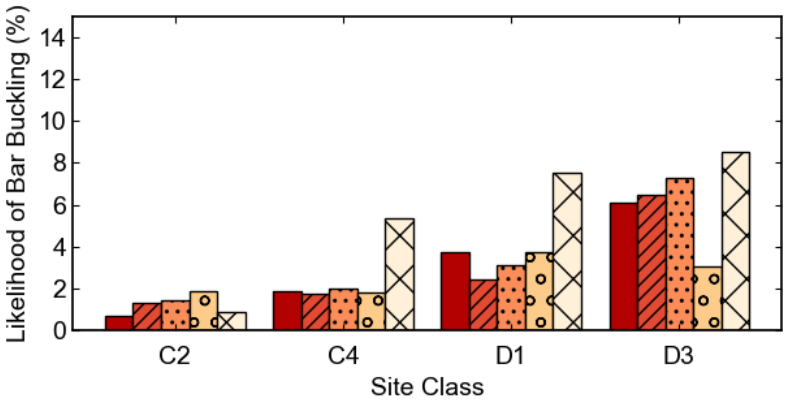

(b) Port Angeles

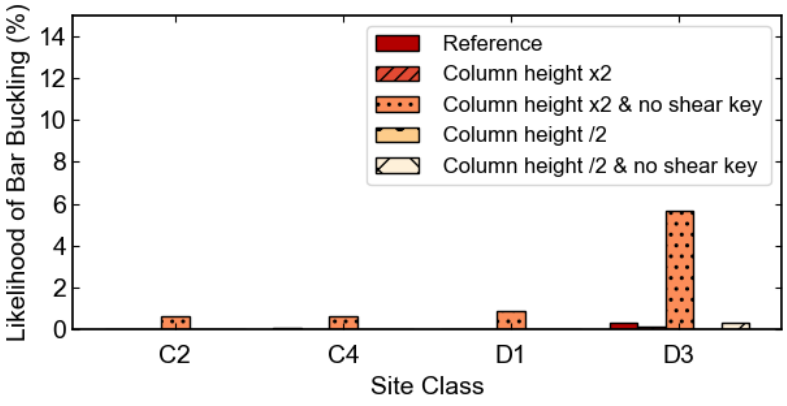

(c) Seattle

Figure 8.4: Effects of column height on the likelihood of the onset of buckling of the column longitudinal bars for (a) Ocean Shores, (b) Port Angeles, and (c) Seattle

Table 8.2. Deformation and damage results for Port Angeles, Site Class D1

Condition	Median End Displacement (in.)	Median Column Drift Ratio (%)	Median Drift Ratio at Spalling (%)	Likelihood of Spalling (%)	Median Drift Ratio at Onset of Bar Buckling (%)	Likelihood of Onset of Bar Buckling (%)
Reference	2.19	0.97	2.06	15.6	4.18	3.7
Double column height (Case 7)	3.13	0.66	2.60	10.4	13.0	2.4
Double column height without shear key (Case 8)	8.90	1.71	2.60	30.5	5.28	3.1
Half column height (Case 9)	1.10	0.48	1.79	19.4	3.64	3.7
Half column height without shear key (Case 10)	1.27	0.49	1.79	23.6	3.64	7.5

The effects of removing shear keys and doubling (or halving) the column heights varied according to the location. Doubling the column height (while maintaining the shear-key resistance) reduced likelihoods of spalling and buckling in Ocean Shores (near source, no basin) but had little effect for Port Angeles (moderate distance and moderate basin depth). Doubling the column height (and removing the shear key) tended to increase the level of damage for both cities. This increase was much larger for Port Angeles than Ocean Shores, likely reflecting the presence of the sedimentary basin, which tends to amplify long-period components of ground motions. The bridges with shorter columns tended to have larger likelihoods of flexural damage, reflecting the lower drift ratio at spalling (Table 8.2), as well as the larger variability in the drift ratios (Figure 8.2).

For Seattle (far from the source, with a deep sedimentary basin), only the combination of removing the shear key and doubling the column height resulted in significant likelihoods of concrete spalling. The likelihood was largest for Soil Class D3, reaching a maximum value of 32 percent.

Figure 8.4 shows the effects of varying the column height on the likelihood of buckling of the column longitudinal bars. The likelihood of bar buckling tended to decrease for the case in which the column height was doubled but the shear key resistance was preserved. For this longer column, the likelihood of buckling increased markedly for the

cities of Ocean Shores and Port Angeles, both located on the Olympic Peninsula. For these two cities and the half-column cases, the presence of a shear key did not have a great effect on the likelihood of bar buckling, ranging from approximately 6 percent to 12 percent for Site Class D1.

In Seattle (far from the source, with a deep sedimentary basin), only the combination of removing the shear key and doubling the column height resulted in significant likelihoods of bar buckling. This likelihood was largest for Soil Class D3, reaching a maximum value of 5.6 percent.

8.2.3 Effects on Force Demands

Figure 8.5 shows the maximum sum of column forces for the three cities. When the column height was doubled, the sum of column forces significantly decreased, especially for the case where the shear keys were present. The column forces of bridges without shear keys were consistently greater than those for bridges with shear keys. This was because the shear keys were taking lateral loads as the columns displaced more.

When the column height was reduced by half, the column forces significantly increased, with the median value around two times that of the reference bridge. The maximum recorded median value was about 0.65 of the bridge weight, and the 85th percentile value was about 0.7 of the bridge weight. For the two bridges with half column height, the presence of shear keys did not make a significant difference. Additionally, although the correlation between the column forces and the soil site classes was not obvious, D1 tended to have the largest responses.

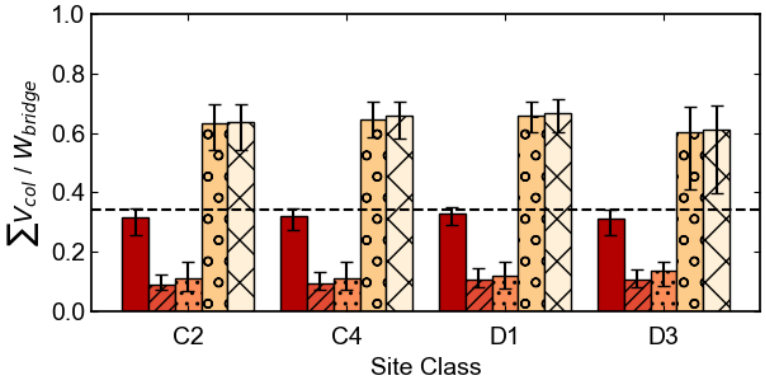

(a) Ocean Shores

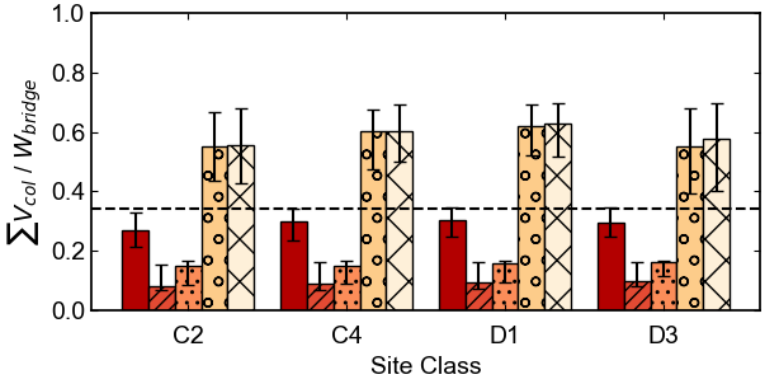

(b) Port Angeles

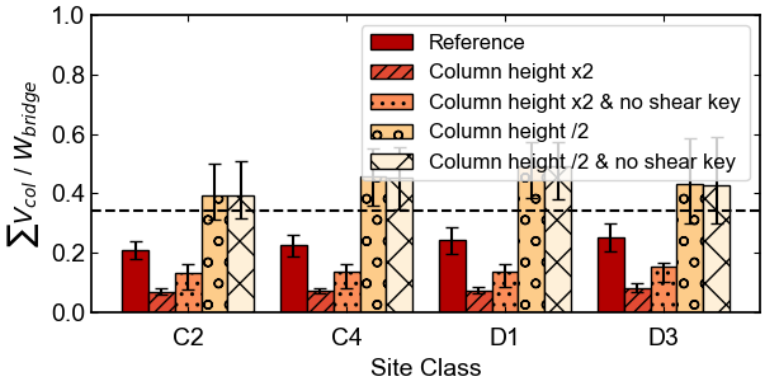

(c) Seattle

Figure 8.5: Effects of column height on the sum of column maximum lateral forces normalized by bridge weight for (a) Ocean Shores, (b) Port Angeles, and (c) Seattle (Dashed line represents the effective yield of bridge columns)

Figure 8.6 shows the maximum sum of shear key forces normalized by bridge weight for the three cities. When the column height was doubled and with shear key, the shear key forces increased, which was consistent with the decrease in column forces shown in Figure 8.5. Except for the case with half column height and shear key, the shear key force ratio tended to increase slightly as the soil condition became softer, with the highest 85^{th} percentile value being no more than 0.7, which was far from reaching the maximum capacity. The shear key force significantly decreased as the column height was reduced to half of its original value, which corresponded to the increase of the horizontal column forces shown in Figure 8.5. And as expected, the shear key forces were zero for the cases where the shear keys were removed.

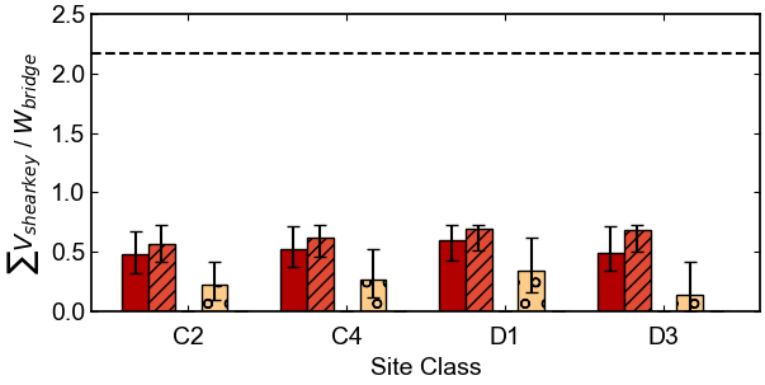

(a) Ocean Shores

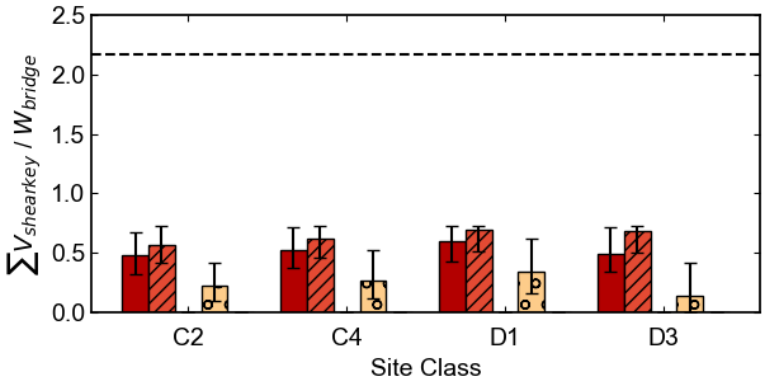

(b) Port Angeles

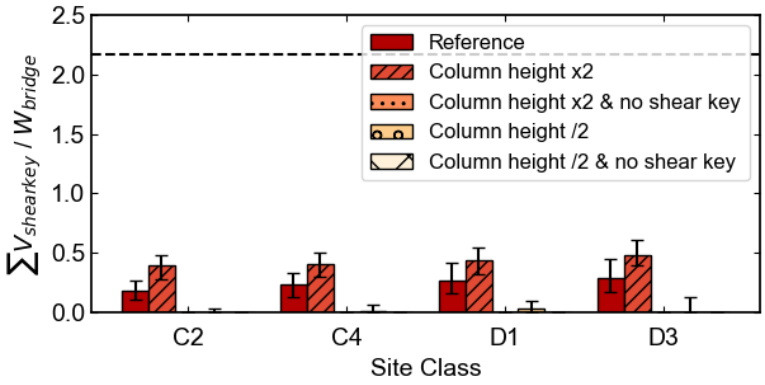

(c) Seattle

Figure 8.6: Effects of column height on the sum of shear key maximum transverse force normalized by bridge weight for (a) Ocean Shores, (b) Port Angeles, and (c) Seattle (Dashed line represents the capacity of shear keys)

8.3 EFFECTS OF COLUMN TRANSVERSE REINFORCEMENT

This section discusses the differences in performance for bridges with varying levels of transverse reinforcement ratios ranging from 0.2 percent (Case 12) to 1.5 percent (Case 11). This change approximated the main difference between bridges designed before and after 1976. Since the transverse reinforcement provides confinement to the concrete core, higher transverse reinforcement ratio values indicate higher confined concrete strengths and ductility (Figure 4.5). The differences were most apparent when columns were subjected to large displacements.

8.3.1 Effects on Deformation Demands

Figures 8.7 and 8.8 show the deformation responses of the reference bridge, a bridge with a lower column transverse reinforcement ratio (Case 12), and a bridge with a higher column transverse reinforcement ratio (Case 11). The end displacements and bent drift ratios were nearly identical for all 15 combinations of three locations and five site conditions.

This similarity was expected because transverse reinforcement has little effect on the column properties for low levels of column deformation. In both cases, the shear keys restricted the transverse deformation demands. Out of all these cases, the maximum median bent drift ratio was only 1.3 percent (Ocean Shores, Site Class D1).

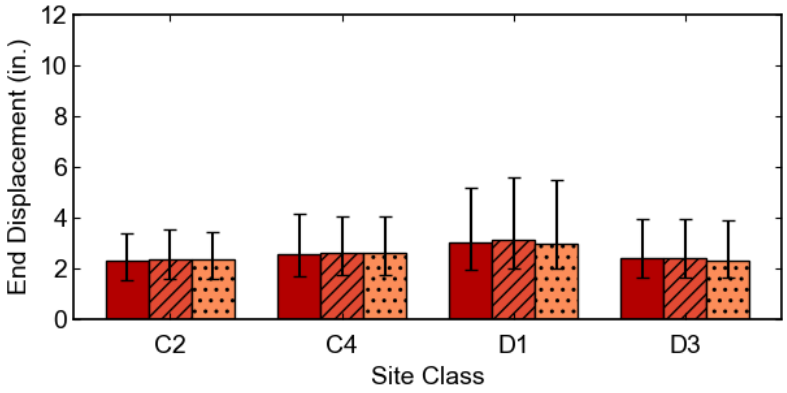

(a) Ocean Shores

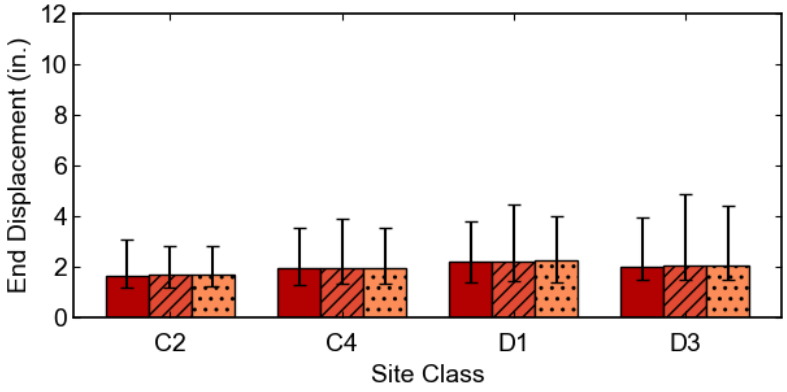

(b) Port Angeles

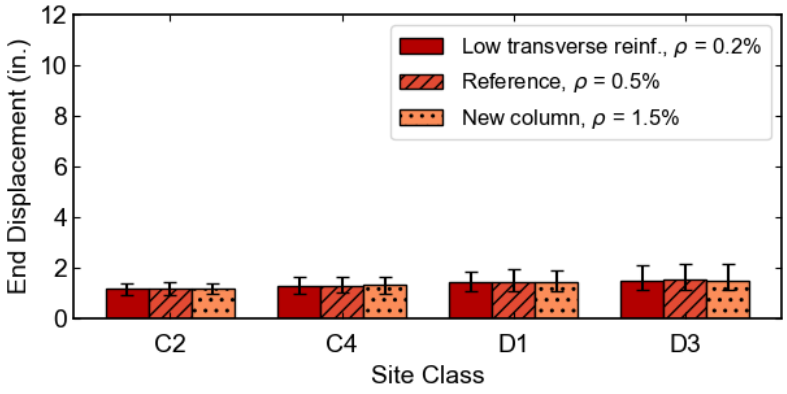

(c) Seattle

Figure 8.7: Effects of transverse reinforcement on maximum displacements at the end of the deck for (a) Ocean Shores, (b) Port Angeles, and (c) Seattle

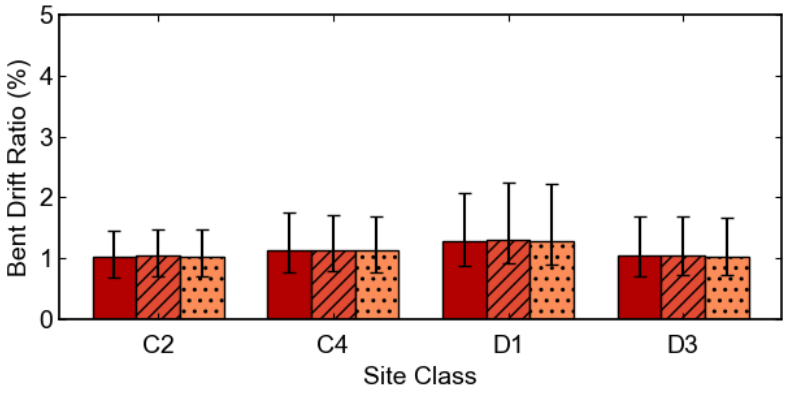

(a) Ocean Shores

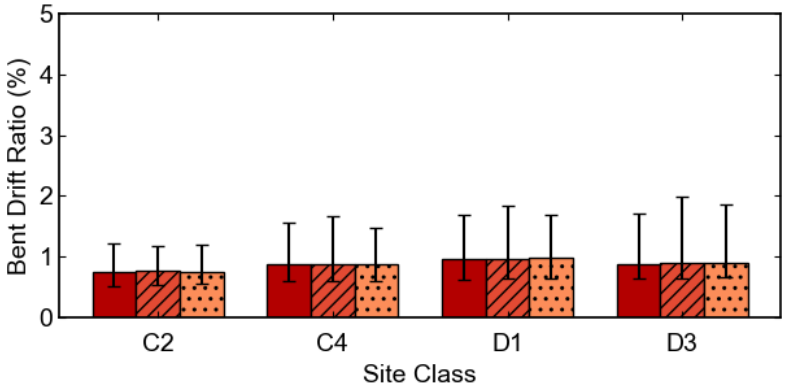

(b) Port Angeles

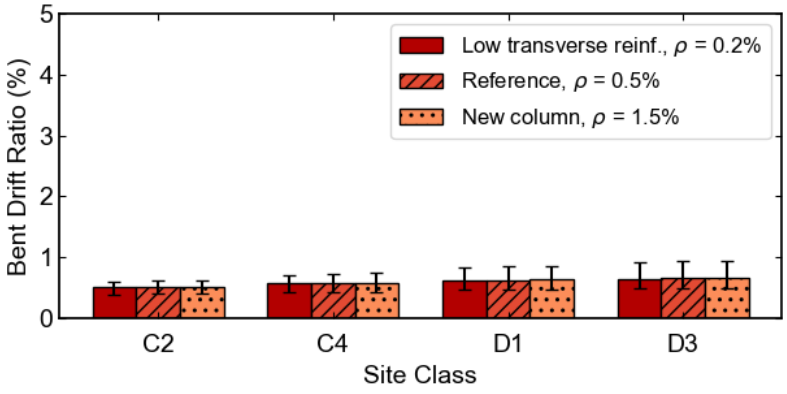

(c) Seattle

Figure 8.8: Maximum bent drift ratios for (a) Ocean Shores, (b) Port Angeles, and (c) Seattle

8.3.2 Effects on the Likelihood of Column Damage

Figure 8.9 shows effects of transverse reinforcement on the likelihood of spalling of the column concrete cover. The likelihood of spalling was calculated following the procedure described in Section 6.4. The calculated drift ratio at concrete cover spalling (Equation 6-1) does not vary with the amount of transverse reinforcement because the cover is outside the transverse reinforcement. Consequently, the likelihoods of spalling were similar for the columns with all levels of transverse reinforcement.

Figure 8.10 shows effects of the transverse reinforcement ratio on the likelihood of buckling of the column longitudinal bars. The likelihood of the onset of buckling of the longitudinal bars was calculated following the procedure described in Section 6.5. As shown in Equation 6-2, the drift ratio at the onset of bar buckling does vary with the amount of transverse reinforcement; in this case, the median drift ratio at the onset of bar buckling decreased from 7.3 percent to 4.7 percent when the transverse reinforcement ratio was increased from 0.2 percent to 1.5 percent with the value from the reference bridge falling in between. As expected, the increased amount of transverse reinforcement tended to decrease the likelihood of bar buckling.

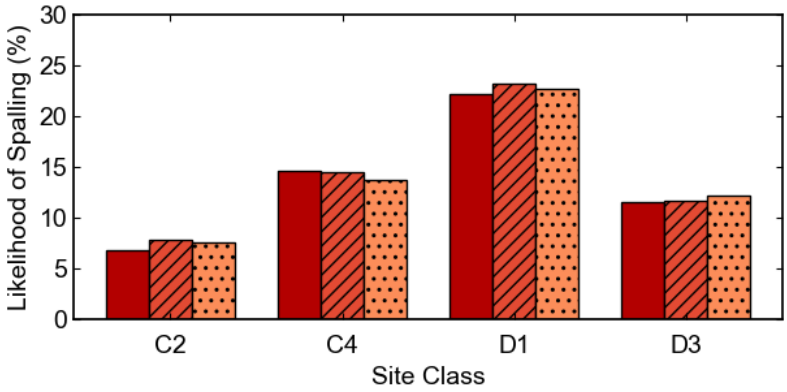

(a) Ocean Shores

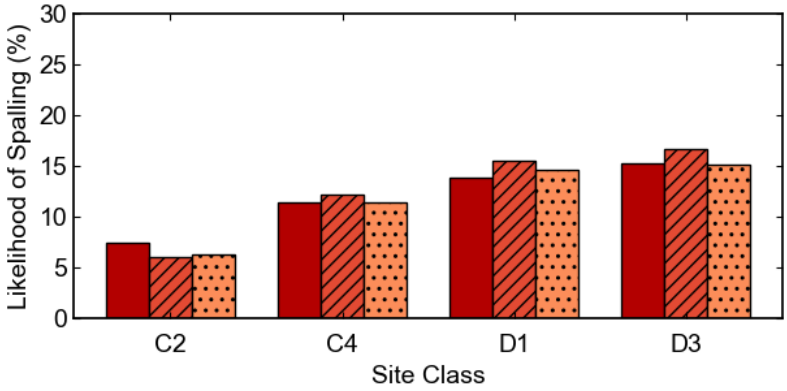

(a) Port Angeles

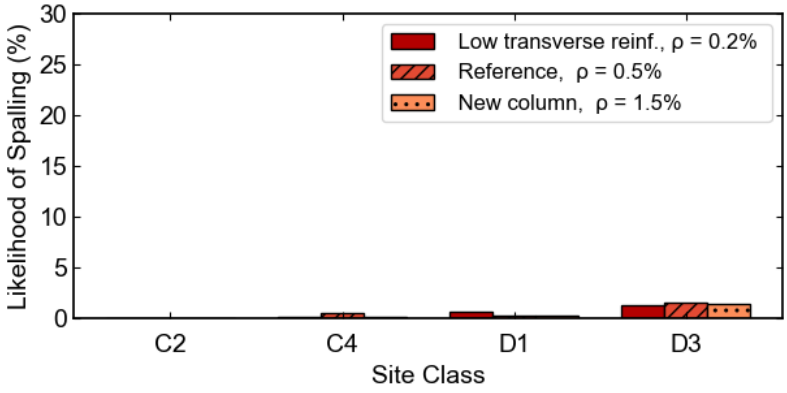

(c) Seattle

Figure 8.9: Effects of transverse reinforcement on the likelihood of spalling of the column cover concrete for (a) Ocean Shores, (b) Port Angeles, and (c) Seattle

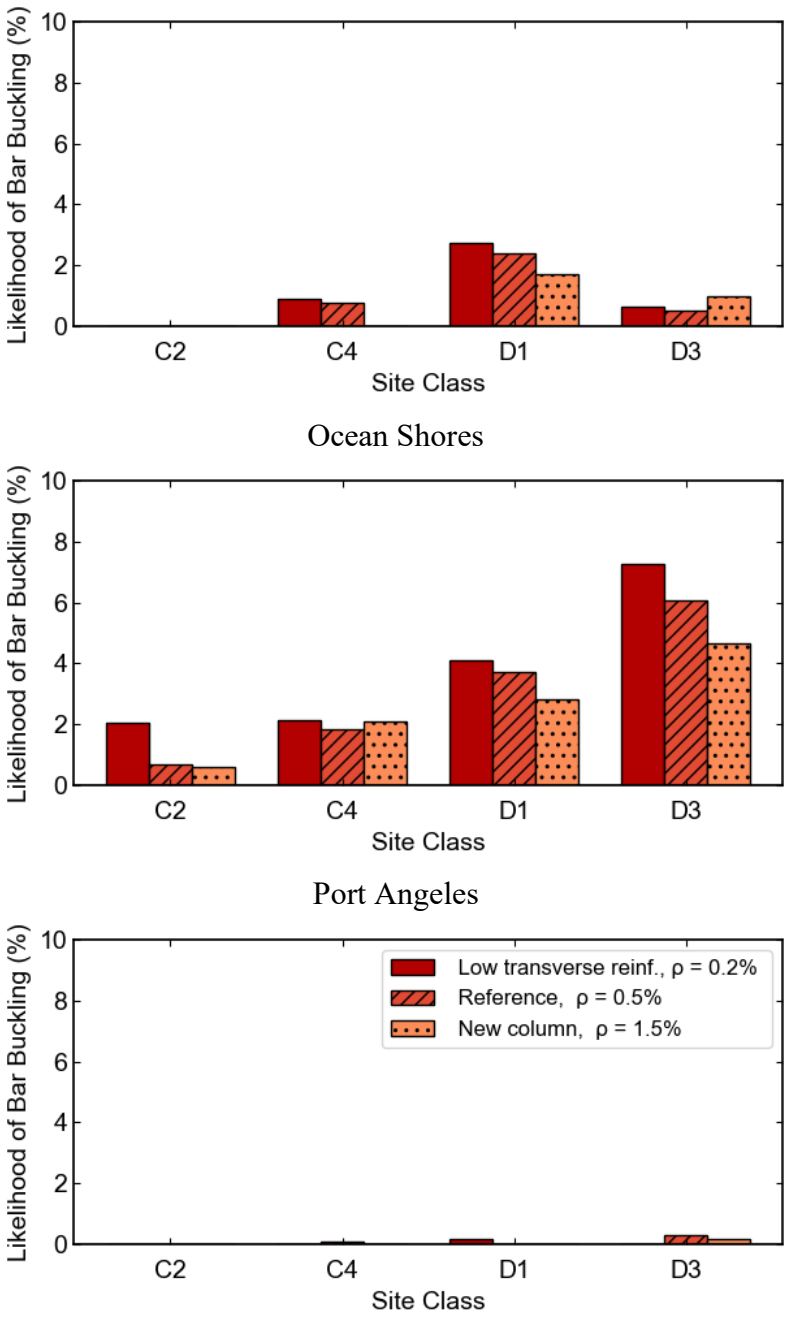

Figure 8.10: Effects of transverse reinforcement on the likelihood of the onset of buckling of the column longitudinal bars for: (a) Ocean Shores, (b) Port Angeles, and (c) Seattle

8.3.3 Effects on Force Demands

The change in transverse reinforcement ratio had almost no effect on the maximum column and shear-key forces. As shown in figures 8.11 and 8.12, the median values for column lateral forces did not reach the yield lateral force for either sets of analyses. For the shear key forces, as for the reference bridge, none of the cases reached the maximum shear-key capacity.

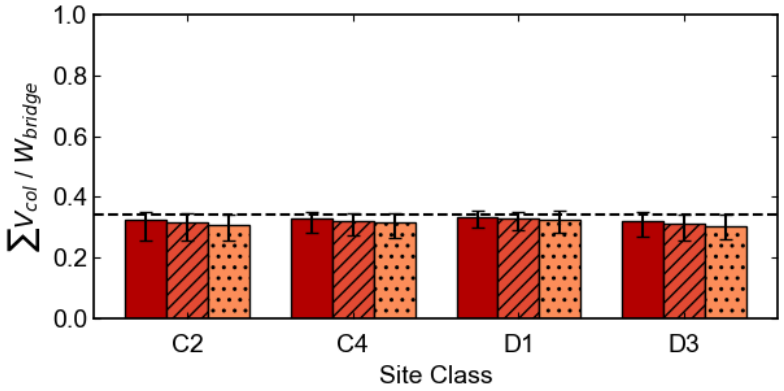

a) Ocean Shores

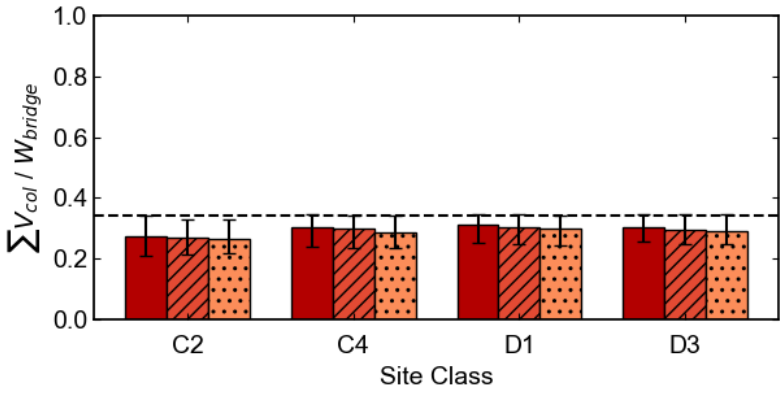

(b) Port Angeles

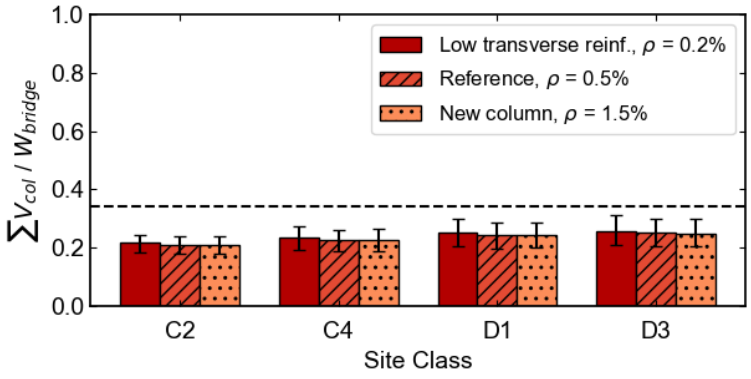

(c) Seattle

Figure 8.11: Effects of transverse reinforcement on the sum of column maximum lateral forces normalized by bridge weight for: (a) Ocean Shores, (b) Port Angeles, and (c) Seattle (Dashed line represents the effective yield of bridge columns)

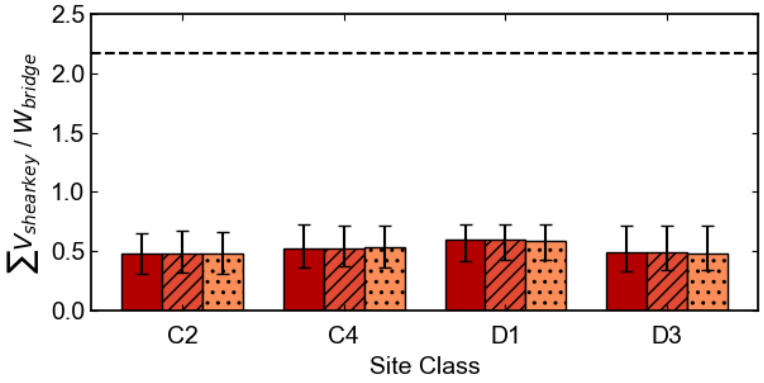

(a) Ocean Shores

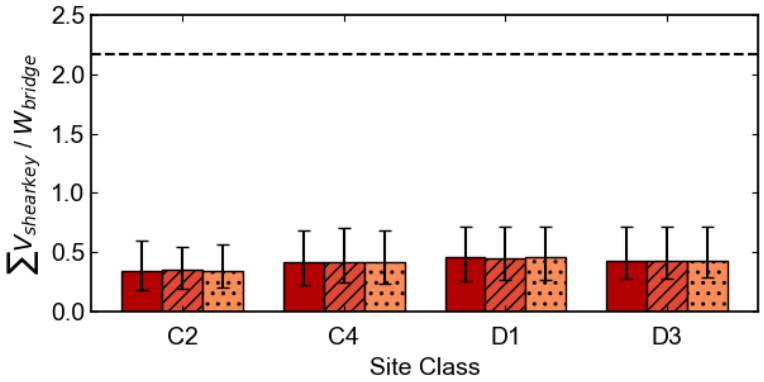

(b) Port Angeles

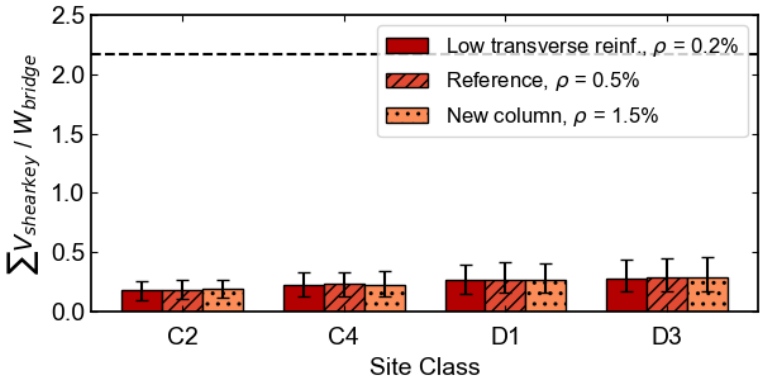

(c) Seattle

Figure 8.12: Effects of transverse reinforcement on the sum of the shear key maximum transverse forces normalized by bridge weight for (a) Ocean Shores, (b) Port Angeles, and (c) Seattle (Dashed line represents the capacity of shear keys)

CHAPTER 9 CONCLUSIONS

9.1 RESEARCH MOTIVATION

The western portions of Northern California, Oregon, and Washington state are at risk for M9 earthquakes generated by the Cascadia Subduction Zone (CSZ), which would likely cause tremendous damage to the many communities. These communities rely on a functional transportation infrastructure for pre-tsunami evacuations (for cities near the coast), post-earthquake emergency response, and economic recovery. Consequently, the performance of bridges in a CSZ event is an essential feature of the resilience of these communities.

Coastal cities in Western Washington are close to the subduction zone, so motions are expected to be intense there. Seattle, along with many other cities in the Puget Sound region, are far from the subduction zone, but they are underlain by deep sedimentary basins. Such basins have been shown to amplify long-period components of earthquake ground motions.

This study examined the effects of M9 earthquakes on typical bridges for a variety of site classes, source distances, basin presence, and key features of bridges, considering six representative cities in Western Washington. This research built directly upon the results of recent research of simulations of M9 earthquakes (Frankel et al. 2018), SDOF modeling of the effects of local site conditions (de Zamacona 2019, and Kortum et al. 2022), and a detailed bridge database compiled by WSDOT and researchers from the University of Washington.

9.2 RESEARCH APPROACH

The baseline (Frankel et al. 2018) and soil-adjusted M9 ground motions (de Zamacona 2019, Marafi et al. 2021) were used to conduct parametric studies to investigate the performance of bridges in Washington state. Six representative cities were selected to consider four geological conditions in Western Washington: coastal outside of basin (Forks and Ocean Shores), inland shallow basin (Port Angeles), inland outside of basin (Olympia), and inland deep basin (Seattle and Everett). Note that Port Angeles is located on the

Olympic Peninsula, so its site-to-source distance is considerably shorter than that of the other "inland" sites.

- WSDOT engineers and University of Washington researchers compiled a database of 582 highway bridges along major highways in the Puget Sound region (Chapter 3). A study of this database made it possible to identify properties that were common in typical bridges.
- A detailed three-dimensional, finite-element model was developed for a reference bridge that would be representative of typical highway bridges in Washington state.
- The performance of the reference bridge model was evaluated with a series of pushover and cyclic analyses and by comparing the dynamic response of the MDOF model with the results of SDOF analyses performed by Kortum et al. (2022).
- A series of parametric studies was performed to investigate the simulated performance of the reference bridge during an M9 earthquake. The first study (Chapter 6) investigated the effects of geographic location, site class, and 30 different earthquake rupture scenarios for the six representative cities. The second parametric study (Chapter 7) evaluated the effects of abutment characteristics for three representative cities. The third study (Chapter 8) evaluated the effects of column characteristics, both with and without shear keys.

9.3 PROPERTIES OF TYPICAL BRIDGES

Most of the bridges along major highways in the Puget Sound region were built before the incorporation of ductile detailing. Of the 582 bridges documented in the database, 435 (74.7 percent) were built before 1976. A total of 74 bridges had a single span, whose failure mode tends to be span unseating, which early WSDOT retrofit efforts have targeted. Out of 508 bridges with multiple spans, 416 (71.6 percent) of the intermediate supports contained at least one reinforced concrete column, which is a common location of bridge damage and failure. As expected, the transverse reinforcement ratio for older reinforced concrete columns (pre-1976) tended to be much smaller than that for newer columns, but interestingly, the longitudinal reinforcement ratio did not vary greatly based on the era of construction (Chapter 3).

A key question addressed in this study was the effectiveness of the abutments in restraining the expected deformations of the bridge. This restraint depends greatly on the continuity of the superstructure and on the presence of transverse shear keys at the abutments. The database study found that 76 percent of pre-1976 bridges had continuous superstructures, and this percentage increased to 97 percent for newer bridges (1976-2018). A study of a subset of 94 bridges for which abutment characteristics were collected found that 90.3 percent (65/72 bridges) of the older bridges and 100 percent (19 bridges) of newer bridges had an internal shear key, an external shear key, or both.

9.4 EARTHQUAKE PERFORMANCE OF REFERENCE BRIDGE

The simulated deformation responses of the typical bridge in the longitudinal direction were consistently smaller than those in the transverse direction because of the high resistance provided by the abutment and backfill soil. For all six locations and four site classes, the 85th percentile longitudinal deformations at the end of the deck were below 2.5 inches, and the bent drift ratio was below 1.0 percent. The following conclusions, drawn from Chapter 6, are provided regarding the response of the bridge in the transverse direction.

In the transverse direction, the coastal locations (Forks and Ocean Shores) had the largest displacement responses. The highest responses for coastal cities were for site class D1, with the 85th percentile responses reaching values of almost 6 inches for the maximum end displacement and almost 2.5 percent for the maximum bent drift ratio. This drift ratio was slightly above the mean drift ratio at spalling (2.3 percent) for reinforced concrete columns, and it was less than half the mean drift ratio at bar buckling for older bridges (4.9 percent).

The responses tended to decrease as the distance from the coast increased. The median transverse displacements were 2 inches or less at the bridge ends, and the median bent drifts were less than 0.8 percent for the two cities located far from the coast and on deep basins (Seattle and Everett).

The force demands on the internal transverse shear keys tended to be far below their nominal capacity. For example, the highest demand corresponded to the city of Forks and

site class D1. In this location, the 85th percentile value for the maximum shear-key force corresponded to only 33 percent of the nominal shear key capacity.

9.5 EFFECTS OF VARIATIONS IN PROPERTIES OF A TYPICAL BRIDGE

The type of abutment (e.g., L-type, semi-integral, and integral) did not significantly affect the transverse response of the bridge, with the median bent drift consistently between 0.5 percent and 1.5 percent. In particular, the L-type abutment and the semi-integral abutment produced similar displacement responses while the integral abutments tended to produce smaller responses.

The abutment foundation type, i.e., piles or spread footings, and the associated soil type, i.e., medium sand and medium clay, did have a small impact on the bridge response. In general, abutments supported on spread footings allowed more transverse displacement than abutments supported on piles, but the magnitude of the increase was dependent on ground motion realization. There was a slight increase in the median bent drift ratio, but it still never exceeded 1.5 percent, and the end displacement was consistently smaller than 3.5 inches. However, the variability in the response increased significantly for spread footing. The 85th percentile value for bent drift ratio was greater than 5 percent, and the 85th percentile value for end displacement was greater than 12 inches for the bridge with spread footings and on medium clay.

A significant increase in transverse displacement response was found with removal of the shear keys and bearing pads, and when the column height was increased. When both the shear keys and bearing pads were removed, the median bent drift ratio was more than three times higher than the original value for the reference bridge, i.e., the end displacement of the deck was close to 8 inches, with the highest 85th-percentile end deck displacement value greater than 12 inches (figures 7.5 and 7.6). This condition, with the shear keys and bearings removed, indirectly approximated the response of bridges with discontinuous superstructures, and the results indicated that such bridges would likely have severe damage. When the shear keys were removed *and* the column height was doubled, the median bent drift ratio further increased to nearly five times that obtained for the reference bridge, with the values of the end deck displacements reaching close to 12 inches. This

indicated that discontinuous bridges with tall columns should be prioritized for seismic evaluation and retrofit.

Decreasing the column height also influenced the response significantly when the shear keys and bearings were not present. When the column height was reduced to half the height for the reference bridge, the median sum of column forces was observed to increase to twice the value for the reference bridge, with the highest sum of column of shear forces reaching 70 percent (1,446 kips) of the bridge weight. This indicated that shorter columns could have shear failure problems and should be prioritized for seismic evaluation and retrofit.

Shear keys provided large resistance for the bridges in the transverse direction. For the reference bridge in this study, the total maximum capacity of the shear keys was 2.17 times the bridge weight. None of the scenarios considered was close to reaching the maximum capacity of the shear keys.

For most scenarios that were considered in this research where shear keys were present, the 85thth percentile values for the sum of the column forces were close to or just reaching the effective yield of the columns.

When the shear keys were included in the analysis, the change of the transverse reinforcement ratio (old and new columns) had minimal effect on the performance of the bridges. In the case where the bridge had old columns and no shear keys, the displacements increased.

In sum, the deformation response of the bridges increased relative to the reference bridge when the abutment resistance was decreased. This effect was observed by replacing the abutment piles with spread footings or by assuming a softer soil at the abutment. This effect was particularly large when the resistance of the shear keys and bearing pads was neglected. Furthermore, bridges with less flexibility were observed to have the largest deformation response in cities closer to the coast (Ocean Shores), while those with higher flexibility had the largest response in the cities on the sedimentary basin (Port Angeles), especially for ground motions generated with the softest soil site class (D3). This observation was consistent with expected effects of basin amplification. In inland cities located on deep basins (e.g., Seattle), the motions were not found to be strong enough to

cause yielding and softening of the bridge; thus their response was smaller than that for cities closer to the coast.

CHAPTER 10 RECOMMENDATIONS FOR WSDOT

The results of this research provide WSDOT with an opportunity to prioritize the seismic evaluation and retrofitting of bridges for CSZ hazards, which can potentially decrease the cost and increase the efficiency of identifying bridges with higher seismic risk. The results also allow WSDOT to develop earthquake scenarios for emergency management planning. While the CSZ represents only one portion of the aggregate seismic hazard, it dominates the hazard along the coast of Washington state. Note that amplification of ground shaking from the deep sedimentary basin that underlies much of the Puget Sound region is also a concern.

Bridge abutments contribute greatly to the seismic performance of typical bridges by restraining the bridge motion, but this restraint depends on the presence of a continuous superstructure and shear keys. Bridges that lack either of these two features, particularly if they were built before 1976, should be a high priority for retrofit, particularly along the coast, where the damage is likely to be the greatest. In the Puget Sound region, bridge deformation response and corresponding column drift demands were found to be largest for bridges that have taller columns, no shear keys, and no bearing pads.

The study also found that the largest bridge responses tended to happen in cities on basins and closer to the rupture zone (e.g., Port Angeles). In these regions the shaking is strong enough at short periods to cause some damage and period elongation of the bridge due to the proximity to the fault plane. These locations amplify somewhat shorter period content of the ground motion, relative to deeper basin locations such as Seattle. That amplified content aligns with the elongated period of the bridge and results in larger response. Therefore, bridge location in terms of both distance from the CSZ fault plane and basin depth may also be used to prioritize bridge evaluation and retrofit.

Notably, the recommendations for WSDOT are limited to the bridges studied and the assumptions used in the modeling. Importantly, shear failure, shear-flexure interaction, and damage from soil liquefaction and lateral spreading were not considered and remain important priorities for bridge seismic retrofit. Additionally, ground motions from only the CSZ source were considered, and crustal faults in the region should be considered in a complete seismic evaluation.

Additional research is needed to fully assess the seismic vulnerability of typical bridges in Washington state. This critical additional research includes the following:

- The effects of soil liquefaction that were not considered in this report. It is likely that soil liquefaction can happen during severe earthquakes.
- Cases in which the bridges are skewed or curved. The symmetricity can significantly influence the response of bridge structures during an earthquake.
- Shear failures of the bridge columns, which were not considered in this study. The column parametric studies in Chapter 8 showed that the lateral force demands at columns significantly increased as the column heights were reduced to half of their original value. This result suggested a higher potential of shear failure for bridges that have shorter column heights. Column shear failure is one of the most common causes of bridge collapse (Moehle and Eberhard 2000).

REFERENCES

AASHTO. 2017. LRFD Bridge Design Specifications. American Association of State Highway and Transportation Officials.

Ahdi, S.K, Stewart, J., Ancheta, T, Kwak, D., and Mitra, D. 2017. "Development of VS Profile Database and Proxy-based Models for VS30 Prediction in the Pacific Northwest Region of North America." Bulletin of the Seismological Society of America 107: 1781-1801.

Berry, M., 2006. "Experimental Calibration of OpenSees Components Using the PEER Column Database." Ph.D. thesis, Department of Civil and Environmental Engineering, University of Washington.

Berry, M.P. and Eberhard, M.O., 2003. "Performance Models for Flexural Damage in Reinforced Concrete Columns," PEER-2003/18, Pacific Earthquake Engineering Research Center, University of California, Berkeley, August.

Berry, M.P., and Eberhard, M.O. 2005. "Practical Performance Model for Bar Buckling." Journal of Structural Engineering, 131(7), 1060-1070.

Berry, M.P. and Eberhard, M.O., 2007. "Performance Modeling Strategies for Modern Reinforced Concrete Bridge Columns," PEER-2007/07, Pacific Earthquake Engineering Research Center, University of California, Berkeley, April.

Berry, M., M. Parrish, and M. Eberhard, 2004. "PEER Structural Performance Database User's Manual." Pacific Earthquake Engineering Research Center, Berkeley, CA.

Bournonville, M., Dahnke, J., and Darwin, D., 2004. "Statistical Analysis of the Mechanical Properties and Weight of Reinforcing Bars." Structural Engineering and Material Laboratory, University of Kansas.

De Zamacona Cervantes, Gloria, 2019. "Response of Idealized Structural Systems to Simulated M9 Cascadia Subduction Zone Earthquakes Considering Local Soil Conditions." Master's Thesis, University of Washington, Seattle.

Elwood, Kenneth, and Eberhard, Marc, 2009. "Effective Stiffness of Reinforced Concrete Columns," ACI Structural Journal, July-August, 106(4), 476-484.

Evans, L. T. and Duncan, J. M., 1982. "Simplified Analysis of Laterally Loaded Piles." No. UCB/GT/82-04, University of California, Berkeley, CA.

FEMA (Federal Emergency Management Agency). 1995. NEHRP Recommended Seismic Provisions for Seismic Regulations for New Buildings (FEMA 222A and 223A).

Frankel, Arthur, Wirth, Erin, Marafi, Nasser. 2018. "The M9 Project Ground Motions", in The M9 Project Ground Motions. DesignSafe-CI. https://doi.org/10.17603/DS2WM3W.

Frankel, Arthur, Erin Wirth, Nasser Marafi, John Vidale, and William Stephenson; 2018. Broadband Synthetic Seismograms for Magnitude 9 Earthquakes on the Cascadia Megathrust Based on 3D Simulations and Stochastic Synthetics, Part 1: Methodology and Overall Results. Bulletin of the Seismological Society of America 2018; 108 (5A): 2347–2369. doi: https://doi.org/10.1785/0120180034

Khaleghi, Bijan. 2019. Memo to All Design Section Staff. Washington State Department of Transportation Bridge and Structures Office.

Kortum, Z, Liu, K.-J., Eberhard, M.O., Berman, J.W., Marafi, N.A., Maurer, B., 2022. "Impacts of Cascadia Subduction Zone M9 Earthquakes on Bridges in Washington State: SDOF Idealized Bridges," Washington State Department of Transportation report WA-RD 908.1.

Lehman, D. E. and J. P. Moehle, 2000. Seismic Performance of Well-Confined Concrete Bridge Columns. PEER 1998/01, Pacific Earthquake Engineering Research Center, Berkeley, CA.

Lignos, D.G. and Krawinkler, H., 2012. "Sidesway collapse of deteriorating structural systems under seismic excitations," Rep.No.TB 177, The John A. Blume Earthquake Engineering Research Center, Stanford University, Stanford, CA.

Mander, J. B., Priestley, M. J. N., and Park, R., 1988. "Theoretical Stress-Strain Model for Confined Concrete" Journal of Structural Engineering, 114(8): 1804-1826.

Mangalathu, Sujith, 2017. "Performance Based Grouping and Fragility Analysis of Box-Girder Bridges in California" Ph.D. thesis, Georgia Institute of Technology, Georgia.

Mangalathu, Sujith, Jeon, Jon-Su, Jian, Jiquing. "Skew Adjustment Factors for Fragilities of California Box-Girder Bridges Subjected to near-Fault and Far-Field Ground Motions." Journal of Bridge Engineering. 24(1). DOI: 10.1061/(ASCE)BE.1943-5592.0001338.

Marafi, N.A. 2018. "Impacts of an M9 Cascadia Subduction Zone Earthquake on Structures Located in Deep Sedimentary Basins." Ph. D. thesis, University of Washington, Seattle.

Marafi, N.A., Eberhard, M.O., Berman, J.W., Wirth, E.A., and Frankel, A.D., 2017. "Effects of Deep Basins on Structural Collapse during Large Subduction Zone Earthquakes." Earthquake Spectra, 33(3), 963-997. https://doi.org/10.1193/071916EQS114M

Marafi, Nasser, Eberhard, Marc, and Berman, Jeffrey, 2019. “Impacts of Simulated M9 Cascadia Subduction Zone Motions on Idealized Systems”. Earthquake Spectra, Vol 35, Issue 3, 2019.

Marafi, N.A., grant, A., Maurer, B.W., Rateria, G., Eberhard. M.O., and Berman, J.W. 2021. “A Generic Soil Velocity Model that Accounts for Near-Surface Conditions and Deeper Geologic Structure,” Soil Dynamics and Earthquake Engineering. 140. DOI: 10.1016/j.soildyn.2020.106461

Marafi, Nasser, Makdisi, Andrew, Eberhard, Marc O., and Berman, Jeffrey. 2020. “Performance of RC Core-Wall Buildings during Simulated M9 Cascadia Subduction Zone Earthquake Scenarios”. Journal of Structural Engineering, Volume 146, Issue 2.

Megally, S. H., Silva, F. P., and Seible, F., 2002. “Seismic Response of Sacrificial Shear Keys in Bridge Abutments.” Report No. SSRP-2001/23, Department of Structural Engineering, University of California, San Diego, CA.

Moehle, J. P., and Eberhard, M. O., 2000. Earthquake damage to bridges. Bridge engineering handbook, 1-34.

Muthukumar, S. and DesRoches, R. 2006. A Hertz contact model with non-linear damping for pounding simulation. Earthquake Engineering and Structural Dynamics, 35, pp:811-828.

Pacific Northwest Seismic Network. “Cascadia Subduction Zone.” https://pnsn.org/outreach/earthquakesources/csz (May 31, 2021)

Palmer, S., Magsin, S., Bilderback, E., Poelstra, J., Folger, D., and Niggemann, R. 2007. “Liquefaction Susceptibility and Site Class Maps of Washington State, By County.” Washington Division of Geology and Earth Resources. Open File Report 2004-20. ftp://ww4.dnr.wa.gov/geology/pubs/ofr04-20/ (June 4, 2019).

Ramanathan, Karthik Narayan, 2012. “Next Generation Seismic Fragility Curves for California Bridges Incorporating the Evolution in Seismic Design Philosophy” Ph. D. thesis, Georgia Institute of Technology, Georgia.

Ranf, R. 2006. Performance Based Evaluation of Seismic Modeling Strategies for Bridges. Ph.D. thesis, University of Washington, Seattle.

Ranf, Richard Tyler, 2007. “Model Selection for Performance-Based Earthquake Engineering of Bridges.” Ph. D. thesis, University of Washington, Seattle.

Shamsabadi, A. and Yan, L. 2008. Closed-form force-displacement backbone curves for bridge abutment-backfill systems. Geotechnical Earthquake Engineering and Soil Dynamics IV. 2008. 1-10.

United States Geological Survey (USGS), 2017, Illustration of Seismic Source Zones in the Pacific Northwest, https://geomaps.wr.usgs.gov/pacnw/pacnweq/pdf/subd_eqpg.pdf

University of Washington-Pacific Earthquake Engineering Research Structural Performance Database. https://nisee.berkeley.edu/spd/. Accessed June 2020.

Wirth, Erin A., Arthur D. Frankel, Nasser Marafi, John E. Vidale, and W. J. Stephenson; 2018. Broadband Synthetic Seismograms for Magnitude 9 Earthquakes on the Cascadia Megathrust Based on 3D Simulations and Stochastic Synthetics, Part 2: Rupture Parameters and Variability. Bulletin of the Seismological Society of America 2018; 108 (5A): 2370–2388. doi: https://doi.org/10.1785/0120180029

Zhu, M., McKenna, F., and Scott, M. H., 2018. "OpenSeesPy: Python Library for the OpenSees Finite Element Framework". Volume 7, School of Civil and Construction Engineering, Oregon State University, OR

APPENDIX A: BRIDGES SELECTED FOR ABUTMENT DATABASE

Table A.1: Selected bridges for abutment database

Bridge Number	Longitude	Latitude	Year
167/110	47.29569	-122.2578	1975
167/122E	47.37778	-122.2444	1967
167/123W	47.3812	-122.2446	1967
167/126E	47.39223	-122.2373	1967
167/128E	47.39825	-122.2284	1967
167/138HOV	47.46492	-122.218	2018
167/16	47.21353	-122.3419	1970
167/20W	47.20189	-122.294	1971
167/38	47.23572	-122.2521	2004
405/104P	47.79386	-122.2124	2007
405/105E	47.79786	-122.2205	1968
405/108W	47.81989	-122.2422	1968
405/10A	47.46489	-122.2482	1994
405/11	47.4637	-122.2459	1964
405/112W	47.83114	-122.2615	1982
405/13	47.46715	-122.2343	2009
405/15	47.46771	-122.2184	1989
405/17	47.47031	-122.2064	2010
405/23E-N	47.50228	-122.1963	1997
405/23W	47.50253	-122.1968	1966

Bridge Number	Longitude	Latitude	Year
405/30E	47.5675	-122.1799	1965
405/35E	47.57939	-122.1741	1969
405/35HOV	47.5799	-122.1744	1969
405/41E	47.60297	-122.1836	1971
405/45.4NE	47.63166	-122.1847	2011
405/45E	47.62978	-122.1883	1965
405/47S-W	47.6341	-122.1882	1966
405/50	47.66945	-122.1878	1970
405/52W	47.67889	-122.1847	1971
405/56W	47.70667	-122.1783	1970
405/59W	47.71822	-122.1876	1970
405/64	47.7425	-122.1875	1969
405/73	47.76855	-122.19	1968
5/439	47.23111	-122.4431	2007
5/445S-S	47.23316	-122.4319	1965
5/455	47.23942	-122.4048	1963
5/457	47.24172	-122.3857	1961
5/461	47.24389	-122.3361	1960
5/461A	47.24467	-122.3363	1962
5/464W	47.252	-122.3328	1960

Bridge Number	Longitude	Latitude	Year
5/504E	47.30033	-122.3028	1959
5/508E	47.35233	-122.2955	1960
5/509E	47.35764	-122.2963	1961
5/516W	47.43119	-122.2715	1963
5/519E	47.45072	-122.2653	1966
5/520HOV	47.45744	-122.2639	1996
5/521E	47.46147	-122.2636	1966
5/522HOV	47.46108	-122.2639	1996
5/522S-E	47.46247	-122.2653	1966
5/525.5H	47.48342	-122.2707	1996
5/526.1	47.48906	-122.2641	1966
5/526E	47.48692	-122.2662	1964
5/532W	47.53528	-122.2972	1967
5/533A	47.54842	-122.3177	1966
5/534N-W	47.55267	-122.3181	1967
5/534W	47.55327	-122.3176	1966
5/535E	47.56055	-122.3213	1966
5/536E-S	47.57108	-122.324	1967
5/537N	47.57322	-122.3159	1967
5/538S-E	47.57428	-122.3202	1967

Bridge Number	Longitude	Latitude	Year
5/538S-W	47.57408	-122.3203	1967
5/539.5	47.58611	-122.3222	1966
5/542E	47.59553	-122.3203	1965
5/542NCD	47.59553	-122.3197	1965
5/543SCD	47.59808	-122.3215	1965
5/545R	47.60414	-122.3274	1964
5/548	47.60872	-122.3314	1964
5/551	47.61417	-122.3306	1965
5/553	47.61845	-122.3293	1962
5/566N-E	47.63325	-122.3235	1963
5/574	47.66497	-122.3225	1962
5/583	47.68682	-122.3269	1964
5/588N-N	47.70841	-122.3294	1995
5/588SCD	47.70842	-122.3304	1964
5/593W	47.74096	-122.329	1964
5/599SCD	47.77739	-122.3183	1995
5/601N-E	47.78272	-122.3162	1995
5/607E	47.80633	-122.3062	1963
5/631E	47.9663	-122.1987	1967
5/638W	47.98083	-122.1885	1967

Bridge Number	Longitude	Latitude	Year
5/646	48.00753	-122.1748	1967
5/647W	48.02314	-122.1758	1968
5/649E	48.04014	-122.179	1968
5/650E	48.0433	-122.1805	1969
5/654A	48.07558	-122.1794	1996
512/10S	47.15894	-122.4158	1966
512/12	47.15903	-122.4057	1965
512/13	47.15867	-122.4026	1965
90/47E-N	47.57989	-122.1753	1969
90/50N	47.58055	-122.1686	1940
90/66N	47.54053	-122.036	1971
90/67E-E	47.53136	-122.0256	2003
90/89S	47.46481	-121.7165	1971
90/99	47.42705	-121.4158	1969

APPENDIX B: STRUCTURAL DRAWINGS FOR BRIDGE 405/23E-N

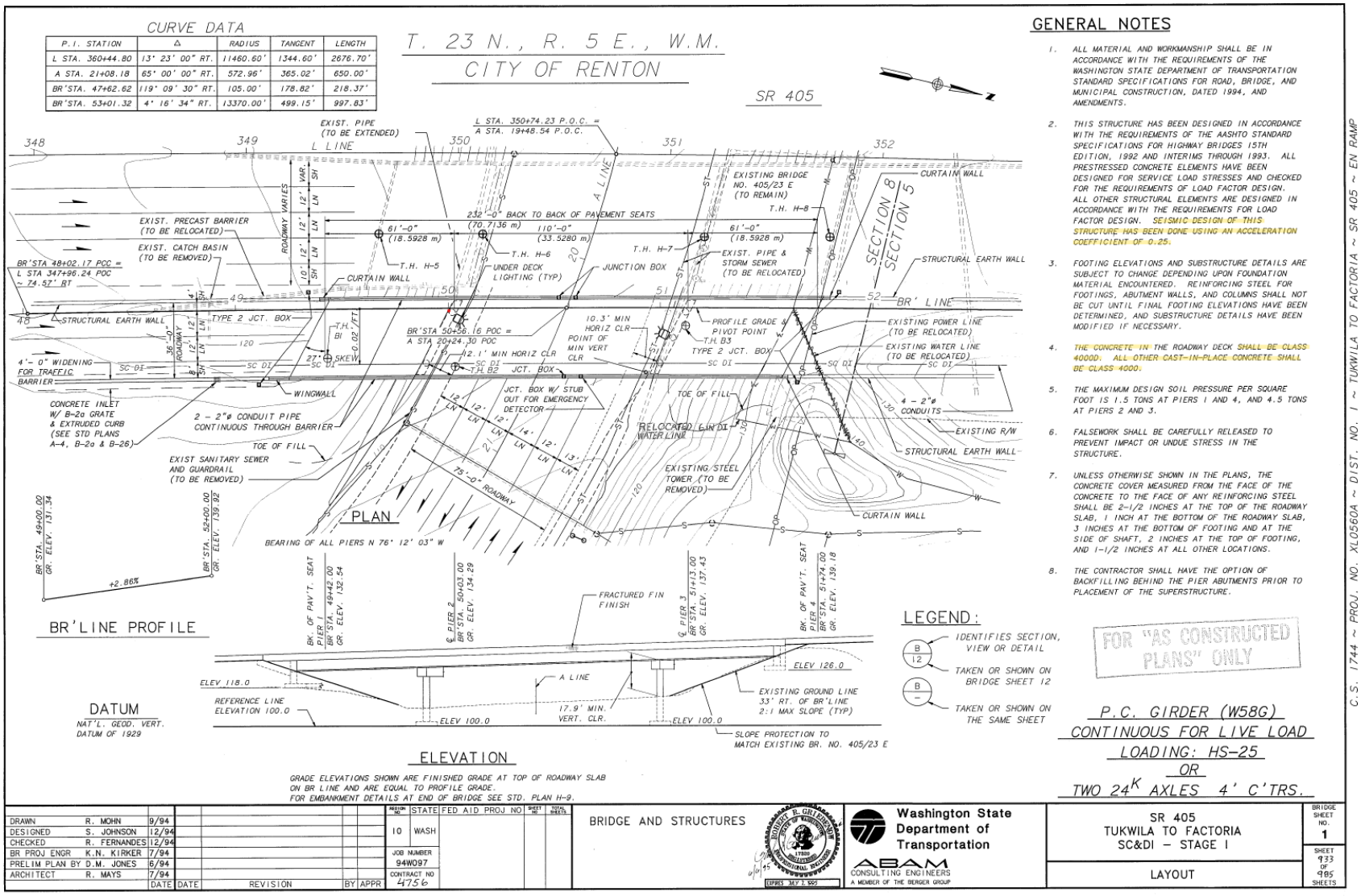
CURVE DATA
P.I. STATION | Δ | RADIUS | TANGENT | LENGTH
L STA. 360+44.80 | 13° 23' 00" RT. | 11460.60' | 1344.60' | 2676.70'
A STA. 21+08.18 | 65° 00' 00" RT. | 572.96' | 365.02' | 650.00'
BR'STA. 47+62.62 | 119° 09' 30" RT. | 105.00' | 178.82' | 218.37'
BR'STA. 53+01.32 | 4° 16' 34" RT. | 13370.00' | 499.15' | 997.83'
T. 23 N., R. 5 E., W.M.
CITY OF RENTON
SR 405
GENERAL NOTES
1. ALL MATERIAL AND WORKMANSHIP SHALL BE IN ACCORDANCE WITH THE REQUIREMENTS OF THE WASHINGTON STATE DEPARTMENT OF TRANSPORTATION STANDARD SPECIFICATIONS FOR ROAD, BRIDGE, AND MUNICIPAL CONSTRUCTION, DATED 1994, AND AMENDMENTS.
2. THIS STRUCTURE HAS BEEN DESIGNED IN ACCORDANCE WITH THE REQUIREMENTS OF THE AASHTO STANDARD SPECIFICATIONS FOR HIGHWAY BRIDGES 15TH EDITION, 1992 AND INTERIMS THROUGH 1993. ALL PRESTRESSED CONCRETE ELEMENTS HAVE BEEN DESIGNED FOR SERVICE LOAD STRESSES AND CHECKED FOR THE REQUIREMENTS OF LOAD FACTOR DESIGN. ALL OTHER STRUCTURAL ELEMENTS ARE DESIGNED IN ACCORDANCE WITH THE REQUIREMENTS FOR LOAD FACTOR DESIGN. SEISMIC DESIGN OF THIS STRUCTURE HAS BEEN DONE USING AN ACCELERATION COEFFICIENT OF 0.25.
3. FOOTING ELEVATIONS AND SUBSTRUCTURE DETAILS ARE SUBJECT TO CHANGE DEPENDING UPON FOUNDATION MATERIAL ENCOUNTERED. REINFORCING STEEL FOR FOOTINGS, ABUTMENT WALLS, AND COLUMNS SHALL NOT BE CUT UNTIL FINAL FOOTING ELEVATIONS HAVE BEEN DETERMINED, AND SUBSTRUCTURE DETAILS HAVE BEEN MODIFIED IF NECESSARY.
4. THE CONCRETE IN THE ROADWAY DECK SHALL BE CLASS 4000D. ALL OTHER CAST-IN-PLACE CONCRETE SHALL BE CLASS 4000.
5. THE MAXIMUM DESIGN SOIL PRESSURE PER SQUARE FOOT IS 1.5 TONS AT PIERS 1 AND 4, AND 4.5 TONS AT PIERS 2 AND 3.
6. FALSEWORK SHALL BE CAREFULLY RELEASED TO PREVENT IMPACT OR UNDUE STRESS IN THE STRUCTURE.
7. UNLESS OTHERWISE SHOWN IN THE PLANS, THE CONCRETE COVER MEASURED FROM THE FACE OF THE CONCRETE TO THE FACE OF ANY REINFORCING STEEL SHALL BE 2-1/2 INCHES AT THE TOP OF THE ROADWAY SLAB, 1 INCH AT THE BOTTOM OF THE ROADWAY SLAB, 3 INCHES AT THE BOTTOM OF FOOTING AND AT THE SIDE OF SHAFT, 2 INCHES AT THE TOP OF FOOTING, AND 1-1/2 INCHES AT ALL OTHER LOCATIONS.
8. THE CONTRACTOR SHALL HAVE THE OPTION OF BACKFILLING BEHIND THE PIER ABUTMENTS PRIOR TO PLACEMENT OF THE SUPERSTRUCTURE.
PLAN
BR'LINE PROFILE
ELEVATION
DATUM
NAT'L. GEOD. VERT. DATUM OF 1929
LEGEND:
IDENTIFIES SECTION, VIEW OR DETAIL
TAKEN OR SHOWN ON BRIDGE SHEET 12
TAKEN OR SHOWN ON THE SAME SHEET
FOR "AS CONSTRUCTED PLANS" ONLY
P.C. GIRDER (W58G)
CONTINUOUS FOR LIVE LOAD
LOADING: HS-25
OR
TWO 24K AXLES 4' C'TRS.
GRADE ELEVATIONS SHOWN ARE FINISHED GRADE AT TOP OF ROADWAY SLAB ON BR LINE AND ARE EQUAL TO PROFILE GRADE.
FOR EMBANKMENT DETAILS AT END OF BRIDGE SEE STD. PLAN H-9.
DRAWN R. MOHN 9/94
DESIGNED S. JOHNSON 12/94
CHECKED R. FERNANDES 12/94
BR PROJ ENGR K.N. KIRKER 7/94
PRELIM PLAN BY D.M. JONES 6/94
ARCHITECT R. MAYS 7/94
DATE DATE REVISION BY APPR
REGION NO. 10 STATE WASH FED AID PROJ NO
JOB NUMBER 94W097
CONTRACT NO 4756
BRIDGE AND STRUCTURES
ROBERT B. GRETZINGER
EXPIRES JULY 7, 1995
Washington State Department of Transportation
ABAM CONSULTING ENGINEERS
A MEMBER OF THE BERGER GROUP
SR 405
TUKWILA TO FACTORIA
SC&DI - STAGE 1
LAYOUT
BRIDGE SHEET NO. 1
SHEET 933 OF 985 SHEETS
SR 405 JOB NO. 7062 SHEET 1 OF 22
C.S. 1744 ~ PROJ. NO. XL0560A ~ DIST. NO. 1 ~ TUKWILA TO FACTORIA ~ SR 405 ~ EN RAMP

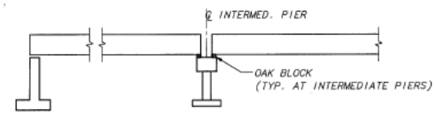

STAGE 1 – SET GIRDERS IN PLACE

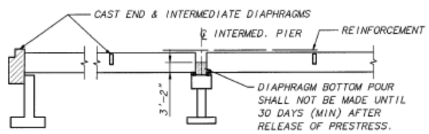

STAGE 2 – POUR DIAPHRAGMS
AND PLACE REINFORCEMENT

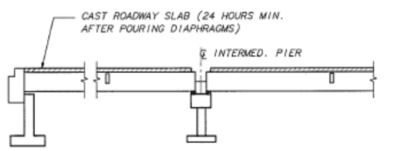

STAGE 3 – POUR ROADWAY SLAB

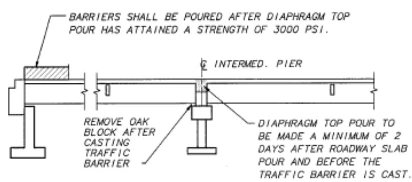

STAGE 4 – POUR DIAPHRAGMS
AT INTERMEDIATE PIERS AND BARRIERS

CONSTRUCTION SEQUENCE – SUPERSTRUCTURE

EXISTING ELEVATION A LINE			
STATION	ELEVATION LT SHOULDER	ELEVATION CENTER LINE	ELEVATION RT SHOULDER
19+00.00	–	–	102.32
19+20.00	–	105.35	103.06
19+40.00	107.59	106.06	103.79
19+60.00	108.26	106.74	104.50
19+80.00	108.95	107.44	105.28
20+00.00	109.68	108.16	105.14
20+20.00	110.45	109.16	107.03
20+40.00	111.15	109.81	107.88
20+60.00	111.88	110.58	108.73
20+80.00	112.69	111.42	109.58
21+00.00	113.64	112.28	110.47
21+20.00	114.36	113.11	111.42
21+40.00	115.16	113.92	112.39

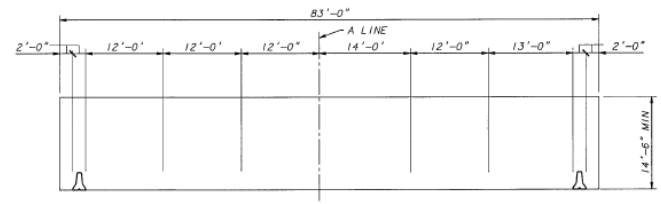

CONSTRUCTION OPENING DIAGRAM
NORMAL TO A LINE

FOR "AS CONSTRUCTED PLANS" ONLY

SR 405 JOB NO. Z06Z SHEET 2 OF 22

DRAWN	R. MOHN	9/94	
DESIGNED	E. DORNSEIF	12/94	
CHECKED	R. FERNANDES	12/94	
BR PROJ ENGR			
PRELIM PLAN BY			
ARCHITECT			
		DATE	DATE / REVISION / BY / APPR

REGION NO. 10 | STATE WASH | FED AID PROJ NO | SHEET NO. | TOTAL SHEETS
JOB NUMBER 94W097
CONTRACT NO 4756

BRIDGE AND STRUCTURES

1-3-95

Washington State Department of Transportation

ABAM CONSULTING ENGINEERS
A MEMBER OF THE BERGER GROUP

SR 405
TUKWILA TO FACTORIA
SC&DI - STAGE 1

CONSTRUCTION SEQUENCE AND PROFILE GEOMETRY

BRIDGE SHEET NO. 2
SHEET 934 OF 985 SHEETS

SR 405/417

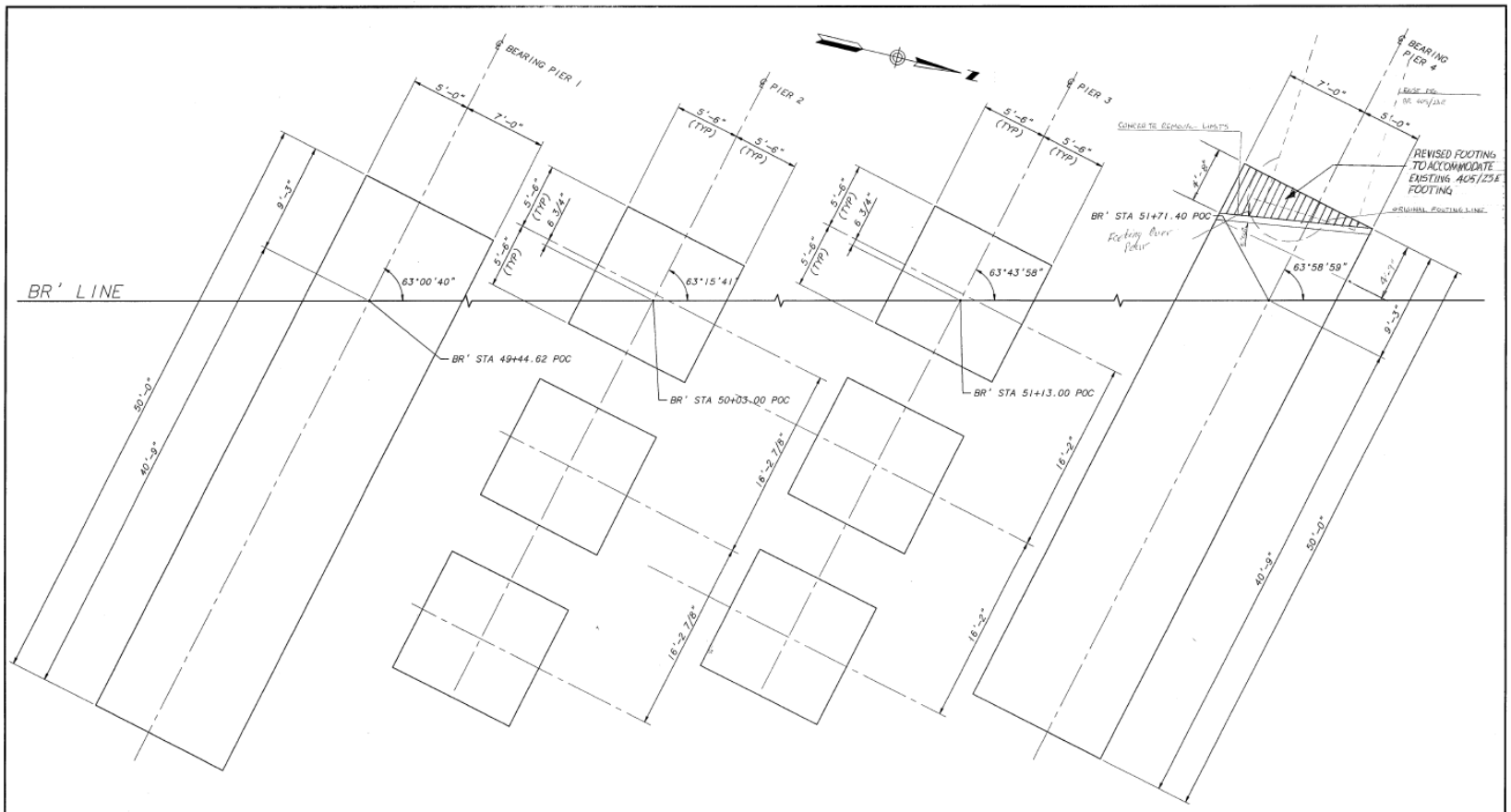

DRAWN	B. HUYNH	9/94				REGION NO.	STATE	FED AID PROJ NO	SHEET NO	TOTAL SHEETS	BRIDGE AND STRUCTURES
DESIGNED	E. DORNSEIF	12/94				10	WASH				
CHECKED	R. FERNANDES	12/94				JOB NUMBER	94W097				
BR PROJ ENGR						CONTRACT NO	4756				
PRELIM PLAN BY											
ARCHITECT											
		DATE	DATE	REVISION	BY	APPR					

Washington State Department of Transportation

ABAM CONSULTING ENGINEERS
A MEMBER OF THE BERGER GROUP

SR 405
TUKWILA TO FACTORIA
SC&DI - STAGE 1

FOOTING LAYOUT

BRIDGE SHEET NO. 3

SHEET 5755 OF 5895 SHEETS

SR 405 JOB NO. 7067 SHEET 3 OF 22

SR 405/417

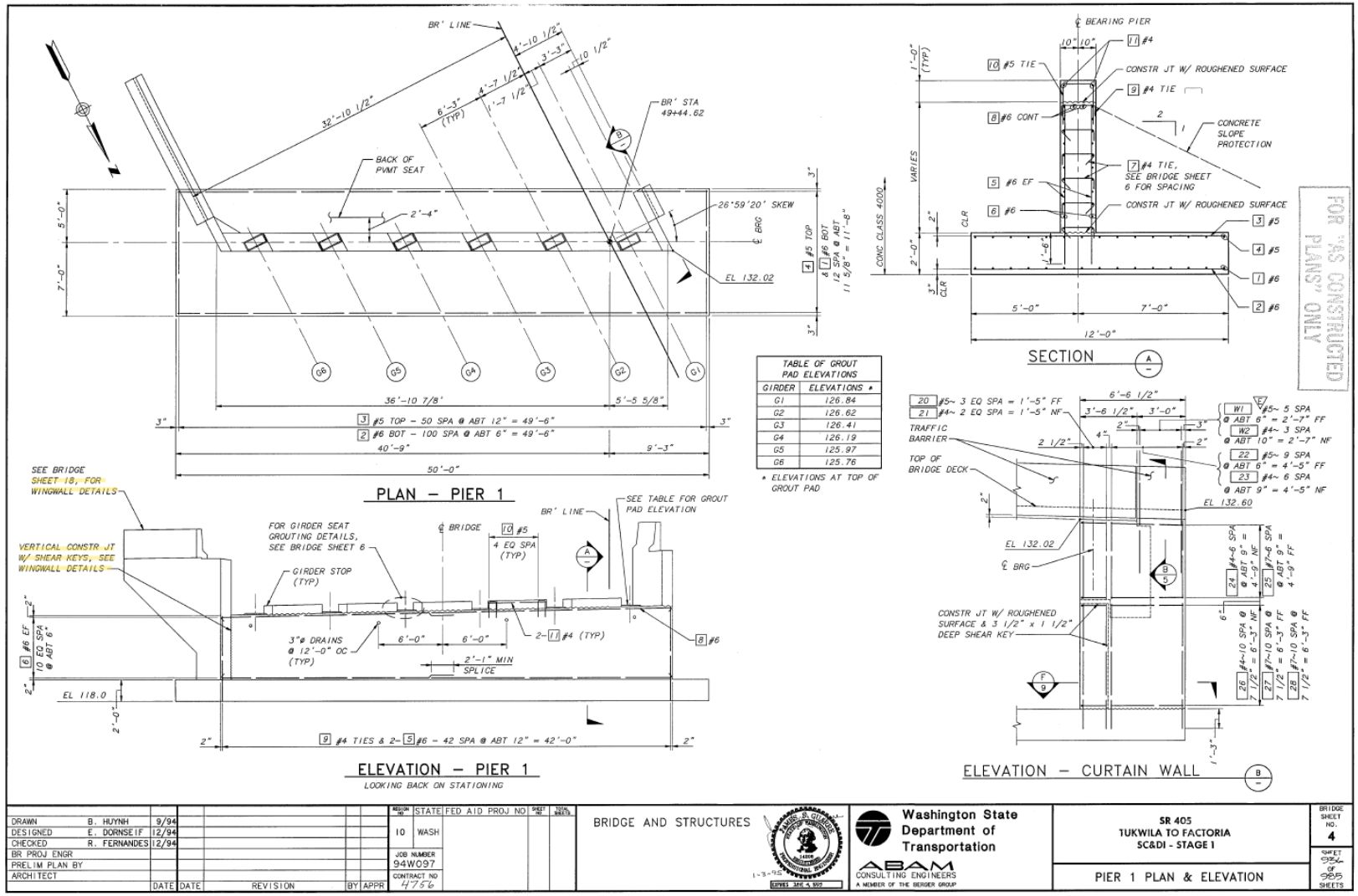

DRAWN	B. HUYNH	9/94			REGION NO	STATE	FED AID PROJ NO	SHEET NO	TOTAL SHEETS	BRIDGE AND STRUCTURES
DESIGNED	E. DORNSEIF	12/94			10	WASH				
CHECKED	R. FERNANDES	12/94			JOB NUMBER 94W097					
BR PROJ ENGR					CONTRACT NO 4756					
PRELIM PLAN BY										
ARCHITECT										
	DATE	DATE	REVISION	BY	APPR					

Washington State Department of Transportation

ABAM CONSULTING ENGINEERS
A MEMBER OF THE BERGER GROUP

SR 405
TUKWILA TO FACTORIA
SC&DI - STAGE 1

PIER 1 PLAN & ELEVATION

BRIDGE SHEET NO. 4

SHEET 934 OF 985 SHEETS

SR 405 JOB NO. 2062 SHEET 4 OF 22

SR405/417

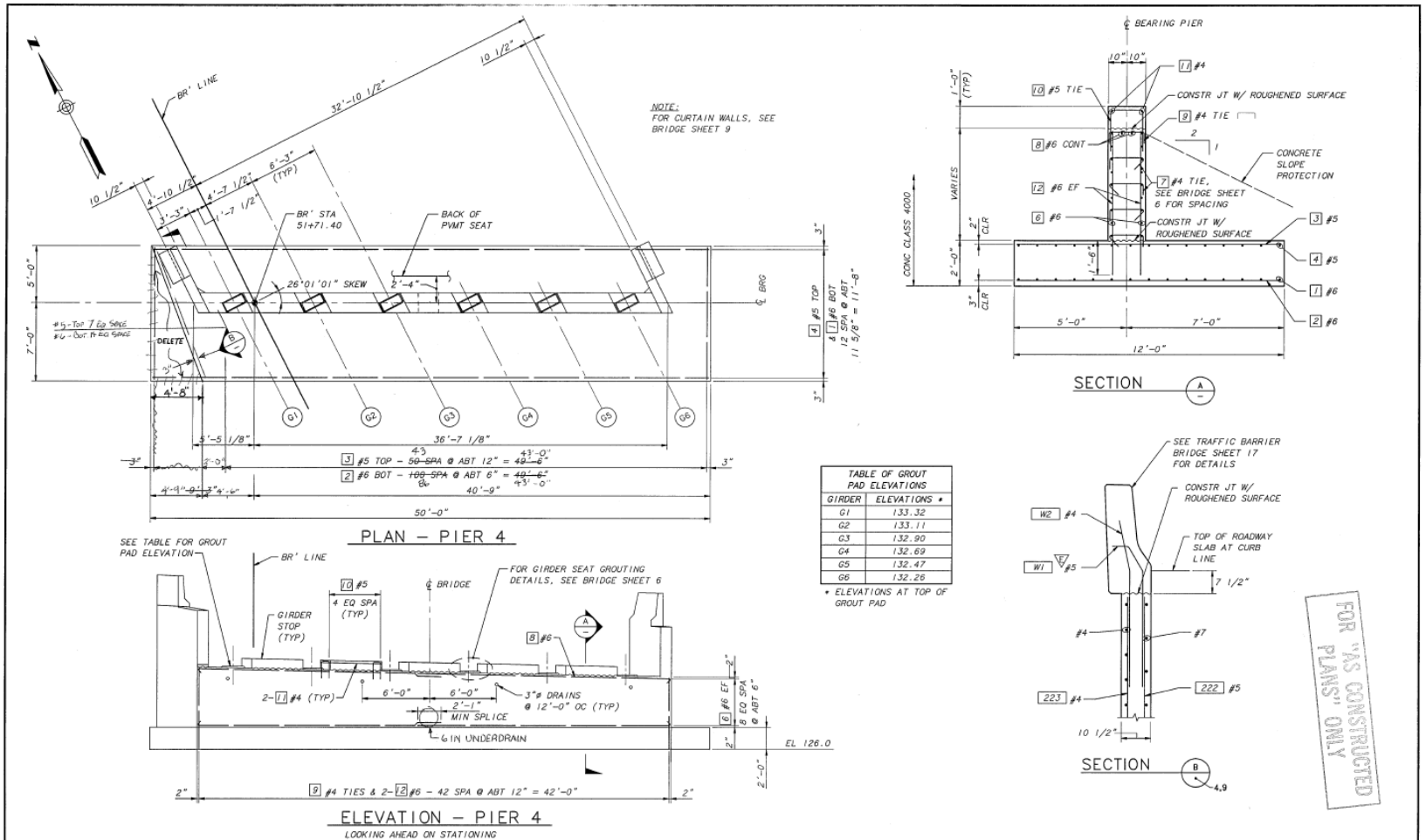

TABLE OF GROUT PAD ELEVATIONS	
GIRDER	ELEVATIONS *
G1	133.32
G2	133.11
G3	132.90
G4	132.69
G5	132.47
G6	132.26

* ELEVATIONS AT TOP OF GROUT PAD

DRAWN	B. HUYNH	9/94						REGION NO	STATE	FED AID PROJ NO	SHEET NO	TOTAL SHEETS
DESIGNED	E. DORNSEIF	12/94						10	WASH			
CHECKED	R. FERNANDES	12/94						JOB NUMBER	94W097			
BR PROJ ENGR								CONTRACT NO	4756			
PRELIM PLAN BY												
ARCHITECT												
		DATE	DATE	REVISION		BY	APPR					

BRIDGE AND STRUCTURES

Washington State Department of Transportation

ABAM CONSULTING ENGINEERS
A MEMBER OF THE BERGER GROUP

SR 405
TUKWILA TO FACTORIA
SC&DI - STAGE 1

PIER 4 PLAN & ELEVATION

BRIDGE SHEET NO. 5

SHEET 957 OF 985 SHEETS

SR 405 JOB NO. 7067 SHEET 5 OF 22

SR 405/417

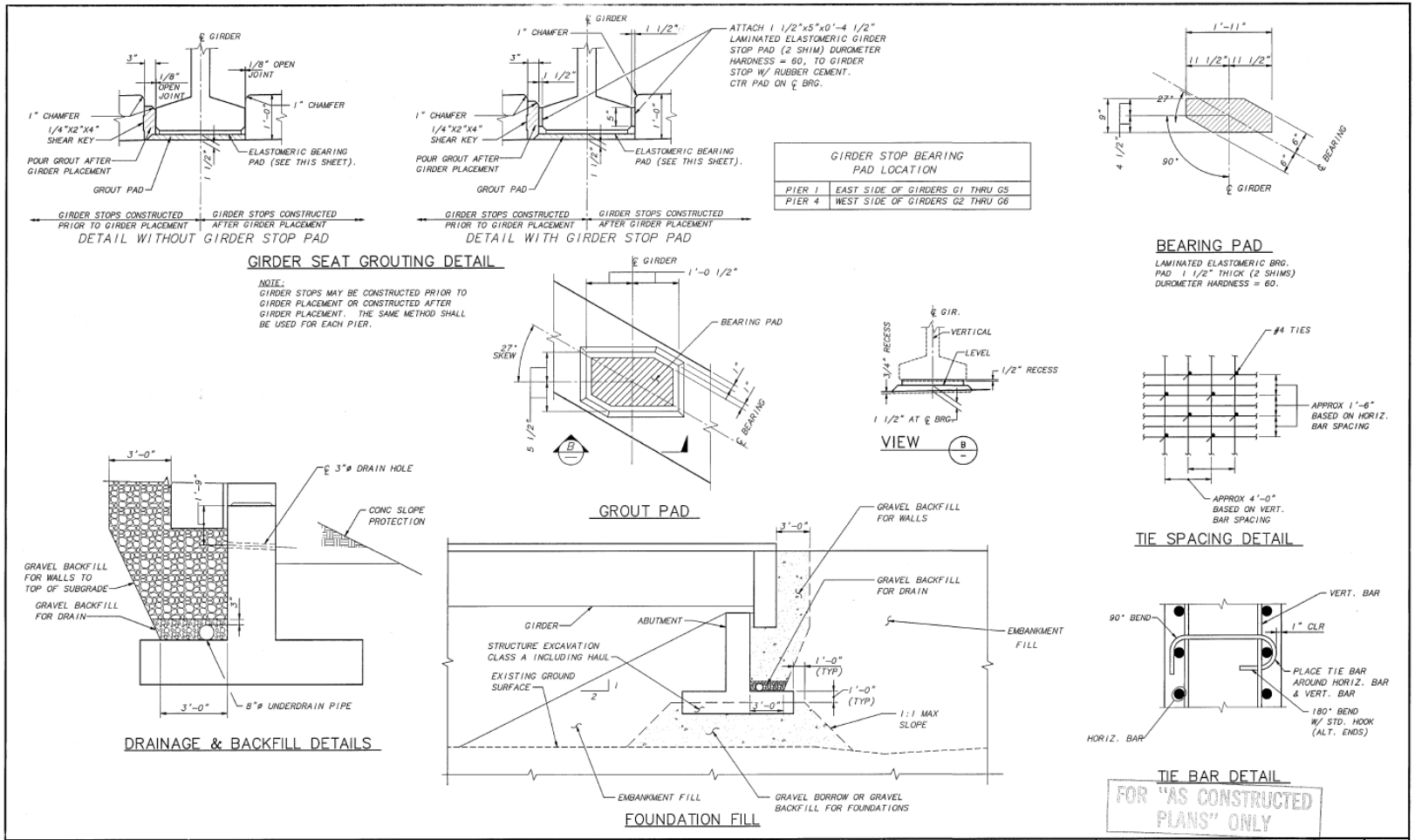

SR 405 JOB NO. 2067 SHEET 6 OF 22

DRAWN	R. MOHN	9/94
DESIGNED	E. DORNSEIF	12/94
CHECKED	R. FERNANDES	12/94
BR PROJ ENGR		
PRELIM PLAN BY		
ARCHITECT		

DATE	REVISION	BY	APPR

REGION NO	STATE	FED AID PROJ NO	SHEET NO	TOTAL SHEETS
10	WASH			
JOB NUMBER 94W097				
CONTRACT NO 4756				

BRIDGE AND STRUCTURES

JAMES R. QUADRO — REGISTERED PROFESSIONAL ENGINEER — STATE OF WASHINGTON — 14888 — PROFESSIONAL ENGINEER — EXPIRES JUNE 4, 1995

Washington State Department of Transportation

ABAM CONSULTING ENGINEERS
A MEMBER OF THE BERGER GROUP

SR 405
TUKWILA TO FACTORIA
SC&DI - STAGE 1

ABUTMENT DETAILS

BRIDGE SHEET NO. 6

SHEET 938 OF 955 SHEETS

SR 405/417

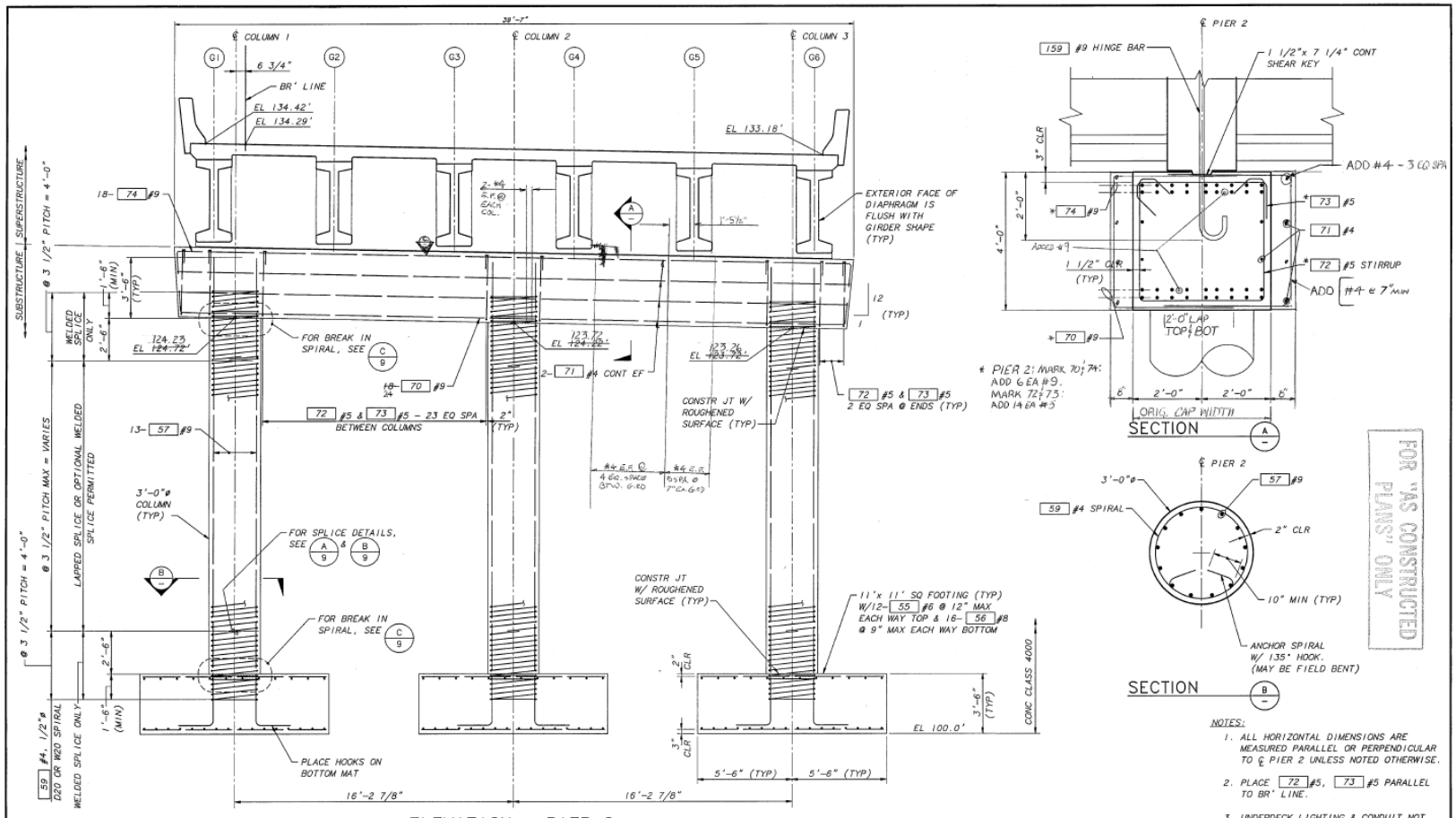

DRAWN	R. MOHN	10/94								
DESIGNED	E. DORNSEIF	12/94								
CHECKED	R. FERNANDES	12/94								
BR PROJ ENGR										
PRELIM PLAN BY										
ARCHITECT										
		DATE	DATE	REVISION	BY	APPR	REGION NO	STATE	FED AID PROJ NO	SHEET NO	TOTAL SHEETS
								10	WASH		
								JOB NUMBER 94W097			
								CONTRACT NO 4756			

BRIDGE AND STRUCTURES

JAMES SIGURDSON, STATE OF WASHINGTON, 14808, REGISTERED PROFESSIONAL ENGINEER, EXPIRES JUNE 4, 1995

Washington State Department of Transportation

ABAM CONSULTING ENGINEERS
A MEMBER OF THE BERGER GROUP

SR 405
TUKWILA TO FACTORIA
SC&DI - STAGE 1

PIER 2 ELEVATION & DETAILS

BRIDGE SHEET NO. 7

SHEET 959 OF 985 SHEETS

SR 405 JOB NO. 7067 SHEET 1 OF 22

SR 405/417

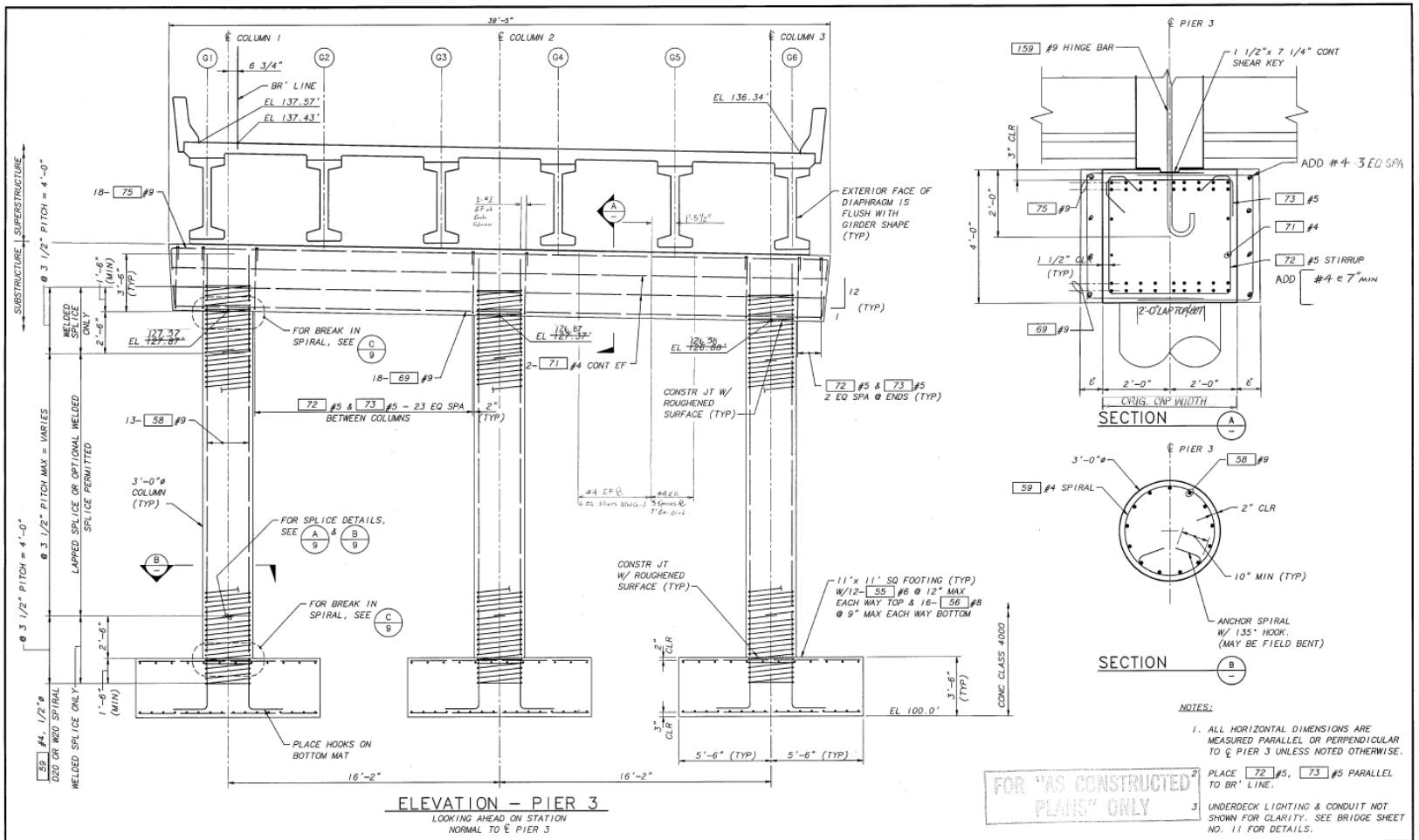

DRAWN	R. MOHN	10/94			REGION NO	STATE	FED AID PROJ NO	SHEET NO	TOTAL SHEETS
DESIGNED	E. DORNSEIF	12/94			10	WASH			
CHECKED	R. FERNANDES	12/94			JOB NUMBER 94W097				
BR PROJ ENGR					CONTRACT NO 4756				
PRELIM PLAN BY									
ARCHITECT									
	DATE	DATE	REVISION	BY	APPR				

BRIDGE AND STRUCTURES

Washington State Department of Transportation

ABAM CONSULTING ENGINEERS
A MEMBER OF THE BERGER GROUP

SR 405
TUKWILA TO FACTORIA
SC&DI - STAGE 1

PIER 3 ELEVATION & DETAILS

BRIDGE SHEET NO. 8

SHEET 940 OF 985 SHEETS

SR 405 JOB NO. 7067 SHEET 8 OF 22

SR 405/417

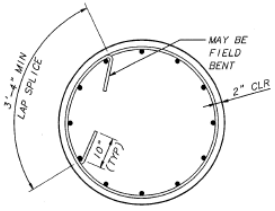

HOOKS SHALL BE PLACED TO AVOID VERTICAL REINF
NOTE: FOR WELDED SPLICE ALTERNATE SEE (B/-)

DETAIL – LAP SPLICE (A/-)

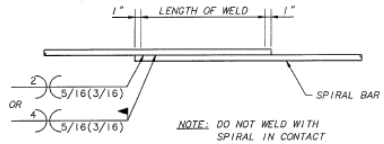

NOTE: DO NOT WELD WITH SPIRAL IN CONTACT WITH VERTICAL REINFORCING. ISOLATE VERTICAL REINFORCING FROM HEAT AND SPLATTER.

DETAIL (B/-)
WELDED SPLICE ALTERNATE

NOTES:

1. COLUMN SPIRAL BARS SHALL BE #4 DEFORMED BAR, 1/2" DIAMETER PLAIN STEEL BAR, OR W20 COLD DRAWN WIRE.
2. LAP SPLICES SHALL BE PERMITTED ONLY WITHIN THE CENTER HALF OF COLUMN HEIGHT. WELD SPLICE SHALL BE PERMITTED ENTIRE LENGTH OF COLUMN.

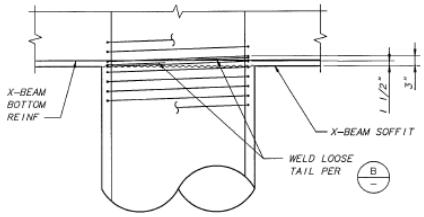

NOTES:

1. PROVIDE BREAK IN SPIRAL TO ALLOW PLACEMENT OF CROSSBEAM BOTTOM REINF OR FOOTING TOP REINF.
2. CROSSBEAM DETAILS SHOWN, FOOTING DETAILS SIMILAR.

DETAIL – SPIRAL BREAK (C/-)

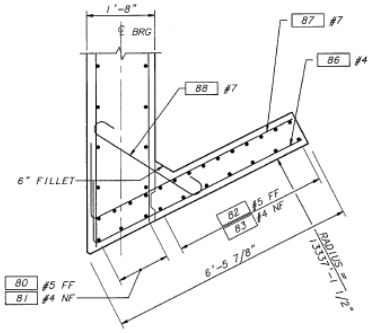

SECTION – EAST CURTAIN WALL @ PIER 4 (D/-)

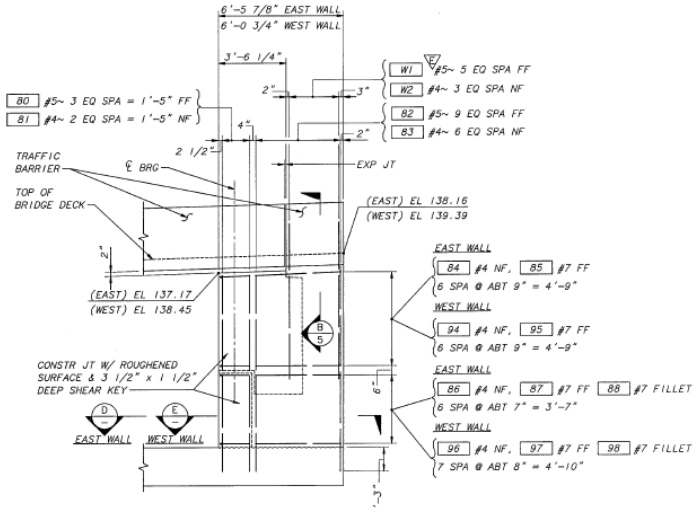

ELEVATION – PIER 4 EAST CURTAIN WALL (AS SHOWN)
PIER 4 WEST CURTAIN WALL (OPP HAND) (C/-)

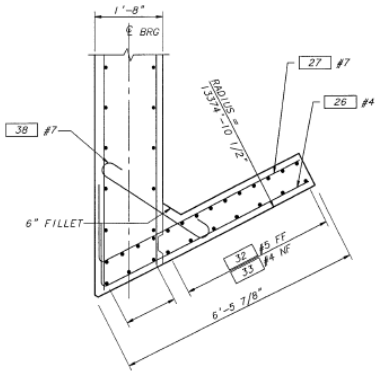

SECTION – WEST CURTAIN WALL @ PIER 1 (F/4)

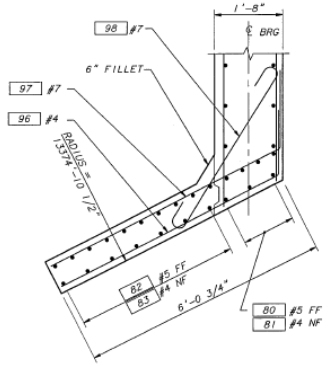

SECTION – WEST CURTAIN WALL @ PIER 4 (E/-)

FOR "AS CONSTRUCTED PLANS" ONLY

DRAWN	R. MOHN	9/94					REGION NO	STATE	FED AID PROJ NO	SHEET NO.	TOTAL SHEETS
DESIGNED	E. DORNSEIF	12/94					10	WASH			
CHECKED	R. FERNANDES	12/94					JOB NUMBER 94W097				
BR PROJ ENGR							CONTRACT NO 4756				
PRELIM PLAN BY											
ARCHITECT											
		DATE	DATE	REVISION	BY	APPR					

BRIDGE AND STRUCTURES

Washington State Department of Transportation

ABAM CONSULTING ENGINEERS
A MEMBER OF THE BERGER GROUP

SR 405
TUKWILA TO FACTORIA
SC&DI - STAGE 1

MISCELLANEOUS PIER DETAILS

BRIDGE SHEET NO. 9
SHEET 941 OF 985 SHEETS

SR 405 JOB NO. 7067 SHEET 9 OF 22

SR 405/417

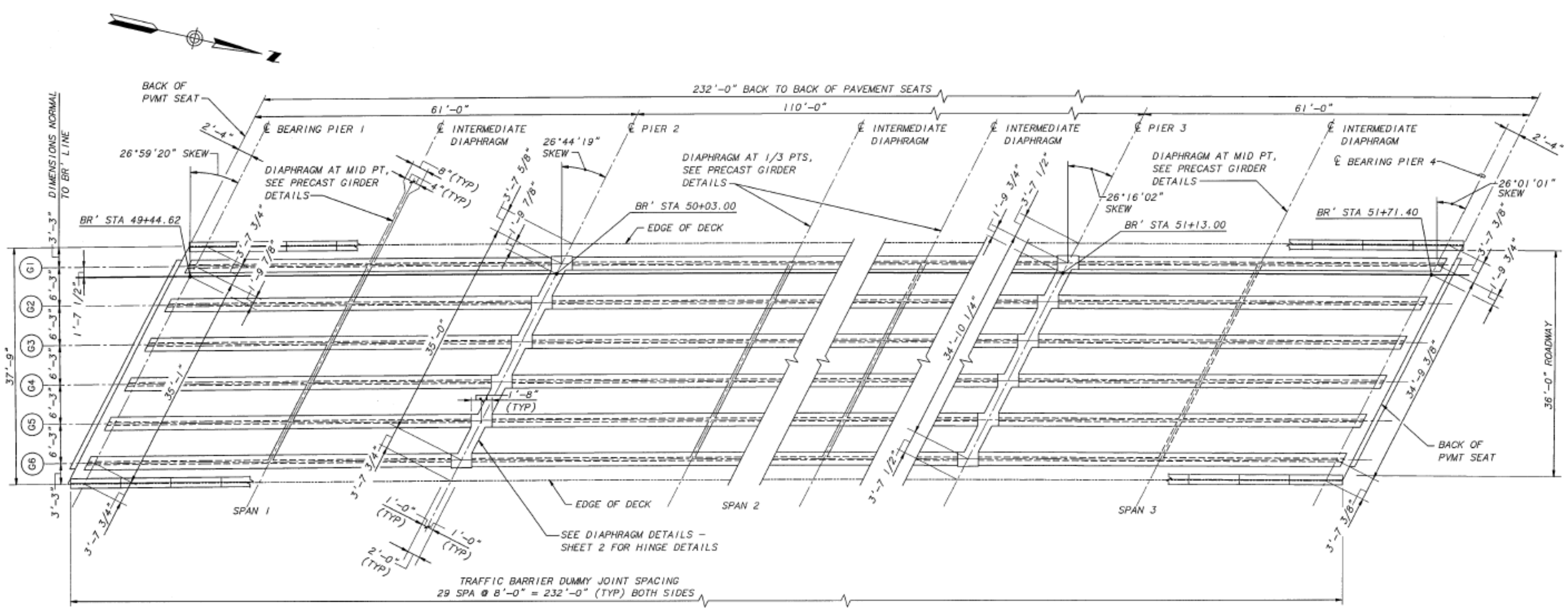

FRAMING PLAN

BEARING OF ALL PIERS AND DIAPHRAGMS = ~~N 76°12'03" W~~ N 76°44'03" W

FOR "AS CONSTRUCTED PLANS" ONLY

SR 405 JOB NO. 7067 SHEET 10 OF 22

DRAWN	R. MOHN	9/94				
DESIGNED	E. DORNSEIF	12/94				
CHECKED	R. FERNANDES	12/94				
BR PROJ ENGR						
PRELIM PLAN BY						
ARCHITECT						
		DATE	DATE	REVISION	BY	APPR

REGION NO. 10 · STATE WASH · FED AID PROJ NO · SHEET NO · TOTAL SHEETS

JOB NUMBER 94W097

CONTRACT NO 4756

BRIDGE AND STRUCTURES

1-3-95

Washington State Department of Transportation

ABAM CONSULTING ENGINEERS
A MEMBER OF THE BERGER GROUP

SR 405
TUKWILA TO FACTORIA
SC&DI - STAGE 1

FRAMING PLAN

BRIDGE SHEET NO. 10

SHEET 942 OF 985 SHEETS

SR 405/417

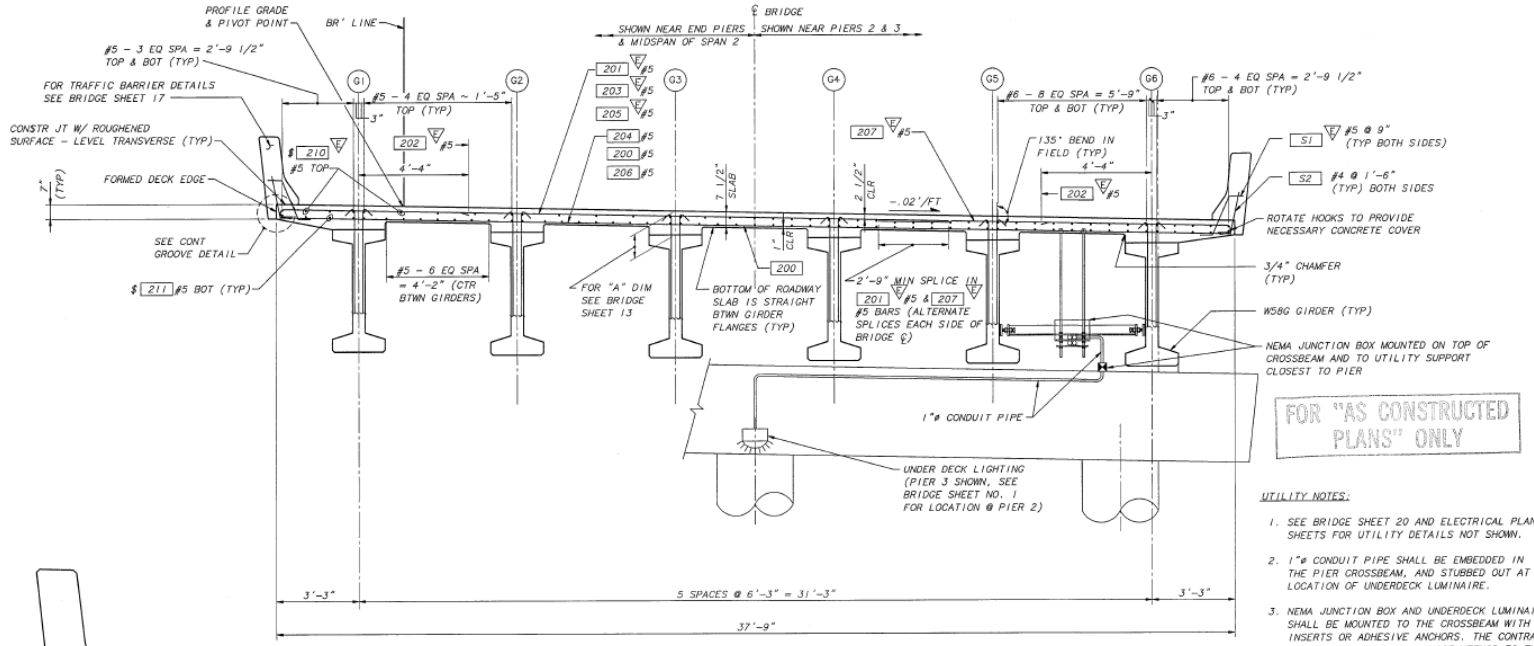

FOR "AS CONSTRUCTED PLANS" ONLY

BRIDGE CROSS SECTION

SHOWN LOOKING AHEAD ON STATIONING

▽E DENOTES EPOXY COATED BARS

$ - LENGTH OF BARS TO BE DETERMINED BY CONTRACTOR

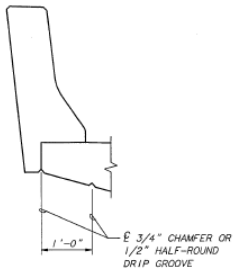

DETAIL - CONTINUOUS GROOVE

UTILITY NOTES:

1. SEE BRIDGE SHEET 20 AND ELECTRICAL PLAN SHEETS FOR UTILITY DETAILS NOT SHOWN.
2. 1"ø CONDUIT PIPE SHALL BE EMBEDDED IN THE PIER CROSSBEAM, AND STUBBED OUT AT LOCATION OF UNDERDECK LUMINAIRE.
3. NEMA JUNCTION BOX AND UNDERDECK LUMINAIRE SHALL BE MOUNTED TO THE CROSSBEAM WITH INSERTS OR ADHESIVE ANCHORS. THE CONTRACTOR SHALL SUBMIT THE ANCHORAGE METHOD TO THE ENGINEER FOR APPROVAL.
4. THE CONTRACTOR SHALL SUBMIT DETAILS FOR ATTACHMENT OF THE NEMA JUNCTION BOX AT THE UTILITY SUPPORT TO THE ENGINEER FOR APPROVAL.
5. ALL CONDUIT AND ALL STEEL IN UTILITY SUPPORTS, INCLUDING FASTENINGS AND ANCHORAGES, SHALL BE GALVANIZED UNLESS OTHERWISE SPECIFIED.
6. DRILLING THROUGH REINFORCING STEEL WILL NOT BE PERMITTED. IF STEEL IS HIT WHEN DRILLING FOR ADHESIVE ANCHORS, THE ANCHORAGE LOCATION SHALL BE MOVED AND THE ABANDONED HOLE FILLED WITH GROUT.

DRAWN	R. MOHN	9/94				REGION NO	STATE	FED AID PROJ NO	SHEET NO	TOTAL SHEETS
DESIGNED	E. DORNSEIF	12/94				10	WASH			
CHECKED	R. FERNANDES	12/94				JOB NUMBER 94W097				
BR PROJ ENGR						CONTRACT NO 4756				
PRELIM PLAN BY										
ARCHITECT										
	DATE	DATE	REVISION	BY	APPR					

BRIDGE AND STRUCTURES

Washington State Department of Transportation

ABAM CONSULTING ENGINEERS
A MEMBER OF THE BERGER GROUP

SR 405
TUKWILA TO FACTORIA
SC&DI - STAGE I

BRIDGE CROSS SECTION

BRIDGE SHEET NO. 11

SHEET 943 OF 965 SHEETS

SR 405 JOB NO. 7062 SHEET 11 OF 22

SR 405/4/7

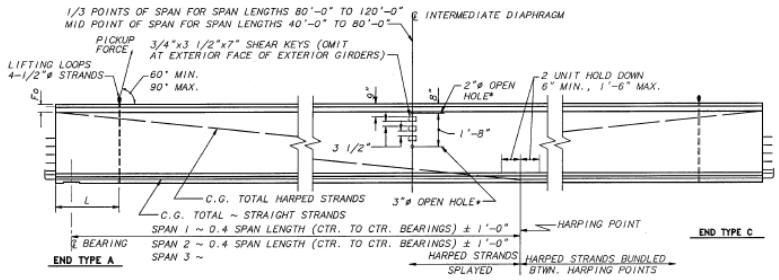

GIRDER ELEVATION

*OMIT HOLES AND PLACE INSERTS ON THE INTERIOR FACE OF EXTERIOR GIRDERS. PLACE HOLES AND INSERTS PARALLEL TO SKEW. INSERTS SHALL BE 1" RICHMOND ROCKET, BURKE HI-TENSILE, LANCASTER MALLEABLE OR APPROVED EQUAL.

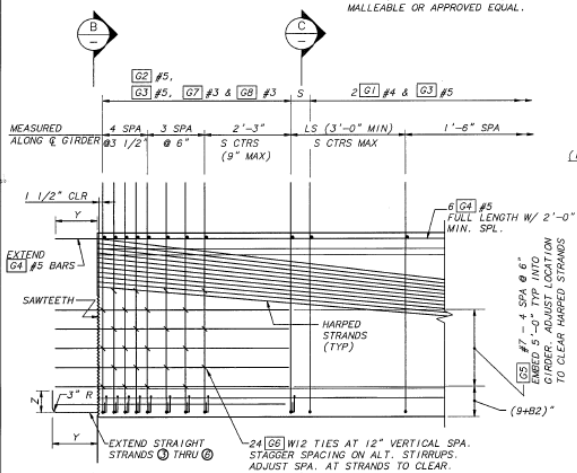

TYPICAL END ELEVATION

END TYPE C SHOWN ~ OTHER ENDS SIMILAR

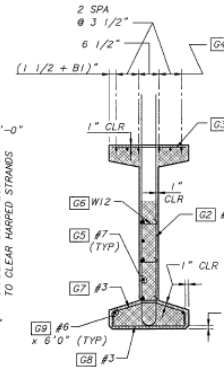

SECTION B

SAWTEETH SHOWN BY SHADED AREA.

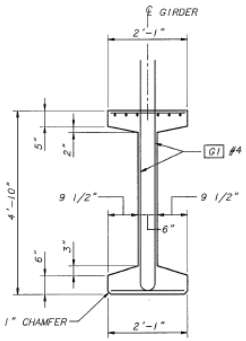

SECTION C

NOTES

ALL DETAILS ON THIS SHEET ARE FOR PRETENSIONED DESIGN ONLY.

PLAN LENGTH SHALL BE INCREASED AS NECESSARY TO COMPENSATE FOR SHORTENING DUE TO PRESTRESS AND SHRINKAGE.

EXTRA CAUTION MUST BE EXERCISED IN HANDLING AND PLACING ALL GIRDERS.

ALL GIRDERS OVER 105' LONG SHALL BE BRACED LATERALLY TO PREVENT TIPPING OR BUCKLING.

THE TOP SURFACE OF THE GIRDER FLANGE SHALL BE ROUGHENED IN ACCORDANCE WITH SECTION 6-02.3(25)H OF THE STANDARD SPECIFICATIONS.

IF THE LIFTING LOOPS EXTEND WITHIN 3" OF THE TOP OF THE ROADWAY SLAB THEY SHALL BE CUT OFF PRIOR TO POURING THE ROADWAY SLAB. ALL LIFTING STRANDS SHALL BE OF THE SAME MATERIAL AND STRENGTH AS THE PRESTRESSING STRANDS. WRAP THE LIFTING LOOPS SO THAT EACH STRAND WILL CARRY ITS SHARE OF THE TOTAL LOAD. EXTEND LIFTING LOOPS ENDING WITH A 9" LONG 90° HOOK TO WITHIN 3" CLEAR OF THE BOTTOM OF THE GIRDER.

CUT ALL STRANDS FLUSH WITH THE GIRDER ENDS AND PAINT WITH AN APPROVED EPOXY RESIN EXCEPT FOR EXTENDED STRANDS AS SHOWN.

FORMS FOR BEARING PAD RECESSES SHALL BE CONSTRUCTED AND FASTENED IN SUCH A MANNER AS NOT TO CAUSE DAMAGE TO THE GIRDER DURING THE STRAND RELEASE OPERATION.

ALL STRANDS ARE 1/2"ø LOW RELAXATION STRANDS (AASHTO M203 GRADE 270).

EXTENDED STRANDS AND BARS ARE PARALLEL TO GIRDER.

FOR SAWTOOTH DETAILS, SEE W58G GIRDER DETAILS II.

ENDS AHEAD ON STATION
G5 BARS LEFT OF ℄
B1 = 0"
B2 = 0"
ENDS BACK ON STATION
G5 BARS RIGHT OF ℄
B1 = 1 1/2"
B2 = 3"

END TYPE	BEARING RECESS	Y	Z	SAWTEETH
A	YES	9"	1'-6"	YES
C	NO	1'-10"	9"	YES

BENDING DIAGRAM

ALL DIMENSIONS ARE OUT TO OUT

MARK	LOCATION	SIZE	
G1	GIRDER STIRRUPS	4	
G2	GIRDER END STIRRUPS	5	
G3	GIRDER TOP FLANGE	5	STR
G4	GIRDER LONGIT FULL LENGTH	5	STR
G5	GIRDER END LONGIT	7	STR
G6	GIRDER END TIES	W12	‡
G7	GIRDER END TIES	3	
G8	GIRDER END TIES	3	
G9	GIRDER LONGIT	6	STR

‡ #3 OR #4 MAY BE SUBSTITUTED FOR W12, FIELD BENDING IS OPTIONAL

** = VARIES FOR SKEWED SPANS

NOTE: FOR DIMENSION A, SEE "GIRDER SCHEDULE"

FOR "AS CONSTRUCTED PLANS" ONLY

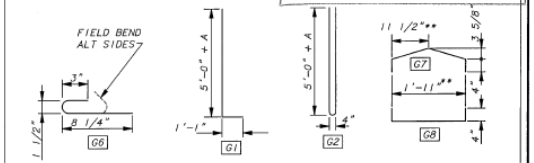

DRAWN	R. MOHN	9/94				REGION NO	STATE	FED AID PROJ NO	SHEET NO	TOTAL SHEETS	BRIDGE AND STRUCTURES
DESIGNED	E. DORNSEIF	12/94				10	WASH				
CHECKED	R. FERNANDES	12/94				JOB NUMBER	94W097				
BR PROJ ENGR						CONTRACT NO	4756				
PRELIM PLAN BY											
ARCHITECT											
		DATE	DATE	REVISION	BY	APPR					

Washington State Department of Transportation

ABAM CONSULTING ENGINEERS
A MEMBER OF THE BERGER GROUP

SR 405
TUKWILA TO FACTORIA
SC&DI - STAGE 1

W58G GIRDER DETAILS – SHEET 1

BRIDGE SHEET NO. 12

SHEET 944 OF 985 SHEETS

SR 405 JOB NO. 2067 SHEET 12 OF 32

SK 405/417

GIRDER SCHEDULE

DIMENSION A AT ℄ BEARINGS = 11.00"
BASED ON GIRDER DEFLECTION = D AT TIME OF SLAB POUR (120 DAYS)

SPAN	GIRDER	END 1 TYPE	END 2 TYPE	L	θ1	θ2	N1	N2	P1	P2	PLAN LENGTH (ALONG GIRDER GRADE)	MIN CONC COMPR STRENGTH 28 DAYS F'C KSI	MIN CONC COMPR STRENGTH RELEASE F'CI KSI	S (IN)	LS (FT)	HARPED NO. OF STRANDS	HARPED JACKING FORCE (KIPS)	STRAIGHT NO. OF STRANDS	STRAIGHT JACKING FORCE (KIPS)	LOCATION OF C.G. STRANDS (IN) E	F℄	Fb	Fo	*C (IN)	D (IN)	Ld (IN)	X (IN)
1	ALL	A	C	4.25'	117°	90°	1'-3"	1 1/2"	1'4 7/8"	0'-1 1/2"	58'-2"	6.0	4.5	9	3'-0"	4	124	10	310	1.88	0	3.0	7.0	0.15	0.51	0	0
2	ALL	C	C	4.25'	90°	90°	1 1/2"	1 1/2"	0'-1 1/2"	0'-1 1/2"	106' - 9"	7.0	6.0	9	3'-0"	14	434	26	806	3.57	3.42	3.0	3.0	1.72	3.58	0	0
3	ALL	C	A	4.25'	90°	117°	1 1/2"	1'-3"	0'-1 1/2"	1'-4 7/8"	58'- 2"	6.0	4.5	9	3'-0"	4	124	10	310	1.88	0	3.0	7.0	0.15	0.51	0	0

* SEE BRIDGE SHEET 16 FOR SCREED SETTING DIAGRAM

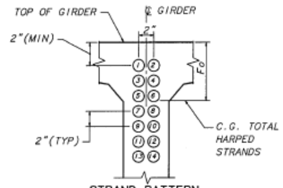

STRAND PATTERN AT GIRDER END

HARPED STRAND LOCATION SEQUENCE SHALL BE AS SHOWN ①, ② ETC.

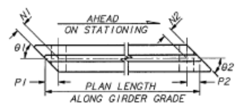

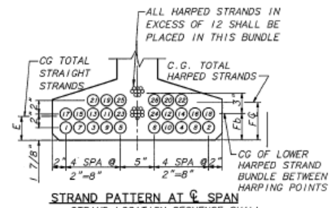

STRAND PATTERN AT ℄ SPAN

STRAND LOCATION SEQUENCE SHALL BE AS SHOWN ①, ② ETC.

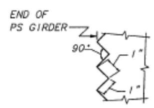

SAWTOOTH DETAILS

SAWTEETH ARE FULL WIDTH – USE SAWTOOTH KEYS FROM BOTTOM OF BOTTOM FLANGE TO BOTTOM OF LOWEST HARPED STRAND AS WELL AS TOP FLANGE ADJACENT TO HARPED STRANDS AS SHOWN IN SECTION B.

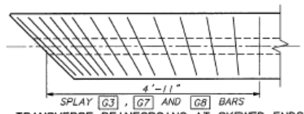

TRANSVERSE REINFORCING AT SKEWED ENDS

ONLY TRANSVERSE REINF. SHOWN.

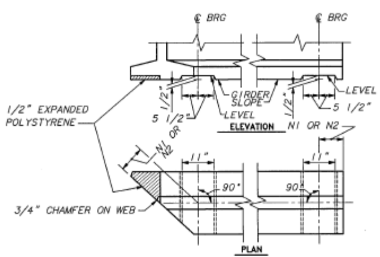

BEARING RECESS DETAIL

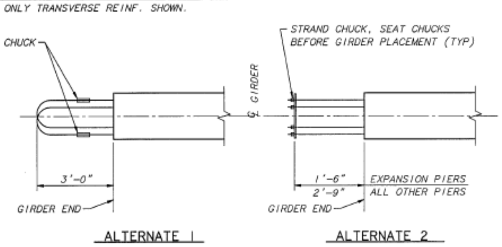

STRAND EXTENSION DETAIL

NOTE TO DESIGNERS:
STRAND EXTENSION DETAIL TO BE USED FOR CONTINUOUS SPANS AT MOMENT-RESISTING DIAPHRAGM. THIS DETAIL NOT APPLICABLE TO CONTINUOUS SPANS UTILIZING HINGE DIAPHRAGMS.

FOR "AS CONSTRUCTED PLANS" ONLY

DRAWN	R. MOHN	9/94
DESIGNED	E. DORNSEIF	12/94
CHECKED	R. FERNANDES	12/94
BR PROJ ENGR		
PRELIM PLAN BY		
ARCHITECT		

DATE | DATE | REVISION | BY | APPR

REGION NO. 10 | STATE WASH | FED AID PROJ NO
JOB NUMBER 94W097
CONTRACT NO 4756

BRIDGE AND STRUCTURES

Washington State Department of Transportation

ABAM CONSULTING ENGINEERS
A MEMBER OF THE BERGER GROUP

SR 405
TUKWILA TO FACTORIA
SC&DI - STAGE 1

W58G GIRDER DETAILS – SHEET 2

BRIDGE SHEET NO. 13

SHEET 945 OF 985 SHEETS

SR 405/417

SR 405 JOB NO. Z067 SHEET 13 OF 22

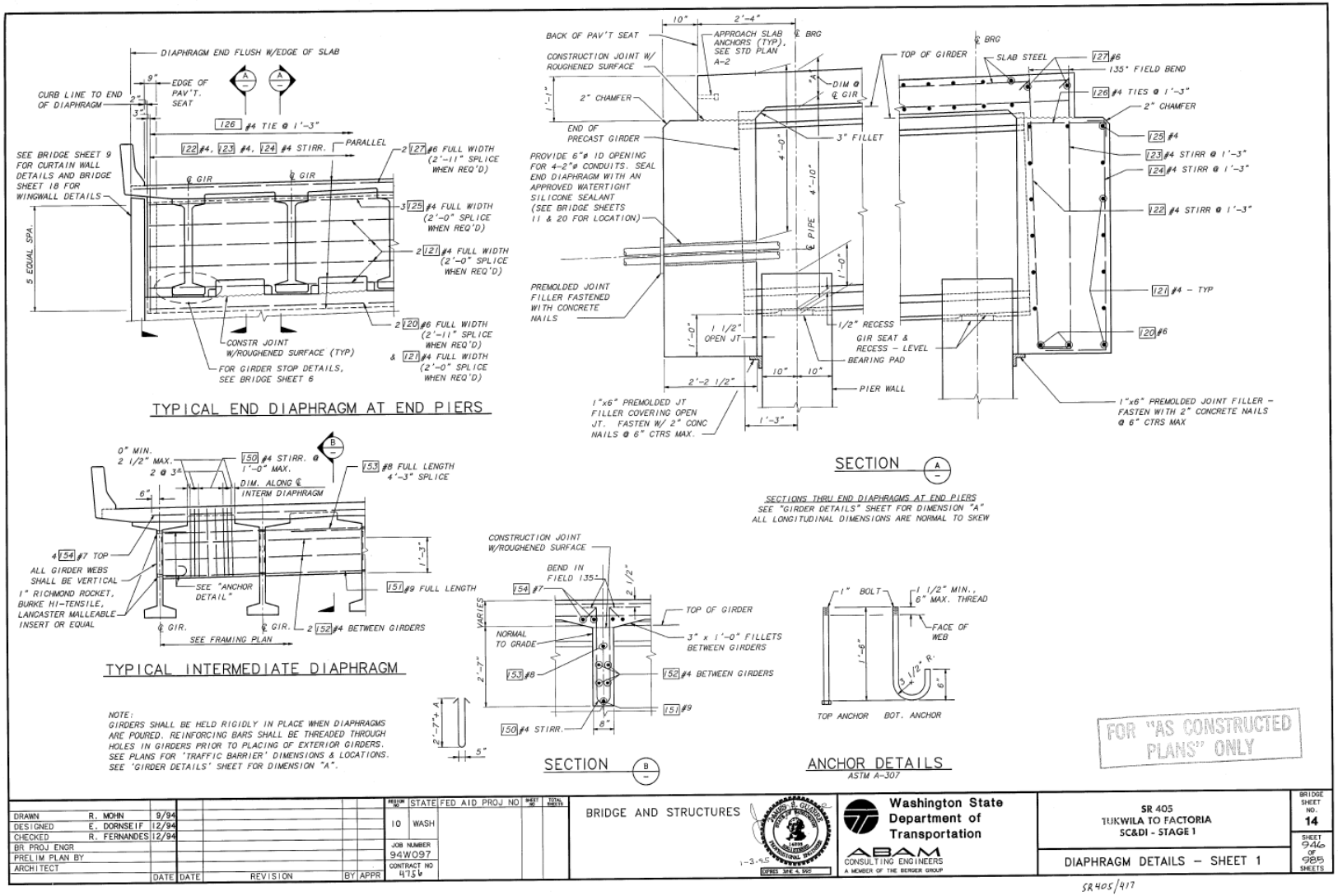

SR 405 JOB NO. 2067 SHEET 14 OF 22

DRAWN	R. MOHN	9/94
DESIGNED	E. DORNSEIF	12/94
CHECKED	R. FERNANDES	12/94
BR PROJ ENGR		
PRELIM PLAN BY		
ARCHITECT		

DATE	REVISION	BY	APPR

REGION NO.	STATE	FED AID PROJ NO	SHEET NO.	TOTAL SHEETS
10	WASH			

JOB NUMBER 94W097
CONTRACT NO 4756

BRIDGE AND STRUCTURES

Washington State Department of Transportation

ABAM CONSULTING ENGINEERS
A MEMBER OF THE BERGER GROUP

SR 405
TUKWILA TO FACTORIA
SC&DI - STAGE 1

DIAPHRAGM DETAILS - SHEET 1

BRIDGE SHEET NO. 14

SHEET 946 OF 985 SHEETS

SR 405/417

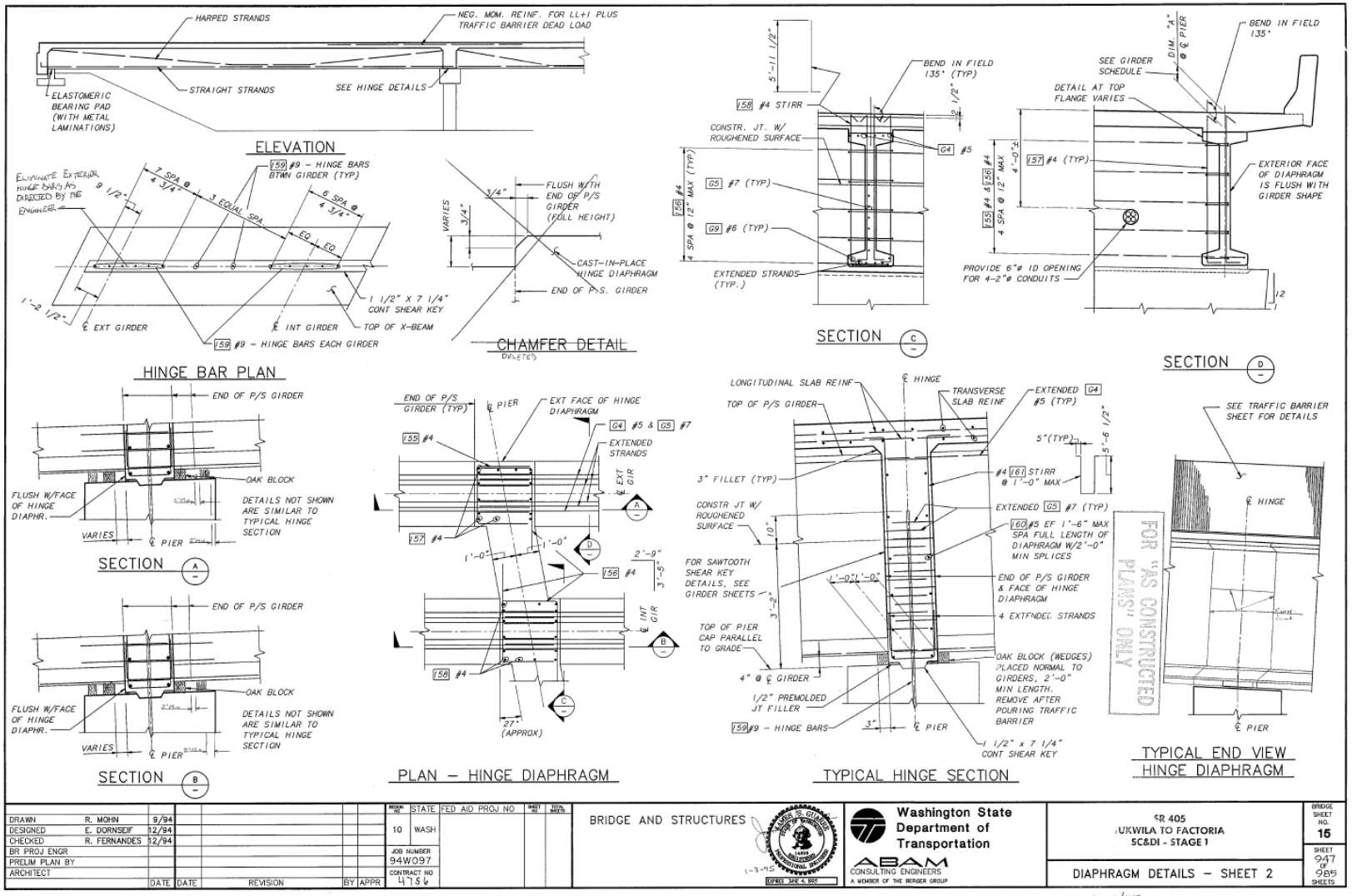

SR 405 JOB NO. 2062 SHEET 15 OF 22

DRAWN	R. MOHN	9/94					REGION NO	STATE	FED AID PROJ NO	SHEET NO	TOTAL SHEETS
DESIGNED	E. DORNSEIF	12/94					10	WASH			
CHECKED	R. FERNANDES	12/94					JOB NUMBER 94W097				
BR PROJ ENGR							CONTRACT NO 4756				
PRELIM PLAN BY											
ARCHITECT											
		DATE	DATE	REVISION	BY	APPR					

BRIDGE AND STRUCTURES

Washington State Department of Transportation

ABAM CONSULTING ENGINEERS
A MEMBER OF THE BERGER GROUP

SR 405
TUKWILA TO FACTORIA
SC&DI - STAGE 1

DIAPHRAGM DETAILS - SHEET 2

BRIDGE SHEET NO. 15

SHEET 947 OF 985 SHEETS

SR 405/417

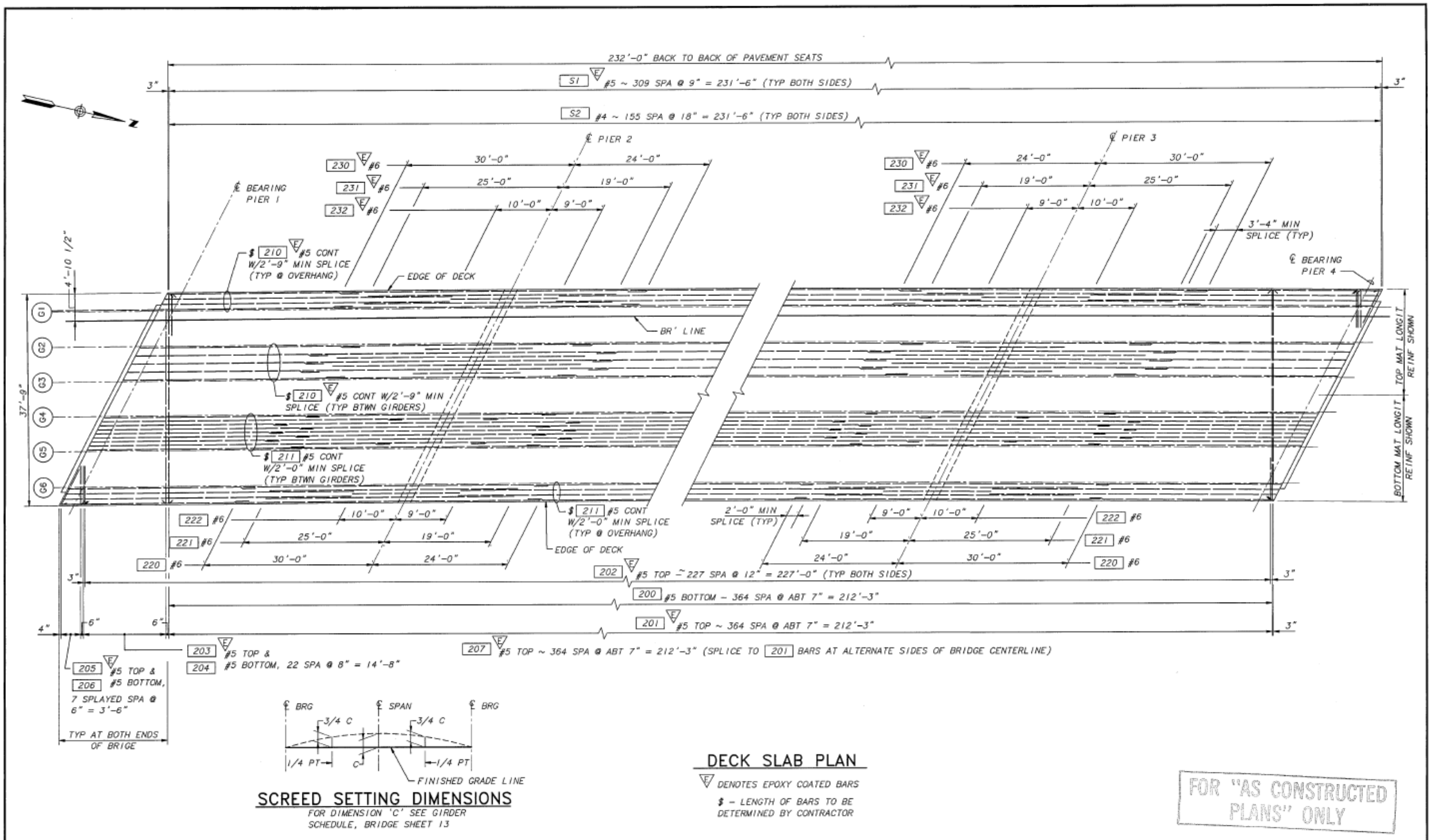

DRAWN	R. MOHN	9/94			
DESIGNED	E. DORNSEIF	12/94			
CHECKED	R. FERNANDES	12/94			
BR PROJ ENGR					
PRELIM PLAN BY					
ARCHITECT					
		DATE	DATE	REVISION	BY APPR

REGION NO: 10 | STATE: WASH | FED AID PROJ NO

JOB NUMBER 94W097

CONTRACT NO 4756

BRIDGE AND STRUCTURES

1-3-95

Washington State Department of Transportation

ABAM CONSULTING ENGINEERS
A MEMBER OF THE BERGER GROUP

SR 405
TUKWILA TO FACTORIA
SC&DI - STAGE 1

DECK SLAB PLAN

BRIDGE SHEET NO. 16

SHEET 948 OF 985 SHEETS

SR 405 JOB NO. 7067 SHEET 16 OF 22

SR405/417

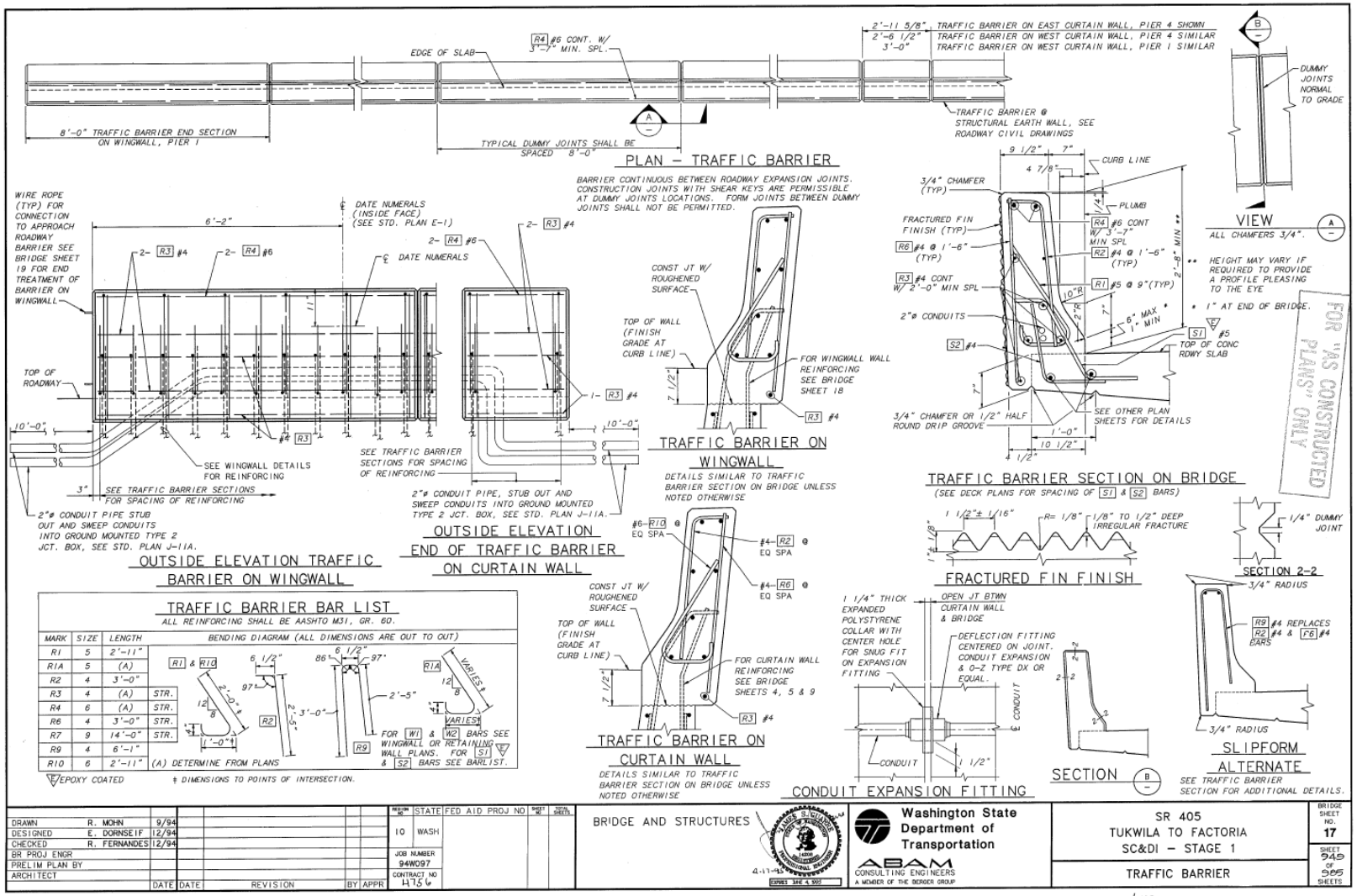
PLAN – TRAFFIC BARRIER
BARRIER CONTINUOUS BETWEEN ROADWAY EXPANSION JOINTS. CONSTRUCTION JOINTS WITH SHEAR KEYS ARE PERMISSIBLE AT DUMMY JOINTS LOCATIONS. FORM JOINTS BETWEEN DUMMY JOINTS SHALL NOT BE PERMITTED.
EDGE OF SLAB
R4 #6 CONT. W/ 3'-7" MIN. SPL.
2'-11 5/8" TRAFFIC BARRIER ON EAST CURTAIN WALL, PIER 4 SHOWN
2'-6 1/2" TRAFFIC BARRIER ON WEST CURTAIN WALL, PIER 4 SIMILAR
3'-0" TRAFFIC BARRIER ON WEST CURTAIN WALL, PIER 1 SIMILAR
8'-0" TRAFFIC BARRIER END SECTION ON WINGWALL, PIER 1
TYPICAL DUMMY JOINTS SHALL BE SPACED 8'-0"
TRAFFIC BARRIER @ STRUCTURAL EARTH WALL, SEE ROADWAY CIVIL DRAWINGS
DUMMY JOINTS NORMAL TO GRADE
VIEW
ALL CHAMFERS 3/4".
WIRE ROPE (TYP) FOR CONNECTION TO APPROACH ROADWAY BARRIER SEE BRIDGE SHEET 19 FOR END TREATMENT OF BARRIER ON WINGWALL
℄ DATE NUMERALS (INSIDE FACE) (SEE STD. PLAN E-1)
℄ DATE NUMERALS
2- R3 #4
2- R4 #6
2- R3 #4
2- R4 #6
1- R3 #4
TOP OF ROADWAY
10'-0"
10'-0"
R3 #4
SEE WINGWALL DETAILS FOR REINFORCING
SEE TRAFFIC BARRIER SECTIONS FOR SPACING OF REINFORCING
3"
SEE TRAFFIC BARRIER SECTIONS FOR SPACING OF REINFORCING
2"ø CONDUIT PIPE STUB OUT AND SWEEP CONDUITS INTO GROUND MOUNTED TYPE 2 JCT. BOX, SEE STD. PLAN J-11A.
OUTSIDE ELEVATION TRAFFIC BARRIER ON WINGWALL
2"ø CONDUIT PIPE, STUB OUT AND SWEEP CONDUITS INTO GROUND MOUNTED TYPE 2 JCT. BOX, SEE STD. PLAN J-11A.
OUTSIDE ELEVATION END OF TRAFFIC BARRIER ON CURTAIN WALL
CONST JT W/ ROUGHENED SURFACE
TOP OF WALL (FINISH GRADE AT CURB LINE)
7 1/2"
FOR WINGWALL WALL REINFORCING SEE BRIDGE SHEET 18
R3 #4
TRAFFIC BARRIER ON WINGWALL
DETAILS SIMILAR TO TRAFFIC BARRIER SECTION ON BRIDGE UNLESS NOTED OTHERWISE
9 1/2"
7"
4 7/8"
CURB LINE
3/4" CHAMFER (TYP)
PLUMB
FRACTURED FIN FINISH (TYP)
R4 #6 CONT W/ 3'-7" MIN SPL
R6 #4 @ 1'-6" (TYP)
R2 #4 @ 1'-6" (TYP)
R3 #4 CONT W/ 2'-0" MIN SPL
R1 #5 @ 9"(TYP)
2'-8" MIN **
** HEIGHT MAY VARY IF REQUIRED TO PROVIDE A PROFILE PLEASING TO THE EYE
* 1" AT END OF BRIDGE.
10"R
2"R
7"
6" MAX *
1" MIN
2"ø CONDUITS
S2 #4
S1 #5
TOP OF CONC RDWY SLAB
7"
3/4" CHAMFER OR 1/2" HALF ROUND DRIP GROOVE
SEE OTHER PLAN SHEETS FOR DETAILS
1'-0"
10 1/2"
4 1/2"
TRAFFIC BARRIER SECTION ON BRIDGE
(SEE DECK PLANS FOR SPACING OF S1 & S2 BARS)
FOR "AS CONSTRUCTED PLANS" ONLY
1 1/2"± 1/16"
R= 1/8"
1/8" TO 1/2" DEEP IRREGULAR FRACTURE
1"±1/8"
FRACTURED FIN FINISH
1/4" DUMMY JOINT
SECTION 2-2
3/4" RADIUS
R9 #4 REPLACES R2 #4 & F6 #4 BARS
3/4" RADIUS
SLIPFORM ALTERNATE
SEE TRAFFIC BARRIER SECTION FOR ADDITIONAL DETAILS.
#6-R10 @ EQ SPA
#4-R2 @ EQ SPA
#4-R6 @ EQ SPA
CONST JT W/ ROUGHENED SURFACE
TOP OF WALL (FINISH GRADE AT CURB LINE)
7 1/2"
FOR CURTAIN WALL REINFORCING SEE BRIDGE SHEETS 4, 5 & 9
R3 #4
TRAFFIC BARRIER ON CURTAIN WALL
DETAILS SIMILAR TO TRAFFIC BARRIER SECTION ON BRIDGE UNLESS NOTED OTHERWISE
1 1/4" THICK EXPANDED POLYSTYRENE COLLAR WITH CENTER HOLE FOR SNUG FIT ON EXPANSION FITTING
OPEN JT BTWN CURTAIN WALL & BRIDGE
DEFLECTION FITTING CENTERED ON JOINT. CONDUIT EXPANSION & O-Z TYPE DX OR EQUAL.
℄ CONDUIT
CONDUIT
1 1/2"
CONDUIT EXPANSION FITTING
SECTION
TRAFFIC BARRIER BAR LIST
ALL REINFORCING SHALL BE AASHTO M31, GR. 60.
MARK | SIZE | LENGTH | BENDING DIAGRAM (ALL DIMENSIONS ARE OUT TO OUT)
R1 | 5 | 2'-11"
R1A | 5 | (A)
R2 | 4 | 3'-0"
R3 | 4 | (A) | STR.
R4 | 6 | (A) | STR.
R6 | 4 | 3'-0" | STR.
R7 | 9 | 14'-0" | STR.
R9 | 4 | 6'-1"
R10 | 6 | 2'-11" | (A) DETERMINE FROM PLANS
R1 & R10
6 1/2"
97°
2'-0"
12
8
1'-0"
R2
2'-5"
3'-0"
86°
R1A
VARIES
2'-5"
R9
FOR W1 & W2 BARS SEE WINGWALL OR RETAINING WALL PLANS. FOR S1 & S2 BARS SEE BARLIST.
EPOXY COATED
DIMENSIONS TO POINTS OF INTERSECTION.
SR 405 JOB NO. 7067 SHEET 17 OF 28
DRAWN R. MOHN 9/94
DESIGNED E. DORNSEIF 12/94
CHECKED R. FERNANDES 12/94
BR PROJ ENGR
PRELIM PLAN BY
ARCHITECT
DATE | DATE | REVISION | BY | APPR
REGION NO 10 | STATE WASH | FED AID PROJ NO
JOB NUMBER 94W097
CONTRACT NO H7156
BRIDGE AND STRUCTURES
STATE OF WASHINGTON JAMES S. WOLD 19808 REGISTERED PROFESSIONAL ENGINEER
4-11-95
EXPIRES JUNE 4, 1995
Washington State Department of Transportation
ABAM CONSULTING ENGINEERS
A MEMBER OF THE BERGER GROUP
SR 405
TUKWILA TO FACTORIA
SC&DI – STAGE 1
TRAFFIC BARRIER
BRIDGE SHEET NO. 17
SHEET 949 OF 995 SHEETS
SR 405/117

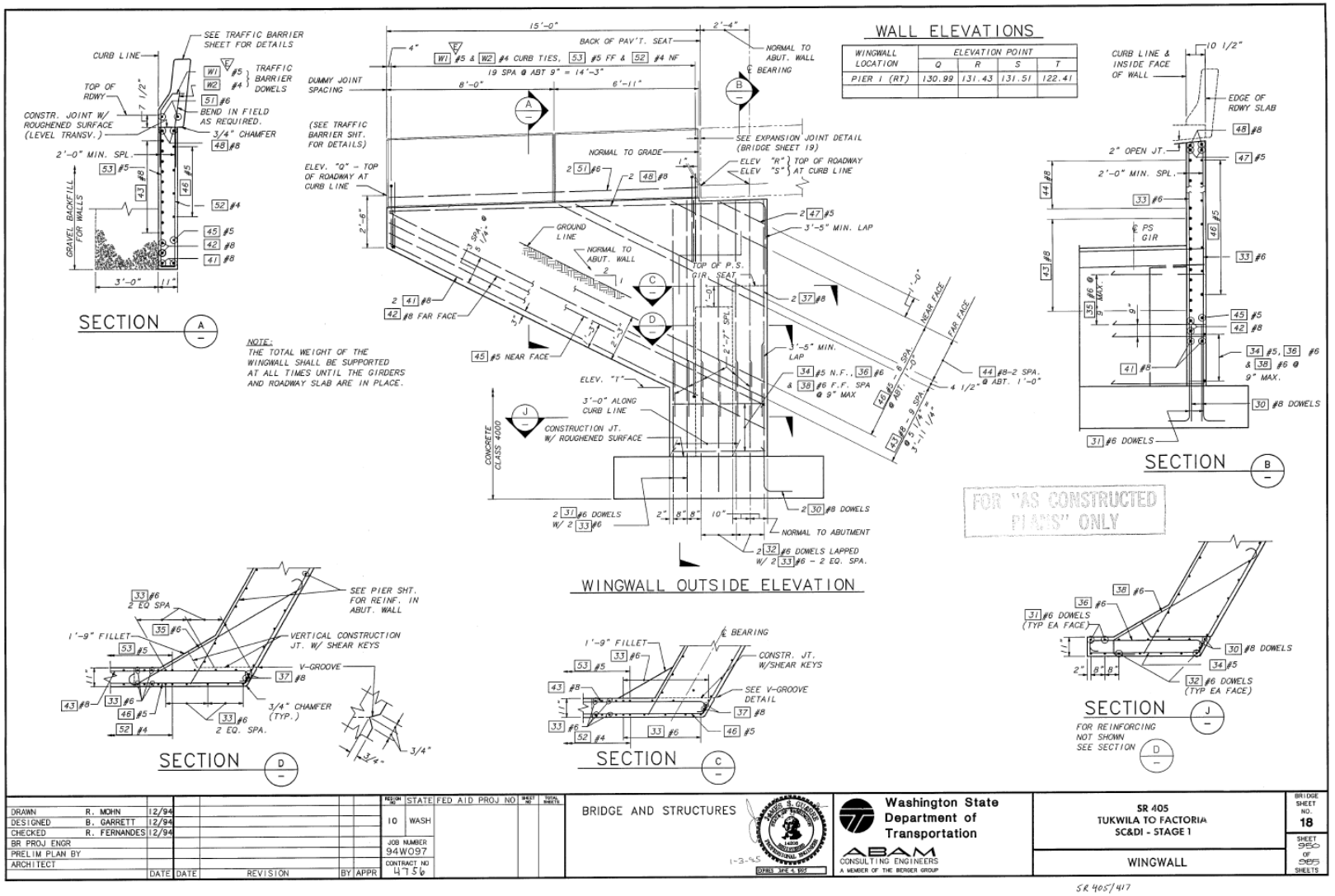

DRAWN	R. MOHN	12/94			REGION NO	STATE	FED AID PROJ NO	SHEET NO	TOTAL SHEETS
DESIGNED	B. GARRETT	12/94			10	WASH			
CHECKED	R. FERNANDES	12/94			JOB NUMBER	94W097			
BR PROJ ENGR					CONTRACT NO	4756			
PRELIM PLAN BY									
ARCHITECT									
	DATE	DATE	REVISION	BY	APPR				

BRIDGE AND STRUCTURES

1-3-95

Washington State Department of Transportation

ABAM CONSULTING ENGINEERS
A MEMBER OF THE BERGER GROUP

SR 405
TUKWILA TO FACTORIA
SC&DI - STAGE 1

WINGWALL

BRIDGE SHEET NO. 18

SHEET 950 OF 2695 SHEETS

SR 405 JOB NO. 7062 SHEET 18 OF 22

SR 405/417

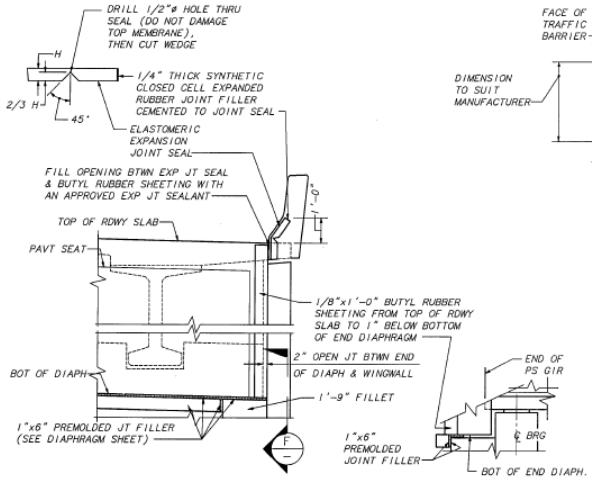

SECTION E

SECTION F

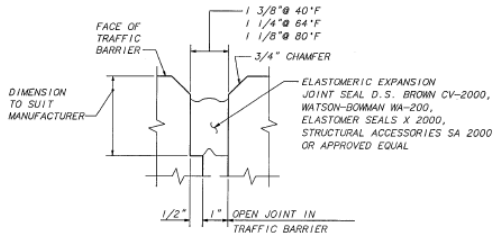

SECTION G

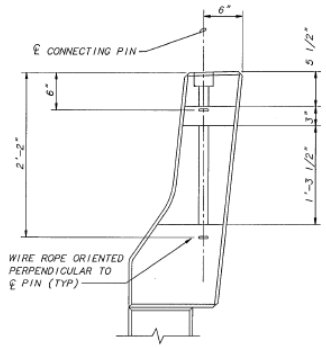

END VIEW

BARRIER ON WINGWALL

SEE STANDARD PLAN C-8 FOR ADDITIONAL END CONFIGURATION DETAILS AND WIRE ROPE DETAILS

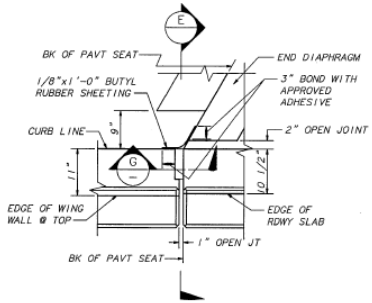

EXPANSION JOINT DETAIL

FOR "AS CONSTRUCTED PLANS" ONLY

DRAWN	R. MOHN	12/94				REGION NO	STATE	FED AID PROJ NO	SHEET NO	TOTAL SHEETS	BRIDGE AND STRUCTURES
DESIGNED	B. GARRETT	12/94				10	WASH				
CHECKED	R. FERNANDES	12/94				JOB NUMBER	94W097				
BR PROJ ENGR						CONTRACT NO	4756				
PRELIM PLAN BY											
ARCHITECT											
		DATE	DATE	REVISION	BY	APPR					

Washington State Department of Transportation

ABAM CONSULTING ENGINEERS
A MEMBER OF THE BERGER GROUP

SR 405
TUKWILA TO FACTORIA
SC&DI - STAGE 1

WINGWALL DETAILS

BRIDGE SHEET NO. 19

SHEET 951 OF 985 SHEETS

SR 405 JOB NO. 706Z SHEET 19 OF 22

SR 405/417

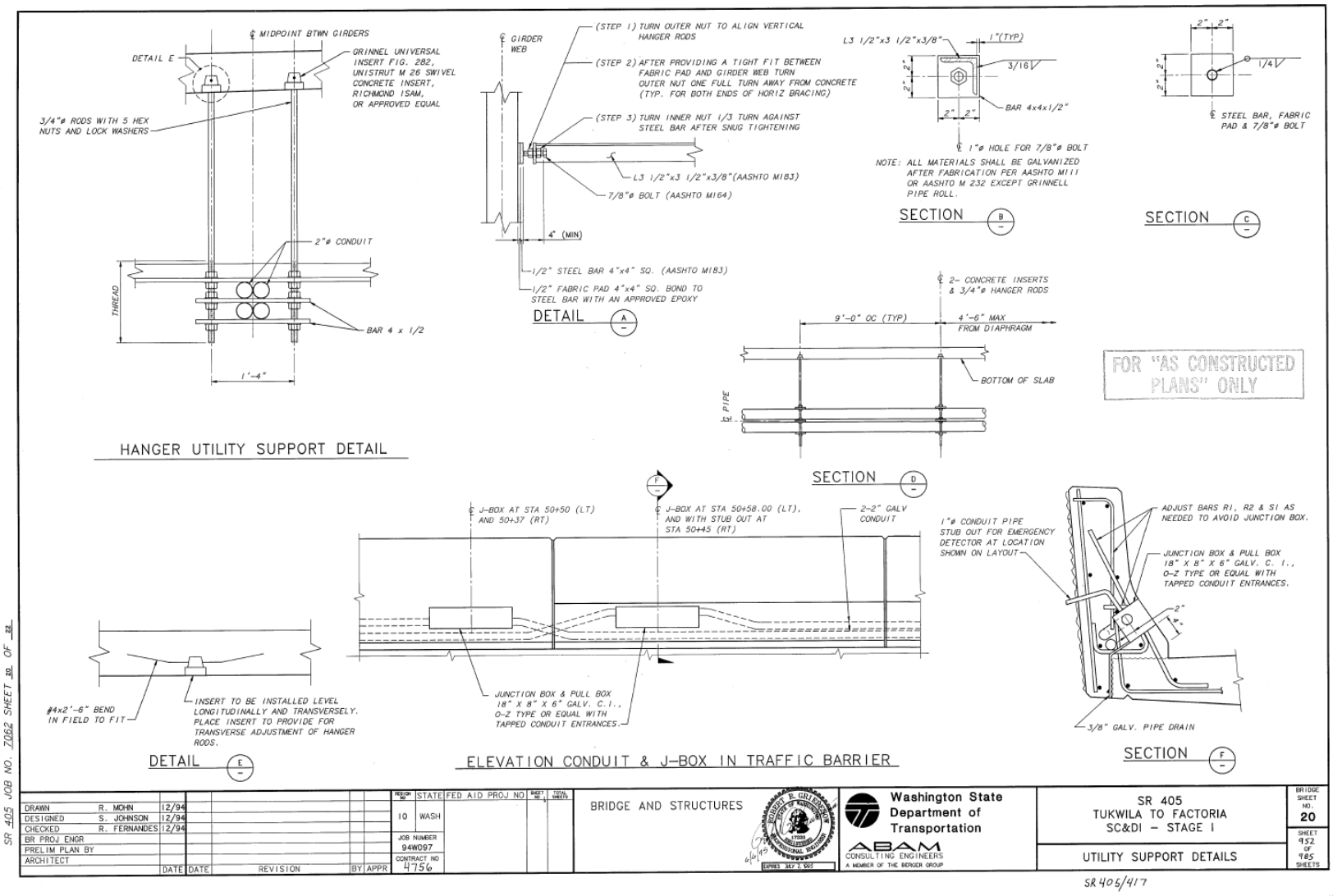
℄ MIDPOINT BTWN GIRDERS
DETAIL E
GRINNEL UNIVERSAL INSERT FIG. 282, UNISTRUT M 26 SWIVEL CONCRETE INSERT, RICHMOND ISAM, OR APPROVED EQUAL
3/4"ø RODS WITH 5 HEX NUTS AND LOCK WASHERS
2"ø CONDUIT
THREAD
BAR 4 x 1/2
1'-4"
HANGER UTILITY SUPPORT DETAIL
℄ GIRDER WEB
(STEP 1) TURN OUTER NUT TO ALIGN VERTICAL HANGER RODS
(STEP 2) AFTER PROVIDING A TIGHT FIT BETWEEN FABRIC PAD AND GIRDER WEB TURN OUTER NUT ONE FULL TURN AWAY FROM CONCRETE (TYP. FOR BOTH ENDS OF HORIZ BRACING)
(STEP 3) TURN INNER NUT 1/3 TURN AGAINST STEEL BAR AFTER SNUG TIGHTENING
L3 1/2"x3 1/2"x3/8"(AASHTO M183)
7/8"ø BOLT (AASHTO M164)
4" (MIN)
1/2" STEEL BAR 4"x4" SQ. (AASHTO M183)
1/2" FABRIC PAD 4"x4" SQ. BOND TO STEEL BAR WITH AN APPROVED EPOXY
DETAIL A
L3 1/2"x3 1/2"x3/8"
1"(TYP)
3/16
BAR 4x4x1/2"
℄ 1"ø HOLE FOR 7/8"ø BOLT
NOTE: ALL MATERIALS SHALL BE GALVANIZED AFTER FABRICATION PER AASHTO M111 OR AASHTO M 232 EXCEPT GRINNELL PIPE ROLL.
SECTION B
1/4
℄ STEEL BAR, FABRIC PAD & 7/8"ø BOLT
SECTION C
℄ 2- CONCRETE INSERTS & 3/4"ø HANGER RODS
9'-0" OC (TYP)
4'-6" MAX FROM DIAPHRAGM
BOTTOM OF SLAB
℄ PIPE
SECTION D
FOR "AS CONSTRUCTED PLANS" ONLY
℄ J-BOX AT STA 50+50 (LT) AND 50+37 (RT)
℄ J-BOX AT STA 50+58.00 (LT), AND WITH STUB OUT AT STA 50+45 (RT)
2-2" GALV CONDUIT
JUNCTION BOX & PULL BOX 18" X 8" X 6" GALV. C.I., O-Z TYPE OR EQUAL WITH TAPPED CONDUIT ENTRANCES.
#4x2'-6" BEND IN FIELD TO FIT
INSERT TO BE INSTALLED LEVEL LONGITUDINALLY AND TRANSVERSELY. PLACE INSERT TO PROVIDE FOR TRANSVERSE ADJUSTMENT OF HANGER RODS.
DETAIL E
ELEVATION CONDUIT & J-BOX IN TRAFFIC BARRIER
1"ø CONDUIT PIPE STUB OUT FOR EMERGENCY DETECTOR AT LOCATION SHOWN ON LAYOUT
ADJUST BARS R1, R2 & S1 AS NEEDED TO AVOID JUNCTION BOX.
JUNCTION BOX & PULL BOX 18" X 8" X 6" GALV. C. I., O-Z TYPE OR EQUAL WITH TAPPED CONDUIT ENTRANCES.
2"
3/8" GALV. PIPE DRAIN
SECTION F
SR 405 JOB NO. 7062 SHEET 20 OF 22
DRAWN R. MOHN 12/94
DESIGNED S. JOHNSON 12/94
CHECKED R. FERNANDES 12/94
BR PROJ ENGR
PRELIM PLAN BY
ARCHITECT
DATE DATE REVISION BY APPR
REGION NO. 10 STATE WASH
JOB NUMBER 94WD97
CONTRACT NO 4756
FED AID PROJ NO
SHEET NO.
TOTAL SHEETS
BRIDGE AND STRUCTURES
ROBERT R. GRUENDER STATE OF WASHINGTON 13868 REGISTERED PROFESSIONAL ENGINEER EXPIRES JULY 3, 1995
Washington State Department of Transportation
ABAM CONSULTING ENGINEERS A MEMBER OF THE BERGER GROUP
SR 405 TUKWILA TO FACTORIA SC&DI - STAGE I
UTILITY SUPPORT DETAILS
BRIDGE SHEET NO. 20
SHEET 952 OF 985 SHEETS
SR405/417

S=BAR IS INCLUDED IN SUBSTRUCTURE QUANTITIES
LUMP SUM QUANTITY
T OR S=TIE OR STIRRUP RADIUS
E=EARTHQUAKE TAIL W/ TIE OR STIRRUP RADIUS
E=BAR IS EPOXY COATED
V=BAR DIMENSIONS VARY BETWEEN DIMENSIONS SHOWN ON THIS LINE AND THE FOLLOWING LINE

MARK NO.	LOCATION	SIZE	NO. REQ'D	BEND TYPE	BEND RADIUS	LUMP SUM	SUBSTRUCT	EPOXY COATED	VARIES	U FT	U IN.	W FT	W IN.	X FT	X IN.	Y FT	Y IN.	Z FT	Z IN.	θ1 DEG	θ2 DEG	LENGTH (EACH) FT	LENGTH (EACH) IN.	TOTAL WEIGHT LBS
	SUBSTRUCTURE																							
	PIER 1																							
1	FOOTING BOTTOM	6	13	50			S			49	6.0											49	6	967
2	FOOTING BOTTOM	6	101	50			S			11	6.0											11	6	1745
3	FOOTING TOP	5	51	50			S			11	6.0											11	6	612
4	FOOTING TOP	5	13	50			S			49	6.0											49	6	671
5	ABUTMENT VERTICAL	6	86	50			S		V	8	4.0											8	4	
										7	1.0											7	1	996
6	ABUTMENT HORIZONTAL	6	44	51			S			23	1.0											23	9	1571
7	ABUTMENT TIES	4	60	58	T		S			1	6.0											2	2	87
8	ABUTMENT TOP HORIZONTAL	6	4	51			S			23	1.0											23	9	143
9	ABUTMENT TOP TIES	4	43	56	T		S			1	6.0											2	1	60
10	GIRDER STOP	5	25	61	T		S			1	5.0	2	0.0	2	0.0							5	3	136
11	GIRDER STOP HORIZONTAL	4	10	50			S			3	5.0											3	5	23
	PIER 1 CURTAIN WALL																							
20	VERT FF	5	4	50			S			13	0.0											13	0	54
21	VERT NF	4	3	50			S			13	0.0											13	0	26
22	VERT FF	5	10	50			S			13	0.0											13	0	136
23	VERT NF	4	7	50			S			13	0.0											13	0	61
24	HORIZ TOP NF	4	7	80			S			6	0.0			0	10.0			0	1.5		62	6	10	32
25	HORIZ TOP FF	7	7	80			S			5	9.0			1	6.0			0	3.0		62	7	3	104
26	HORIZ TOP NF	4	11	80			S			6	0.0			0	10.0			0	1.5		62	6	10	50
27	HORIZ TOP FF	7	11	80			S			5	9.0			1	6.0			0	3.0		62	7	3	163
28	HORIZ AT FILLET	7	11	52			S			3	0.0											4	7	104
W1	TRAFFIC BARRIER DOWEL	5	6	91			S	E														4	1	26
W2	TRAFFIC BARRIER DOWEL	4	4	92			S															4	3	11
	PIER 1 WINGWALL																							
30	DOWEL	8	2	54			S			6	0.0											7	2	38
31	DOWEL	6	4	54			S			6	0.0											6	10	41
32	DOWEL	6	10	54			S			6	0.0											6	10	103
33	VERTICAL	6	14	50			S			8	10.0											8	10	186
34	STUB HORIZONTAL	5	6	80			S			4	2.0	0	8.0	0	9.0	0	2.5	0	2.5	90	117	5	5	34
35	FILLET HORIZONTAL	6	3	52			S			7	0.0											8	5	38
36	STUB HORIZONTAL	6	6	52			S			4	4.0											5	9	51
37	VERTICAL	8	2	50			S			9	9.0											9	9	52
38	FILLET HORIZONTAL	6	6	79			S			0	8.0	1	0.0	5	9.0	0	3.0	0	3.0	90	120	7	11	71
41	BOTTOM OUTSIDE FACE	8	2	51			S			19	5.0											20	4	109
42	SLOPE INSIDE FACE	8	2	51			S			19	5.0											20	4	109
43	SLOPE INSIDE FACE	8	10	51			S		V	19	5.0											20	4	
										9	9.0											10	8	414
44	SLOPE INSIDE FACE	8	3	51			S		V	8	9.0											9	8	
										4	2.0											5	1	59
45	SLOPE OUTSIDE FACE	5	1	51			S			19	5.0											20	0	21
46	SLOPE OUTSIDE FACE	5	7	51			S		V	17	11.0											18	6	
										4	2.0											4	9	85
47	TOP CORNER	5	2	51			S		V	1	4.0											1	11	
										1	2.0											1	9	4
48	TOP HORIZONTAL	8	2	61			S		V	17	11.0	3	9.0									21	6	
										17	9.0	3	9.0									21	4	114
51	CURB TOP HORIZONTAL	6	2	50			S			14	8.0											14	8	44
52	VERTICAL	4	20	54			S		V	1	6.0											2	1	
										8	5.0											9	0	74

S=BAR IS INCLUDED IN SUBSTRUCTURE QUANTITIES
LUMP SUM QUANTITY
T OR S=TIE OR STIRRUP RADIUS
E=EARTHQUAKE TAIL W/ TIE OR STIRRUP RADIUS
E=BAR IS EPOXY COATED
V=BAR DIMENSIONS VARY BETWEEN DIMENSIONS SHOWN ON THIS LINE AND THE FOLLOWING LINE

MARK NO.	LOCATION	SIZE	NO. REQ'D	BEND TYPE	BEND RADIUS	LUMP SUM	SUBSTRUCT	EPOXY COATED	VARIES	U FT	U IN.	W FT	W IN.	X FT	X IN.	Y FT	Y IN.	Z FT	Z IN.	θ1 DEG	θ2 DEG	LENGTH (EACH) FT	LENGTH (EACH) IN.	TOTAL WEIGHT LBS
53	VERTICAL	5	20	54			S		V	1	6.0											2	3	
										8	5.0											9	2	118
W1	TRAFFIC BARRIER DOWEL	5	20	91			S	E														4	1	87
W2	TRAFFIC BARRIER DOWEL	4	20	92			S															4	3	55
	PIER 2																							
55	FOOTING	6	72	50			S			10	6.0											10	6	1136
56	FOOTING	8	96	50			S			10	6.0											10	6	2691
57	COLUMN VERTICAL	9	39	68			S			1	8.0	27	3.0									28	6	3777
59	COLUMN SPIRAL	4	3	67			S			2	8.0	81	0.0	0	3.5							678	6	1360
70	CROSS BEAM HORIZONTAL BOTTOM	9	24 ~~34~~	50			S			38	10.0											38	10	7130
71	CROSS BEAM HORIZONTAL	4	4 ~~12~~	50			S			34	1.0											34	1	273
72	CROSS BEAM STIRRUP	5	60 ~~36~~	72	S		S			3	9.0	3	7.0	3	7.0							11	8	703
73	CROSS BEAM TOP TIE	5	60 ~~36~~	58	T		S			3	9.0											4	7	277
74	CROSS BEAM HORIZONTAL	9	24 ~~34~~	50			S			39	2.0											39	2	7191
	PIER 3																							
55	FOOTING	6	72	50			S			10	6.0											10	6	1136
56	FOOTING	8	96	50			S			10	6.0											10	6	2691
58	COLUMN VERTICAL	9	39	68			S			1	8.0	30	4.0									31	7	4186
59	COLUMN SPIRAL	4	3	67			S			2	8.0	92	0.0			5	0.0					770	9	1545
69	CROSS BEAM HORIZONTAL BOTTOM	9	18 ~~34~~	50			S			38	8.0											38	8	7099
71	CROSS BEAM HORIZONTAL	4	4 ~~12~~	50			S			34	1.0											34	1	273
72	CROSS BEAM STIRRUP	5	54 ~~36~~	72	S		S			3	9.0	3	7.0	3	7.0							11	8	703
73	CROSS BEAM TOP TIE	5	54 ~~36~~	58	T		S			3	9.0											4	7	277
74	CROSS BEAM HORIZONTAL	9	18 ~~34~~	50			S			39	0.0											39	0	7160
	PIER 4																							
1	FOOTING BOTTOM	6	13	50			S			49	6.0											49	6	967
2	FOOTING BOTTOM	6	101	50			S			11	6.0											11	6	1745
3	FOOTING TOP	5	51	50			S			11	6.0											11	6	612
4	FOOTING TOP	5	13	50			S			49	6.0											49	6	671
6	ABUTMENT HORIZONTAL	6	44	51			S			23	1.0											23	9	1571
7	ABUTMENT TIES	4	48	58	T		S			1	6.0											2	2	69
8	ABUTMENT TOP HORIZONTAL	6	4	51			S			23	1.0											23	9	143
9	ABUTMENT TOP TIES	4	43	56	T		S			1	6.0											2	1	60
10	GIRDER STOP	5	25	61	T		S			1	5.0	2	0.0	2	0.0							5	3	136
11	GIRDER STOP HORIZONTAL	4	10	50			S			3	5.0											3	5	23
12	ABUTMENT VERTICAL	6	86	50			S		V	7	0.0											7	0	
										5	7.0											5	7	813
	PIER 4 CURTAIN WALL EAST																							
80	VERT FF	5	4	50			S			10	6.0											10	6	44
81	VERT NF	4	3	50			S			10	6.0											10	6	21
82	VERT FF	5	10	50			S			10	6.0											10	6	110
83	VERT NF	4	7	50			S			10	6.0											10	6	49
84	HORIZ TOP NF	4	7	80			S			5	11.0			0	10.0			0	1.5		64	6	9	32
85	HORIZ TOP FF	7	7	80			S			5	8.0			1	6.0			0	3.0		64	7	2	103
86	HORIZ TOP NF	4	7	80			S			5	11.0			0	10.0			0	1.5		64	6	9	32
87	HORIZ TOP FF	7	7	80			S			5	8.0			1	6.0			0	3.0		64	7	2	103
88	HORIZ AT FILLET	7	7	52			S			3	0.0											4	7	66
W1	TRAFFIC BARRIER DOWEL	5	6	91			S	E														4	1	26
W2	TRAFFIC BARRIER DOWEL	4	4	92			S															4	3	11

BENDING DIAGRAMS

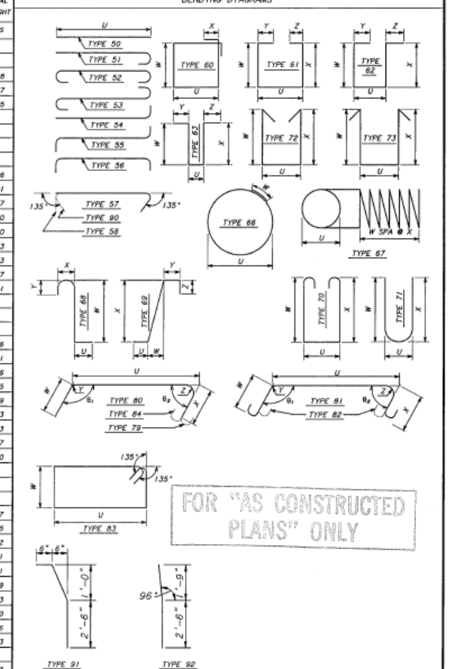

NOTES:

1. ALL REINFORCING BARS ON THIS SHEET SHALL BE AASHTO M31 GRADE 60 UNLESS SHOWN OTHERWISE.
2. REINFORCING FOR TRAFFIC BARRIER IS NOT SHOWN IN THIS BAR LIST EXCEPT FOR BARS S1, S2, W1, AND W2. SEE TRAFFIC BARRIER, SHEET 17.
3. BEND FOR TRANSVERSE BARS DUE TO ROADWAY CROWN CONDITIONS HAVE NOT BEEN SHOWN. THESE BARS SHALL BE BENT AS REQUIRED TO CONFORM TO THE CONFIGURATION OF THE STRUCTURE.
4. $ NUMBER AND LENGTH OF BARS TO BE DETERMINED BY THE CONTRACTOR FROM THE PLANS.
5. LENGTHS OF SPIRAL SHOWN IN BARLIST DOES NOT INCLUDE LENGTH OF SPLICES
6. DIMENSIONS FOR BENT REINFORCING BARS (INCLUDING LENGTH) ARE POINTS OF INTERSECTION (OUT TO OUT).

SR 405 JOB NO. 7067 SHEET 21 OF 22

DRAWN	R. MOHN	10/94
DESIGNED	E. DORNSEIF	12/94
CHECKED	R. FERNANDES	12/94
BR PROJ ENGR		
PRELIM PLAN BY		
ARCHITECT		
		DATE

DATE | REVISION | BY | APPR

REGION NO. 10 | STATE WASH | FED AID PROJ NO | SHEET NO | TOTAL SHEETS
JOB NUMBER 94W097
CONTRACT NO 4756

BRIDGE AND STRUCTURES

JAMES S. GIAMPAGLIA, STATE OF WASHINGTON, 14006, REGISTERED PROFESSIONAL ENGINEER
1-3-95
EXPIRES JUNE 4, 1995

Washington State Department of Transportation

ABAM CONSULTING ENGINEERS
A MEMBER OF THE BERGER GROUP

SR 405
TUKWILA TO FACTORIA
SC&DI - STAGE 1

BAR LIST – SHEET 1

BRIDGE SHEET NO. 21
SHEET 953 OF 985 SHEETS

SR 405/417

S=BAR IS INCLUDED IN SUBSTRUCTURE QUANTITIES
LUMP SUM QUANTITY
T OR S=TIE OR STIRRUP RADIUS
E=EARTHQUAKE TAIL W/ TIE
OR STIRRUP RADIUS
E=BAR IS EPOXY COATED
V=BAR DIMENSIONS VARY BETWEEN DIMENSIONS SHOWN ON THIS LINE AND THE FOLLOWING LINE

MARK NO.	LOCATION	SIZE	NO. REQ'D	BEND TYPE	BEND RADIUS	S=BAR	LUMP SUM	SUBSTRUCT	EPOXY COATED	VARIES	DIMENSIONS U FT	U IN.	W FT	W IN.	X FT	X IN.	Y FT	Y IN.	Z FT	Z IN.	θ_1 DEG	θ_2 DEG	LENGTH (EACH) FT	LENGTH (EACH) IN.	TOTAL WEIGHT LBS
	PIER 4 CURTAIN WALL WEST																								
80	VERT FF	5	4	50			S				11	9.0											11	9	49
81	VERT NF	4	3	50			S				11	9.0											11	9	24
82	VERT FF	5	10	50			S				11	9.0											11	9	123
83	VERT NF	4	7	50			S				11	9.0											11	9	55
94	HORIZ TOP NF	4	7	80			S				5	8.0	0	8.0			0	1.5			64		6	2	29
95	HORIZ TOP FF	7	7	80			S				5	11.0	1	2.0			0	3.0			64		6	9	98
96	HORIZ TOP NF	4	8	80			S				5	8.0	0	8.0			0	1.5			64		6	2	33
97	HORIZ TOP FF	7	8	80			S				5	11.0	1	2.0			0	3.0			64		6	9	110
98	HORIZ AT FILLET	7	8	52			S				4	6.0											6	1	100
W1	TRAFFIC BARRIER DOWEL	5	6	91			S	E															4	1	26
W2	TRAFFIC BARRIER DOWEL	4	4	82			S																4	3	11
	SUPERSTRUCTURE																								
	END DIAPHRAGM – PIER 1																								
120	BOTTOM HORIZONTAL	6	2	50							40	11.0											40	11	123
121	HORIZONTAL	4	22	50							21	6.0											21	6	316
122	STIRRUP	4	32	54	S						7	0.0											7	4	156
123	STIRRUP	4	32	54	S						7	0.0											7	4	156
124	STIRRUP	4	32	61	S						5	4.0	1	8.0	0	8.0							7	7	162
125	TOP HORIZONTAL	4	6	50							21	6.0											21	6	86
126	TOP TIES	4	31	56	T						1	7.0											2	2	45
127	TOP HORIZONTAL	6	2	50							40	11.0											40	11	123
	END DIAPHRAGM – PIER 4																								
120	BOTTOM HORIZONTAL	6	2	50							39	5.0											39	5	118
121	HORIZONTAL	4	11	50							38	1.0											38	1	280
122	STIRRUP	4	32	54	S						7	0.0											7	4	156
123	STIRRUP	4	32	54	S						7	0.0											7	4	156
124	STIRRUP	4	32	61	S						5	4.0	1	9.0	0	8.0							7	7	162
125	TOP HORIZONTAL	4	3	50							39	5.0											39	5	79
126	TOP TIES	4	31	56	T						1	8.0											2	3	47
127	TOP HORIZONTAL	6	2	50							39	5.0											39	5	118
	INTERMEDIATE DIAPHRAGMS																								
150	STIRRUP	4	180	71	S						0	5.0	4	8.5	4	8.5							9	7	1153
151	BOTTOM HORIZONTAL	9	4	50							34	1.0											34	1	464
152	HORIZONTAL BETWEEN GIRDERS	4	180	50							6	2.0											6	2	741
153	HORIZONTAL FULL LENGTH	8	4	50							34	1.0											34	1	364
154	TOP HORIZONTAL	7	16	50							35	11.0											35	11	1175
	INTERMEDIATE HINGE DIAPHRAGM																								
155	HORIZONTAL TIE	4	20	61	S						1	0.5	2	9.0	2	9.0							6	5	85
156	HORIZONTAL TIE	4	100	61	T						2	9.0	3	5.0									6	1	406
157	STIRRUP	4	60	54	S						5	5.0											5	9	229
158	STIRRUP	4	120	54	S						5	11.5											6	3	501
159	HINGE BAR	9	64	51							6												7	3	1575
160	HORIZONTAL	5	20	50							36	9.0											36	9	767
161	STIRRUP	4	50	63	S						1	9.0	5	6.5	5	6.5	0	5.0	0	5.0			13	4	445

S=BAR IS INCLUDED IN SUBSTRUCTURE QUANTITIES
LUMP SUM QUANTITY
T OR S=TIE OR STIRRUP RADIUS
E=EARTHQUAKE TAIL W/ TIE
OR STIRRUP RADIUS
E=BAR IS EPOXY COATED
V=BAR DIMENSIONS VARY BETWEEN DIMENSIONS SHOWN ON THIS LINE AND THE FOLLOWING LINE

MARK NO.	LOCATION	SIZE	NO. REQ'D	BEND TYPE	BEND RADIUS	S=BAR	LUMP SUM	SUBSTRUCT	EPOXY COATED	VARIES	DIMENSIONS U FT	U IN.	W FT	W IN.	X FT	X IN.	Y FT	Y IN.	Z FT	Z IN.	θ_1 DEG	θ_2 DEG	LENGTH (EACH) FT	LENGTH (EACH) IN.	TOTAL WEIGHT LBS
	ROADWAY SLAB																								
200	TRANSVERSE BOTTOM	5	365	50					E		37	6.0											37	6	14276
201	TRANSVERSE TOP	5	365	51					E		26	5.0											27	0	10275
202	CANTILEVER	5	456	51					E		7	4.0											7	11	3760
203	TRANSVERSE TOP END	5	48	51					E	V	34	3.0											34	10	
											7	9.0											8	4	1035
204	TRANSVERSE BOTTOM END	5	48	50						V	34	3.0											34	3	
											7	7.0											7	7	1004
205	TRANSVERSE TOP SPLAYED	5	16	51					E	V	5	1.0											5	8	
											7	7.0											8	2	115
206	TRANSVERSE BOTTOM SPLAYED	5	16	50						V	5	1.0											5	1	
											7	7.0											7	7	106
207	TRANSVERSE TOP	5	365	51					E		13	11.0											14	6	5516
210	LONGITUDINAL TOP	5	$	50		L		E			$	$											$	$	5321
211	LONGITUDINAL BOTTOM	5	$	50		L					$	$											$	$	8887
220	PIER LONGITUDINAL BOTTOM	6	38	50							54	0.0											54	0	3082
221	PIER LONGITUDINAL BOTTOM	6	48	50							44	0.0											44	0	3172
222	PIER LONGITUDINAL BOTTOM	6	24	50							19	0.0											19	0	685
230	PIER LONGITUDINAL TOP	6	38	50					E		54	0.0											54	0	3082
231	PIER LONGITUDINAL TOP	6	48	50					E		44	0.0											44	0	3172
232	PIER LONGITUDINAL TOP	6	24	50					E		19	0.0											19	0	685
S1	TRAFFIC BARRIER TIE	5	620	69					E		0	6.0	0	9.0	1	6.0	0	6.0					2	7	1890
S2	TRAFFIC BARRIER TIE	4	312	69							1	6.0	0	2.0	1	6.0							2	11	610

BENDING DIAGRAMS

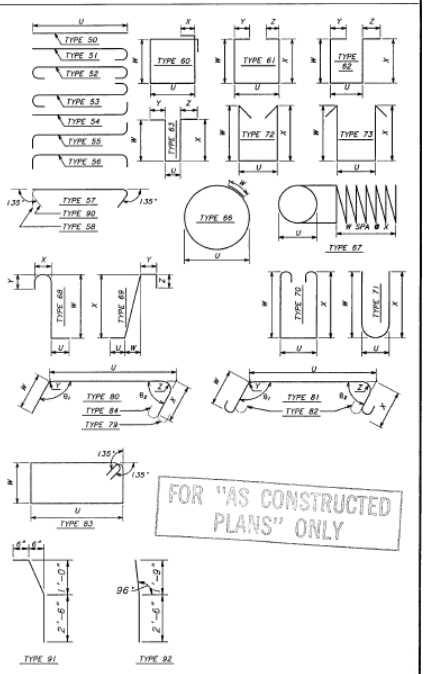

NOTES:

1. ALL REINFORCING BARS ON THIS SHEET SHALL BE AASHTO M31 GRADE 60 UNLESS SHOWN OTHERWISE.
2. REINFORCING FOR TRAFFIC BARRIER IS NOT SHOWN IN THIS BAR LIST EXCEPT FOR BARS S1, S2, W1, AND W2. SEE TRAFFIC BARRIER, SHEET 17.
3. BEND FOR TRANSVERSE BARS DUE TO ROADWAY CROWN CONDITIONS HAVE NOT BEEN SHOWN. THESE BARS SHALL BE BENT AS REQUIRED TO CONFORM TO THE CONFIGURATION OF THE STRUCTURE.
4. # NUMBER AND LENGTH OF BARS TO BE DETERMINED BY THE CONTRACTOR FROM THE PLANS.
5. LENGTHS OF SPIRAL SHOWN IN BARLIST DOES NOT INCLUDE LENGTH OF SPLICES
6. DIMENSIONS FOR BENT REINFORCING BARS (INCLUDING LENGTH) ARE POINTS OF INTERSECTION (OUT TO OUT).

FOR "AS CONSTRUCTED PLANS" ONLY

SR 405 JOB NO. 7067 SHEET 22 OF 22

DRAWN	R. MOHN	10/94
DESIGNED	E. DORNSEIF	12/94
CHECKED	R. FERNANDES	12/94
BR PROJ ENGR		
PRELIM PLAN BY		
ARCHITECT		

DATE	REVISION	BY	APPR

REGION NO	STATE	FED AID PROJ NO	SHEET NO	TOTAL SHEETS
10	WASH			
JOB NUMBER	94W097			
CONTRACT NO	4756			

BRIDGE AND STRUCTURES

1-3-95 EXPIRES: JUNE 4, 1995

Washington State Department of Transportation

ABAM CONSULTING ENGINEERS
A MEMBER OF THE BERGER GROUP

SR 405
TUKWILA TO FACTORIA
SC&DI - STAGE 1

BAR LIST – SHEET 2

BRIDGE SHEET NO. 22

SHEET ITEM OF SHEETS SHEETS

SR 405/417

APPENDIX C: SUMMARY OF BRIDGE PERFORMANCE STATISTICS

Table C.1: Summary of statistics for the reference bridge

Location	Soil Class	Abutment Displacement (in.)			Bent Drift Ratio (%)			Likelihood of Spalling (%)	Likelihood of Bar Buckling (%)
		15%	50%	85%	15%	50%	85%		
Z0FORK	Baseline	1.51	2.72	3.43	0.64	1.16	1.47	8.69	0.00
Z0FORK	C2	1.46	2.95	3.77	0.67	1.24	1.63	12.60	0.03
Z0FORK	C4	1.76	3.43	4.99	0.84	1.49	2.06	24.10	0.54
Z0FORK	D1	2.12	3.74	5.81	0.97	1.65	2.31	31.30	1.30
Z0FORK	D3	1.88	2.77	5.91	0.82	1.18	2.35	23.33	2.83
Z0XOCS	Baseline	1.55	2.26	3.26	0.71	0.99	1.37	6.43	0.01
Z0XOCS	C2	1.58	2.37	3.51	0.71	1.04	1.48	7.85	0.01
Z0XOCS	C4	1.74	2.59	4.05	0.78	1.13	1.72	14.46	1.10
Z0XOCS	D1	2.02	3.12	5.61	0.91	1.31	2.25	23.22	3.44
Z0XOCS	D3	1.66	2.39	3.97	0.72	1.05	1.69	11.72	0.88
Z0XANG	Baseline	1.13	1.64	3.00	0.50	0.75	1.26	4.23	0.00
Z0XANG	C2	1.19	1.71	2.83	0.53	0.77	1.18	6.07	0.76
Z0XANG	C4	1.35	1.97	3.92	0.61	0.89	1.66	12.12	2.57
Z0XANG	D1	1.42	2.19	4.47	0.64	0.97	1.84	15.57	4.96
Z0XANG	D3	1.48	2.06	4.85	0.65	0.90	1.99	16.60	7.89
Z00CPW	Baseline	1.01	1.20	1.67	0.45	0.53	0.79	0.37	0.00
Z00CPW	C2	0.99	1.31	1.82	0.44	0.59	0.84	0.52	0.00

Location	Soil Class	Abutment Displacement (in.)			Bent Drift Ratio (%)			Likelihood of Spalling (%)	Likelihood of Bar Buckling (%)
		15%	50%	85%	15%	50%	85%		
Z00CPW	C4	1.16	1.55	2.16	0.53	0.70	0.96	1.36	0.00
Z00CPW	D1	1.24	1.73	2.53	0.54	0.78	1.10	2.99	0.01
Z00CPW	D3	1.60	2.00	2.89	0.70	0.89	1.23	4.59	0.01
Z0XWLK	Baseline	0.94	1.13	1.35	0.41	0.48	0.58	0.04	0.00
Z0XWLK	C2	0.93	1.18	1.42	0.41	0.51	0.62	0.03	0.00
Z0XWLK	C4	1.00	1.30	1.63	0.43	0.57	0.73	0.47	0.19
Z0XWLK	D1	1.08	1.43	1.92	0.47	0.63	0.85	0.31	0.00
Z0XWLK	D3	1.14	1.52	2.16	0.50	0.66	0.94	1.53	0.35
Z0EVCC	Baseline	0.82	1.04	1.19	0.35	0.45	0.52	0.00	0.00
Z0EVCC	C2	0.78	1.09	1.36	0.32	0.48	0.59	0.04	0.00
Z0EVCC	C4	0.88	1.21	1.57	0.38	0.54	0.70	0.06	0.00
Z0EVCC	D1	0.96	1.32	1.78	0.41	0.59	0.79	0.17	0.00
Z0EVCC	D3	1.05	1.39	2.02	0.46	0.60	0.89	0.62	0.00

Table C.2: Summary of statistics for integral abutments (Case 1)

Location	Soil Class	Abutment Displacement (in.)			Bent Drift Ratio (%)			Likelihood of Spalling (%)	Likelihood of Bar Buckling (%)
		15%	50%	85%	15%	50%	85%		
Z0XOCS	Baseline	1.37	1.89	2.72	0.59	0.82	1.15	3.16	0.00
Z0XOCS	C2	1.40	2.06	3.33	0.60	0.88	1.40	5.36	0.00
Z0XOCS	C4	1.52	2.40	4.09	0.66	1.03	1.67	10.99	0.01
Z0XOCS	D1	1.79	2.59	4.91	0.77	1.10	1.99	18.22	0.57
Z0XOCS	D3	0.99	1.76	3.54	0.42	0.75	1.48	7.88	0.03
Z0XANG	Baseline	0.88	1.33	2.41	0.39	0.58	0.99	1.01	0.00
Z0XANG	C2	0.88	1.45	2.51	0.38	0.62	1.05	1.70	0.00
Z0XANG	C4	1.07	1.71	2.95	0.46	0.74	1.24	5.63	0.77
Z0XANG	D1	1.27	1.96	3.35	0.55	0.84	1.39	9.23	2.18
Z0XANG	D3	0.89	1.69	3.47	0.38	0.71	1.44	11.32	3.96
Z0XWLK	Baseline	0.61	0.79	0.97	0.26	0.35	0.43	0.00	0.00
Z0XWLK	C2	0.66	0.86	1.09	0.28	0.37	0.46	0.00	0.00
Z0XWLK	C4	0.74	1.03	1.37	0.32	0.44	0.59	0.03	0.00
Z0XWLK	D1	0.87	1.21	1.56	0.37	0.53	0.67	0.09	0.00
Z0XWLK	D3	0.69	1.01	1.74	0.30	0.44	0.75	0.60	0.04

Table C.3: Summary of statistics for semi-integral abutment (Case2)

Location	Soil Class	Abutment Displacement (in.)			Bent Drift Ratio (%)			Likelihood of Spalling (%)	Likelihood of Bar Buckling (%)
		15%	50%	85%	15%	50%	85%		
Z0XOCS	Baseline	1.69	2.42	3.42	0.70	0.99	1.42	5.69	0.00
Z0XOCS	C2	1.66	2.45	3.73	0.69	1.01	1.51	8.79	0.00
Z0XOCS	C4	1.84	2.86	5.32	0.77	1.16	1.97	17.89	0.88
Z0XOCS	D1	2.11	3.16	5.80	0.88	1.30	2.22	23.87	3.02
Z0XOCS	D3	1.66	2.46	4.53	0.69	1.00	1.75	13.33	0.87
Z0XANG	Baseline	1.26	1.65	2.56	0.51	0.67	1.05	3.49	0.00
Z0XANG	C2	1.30	1.76	2.95	0.53	0.72	1.18	7.04	2.70
Z0XANG	C4	1.47	2.08	3.45	0.59	0.85	1.41	12.25	5.85
Z0XANG	D1	1.49	2.29	4.36	0.62	0.95	1.76	15.65	7.88
Z0XANG	D3	1.50	2.14	4.80	0.62	0.88	1.80	15.78	7.59
Z0XWLK	Baseline	0.88	1.06	1.37	0.36	0.44	0.56	0.02	0.00
Z0XWLK	C2	0.91	1.19	1.42	0.37	0.49	0.59	0.02	0.00
Z0XWLK	C4	1.04	1.35	1.81	0.43	0.56	0.75	0.13	0.00
Z0XWLK	D1	1.11	1.49	2.02	0.45	0.62	0.84	0.37	0.00
Z0XWLK	D3	1.12	1.47	2.25	0.45	0.61	0.90	1.47	0.33

Table C.4: Summary of statistics for spread footing (Case 3)

Location	Soil Class	Abutment Displacement (in.)			Bent Drift Ratio (%)			Likelihood of Spalling (%)	Likelihood of Bar Buckling (%)
		15%	50%	85%	15%	50%	85%		
Z0XOCS	Baseline	1.81	2.44	3.92	0.71	0.97	1.54	11.88	3.34
Z0XOCS	C2	1.80	2.51	4.17	0.71	0.99	1.64	13.19	1.84
Z0XOCS	C4	1.91	2.76	4.83	0.75	1.09	1.90	16.79	2.01
Z0XOCS	D1	2.15	3.09	5.95	0.83	1.22	2.33	23.56	2.15
Z0XOCS	D3	2.07	2.94	5.24	0.81	1.16	2.07	20.90	3.91
Z0XANG	Baseline	1.29	2.17	10.65	0.54	0.85	4.16	24.36	10.75
Z0XANG	C2	1.31	2.17	7.37	0.54	0.85	2.90	22.14	9.13
Z0XANG	C4	1.45	2.49	7.25	0.60	0.98	2.83	26.32	9.34
Z0XANG	D1	1.66	2.66	11.55	0.66	1.06	4.53	29.85	12.34
Z0XANG	D3	1.91	3.07	17.91	0.75	1.20	6.92	33.30	18.48
Z0XWLK	Baseline	1.02	1.28	1.71	0.42	0.53	0.66	0.36	0.00
Z0XWLK	C2	1.04	1.35	1.80	0.43	0.55	0.71	0.32	0.00
Z0XWLK	C4	1.16	1.51	2.09	0.47	0.61	0.83	0.81	0.00
Z0XWLK	D1	1.18	1.68	2.36	0.49	0.67	0.94	2.20	0.02
Z0XWLK	D3	1.36	1.95	3.02	0.56	0.77	1.18	5.50	0.37

Table C.5: Summary of statistics for medium clay (Case 4)

Location	Soil Class	Abutment Displacement (in.)			Bent Drift Ratio (%)			Likelihood of Spalling (%)	Likelihood of Bar Buckling (%)
		15%	50%	85%	15%	50%	85%		
Z0XOCS	Baseline	1.59	2.12	3.79	0.66	0.86	1.53	8.92	3.32
Z0XOCS	C2	1.58	2.26	3.71	0.66	0.92	1.49	8.60	2.05
Z0XOCS	C4	1.80	2.56	4.51	0.73	1.03	1.82	14.93	2.00
Z0XOCS	D1	2.02	2.92	5.55	0.82	1.19	2.22	22.45	2.23
Z0XOCS	D3	1.71	2.68	4.71	0.71	1.09	1.88	16.43	1.84
Z0XANG	Baseline	1.18	1.80	6.60	0.52	0.74	2.66	18.40	6.42
Z0XANG	C2	1.25	1.85	5.13	0.53	0.76	2.07	15.72	5.12
Z0XANG	C4	1.40	2.16	8.77	0.60	0.87	3.47	20.27	8.89
Z0XANG	D1	1.49	2.33	8.37	0.63	0.95	3.34	24.18	10.47
Z0XANG	D3	1.63	2.51	10.26	0.67	1.01	3.99	26.27	12.37
Z0XWLK	Baseline	0.94	1.15	1.38	0.40	0.49	0.58	0.01	0.00
Z0XWLK	C2	0.98	1.21	1.53	0.41	0.52	0.64	0.06	0.00
Z0XWLK	C4	1.00	1.35	1.79	0.43	0.58	0.72	0.53	0.01
Z0XWLK	D1	1.05	1.52	2.00	0.45	0.63	0.81	0.51	0.00
Z0XWLK	D3	1.18	1.67	2.44	0.50	0.68	0.99	2.68	0.30

Table C.6: Summary of statistics for no shear key (Case 5)

Location	Soil Class	Abutment Displacement (in.)			Bent Drift Ratio (%)			Likelihood of Spalling (%)	Likelihood of Bar Buckling (%)
		15%	50%	85%	15%	50%	85%		
Z0XOCS	Baseline	1.80	2.57	4.44	0.71	1.00	1.74	13.78	0.10
Z0XOCS	C2	1.95	2.65	4.29	0.77	1.03	1.68	12.52	0.19
Z0XOCS	C4	2.09	2.87	5.20	0.82	1.13	2.03	19.45	1.73
Z0XOCS	D1	2.21	3.32	6.19	0.86	1.29	2.42	25.92	3.55
Z0XOCS	D3	2.22	3.38	6.90	0.86	1.33	2.70	27.73	4.77
Z0XANG	Baseline	1.33	2.28	7.68	0.53	0.89	3.00	26.24	8.25
Z0XANG	C2	1.36	2.38	8.71	0.54	0.93	3.41	28.53	8.93
Z0XANG	C4	1.52	2.81	9.93	0.61	1.11	3.89	30.83	10.61
Z0XANG	D1	1.67	2.86	11.66	0.66	1.12	4.55	32.39	12.51
Z0XANG	D3	2.12	3.80	15.16	0.83	1.48	5.92	40.69	17.09
Z0XWLK	Baseline	1.03	1.41	2.00	0.41	0.56	0.78	1.85	0.00
Z0XWLK	C2	1.07	1.44	1.99	0.43	0.57	0.78	0.84	0.00
Z0XWLK	C4	1.18	1.63	2.36	0.47	0.65	0.92	1.89	0.18
Z0XWLK	D1	1.25	1.81	2.68	0.50	0.71	1.05	4.17	0.35
Z0XWLK	D3	1.54	2.18	3.43	0.61	0.84	1.33	8.82	1.34

Table C.7: Summary of statistics for no shear key and no bearing (Case 6)

Location	Soil Class	Abutment Displacement (in.)			Bent Drift Ratio (%)			Likelihood of Spalling (%)	Likelihood of Bar Buckling (%)
		15%	50%	85%	15%	50%	85%		
Z0XOCS	Baseline	1.91	2.93	6.22	0.72	1.11	2.38	21.50	1.75
Z0XOCS	C2	1.87	3.07	6.93	0.71	1.18	2.69	23.43	2.35
Z0XOCS	C4	2.04	3.51	7.94	0.78	1.35	3.08	29.61	4.54
Z0XOCS	D1	2.26	3.84	9.25	0.87	1.48	3.59	35.59	6.45
Z0XOCS	D3	2.61	4.23	12.12	0.99	1.62	4.71	40.41	12.35
Z0XANG	Baseline	1.81	2.95	12.58	0.69	1.14	4.86	37.18	14.46
Z0XANG	C2	1.69	3.28	13.41	0.65	1.26	5.21	36.13	14.04
Z0XANG	C4	1.83	3.86	15.15	0.70	1.48	5.85	40.77	16.77
Z0XANG	D1	1.92	4.08	14.18	0.74	1.58	5.52	43.07	16.91
Z0XANG	D3	2.98	7.13	21.04	1.14	2.75	8.21	60.71	28.88
Z0XWLK	Baseline	1.24	1.90	2.62	0.47	0.72	0.99	5.61	0.01
Z0XWLK	C2	1.27	1.89	3.30	0.47	0.71	1.26	10.33	1.21
Z0XWLK	C4	1.44	2.08	3.80	0.54	0.79	1.46	11.33	1.74
Z0XWLK	D1	1.50	2.20	4.08	0.56	0.82	1.57	12.56	1.59
Z0XWLK	D3	2.12	3.47	10.42	0.81	1.34	4.02	34.84	10.63

Table C.8: Summary of statistics for column height x2 (Case 7)

Location	Soil Class	Abutment Displacement (in.)			Bent Drift Ratio (%)			Likelihood of Spalling (%)	Likelihood of Bar Buckling (%)
		15%	50%	85%	15%	50%	85%		
Z0XOCS	Baseline	1.90	2.86	4.42	0.41	0.62	0.96	0.16	0.00
Z0XOCS	C2	2.09	2.96	4.90	0.43	0.63	1.02	2.99	0.04
Z0XOCS	C4	2.26	3.17	5.88	0.47	0.69	1.18	3.37	0.39
Z0XOCS	D1	2.49	3.70	7.12	0.54	0.80	1.40	4.39	0.30
Z0XOCS	D3	2.63	3.62	6.69	0.56	0.79	1.33	3.24	0.01
Z0XANG	Baseline	1.92	2.46	8.48	0.40	0.52	1.64	6.10	0.01
Z0XANG	C2	1.90	2.53	9.12	0.39	0.54	1.73	7.59	1.32
Z0XANG	C4	2.09	2.94	10.69	0.43	0.62	1.96	10.29	1.74
Z0XANG	D1	2.22	3.13	12.57	0.45	0.66	2.37	13.04	2.43
Z0XANG	D3	2.39	3.35	14.14	0.52	0.72	2.77	15.76	6.46
Z0XWLK	Baseline	1.56	1.81	2.30	0.31	0.39	0.50	0.00	0.00
Z0XWLK	C2	1.53	1.90	2.45	0.32	0.41	0.52	0.04	0.00
Z0XWLK	C4	1.55	2.04	2.54	0.33	0.43	0.53	0.28	0.00
Z0XWLK	D1	1.64	2.15	2.79	0.34	0.45	0.59	0.58	0.00
Z0XWLK	D3	1.93	2.43	3.30	0.41	0.52	0.71	1.72	0.11

Table C.9: Summary of statistics for column height x2 and no shear key (Case 8)

Location	Soil Class	Abutment Displacement (in.)			Bent Drift Ratio (%)			Likelihood of Spalling (%)	Likelihood of Bar Buckling (%)
		15%	50%	85%	15%	50%	85%		
Z0XOCS	Baseline	1.88	4.41	11.32	0.38	0.86	2.21	11.71	2.46
Z0XOCS	C2	2.01	4.36	13.28	0.39	0.85	2.57	13.81	1.79
Z0XOCS	C4	2.20	4.52	13.45	0.43	0.87	2.62	14.64	1.35
Z0XOCS	D1	2.41	4.87	13.66	0.47	0.96	2.67	15.81	1.00
Z0XOCS	D3	2.94	6.13	17.18	0.58	1.18	3.36	22.40	2.37
Z0XANG	Baseline	2.88	9.74	20.07	0.56	1.89	3.93	32.72	1.55
Z0XANG	C2	2.99	7.36	18.85	0.58	1.44	3.68	26.99	1.45
Z0XANG	C4	3.15	7.58	18.73	0.61	1.48	3.65	29.65	2.01
Z0XANG	D1	3.34	8.85	20.23	0.65	1.71	3.95	30.54	3.11
Z0XANG	D3	4.61	11.70	24.90	0.89	2.29	4.88	43.88	7.31
Z0XWLK	Baseline	2.39	6.13	10.18	0.46	1.19	1.98	14.00	1.10
Z0XWLK	C2	2.53	5.62	11.40	0.48	1.10	2.23	13.45	0.60
Z0XWLK	C4	2.79	6.23	11.73	0.54	1.19	2.28	13.70	0.60
Z0XWLK	D1	2.86	6.13	12.39	0.57	1.21	2.41	15.81	0.89
Z0XWLK	D3	3.96	8.67	20.96	0.78	1.69	4.09	31.96	5.63

Table C.10: Summary of statistics for column height /2 (Case 9)

Location	Soil Class	Abutment Displacement (in.)			Bent Drift Ratio (%)			Likelihood of Spalling (%)	Likelihood of Bar Buckling (%)
		15%	50%	85%	15%	50%	85%		
Z0XOCS	Baseline	0.89	1.11	1.92	0.35	0.48	0.85	16.20	0.01
Z0XOCS	C2	0.88	1.26	1.95	0.34	0.55	0.89	20.19	0.01
Z0XOCS	C4	0.96	1.40	2.55	0.39	0.63	1.11	30.78	0.55
Z0XOCS	D1	1.06	1.61	3.16	0.46	0.75	1.38	39.83	4.00
Z0XOCS	D3	0.56	1.02	1.94	0.21	0.43	0.90	16.57	0.44
Z0XANG	Baseline	0.56	0.86	1.42	0.21	0.34	0.60	8.68	3.33
Z0XANG	C2	0.65	0.88	1.49	0.24	0.35	0.66	8.69	1.89
Z0XANG	C4	0.71	1.02	1.93	0.27	0.43	0.83	15.04	1.78
Z0XANG	D1	0.79	1.10	2.07	0.30	0.48	0.91	19.44	3.71
Z0XANG	D3	0.54	0.87	1.89	0.20	0.36	0.84	15.30	3.07
Z0XWLK	Baseline	0.35	0.46	0.68	0.12	0.17	0.25	0.01	0.00
Z0XWLK	C2	0.40	0.51	0.71	0.14	0.19	0.27	0.03	0.00
Z0XWLK	C4	0.48	0.65	0.82	0.17	0.24	0.32	0.20	0.00
Z0XWLK	D1	0.51	0.72	0.90	0.19	0.27	0.36	0.44	0.00
Z0XWLK	D3	0.39	0.60	0.96	0.14	0.22	0.41	1.49	0.00

Table C.11: Summary of statistics for column height /2 and no shear key (Case 10)

Location	Soil Class	Abutment Displacement (in.)			Bent Drift Ratio (%)			Likelihood of Spalling (%)	Likelihood of Bar Buckling (%)
		15%	50%	85%	15%	50%	85%		
Z0XOCS	Baseline	0.99	1.27	2.11	0.37	0.49	0.82	16.80	0.01
Z0XOCS	C2	0.92	1.41	2.56	0.34	0.55	0.98	22.93	0.50
Z0XOCS	C4	1.07	1.73	3.03	0.40	0.67	1.17	32.76	0.98
Z0XOCS	D1	1.22	1.90	4.12	0.46	0.73	1.61	41.92	5.63
Z0XOCS	D3	0.55	1.23	2.65	0.20	0.47	1.03	21.22	1.45
Z0XANG	Baseline	0.57	0.84	2.03	0.21	0.31	0.77	12.30	0.66
Z0XANG	C2	0.63	0.93	2.21	0.23	0.34	0.85	14.22	0.85
Z0XANG	C4	0.76	1.17	2.64	0.28	0.44	1.02	20.48	5.33
Z0XANG	D1	0.79	1.27	2.80	0.29	0.49	1.07	23.55	7.52
Z0XANG	D3	0.54	1.00	2.74	0.20	0.38	1.05	20.84	8.51
Z0XWLK	Baseline	0.36	0.47	0.67	0.13	0.17	0.25	0.02	0.00
Z0XWLK	C2	0.40	0.52	0.75	0.14	0.19	0.28	0.06	0.00
Z0XWLK	C4	0.45	0.65	0.88	0.16	0.24	0.33	0.23	0.00
Z0XWLK	D1	0.50	0.73	0.98	0.18	0.27	0.37	0.62	0.00
Z0XWLK	D3	0.38	0.59	1.11	0.14	0.22	0.42	1.98	0.33

Table C.12: Summary of statistics for new column (Case 11)

Location	Soil Class	Abutment Displacement (in.)			Bent Drift Ratio (%)			Likelihood of Spalling (%)	Likelihood of Bar Buckling (%)
		15%	50%	85%	15%	50%	85%		
Z0XOCS	Baseline	1.47	2.25	3.35	0.64	0.99	1.43	6.83	0.00
Z0XOCS	C2	1.57	2.34	3.45	0.71	1.02	1.48	7.54	0.00
Z0XOCS	C4	1.75	2.61	4.05	0.77	1.14	1.69	13.69	0.01
Z0XOCS	D1	2.01	2.99	5.47	0.89	1.28	2.22	22.67	1.72
Z0XOCS	D3	1.62	2.32	3.91	0.72	1.01	1.68	12.16	1.00
Z0XANG	Baseline	1.17	1.56	2.97	0.52	0.69	1.31	7.98	2.91
Z0XANG	C2	1.22	1.70	2.81	0.55	0.75	1.19	6.24	0.58
Z0XANG	C4	1.33	1.96	3.55	0.60	0.87	1.48	11.35	2.11
Z0XANG	D1	1.41	2.23	4.00	0.63	0.98	1.69	14.67	2.81
Z0XANG	D3	1.49	2.05	4.39	0.66	0.89	1.87	15.09	4.67
Z0XWLK	Baseline	0.98	1.11	1.34	0.42	0.48	0.58	0.01	0.00
Z0XWLK	C2	0.95	1.18	1.41	0.41	0.51	0.62	0.04	0.00
Z0XWLK	C4	0.98	1.31	1.64	0.42	0.57	0.74	0.11	0.00
Z0XWLK	D1	1.07	1.44	1.90	0.47	0.63	0.85	0.29	0.00
Z0XWLK	D3	1.14	1.48	2.15	0.49	0.66	0.94	1.40	0.18

Table C.13: Summary of statistics for low transverse reinforcement ratio (Case 12)

Location	Soil Class	Abutment Displacement (in.)			Bent Drift Ratio (%)			Likelihood of Spalling (%)	Likelihood of Bar Buckling (%)
		15%	50%	85%	15%	50%	85%		
Z0XOCS	Baseline	1.47	2.17	3.23	0.63	0.93	1.37	5.96	0.00
Z0XOCS	C2	1.55	2.33	3.38	0.68	1.03	1.45	6.79	0.00
Z0XOCS	C4	1.70	2.57	4.17	0.77	1.12	1.75	14.57	0.89
Z0XOCS	D1	1.96	3.03	5.17	0.88	1.29	2.07	22.19	2.75
Z0XOCS	D3	1.61	2.39	3.93	0.71	1.04	1.69	11.54	0.64
Z0XANG	Baseline	1.20	1.58	2.36	0.54	0.72	1.02	6.51	3.33
Z0XANG	C2	1.17	1.65	3.09	0.50	0.74	1.22	7.47	2.05
Z0XANG	C4	1.28	1.93	3.51	0.60	0.87	1.55	11.45	2.12
Z0XANG	D1	1.38	2.19	3.80	0.63	0.96	1.68	13.90	4.10
Z0XANG	D3	1.49	2.01	3.93	0.65	0.88	1.70	15.19	7.28
Z0XWLK	Baseline	0.90	1.12	1.30	0.39	0.49	0.57	0.03	0.00
Z0XWLK	C2	0.91	1.17	1.38	0.39	0.51	0.61	0.02	0.00
Z0XWLK	C4	0.99	1.29	1.62	0.43	0.57	0.71	0.12	0.00
Z0XWLK	D1	1.08	1.41	1.85	0.47	0.63	0.83	0.66	0.16
Z0XWLK	D3	1.13	1.46	2.08	0.48	0.65	0.92	1.22	0.01

Title VI Notice to Public

It is the Washington State Department of Transportation's (WSDOT's) policy to assure that no person shall, on the grounds of race, color, or national origin, as provided by Title VI of the Civil Rights Act of 1964, be excluded from participation in, be denied the benefits of, or be otherwise discriminated against under any of its programs and activities. Any person who believes his/her Title VI protection has been violated, may file a complaint with WSDOT's Office of Equity and Civil Rights (OECR). For additional information regarding Title VI complaint procedures and/or information regarding our non-discrimination obligations, please contact OECR's Title VI Coordinator at (360) 705-7090.

Americans with Disabilities Act (ADA) Information

This material can be made available in an alternate format by emailing the Office of Equity and Civil Rights at wsdotada@wsdot.wa.gov or by calling toll free, 855-362-4ADA(4232). Persons who are deaf or hard of hearing may make a request by calling the Washington State Relay at 711.